CONF-771129--

Proceedings of the Fusion Fueling Workshop

Held at Princeton University, Princeton, New Jersey
November 1-3, 1977

March 1978

Funded By
U.S. Department of Energy
Assistant Secretary for Energy Technology
Office of Fusion Energy

Under Contract No. EY-76-C-02-3073

Proceedings of the Fusion Fueling Workshop

Held at Princeton University, Princeton, New Jersey
November 1-3, 1977

March 1978

Funded By
U.S. Department of Energy
Assistant Secretary for Energy Technology
Office of Fusion Energy
Washington, DC 20545

Under Contract No. EY-76-C-02-3073

Available from:

National Technical Information Service (NTIS)
U.S. Department of Commerce
5285 Port Royal Road
Springfield, Virginia 22161

Price:

Printed Copy:	$ 8.00
Microfiche:	$ 3.00

ACKNOWLEDGMENTS

The Fusion Fueling Workshop was organized by Robert G. Mills with the help of Samuel L. Gralnick and Constance C. Hopkins of the PPPL and by Hatice S. Cullingford of the Office of Fusion Energy in DOE. The efforts of many PPPL staff and the DOE staff, especially Cindy Smith for her secretarial assistance in the preparation of this document, are acknowledged with appreciation.

TABLE OF CONTENTS

INTRODUCTION

The Office of Fusion Energy* of the Department of Energy+ (DOE) sponsored a workshop on Fusion Fueling on November 1-3, 1977. The Princeton Plasma Physics Laboratory (PPPL) and the School of Engineering and Applied Science hosted the workshop which was attended by approximately sixty-five participants from eight countries.

The purpose of the workshop was to outline the background and rationale and help set objectives for implementation of a sound fusion fueling development. The meeting provided a medium for extensive interactions among those scientists who are active researchers in the area of fusion fueling. The problems and the solutions associated with fueling of future fusion reactors and near-term machines were discussed in the following sessions: Plasma Guns and Cluster Beams; Neutral Beams; Gas Blankets and Neutral-Plasma Interactions; and Pellet Injection. A technology overview was provided in a separate session. The papers presented in the sessions are included in these proceedings along with the topical summaries which were prepared by those individuals as referenced.

Hatice S. Cullingford
Plasma Engineering Branch
Office of Fusion Energy

*Formerly the Division of Magnetic Fusion Energy (DMFE).

+Prior to its activation in October 1977, the Energy Research and Development Administration (ERDA).

PLASMA GUNS AND CLUSTER BEAMS

Chairman: G. H. Miley
(University of Illinois, U.S.A.)

FUELING BY COAXIAL PLASMA GUNS*

John Marshall

Los Alamos Scientific Laboratory
University of California
Los Alamos, New Mexico 87545

Coaxial Guns

Many kinds of plasma guns have been investigated by various workers and a number of them might be suitable for fueling thermonuclear reactors. I shall limit my attention here however to pulsed coaxial guns, because of their simplicity of construction, high performance, and high efficiency.[1,2]

A coaxial gun consists essentially of two circularly symmetric metal electrodes separated at the breech by an insulator-vacuum seal, and open at the muzzle for the emergence of plasma. The plasma is derived from a puff of gas admitted by a fast valve. This makes it possible for the space beyond the muzzle to remain evacuated except for the plasma admitted by the gun. A high-voltage, high-current power supply such as a capacitor bank or an inductive energy store is connected across the electrodes at the breech. This is switched on, usually with some predetermined delay after gas admission, and produces a radial discharge through the gas between the electrodes. The B_θ magnetic field associated with the radial current produces a $j \times B$ force on the discharge, tending to drive it away from the breech and out through the muzzle. The actual processes involved are exceedingly complicated, involving ionization phenomena, electrode effects, finite gyro orbits of the ions, space charge electric fields and strong differences in currents carried by ions and electrons, described reasonably well as a Hall effect. The performance of a gun depends strongly on its parameters, which might be described by position in a multidimensional space with coordinates describing dimensions, electrode shapes, magnitude and polarity of supply voltage, position of gas inlet, amount of gas admitted, delay after gas admission, insulator design, etc. Optimization of performance is difficult because of the many parameters, and in practice is usually done by maximizing some single criterion of performance, e.g., neutron yield or plasma velocity. The result is a wide variety of designs and performance characteristics.

Performance of appropriately optimized designs is characterized by high efficiency (>50%), high plasma purity, and large plasma energy with state-of-the-art power supplies. The acceleration of the plasma appears in all cases to be expansion of magnetized and moderately heated plasma out through the muzzle, driven by its own internal pressure, kinetic and magnetic. Nearly all coaxial guns are operated with negative center electrode. This is because of better collimation of the emerging plasma with negative polarity. The reason is that, with Hall effect, the current streamlines are tipped backward at the cathode, producing an inward pinching force component along with the axial force responsible for acceleration through the muzzle. The B_θ field is mixed with the plasma during the ionization process. The embedded field is convected out through the muzzle with the plasma, and thus the plasma must carry an extension of the cathode current. This produces a radial pinching force, helping to collimate the plasma beyond the gun muzzle. Electrical resistivity in the emergent plasma leads to magnetic flux annihilation on the axis, and a tendency for plasma to accumulate there as it follows the flux. This is particularly important with high Z plasmas because of electron temperature clamping by line radiation.

Plasma guns have been operated at total emergent plasma energies of 300 kJ and more. There seems to be no serious obstacle to their energies being extended to several megajoules.

Coaxial guns are divided into two types, "snowplow" and "deflagration" guns. In the snowplow gun (Figs. 1, 2) a magnetic piston progresses along the interelectrode space, ionizing the gas, mixing it with field, and pushing it aside to rest against the outer electrode. The embedded magnetic field serves to reduce heat loss to the electrodes, and its pressure subsequently drives the plasma out through the muzzle. The magnetic piston also carries a plasma (more tenuous than the plasma pushed aside and left behind). The snowplow gun is characterized by a wide spread of plasma velocities and densities. Frequently it appears in two distinct "plasmoids", a fast one followed by a slow one. The deflagration gun appears in two distinct types.[3,4] One is the familiar M.P.D. accelerator, and its relatives, operated dc or quasi dc at a few thousand amperes and a few hundred volts. The other is a pulsed variety (Fig. 3).[5,6] In either case a more or less stationary discharge is formed with plasma ionized, magnetized and driven out through the the muzzle continuously. The deflagration gun has been the less thoroughly studied till now. In some embodiments it appears to have superior focussing properties, and to the extent it is steady-state it would appear to produce a stream of plasma with steady characteristics, velocity and density.

The plasma from coaxial guns of the snowplow-type (the ones which have been most investigated) is surprisingly free of contamination by electrode materials (usually Cu). This is due to happy accidents in the mechanisms of current transfer between plasma and electrodes. For example the initial ionizing snowplow appears to derive most of its cathode current from the collection of low-energy ions. This produces little heat at the cathode and leaves there a dense layer of neutrals, which can be ionized later during the plasma expansion acceleration phase to provide electron current without the need of thermionic emission or potential sheaths. The situation in deflagration guns is not clear, although M.P.D. devices, which share some of the characteristics of the class, appear usually to depend on thermionic emission from a hot cathode, and in some cases have shown strong potential sheaths at the anode.[4] There may be substantial differences between pulsed and dc or quasi dc operation.

Injection into Containment Fields

Injection of gun plasma into containment fields involves phenomena at least as complicated as those in the gun. The plasma can be injected into open geometries (straight solenoid or mirror machine). In these cases it is convenient to inject parallel to the field lines. It can also be injected into closed geometries (toroidal devices such as tokamaks or absolute minimum fields as in caulked-cusp toroidal

multipoles). The plasma can be injected into a device which already has a plasma in it, or into a vacuum field. The plasma can have large enough ion energy to provide a trapped plasma at thermonuclear temperatures or it can provide plasma at reduced temperatures suitable for refueling an ignited thermonuclear reactor or to provide a pre-plasma for heating by compression or other process. Injection can be high-beta or low-beta depending on whether the injected plasma substantially excludes magnetic field after injection or not. We have here four pairs of alternatives which can be combined to give sixteen different combinations. The phenomena encountered in the different combinations are generally quite different from each other, and few of them have been adequately investigated experimentally. For this reason I shall mostly limit my discussion to cross-field injection and shall concentrate on the case of injection into systems already containing plasma, the general case for a tokamak.

A number of experiment have been performed in which coaxial gun plasma is injected across a magnetic field at right angles to the direction of the field.[7,8,9,10] At moderate magnetic field strengths, the fast plasma enters the field almost as though it weren't there, and proceeds across the field at its original speed, still collimated into a narrow jet. The plasma is thoroughly permeated by the magnetic field in a low-beta manner, there appearing to be no reduction of field strength inside the plasma. This implies that the plasma was initially at a low temperature, although it has a large streaming energy density, and that it is not heated appreciably upon entering the field. The plasma is observed to contain a transverse electric field commensurate with its velocity and the strength of the magnetic field ($\vec{E} = \vec{v} \times \vec{B}$). The propagation of the plasma across the field appears to be reasonably explainable in terms of polarization charges on its transverse surfaces. Plasma between the charges finds itself in a uniform transverse electric field and thus drifts at speed E/B. A tenuous plasma spreads outward along the field lines passing through the plasma, providing electrical contact between the plasma and whatever lies on the same field lines. This allows potential probing outside of the energetic plasma stream. It is also possible, because of this, to bring the plasma to a stop by discharging its polarization field through a metal plate or through another plasma, moving across the field in the opposite direction and therefore with opposite electric polarization. Substantial currents flow along the field lines and across the plasma. The $\vec{j} \times \vec{B}$ force of this current then stops the plasma.

While the propagation of the magnetized plasma across the field can be rationalized, its entry into the field is not well understood. The question is how are the field and the plasma thoroughly mixed without heating the plasma? We might say that the mechanism is unimportant and that we care only that it does enter the field. The difficulty here is that under some conditions it does not enter the field, and that these are conditions of some practical interest.

We are concerned with the entry of a long stream of plasma into a transverse magnetic field and we know that, once the stream is well inside, it is thoroughly permeated by the field. We can imagine that the ions, because of their larger mass, can penetrate the field farther than the electrons, produce a positive space charge and an electric potential, the gradient of which gives the electric field required for the cross-field drift. Somehow the electric field of this space charge then manages to drag the electrons in to produce quasi-neutrality. The potential of the ion space charge, according to this picture, would be limited by the ion kinetic energy in the plasma stream and this would put a limit on the width of the stream given by $w \leq Mv/2Be$. Further complications are introduced by the loss of ion kinetic energy to be expected when the ions penetrate to the high positive potential produced by their own space charge. In addition the electrons would be expected to gain energy in falling into the positive potential, and this would certainly heat them and produce diamagnetism. Observations show that the diamagnetism is minimal, not over 10% beta, and that no appreciable slowing of the ions occurs. The injection process may involve some kind of clumping of the entering plasma so that ions and electrons enter the positive potential attached to one another so that the gain and loss of energy are minimal.

There is experimental evidence that the presence of a background plasma in the magnetic field interferes with the entry mechanism and prevents low-beta injection. This was discovered during a two-gun injection experiment, where the electric field of each plasma stream was used to depolarize and stop an oppositely directed stream.[9] If one of the guns was fired about one millisecond early, the other gun plasma did not enter the field. The phenomenon was not thoroughly investigated because of the shortness of time, so it is not known whether a change of parameters, e.g., a reduction of field strength, would have allowed the second plasma stream to enter. It is not known whether the cause is interference with the field-plasma mixing process or whether it is line-tying after mixing.

Injection into Reactors

Where does all this leave us with regard to injection into the ambient plasma of an operating reactor? It appears that if line-tying has anything to do with the prevention of low-beta injection by a background plasma, the effect should be even stronger under reactor conditions. This is because at reactor temperatures the effective magnetic Reynolds number should be very large, $R_m = 2\pi w/a \sigma v >> 1$ where w is the width of the plasma stream, a is the minor radius of the plasma, σ is the conductivity (emu), and v is the velocity. This is equivalent to saying that, on the timescale of plasma flow into the field, the magnetic lines of force are well frozen into the plasma. Qualitatively this implies that field lines in the injected plasma are trailed behind it inward into the containment field, slowing it down by their tension and then perhaps pulling it outward again, provided they are anchored at the outside. It should be emphasized that this qualitative picture tends to break down by its very complexity, so that theoretical predictions unsupported by experiment are on shaky ground. However it appears that we should first consider high-beta injection.

In high-beta injection, with reference to Fig. 6, we might expect the plasma stream to impact against the field in a more or less cylindrical form. We assume that the stagnation pressure (nmv^2) is larger than the field pressure. Thus the plasma punches a hole in the field and enters as though it were a conducting metal cylinder. In impacting against the field, the ion temperature of the plasma is raised (Fig. 7). Once inside, the transverse kinetic pressure of the plasma holds back the surrounding magnetic field. There is no equilibrium in this configuration because the pushing aside of the field raises its pressure on the transverse boundaries and lowers it near the plasma in the direction of the field. The plasma thus is compressed transversely and

expands along the field. The result is that the original cylindrical shape of the plasma is transformed into a spatulate shape, twisted like a corkscrew in a sheared field as in a tokamak. The plasma does not really have a thin current sheet separating a field-free region from the containing field. Normally we find a current sheath of the order of an ion-gyro radius thick. A thin sheath implies electric fields to transfer to the ions the $\vec{j} \times \vec{B}$ forces on the electrons. As the cylinder is flattened between the field lines, it eventually becomes so thin that it is all sheath. It has magnetic field soaked into it through its whole thickness. The plasma in the sheath on the surface of the stream is at all times line-tied to the ambient plasma in the field, and tends to drag it along. This slows down the sheath plasma and leaves it behind to flow out along the field lines and mix with the ambient plasma. It is likely to slow down the whole stream because of interchange of ions between sheath and the body of the stream.

Thus we expect that, on some scale, gun plasma with sufficiently high stagnation pressure should enter the containment region of a reactor and mix with the ambient plasma. A denser, faster, larger diameter stream should penetrate farther. The subject is too complicated for reliable predictions to be made. Some relatively simple experimentation would illuminate the subject considerably. It is regrettable that the experiments of Hammel and Kewish were terminated before attaining more data.

REFERENCES

1. J. Marshall and I. Henins, Plasma Phys. and Controlled Nucl. Fus. Research, I.A.E.A Vienna (1966) P. 449.

2. G. N. Aretov, J. N. Burdonskii, Yu. A. Valkov, V. I. Vasil'ev, A. P. Lototskii, Yu. V. Skvortsov, V. G. Solov'ova, Yu. F. Suslov, Proc. of Second Topical Conference on Pulsed High-Beta Plasmas, Garching bei Munchen (1972).

3. M. J. Boyle, K. E. Clark, and R. G. Jahn, AIAA Journal 14 955 (1976).

4. A. I. Morozov, Fiz. Plazmy 1, 179 (1975).

5. Dah Yu Cheng, Nuclear Fusion 10, 305 (1970).

6. E. A. Azizov, I. V. Kochurov, and M. M. Stepanenko, Zh. Tekh. Fiz. 45, 1826 (1975).

7. D. A. Baker and J. E. Hammel, Phys. Fluids 8, 713 (1965).

8. J. E. Hammel and D. A. Baker, Plasma Physics and Controlled Nuclear Fusion Research, I.A.E.A., Vienna (1966) p.499.

9. J. E. Hammel and R. W. Kewish, Jr., Los Alamos Report LA-3994 (1969).

10. I. I. Demidenko, N. S. Lomino, V. G. Padalka and N. A. Khizhnyak, Zh. Tekh. Fiz. 41, 900 (1971).

*Work performed under the auspices of the Department of Energy.

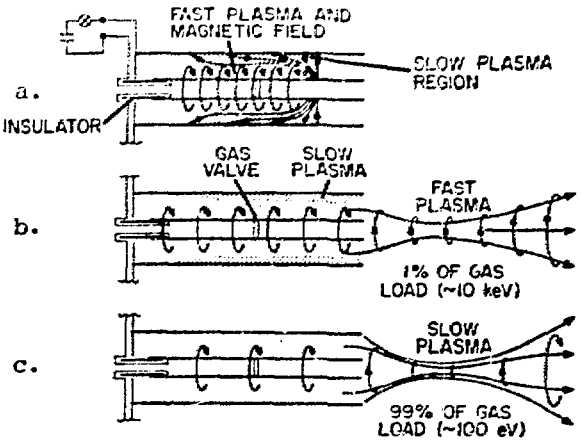

Fig. 1. Coaxial Gun, Snowplow Type.
a. Magnetic piston moves along barrel, dense magnetized plasma pushed aside, tenuous plasma in piston.
b. Piston with "fast plasma" emerges from muzzle.
c. Dense magnetized plasma emerges to produce "slow plasma".

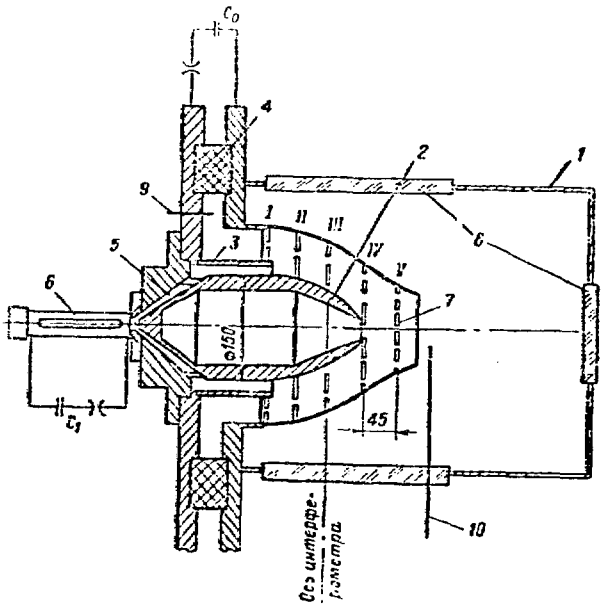

Fig. 2. Coaxial Gun at Kurchatov Institute. Typical of reference (2). Inner electrode diameter 15 cm. Slots are for interferometric observation.

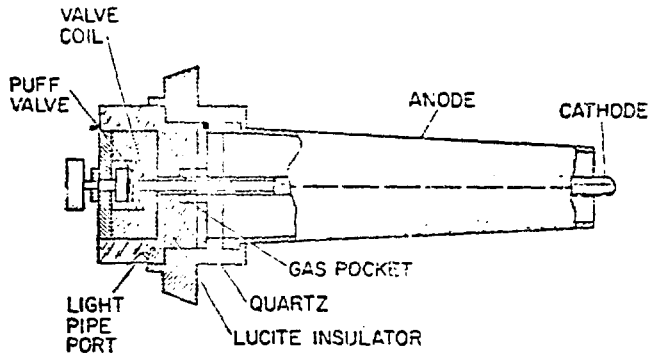

Fig. 3. Deflagration Gun of D. Y. Cheng
Gun ~ 30 cm long.

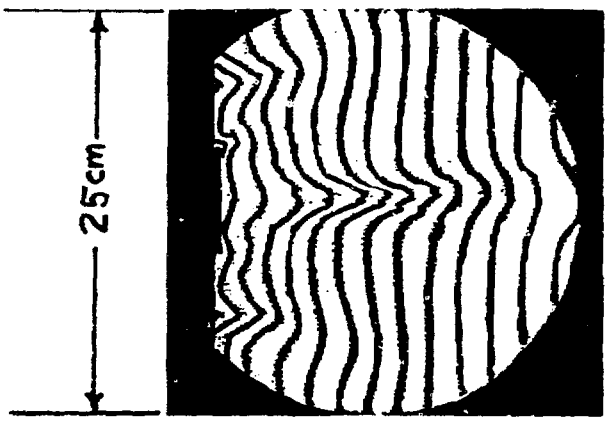

Fig. 4. Ruby Laser Holographic Interferogram (retouched)
One fringe ~ $3 \times 10^{17}/cm^2$; Plasma speed ~ 2×10^7 cm/sec; Central density ~ $10^{17}/cm^3$; Deuterium.

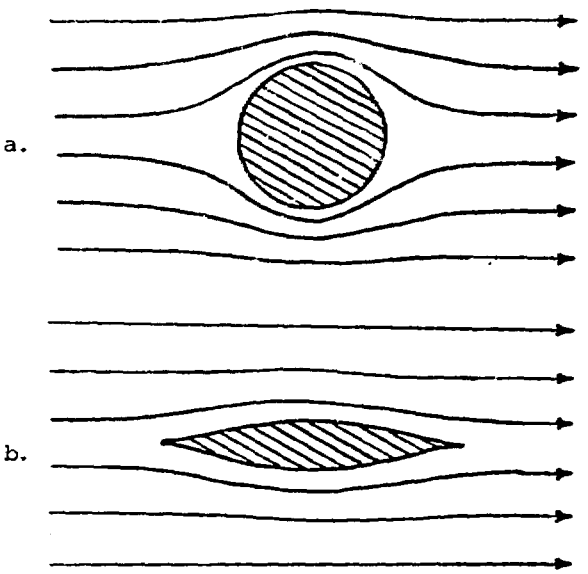

Fig. 6. High-Beta Injection
a. Plasma on first encountering field
b. Plasma after deformation by field

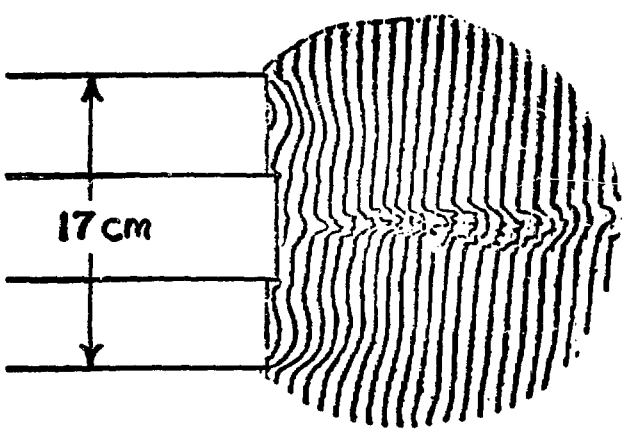

Fig. 5. Holographic Interferogram of Ne Gun Plasma (retouched). Dense condensation on axis is due to resistive flux annihilation.

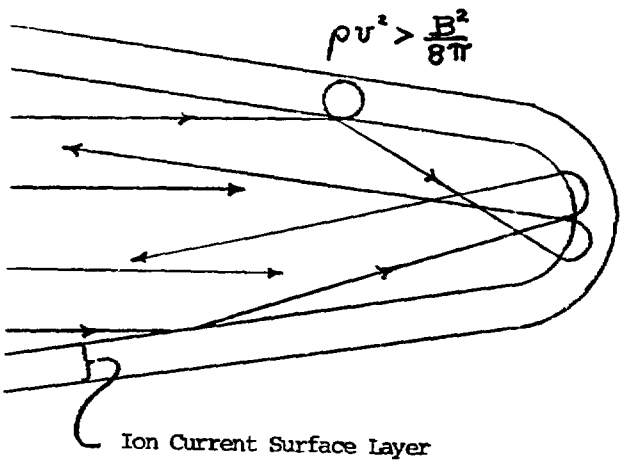

Fig. 7. High-Beta Collisionless Injection.

PROSPECTS FOR DEFLAGRATION GUNS*

Dah Yu Cheng, Prabahakar P. Tripathi and C. N. Chang
Plasma Research Laboratory, School of Engineering
University of Santa Clara
Santa Clara, California 95053

Summary

Deflagration is a process of fluid expansion with energy addition. Its existence in plasma physics was first discovered in the back-strapped T-tube experiments. In the coaxial plasma gun configuration the operation can be simple and yet produce a clean, high density (5×10^{15} cm^{-3}), and high kinetic energy (10 - 50 keV) collimated plasma beam. Plasma acceleration mechanism was thought to be driven by J x B force. Tapered electrodes have been used to obtain plasma beams. Scaling of the gun can be performed according to simple theory based on momentum and energy balance. Proposed plasma fueling and injection to magnetic fusion systems will be discussed.

Introduction

Plasma guns have been considered to be a practical fusion fueling device since the dawn of fusion research. The prospects for colliding high energy dense plasma beams within a guiding magnetic field were discussed many times. Several forms of plasma guns were built; they varied from the back strapped T-tube by Kolb to many forms of rail guns, to the coaxial plasma gun made famous by Marshall.

All the devices built in the 1950's had some things in common, namely: (1) simplicity, (2) high conversion efficiency from stored energy, (3) possibility of using mixture of gases, and (4) relatively high plasma density (10^{15} – 10^{17}/c.c.). They also had the unfortunate character of not being able to reach high enough kinetic energy considered adequate for fusion at that time. T-tube made its way to various university laboratories due to its simplicity and its vlaue as a spectrascopic light source. The most popular gun is the Marshall Gun, which has the most complete diagnostic information and also can produce higher plasma energy than most other devices.

About ten years ago, the deflagration plasma acceleration was discovered experimentally in a T-tube. Deflagration acceleration in a back strapped T-tube can be produced by connecting high voltage capacitors directly to the terminals of the evacuated T-tube and then pulsing the gas in to initiate the discharge. Initially the T-tube is evacuated to a high vacuum (10^{-6} mmHg) to hold off the electric breakdown by using the character of the vacuum side of the Paschen's law. The breakdown is initiated by a puff of gas fed from the back-strap side of the T-tube, while the electric discharge starts at the instant the Paschen breakdown voltage drops below the capacitor voltage.

*This work is sponsored by ERDA Grant No. 4-70-90-71.

The difference of this discharge to that of the ordinary T-tube is that the deflagration plasma is accelerated into a vacuum without collisions with neutrals and the consequent pile-up. The discharge is fed by the neutral gas continuously to form a quasi-steady state plasma flow. The initial measurement of the velocity of the plasma front indicated a value about 10^8cm/sec with hydrogen plasmas. The T-tube represented a modest experimental set up, yet produced plasma kinetic energy on the order of 10 keV. Theoretical study following the observed phenomena led to the study of the deflagration process and other deflagration gun designs.

The following paragraphs will summarize the physical properties of deflagration, the experimental results and relavent plasma properties for fusion research.

Scaling of the plasma gun has also been attempted; the experimental results for different size guns can be predicted with some degree of accuracy using simple theories. The prospect of using the deflagration gun for fueling, ignition or pellet pushing will be discussed also.

What Is Deflagration?

An examination of other plasma devices, indicated that they are invariably snowplow discharges. The acceleration force of the plasma is the J x B force in all cases except that the snowplow discharge has a distinct current sheet and a neutral gas shock layer ahead of the current sheet. The deflagration plasma is also accelerated by the J x B force but can be freely expanded into a vacuum without the neutral gas in its way.

A close examination of the governing equations shows that deflagration and snowplow are two distinct roots of the conservation equations of mass and momentum with energy addition. (Ref. 1). The snowplow discharge occurs with a plasma flow under compression and the deflagration discharge occurs with a plasma flow under expansion. The limiting factors which govern the physical limits of the discharge modes are the heating rate and the entropy production extreme. For a given heating rate, entropy production reaches two maxima. These are known in combusion science as the Rankine-Hugoniot limits (Ref. 2). Due to the distinct nature of the two roots, the snowplow or deflagration discharges have to be specially triggered. The earlier T-tube experimental results can be seen in Figure 1. The two T-tubes had the same capacitor stored energy. Image converter streak pictures showed that one has a jump surface and the other only a faded out moving front. From the T-tube studies, one can see that a coaxial geometry is more suitable for the theoretical and the experimental study of the phenomena. In Figure 2, the cut-away view of the coaxial discharges are shown. In both cases, the plasmas are accelerated by

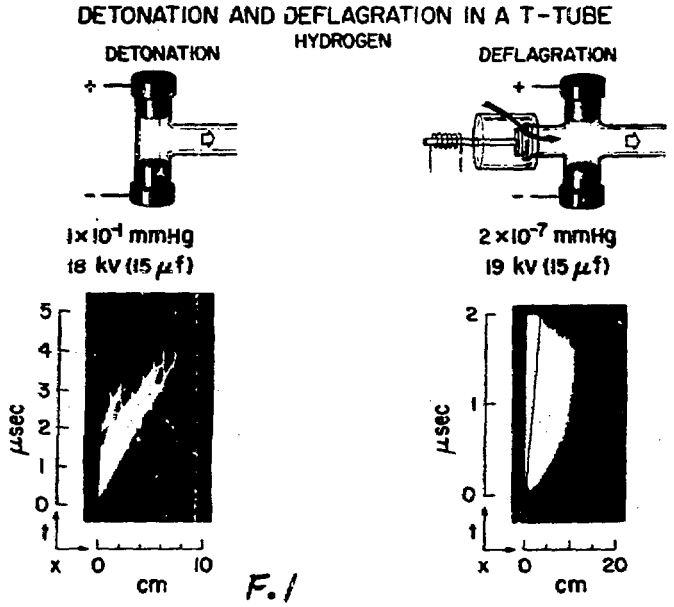

the J x B force; however, the snowplow wave propagates in the same direction as the J x B force but the deflagration wave propagates in the direction opposite to J x B force. Neutral gas can be injected from the insulator wall to create a quasi-steady discharge in the laboratory frame of observation. Thus, the deflagration discharge can be operated as a quasi-steady device, but the snowplow device is limited by the length of the device itself. When the snowplow wave reaches the end of the gun, depending upon the geometry, it can either become a plasma focus or spew out high velocity plasmas. The time period is limited.

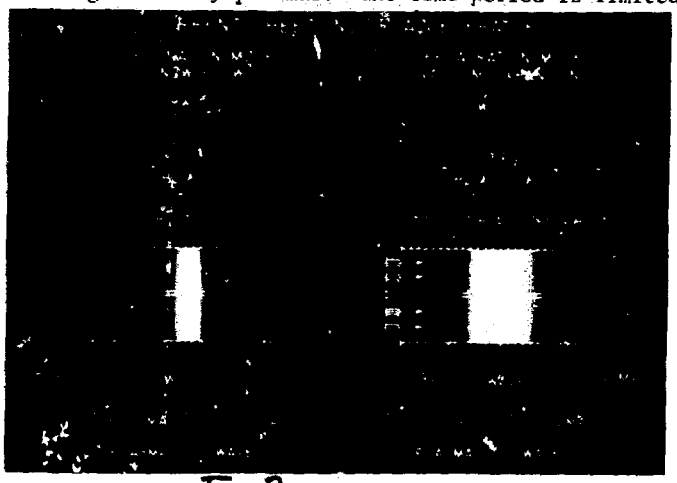

The Coaxial Deflagration Plasma Guns

The first generation coaxial plasma guns can be seen in Figure 3. The plasma gun requires a puff valve to inject gas through the breach insulator of the gun, while the electric field is held off by vacuum. There are small slits cut along the axial direction for photographic pruposes. The time sequential pictures of the switchless discharge, triggered only by the puffed gas, can be seen in Figure 4. A typical time history of current near the gun breech is also shown. Typically, the deflagration discharge in the first half cycle of the discharge current will propel plasma out of the gun muzzle into a vacuum. The stationary nature of the sequential pictures for the first half cycle indicates approach to a quasi-steady state discharge. When capacitor rings, the

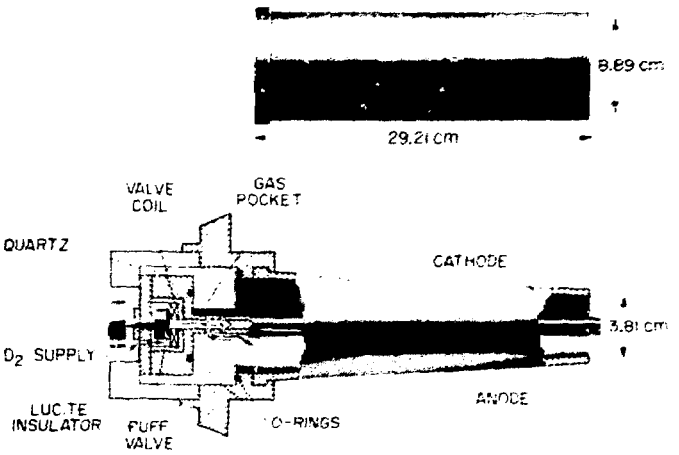

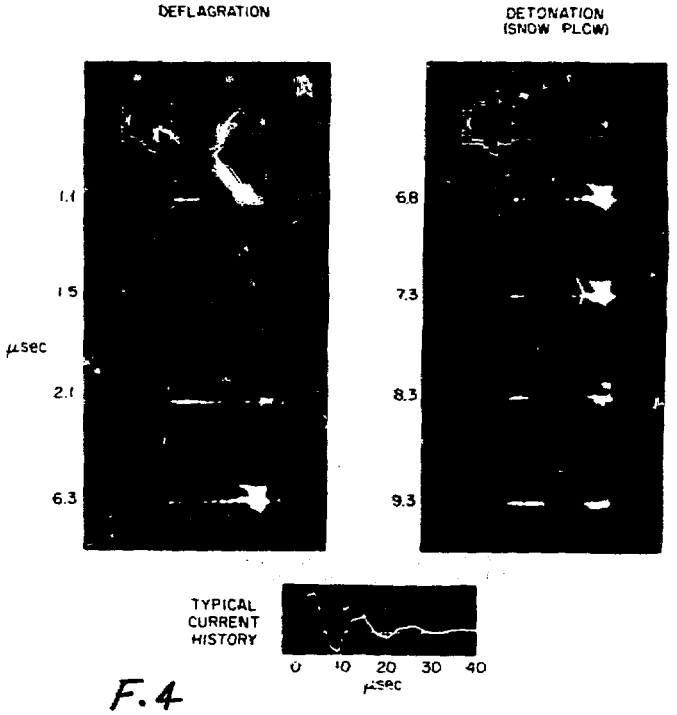

voltage across the gun swings to the other polarity. The restrike along the gun breech occurs now with the presence of neutral gas and produces a snowplow discharge. A typical moving jump surface appears again in the second set of the sequential pictures.

In Figure 5, the magnetic field profiles inside the gun barrel indicate a distributed current for deflagration but a concentrated higher current density sheet for snowplow. Given the same total current it implies a low current density on the electrode surfaces for deflagration and high current density for a snowplow discharge. This also means that the impurities are more likely to be produced by the snowplow discharges than by the deflagration discharges.

In Figure 6, the experimental results of a time resolved measurement by a 1/4 meter monochrometer are shown for the Cu I line (4062Å). According to the gun current traces shown, the first half cycle again produces the deflagration discharge which are followed by several snowplow discharges; only the first snowplow discharge is strong enough to produce impurity lines. When the snowplow discharges were eliminated by a crow-

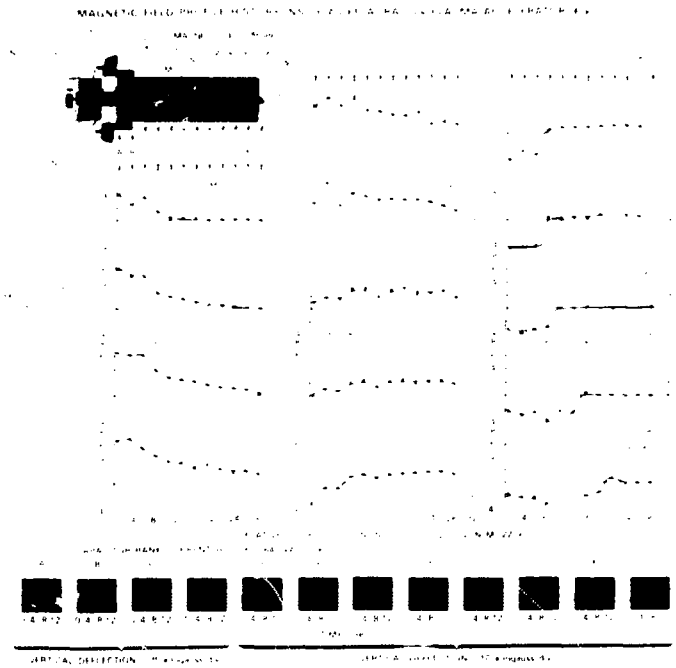

F. 5

bar switch, the impurity line was also eliminated. The same phenomena can be seen in Figure 7 when the monochrometer is tuned to 4651A oxygen II line. Although center electrode erosion is frequently found, it is generally believed that the total current of the deflagration discharge can be substantially increased before impurities would be a problem provided one can eliminate the follow-on snowplow all the time.

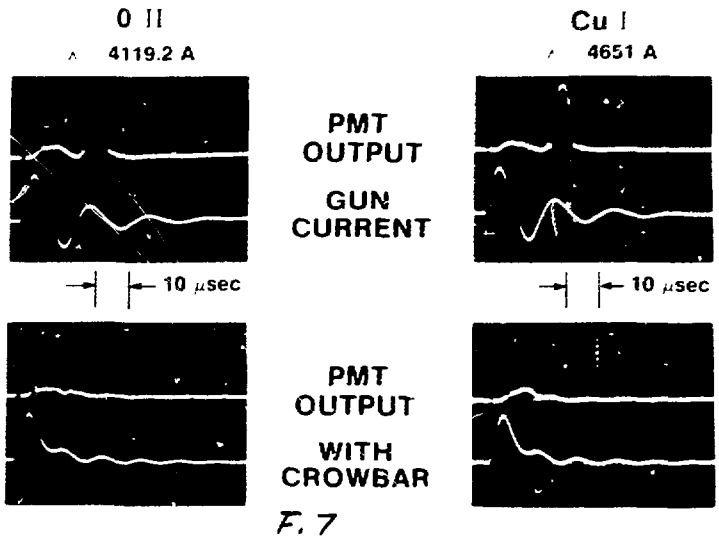

F. 7

[illegible] accelerates, [illegible] greatly [illegible]

[illegible] the [illegible] of the discharge current [illegible] will not [illegible] well understood, because the particles [illegible] accelerated under a very high [illegible] field [illegible] typically [illegible] 50 kilogauss. The [illegible] plasma [illegible] encountered during the acceleration, and eventually the plasma temperature will [illegible] accordingly to the rapid expansion. Finally, when the [illegible] point is [illegible] than it can be [illegible] energy, the deflagration limit is reached.

[illegible] the [illegible] single particle point of view, the charged particle [illegible] accelerated according to [illegible] drift velocity; when the [illegible] lower toward the gun muzzle, the drift velocity becomes higher, thus constituting a natural expansion process. (Figure 8). If the particles are truly accelerated according to the J x B vector [illegible] the gun, then the plasma beam can also be focussed. The focussed plasma beam would have higher density away from the gun electrodes due to its accumulation effect. (Figure 9). This is indeed the case as it was verified by laser interferometric pictures. The ordinary focussed spot can be as small as 1 cm^2. This can be seen in Figure 10 which shows damage pattern on a polished copper.

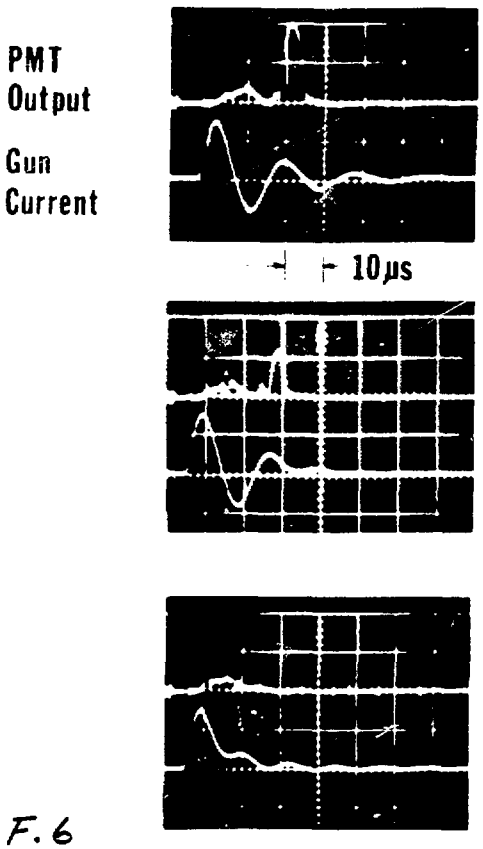

F. 6

If one chooses to ignore the complicated discharge current structure, the plasma kinetic energy can still be estimated from the momentum balance, as the stagnation pressure of the plasma beam should be on the order of the magnetic pressure at the breech of the gun. So the scaling to higher kinetic energy requires smaller electrode diameters, and scaling to higher stored energy handling capability requires larger electrode dimensions. A series of various size guns can be seen in Figure 11.

One of the higher kinetic energy guns shown in Figure 12, was used extensively for scaling law experiments. This gun routinely produces greater than 10 keV plasma kinetic energy. When the gun discharged 8 KJ of energy of plasma beam to a metal target, Figure 13, the sizes of the damage patterns were confined to the outer electrode diameter of the plasma gun. The pictures in Figure 13 were results of a single blast on a polished metal target.

From past experiences and data, the plasma kinetic energy were typically proportional to the magnetic field pressure rather than capacitor voltage. Using plasma

TYPICAL B FIELD
PROFILE AND CHARGED
PARTICLE TRAJECTORIES

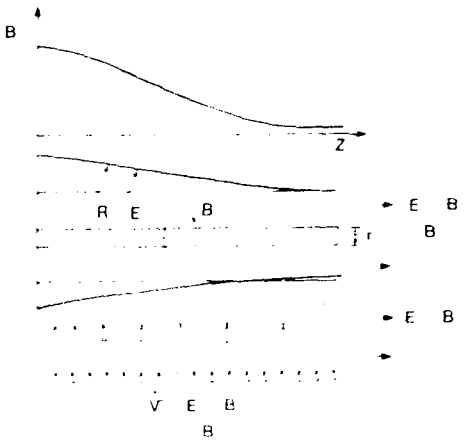

F. 8

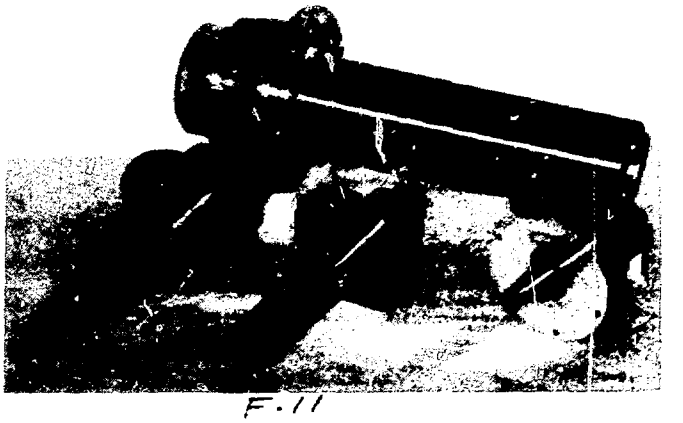

F.11

TAPERED ANODE

HOLLOW COPPER CATHODE

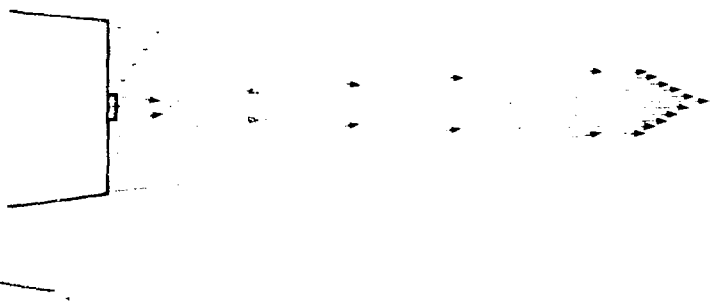

F.9

F.10

density of 10^{16}/c.c. as measured by laser holography, and magnetic probe data one can compute a plasma velocity if the magnetic pressure is totally converted into kinetic energy. This compared will with time of flight velocity measurements using a weak guided axial magnetic field and diamagnetic probes, as this can be seen in Figure 11.

HIGH KINETIC ENERGY GUN
TYPICAL GUN ASSEMBLY

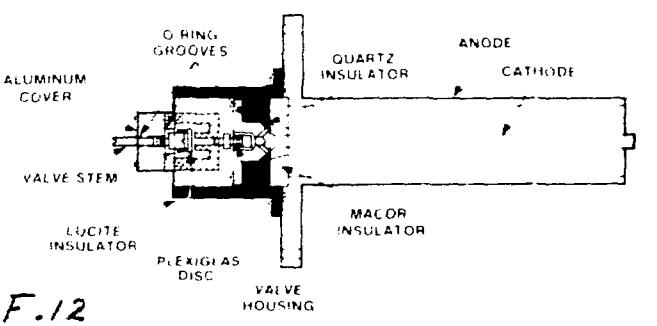

F.12

HIGH K.E. GUN STOPPER PLATE
DAMAGE TEST

12kJ — SINGLE SHOT

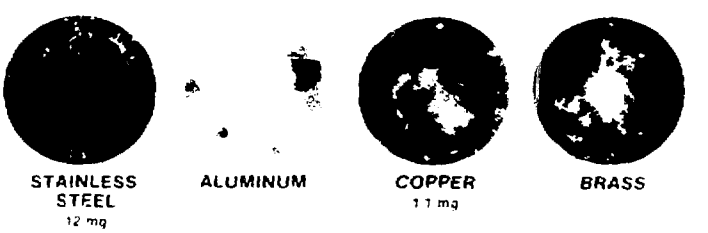

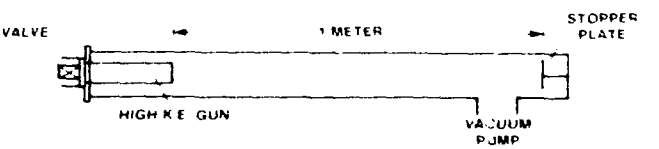

F.13

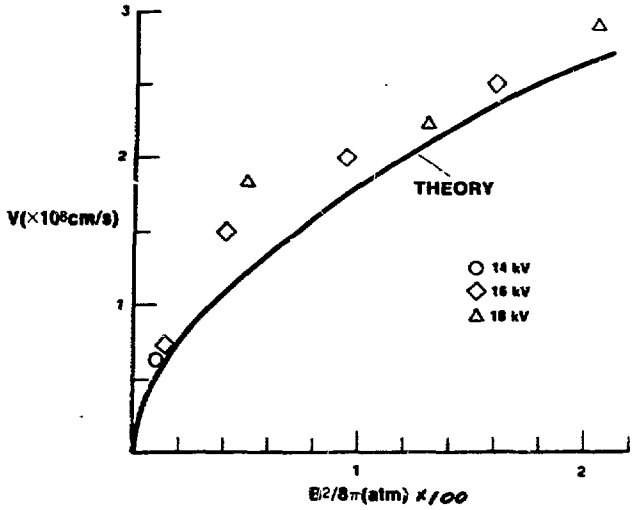

F. 14

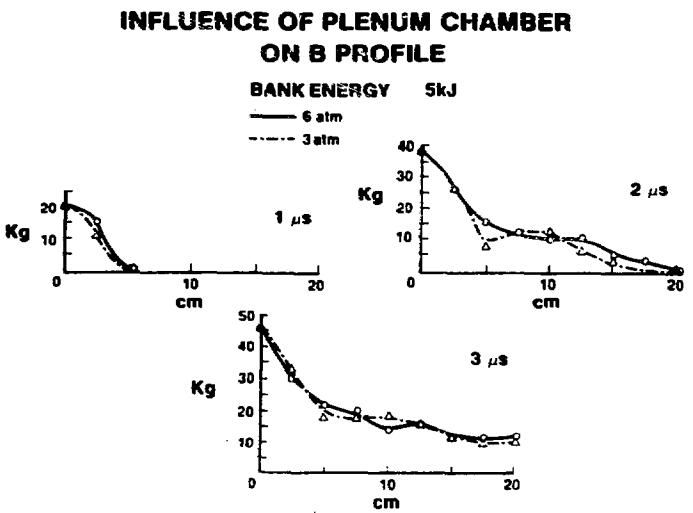

F. 15

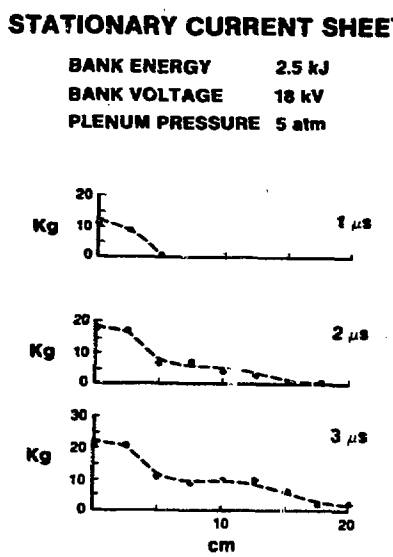

F. 16

From time of flight measurements, plasma kinetic energy as high as 50 kev was obtained. This becomes an interesting energy range for many fusion related applications.

Due to the focussing property of the gun, one can use this plasma gun to penetrate magnetic confinement field through a high Beta hole. The mechanism of cross field penetration is not known since no experiment has been performed. From momentum balance point of view, if the magnetic field strength at the breech of the gun is 100 kiloguass, then the plasma being pushed by this field strength ought to be able to penetrate a confinement field of 25 kiloguass or more. The high density small diameter beam will not disturb the confinement field in a gross way. If the confinement field has a minimum B configuration, the dense plasma will be diffused in travelling towards the minimum B region, and then could not climb the magnetic field wall again. The pulsed plasma energy will be on the order of fusion burning temperature, hence, it not only becomes a deuterium fueling system but also an energy feeding system for ignition pruposes. Since tritium-deuterium mixture can be used without changing the gun parameters, the ignition burning can be enhanced with a controlled D-T mixture.

Cross field experiment may be needed to evaluate the potential of deflagration guns. A proposed arrangement to inject plasmas into a mirror machine can be seen in Figure 17. The gatling gun arrangement can be used to inject plasmas along the field lines. Gatling gun arrangement may be the alternative to long pulse period single gun operation. This also provides flexibility in plasma energy feeding for ignition, fueling or end plugging. If the cross field injection into a mirror is feasible then injection in to Tokamak should become natural. F. 18

Experiments using two plasma guns to inject plasmas from both ends of a B_Z field have been performed (Ref. 3). The stagnation of the plasma inside the field has produced high enough Beta to push

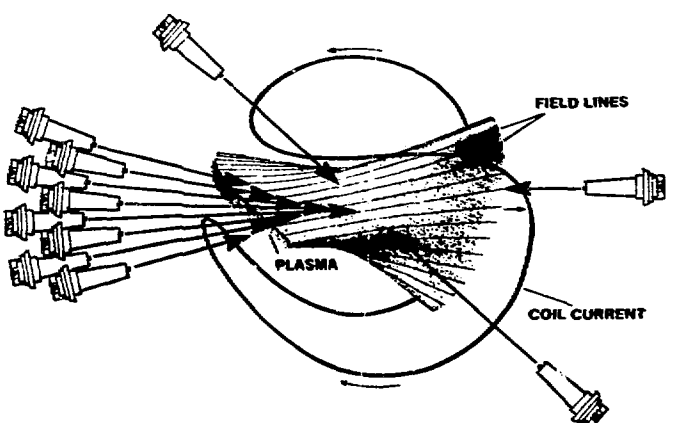

F. 17

magnetic flux away.

Finally, the focussed plasma beam has such a high power density, that if it is a heavy ion plasma and the plasma energy can be scaled to over 1.0 MeV then injecting a number of plasma beams on to a deuterium pellet can be a more effective pusher than laser beam or heavy ion beam (which is low density, high energy [Bev].) pellet fusion schemes. (Ref. 4).

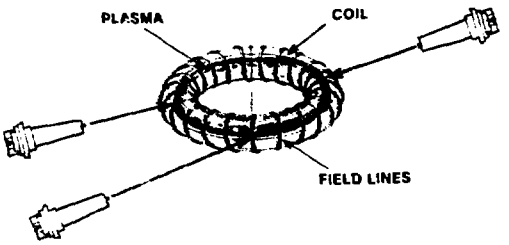

F.18

REFERENCES

1. Dah Yu Cheng, "Plasma Deflagration and the Properties of A Coaxial Plasma Deflagration Gun", NUCLEAR FUSION, Vol. 10, No. 3, 1970, pp. 305-317.

2. K.I. Shchelkin and Ya. K. Troshin, "Gas Dynamics of Combustion", NASA TECHNICAL TRANSLATION, Nasa TT F-231, 1963.

3. Dah Yu Cheng, "The Application of A Deflagration Gun to Fusion System", PROCEEDINGS OF THE HIGH BETA WORKSHOP, Los Alamos, 1975, pp. 680-700.

4. R. Arnold and R. Martin, "Ion Beam Pellet Fusion As CTR Neutron Test Source", Presented at the International Conference on Radiation Test Facilities for CTR Surface and Materials Program, Argonne National Laboratory, July, 1975; J.W. Shearer, "Ion Beam Compression of Thermonuclear Pellets", NUCLEAR FUSION, Vol. 15, 1975, pp. 952-955.

SUMMARY OF FUELING BY PLASMA GUNS

J. Norem
Argonne National Laboratory
Argonne, Illinois 60439

A number of different problems, applications, and technical features of plasma guns were discussed at the conference. These guns have many attractive features such as their simplicity, high particle fluxes (10^{21}/shot), efficiency (90% of input power can be deposited in calorimeters) and their flexibility. The primary problems of these devices, in the context of plasma fueling, seem to be their impurity content and uncertainty regarding their ability to penetrate large plasmas. Existing measurements seem to suggest that impurities are not a serious problem of the gun if operated carefully. The bremsstrahlung spectra from gun plasmas seem to overwhelm impurity line radiation. The plasma that is produced by these guns has been shown to be able to move across a magnetic field and into plasmas. There is very little data on the use of guns with tokamaks; and impurities and penetration problems require considerable study before the problems are fully understood. There seemed to be a general agreement that more experimentation should be done. Theoretical problems, such as the exact mechanisms of penetration were also raised. The effects of such things as the Rayleigh-Taylor instabilities on the plasma stream and the induced oscillations in the target plasma are largely unknown.

The use of plasma guns for preionization of existing machines was also discussed. Injected plasma in a magnetic field moves by polarizing itself such that the electric field created produces the initial drift velocity, $V = E/B$. If two guns are used, it should be possible to stop the plasma in the center of a vacuum chamber in a number of ways. Even if the impurity levels were not negligible in the plasma streams, the trapped plasma could be diluted by adding more neutral gas. Possible geometries for preionization are shown in Figure 1.

Generally the main problem with plasma guns seems to be that the ionization and propulsion fields are the same; thus it is not possible to control separately the content of the plasma and its subsequent motion. If plasmas can be created and moved by different fields, it might be possible to obtain clean plasmas and to direct them towards, and inside of, tokamak plasmas. The simplest example of this would be the creation of a second tokamak discharge alongside an initial discharge. If the currents in these discharges were parallel, they would attract each other and fueling is, in principle, possible. These systems are generally not considered "plasma guns".

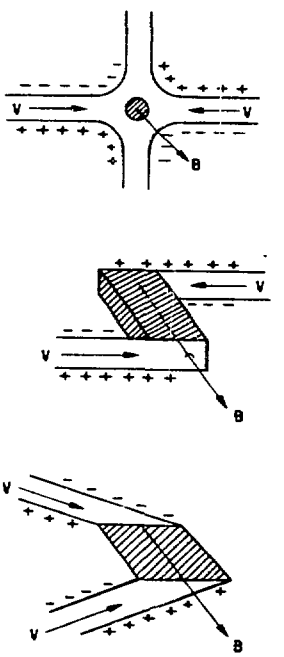

Fig. 1. Possible methods of trapping plasma from plasma guns in a magnetic field.

CLUSTER BEAM INJECTION

F. Bottiglioni, J. Coutant, M. Fois.

ASSOCIATION EURATOM-CEA SUR LA FUSION
Département de Physique du Plasma et de la Fusion Contrôlée
Centre d'Etudes Nucléaires
Boîte Postale n° 6 - 92260 FONTENAY-AUX-ROSES (FRANCE)

Abstract

Areas of possible applications of cluster injection are discussed. The deposition inside the plasma of molecules, issued from the dissociation of the injected clusters, has been computed. Some empirical scaling laws for the penetration are given.

I). Experimental and theoretical research on hydrogen cluster beams, aimed to plasma applications, has been developed in Karlsruhe, Culham, Oak Ridge, Tokyo and Fontenay-aux-Roses. High energy injectors and injection lines are operating or in progress at Karlsruhe, Fontenay and Tokyo. The main components of an injection line, described in paper [1], are :

a/ the cluster source, where intense clustered beams (10 ÷1000 Ae with cluster atomic mass number A ≈10^3÷10^8 a.m.u.) are formed by expanding H_2 in a nozzle cooled at 20÷40°K.

b/ the cluster ionizer, where clusters are ionized and their mass adjusted to the injection requirements (A ≈50÷500 a.m.u.).

c/ the accelerating tube, generally single gap to minimize the risk of neutralizing clusters on residual gas during acceleration.

d/ the drift tube connected to the magnetic trap containing the plasma.

We remind that all units are expressed in the MKS system excepted mass flux (in equivalent Amperes - 1Ae≈6$10^{18}$ $\frac{\text{atoms}}{\text{s}}$) and energies (in eV).

The very low specific charge of cluster ions, by reducing the space charge spread and increasing the larmor radius, allows the injection of charged beams, at least in the toroidal traps of the present generation. The spread of cluster masses is converted after acceleration into a velocity distribution, therefore making plasmas produced or heated by cluster ion beams, less susceptibles of kinetic instabilities in comparison with the injection of monoenergetic atoms.

Some figures of cluster ion beams are listed below in Table I.

It appears that cluster ion beams can be considered, at least for the lines in progress at present *, as atomic sources of high intensity with energy per atom not exceeding 10 KeV. Therefore cluster injection may fit well to build up hot plasmas, to make up for particle losses from plasma and to heat directly ions. Among other applications, cluster beams at about 3 KeV/atom have been proposed to produce negative ions. [2]

* At Fontenay-aux-Roses (F)
* At Karlsruhe (DBR).

Areas of possible applications of fast atoms, cluster ion beams, pellets as well as the requirements to refuel (at the plasma temperature) several toroidal traps and reactors, are shown in FIG.1.

Clusters and pellets have the same crystalline properties. The difference in their sizes leads to different behaviours when interacting with a plasma. We call "clusters" the aggregates with A less than 10^6a.m.u., i.e. less than 400 Å in diameter, and pellets those with A greater than 10^9a.m.u., then with diameters greater than 5000 Å ; these limits corresponding respectively to transparency and opacity to the impinging energy.[3] Main properties of H_2 crystals are listed below in table II.

II). The fastest process undergone by clusters in a plasma is the break up caused mainly by ionizing collisions with electrons, ions and atoms. Clusters split up since they cannot hold more than one charge, when their mass is less than a few thousand of atoms. By transferring momentum to crystal lattice, non ionizing collisions with atoms and ions yield neutral fragments at a rate estimated at 10÷20% of the total fragment production in a plasma. Evaporation has been evaluated to proceed at a slower rate than breakage.[3] The main cross section used to compute the m.f.p. of fragmentation

$$\lambda_b = \frac{V_c}{\sigma_{eN} V_e n_e + \sum_K \sigma_{KN} n_K V_{rK}} \qquad (1)$$

are discussed in paper[1] and summarized in table III. Here V_e, V_r, V_c are respectively the plasma electron velocity, the cluster relative velocity with ions or atoms, the cluster velocity. In FIG. 2 are shown λ_b and λ_{ev}, the m.f.p. of evaporation.

Charged clusters can be neutralized by colliding with gas molecules. The cluster ion neutralization has been measured for H_2 clusters with 10^2÷10^3 atoms and energy Eo up to 10^4eV/atom. An efficiency η_n of the cluster conversion from the charged to the neutral state of about 90 % has been found for an H_2 target thickness one order of magnitude less than that required to neutralize protons with the same energy.[5] The value of a cluster neutralization cross section $\sigma_n \simeq 0{,}3\ S_c$ can be inferred from same other experimental observations.[6] So far, these experimental figures for σ_n are not explained as well as those for cluster ionisation are.[1] Nevertheless, since it is likely the break up by momentum transfer to be the dominant process, together with a very asymmetric fragmentation[6], an high efficiency of neutralization could be expected to keep up in the range of energy Eo=10÷100 $\frac{\text{KeV}}{\text{a.m.u.}}$ even if the cluster reionisation by collisions with molecules must be taken into account.

III). The efficiency of a cluster injection line should therefore be better than that of fast atoms, even when the cluster neutralization is required. This is the case if clusters reach the plasma by having turned considerably, i.e. more than 10°. Actually neutralization is necessary if the distance between the inner of the coils and the plasma edge exceeds 15÷30cm. For low energy injection (Eo≈a few $\frac{KeV}{a.m.u.}$) the losses into local mirrors are not important because of the rapid scattering of the injected particles, which in addition are not deposited on the outer shells of plasmas with $\bar{n} \leq 3 \div 5\ 10^{19} m^{-3}$. The angle of injection is therefore less critical than for fast atoms beams. In table IV are listed some comparative figures of merit for cluster ion and fast atom injection lines. It must be pointed out that fast atom figures have a wide experimental evidence, which is still lacking for the cluster ion injection lines.

IV). The penetration of clusters into a plasma depends strongly on their dissociation hystory. With a magnetic field it can be said that the penetration of charged clusters is determined for large A by the dissociation m.f.p. λ_b and for small A by the magnetic field (see FIG.2). The complete dissociation hystory could be determined if at each collision the mass of the two fragments were known. Some experimental observations indicate a very asymmetric dissociation.[6] FIG.3 sketches some hystograms of the H_2, issued from the dissociation of clusters. Parameters are indicated on the figure. The trajectory of each fragment is followed by a triple MonteCarlo integration The three random variables are the effective path travelled by the cluster between two collisions, the probability of a neutral fragment production and the fragmentation parameter f, ratio of the mass of the lighter fragment to the parent cluster one. The mass of the second fragment is the complement of the first fragment mass. The production rate of H_2 along the plasma radius, deduced from these hystograms, can generally be approximated (if A≥80÷100amu) by the distribution function

$$\frac{dH_2}{dx} \simeq f_{H_2}(x) \simeq C\beta^2 x \exp\left[\frac{-(\beta x)^{\alpha}}{\alpha}\right] \qquad (2)$$

where x is the radial distance from the injection point ; C is normalisation factor, and α is about 1,8÷2. For plasma density constant, β is related to the plasma parameter by the relationships :

$$\beta \simeq 5.8\ 10^{-8} \left(\frac{Bn}{Eo}\right)^{0.5} \qquad \left(Eo \leq 50 \frac{KeV}{a.m.u.}\right) \qquad (3)$$

$$\beta \simeq 3.1\ 10^{-7}\ (Bn)^{0.5}\ Eo^{-0.65} \left(Eo > 100 \frac{KeV}{a.m.u.}\right) \qquad (4)$$

The maximum of f_{H_2} occurs at $L_o = \frac{1}{\beta}$.

The limiting value of $f_{H_2}(x)$ for B=0 is approximated by the distribution fonction :

$f_{H_2}(x) \propto \beta^2 x \exp(-\beta x)$, with $\beta \simeq \frac{1}{\lambda_o}$ and λ_o, the m.f.p. of the cluster atoms. The density of molecules deposited by injecting a cluster beam with intensity ϕ is :

$$n(\gamma) \simeq \frac{\phi}{2\pi a(1-\gamma)} f_{H_2}(\gamma) = \frac{C\phi}{2\pi a^2} \frac{K^2}{1-\gamma} \exp\left(-\frac{K^2\gamma^2}{2}\right) \qquad (5)$$

where a is the plasma radius, $\gamma = \frac{x}{a}$ the normalized radial distance from the plasma edge, $K = \beta a = \frac{a}{L_o}$.

FIG.4 shows eq.(5) for cluster and atomic beams for different values of K. It can be seen that cluster beams do not enhance energy and density gradients at the plasma edge. A good compromise for a correct refuelling of the plasma core could be K = 3÷3,5. With K = 4 the center could be refuelled by inward diffusion of the density distribution peaked at γ = 0.3. By putting in evidence λ_o (computed for $10^3 \leq Te \leq 10^4$eV; Ti = 10^4eV if $Eo \geq 10^4 \frac{eV}{a.m.u.}$ or Ti = Eo if $Eo \leq 10^4 \frac{eV}{a.m.u.}$) in eq.(3) and (4), the ratio $\frac{L_o}{\lambda_o}$ can be expressed. Since the e-folding lenght Le of a cluster beam is related to Lo, the ratio $\frac{Le}{\lambda_o}$ can be approximated by the following relationships :

$$\frac{Le}{\lambda_o} \simeq 2.3\ 10^{-10} \left(\frac{n}{B}\right)^{0.5} \qquad Eo \leq 50 \frac{KeV}{a.m.u.}$$

$$\frac{Le}{\lambda_o} \simeq 8.\ 10^{-10} \left(\frac{n}{B}\right)^{0.5} Eo^{-0.15} \qquad Eo > 100 \frac{KeV}{a.m.u.} \qquad (6)$$

which are represented in FIG.5. It appears that Le/λ_o can be greater than unity when the ratio $\frac{n}{B}$ is greater than a critical value E_c which increases with Eo. It can be concluded that cluster injection is particularly interesting in machines with high ratio density over magnetic field. FIG.6 and 7 show the hystograms of H_2 deposition, with $\frac{Eo}{n}$ = cte. The density has been doubled (from 4 to 8 $10^{19} m^{-3}$) so as the energy Eo (from 30 to 60 $\frac{KeV}{a.m.u.}$). It can be shown that Lo, Le and the shape of the $f_{H_2}(x)$ are rather unchanged. However the region with $\frac{Le}{\lambda_o} \gg 1$ can hardly be reached by only increasing the density. As a matter of fact the critical value E_c, increases with Eo, which in turn must be raised to hold the penetration Lo constant. Furthermore energies greater than 100 KeV/a.m.u. are presently out of the reach of cluster beams, because of too high electrostatic potentials necessary to accelerate aggregates with A>50÷100 a.m.u.

In FIG.8 the range of applicability of cluster injection at energies below 30 KeV/a.m.u. is shown. It appears that with K = 3,5÷4 the present energy per atom could be sufficient to refuel and heat plasmas with $Bn \simeq 10^{+20}$ Tm^{-3} and radius up to 1.2 m. The refuelling of this latter plasma (Vol 60 m^3, $\tau_{diffusion}$ = 1÷2s) requires about (1÷2) 10^{21} $\frac{atoms}{s}$. This figure could be realized by a cluster beam with Eo = 30 KeV/a.m.u, A = 100 a.m.u. , I^+ = 1,5÷3A, accelerating voltage V = 3 MV. The power given to the plasma ions would be 4,5÷9 MW, which is in the range of the power necessary to heat the plasma. Therefore by injecting clusters both the refuelling and the heating could be realized. At very low energy per atom (Eo≤200 eV) clusters can be used to create a cold plasma blanket in order to diminish the sputtering from the walls and the influx of impurity into the hot plasma.

V).To refuel a reactor with 2000 MW_{th}, a = 2m, R = 10m, B= 5T, $n = 10^{20} \div 2\ 10^{20} m^{-3}$, $T_e = T_i = 10^4$ eV, $Z_e \geq 4$, burn-up fraction $f_b \simeq 4\%$ about $4\ 10^{22}$ atoms per second are required.

FIG.9 shows the factor G, ratio of the circulating power to the gross output power, versus the energy E of the injected atoms (protons or deuterons) :

$$G = \frac{P_{circulated}}{P_{net} + P_{circulated}} \simeq \frac{1}{\eta_b \eta_1 \frac{f_b}{2} \frac{W_{DT}}{E} + \eta_2} \quad (7)$$

where η_b is the overall efficiency of the injection line, η_1 and η_2 the efficiency of the electric energy recovery respectively from neutrons and charged particles, W_{DT} the energy of fusion reactions ($\simeq$17,5 MeV).
As far as the necessity of directly refuelling the center of the plasma is postulated, neither fast atoms nor cluster are within the reach because G would be higher than unity. Only pellets seem attractive because of their probable shielding from the plasma energy. In this case, the very difficulty deals with the possibility to give pellets velocities of about 10^4 m s^{-1} (corresponding to about 1 eV/deuteron), which are necessary to make pellets get to the center of the plasma. The penetration length can be increased by a large factor by injecting beams vertically in a significant ripple of the magnetic field below the midplane.[7-8].

In this case, the energy per a.m.u. Eo necessary to deposit atoms at a distance L_1 from the plasma edge is :

$$Eo^{5/2} \geq 4{,}3\ 10^{13} \frac{R\ lu\Lambda\ L_1\ Bn\ Z_e}{\xi o\ A_1} \left(\frac{A_1 + A\rho}{A_1 A_\rho}\right)^2 \quad (8)$$

$\xi_o = \frac{\delta B}{B}$ is the ripple ofB in the plane where atoms are trapped in a banana orbit, A_1 and $A\rho$ respectively the mass number of beam and plasma particles. FIG.10 sketches the relationship(8).For the reactor of figure a refuelling with K = 2 would give :
$nLBZe \simeq (0{,}5 \div 1)\ 10^{20} Ze$ which for Ze = 5 becomes: $nLBZe \simeq (2{,}5 \div 5)\ 10^{20}$. The energy per a.m.u. of the injected deuterons is therefore reduced from the range of 200 KeV/a.m.u. down to 50÷70 KeV/a.m.u. (100÷140 KeV/deuteron).

The corresponding value of G is still unacceptable unless an efficient recovery of the charged particles energy in the neutralizer ($\eta_n \geq 0.7$) and in the blanket ($\eta_2 \geq 0.7$) could be provided. If so, the reactor would be refuelled with G≃0,7÷0,85. When considering cluster injection, the scaling down of Eo with A_1 cannot exceed 15% ; otherwise clusters, which are rapidly broken up, would deposit their mass too far away from the center of the plasma. This gain in energy can be expressed approximately as :

$$\frac{\Delta E}{E} \simeq 9\ 10^{6K} \left(\frac{Eo}{nB}\right)^{0.5} \quad (9)$$

In addition, it is expected all the coulomb-type cross sections of clusters (therefore the ionisation cross section) to be rather insensitive to impurities, since the cross section top values are the cluster geometrical cross-section S_c.

The ionisation cross section is, in average, increased by no more than 1,5 when $Z_e \geq 2$. Therefore the parameter $nLBZ_e$ scales from $(2{,}5 \div 5)\ 10^{21}$ down to $(0{,}8 \div 1{,}6)\ 10^{21}$. The energy Eo could be in the range of 30÷35 KeV/a.m.u., that is 60÷70 KeV/deuteron when injecting deuteron clusters into a deuteron plasma. By injecting deuteron cluster into a tritium plasma, the energy becomes 50÷60 KeV/deuteron. If the high neutralization efficiency for clusters is confirmed in this range of energy, the reactor could be refuelled with a circulating power factor G≃0,45÷0,65 by injecting clusters in a ripple of the magnetic field ($\xi o = 10^{-2}$ at 2 = 1m).

Table V below summarizes the values of energy and current necessary to refuel a reactor.

VI).To conclude, in the present size toroidal devices, cluster injection can either make up for particle losses or even increase the plasma density. At the same time, ions can be directly heated. The expected effects of the injection of a beam of 150 KW at 3 KeV/atom in TFR are shown in FIG.11.

The experiments under way aim to prove the feasibility of the method, to determine experimentally the efficiency of cluster injection line and to verify the pysical assumptions used to compute the cluster behaviour in a plasma.

REFERENCES

(1) F. Bottiglioni, J.Coutant, M.Fois - Proc.of 3rd Int.Meeting on "Theoretical and Experimental Aspects of Heating of toroidal Plasmas" - Grenoble-1976 - Vol.II pg 1.

(2) E.W. Becker et al - Nucl.Fusion 17, 3, (1977) 617.

(3) F. Bottiglioni, J.Coutant, M.Fois - Nucl. Fus. 14 (1974) 365

(4) J.R. Hiskes Nucl.Fus. 12 (1972) 423.

(5) O.F. Hagena, W. Henkes, V. Pfeiffer - Proc. of 9th Symposium on Fusion Technology - Garmisch Partenkirchen 1976 - pg. 885.

(6) F. Bottiglioni, J. Coutant, M.Fois - Proc. of 6th Europ. Conf.Controlled Fusion and Plasma Physics. Moscou 1973 - Vol.1 - pg. 381.

(7) R. Deicas, A. Samain - Rapport activité Association EUR-CEA 1975
EUR-CEA-FC-810

(8) D.L. Jassby, K.J. Goldston - Princeton Plasma Phys. Lab. MATT-1206 (1976).

TABLE I - Figures for cluster ion beams

Parameter	Prototypes in progress at present	Short term extrapolations	Possible extrapolation towards high equiv. current	Possible extrapolation towards high accel.voltages
$\bar{A}$	100÷1000 a.m.u.	50÷100 a.m.u.	$5\ 10^2$÷$5\ 10^3$ a.m.u.	50÷100 a.m.u.
f(A)	$A^{5/6}\exp(-2A/\bar{A})$	id	id	id
a	10÷100 A_o	10÷100 A_o	10^3÷10^4 A_o	10÷100 A_o
$\alpha\frac{I}{S}$	400÷2000 $\frac{mA}{cm^2}$	400÷2000 $\frac{mA}{cm^2}$	10÷30 $\frac{Kg}{cm^2}$	400÷2000 $\frac{mA}{cm^2}$
Θ	±1° half angle	id	id	id
I^+	200÷100 mA	200 mA÷1 A	~2 A	200 mA÷1 A
V	0,5÷1 MV	0,5÷1 MV	~1 MV	1÷5 MV
Eo	1÷10 $\frac{KeV}{a.m.u.}$	5÷20 $\frac{KeV}{a.m.u.}$	100÷1000 $\frac{eV}{a.m.u}$	10÷100 $\frac{KeV}{a.m.u}$
P	100÷200 MW	0,1÷1 MW	~2 MW	0,2÷2,5 MW
operation	steady or pulsed	pulsed	pulsed	pulsed

TABLE II - Properties of H_2 crystals.

density	$n_c \simeq 2.2\ 10^{28}$ $\frac{\text{molecules}}{m^3}$ or 73,6 $\frac{Kg}{m^3}$
intermolecular distance	$d_o \simeq 3.6\ 10^{-10}$ m
geometrical cross-section	$S_c \simeq 10^{-19}\ A^{2/3} m^2$
mean diameter	$\bar{D}_c \simeq 2.4\ 10^{-10}\ A^{1/3} m$
intermolecular binding energy	$W_D \simeq 10^{-2}$ eV (Van der Waals forces)
relative dielectric constant	$\epsilon_r \simeq 1.21$

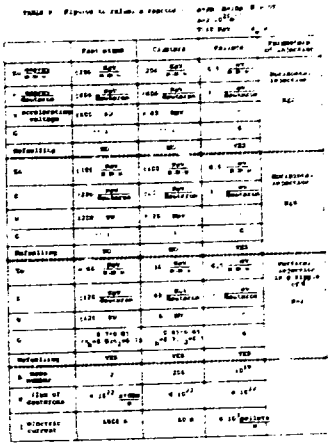

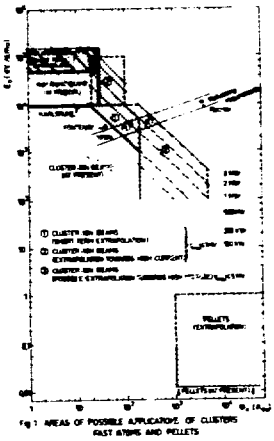

Fig 1 AREAS OF POSSIBLE APPLICATIONS OF CLUSTERS FAST ATOMS AND PELLETS

TABLE III - Cross sections for cluster fragmentation and evaporation.

- ionisation by electrons	$\sigma_{1(eN)} \simeq \sigma_{1(e,1)} A$	As 200 a.m.u.
- ionisation by protons	$\sigma_{2(1N)} \simeq \sigma_{2(1,1)} A$	As 200 a.m.u.
- charge exch leading to cluster ionisation	$\sigma_{3(exN)} \simeq \sigma_{3(ex1)} A$	As 20 30 a.m.u.
- break up by momentum transfer	$\sigma_{4(bN)} \simeq \sigma_{4(b1)} A$	As 10 20 a.m.u.
- evaporation	$\sigma_{5(eVN)} \simeq \sigma_{5(ev1)} A^{0,6}$	(3)

- when the linear dependence on A fails, σ_N varies as $A^{2/3}$.
- $\sigma_{1(e,1)}$; $\sigma_{2(i,1)}$; $\sigma_{3(ex,1)}$ are respectively the cross section of ionisation by electrons, ionisation by protons, charge exchange on protons of cluster atoms.
- $\sigma_{4(b,1)} \simeq 2\ 10^{-20} m^2$ (4).

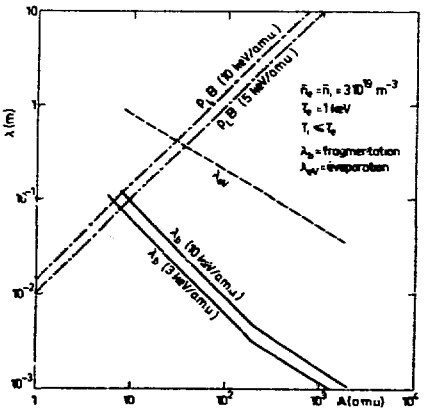

Fig 2 CLUSTER MEAN FREE PATHS OF FRAGMENTATION (λ_b), EVAPORATION (λ_{ev}) AND LARMOR RADIUS (ρ_L)

TABLE IV - Comparative figures for cluster and fast atoms injection lines.

Parameter	Cluster ions	Fast atoms
Gas efficiency	(Ioniser)$\eta_g = \frac{N^+}{N} \geq 70\%$	$\eta_g = \frac{N^+}{N} \simeq 50\%$
Energy efficiency at acceleration stage (secondary electrons suppressed)	$\eta_a \leq 90\%$	$\eta_a \leq 90\%$
Neutralisation efficiency	$\eta_n \simeq 100\%$ if neutralisation necessary : $70\% \leq \eta_n \leq 90\%$ 100 $\frac{KeV}{a.m.u}$ ≥ Eo≥ a few $\frac{KeV}{a.m.u}$	$60\% \leq \eta_n \leq 90\%$ 40 $\frac{KeV}{a.m.u}$ ≥ Eo≥ a few $\frac{KeV}{a.m.u}$
Energy efficiency of the beam transfert	$\eta_t \leq 90\%$	$\eta_t \leq 90\%$
Capture in the plasma. Vertical drift losses F_D	Depending on plasma parameters. Rather insensitive to injection angle(Eo≥10 KeV/a.m.u) $0° \leq \alpha \leq 10°$ $10\% \leq f_D \leq 25\%$	Avoid normal injection $5° \leq \alpha \leq 10°$ $25\% \leq f_D \leq 50\%$

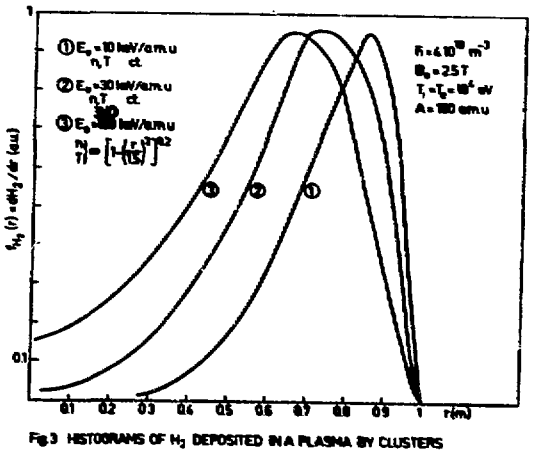

Fig 3 HISTOGRAMS OF H_2 DEPOSITED IN A PLASMA BY CLUSTERS

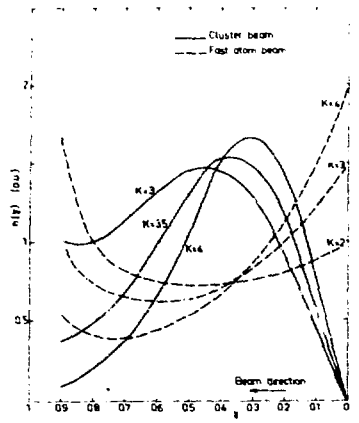

Fig 4 H_2 DENSITY YIELDED BY CLUSTER INJECTION

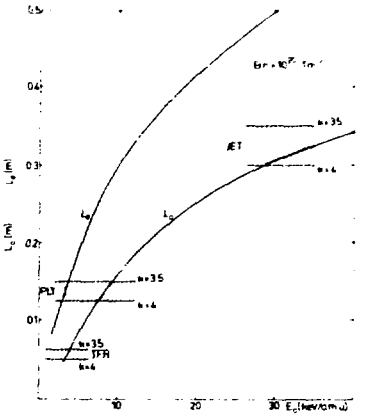

Fig 8 CLUSTER PENETRATION (L_p) VS CLUSTER ENERGY PER AMU (E_o)

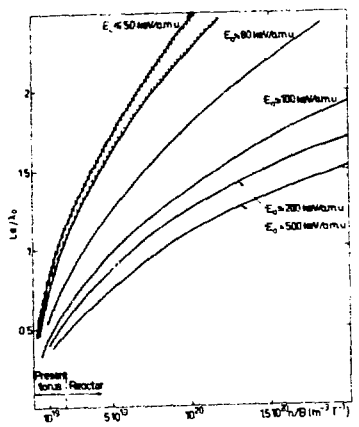

Fig 5 RATIO L_p/λ_o VS n/B

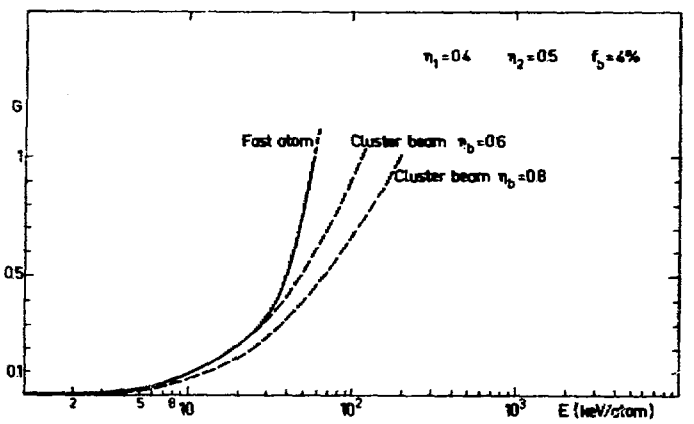

Fig 9 CIRCULATING POWER FACTOR (G) VS CLUSTER ENERGY PER ATOM (E)

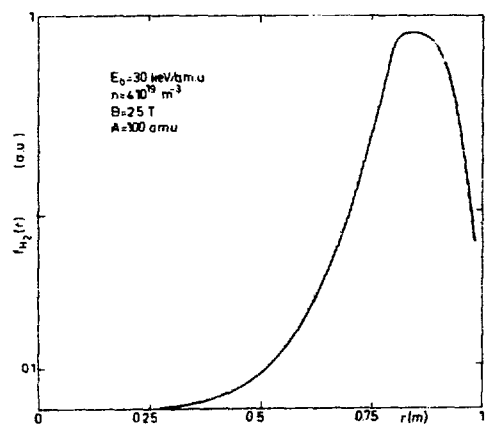

Fig 6 HISTOGRAM OF H_2 DEPOSITED IN A PLASMA BY CLUSTERS

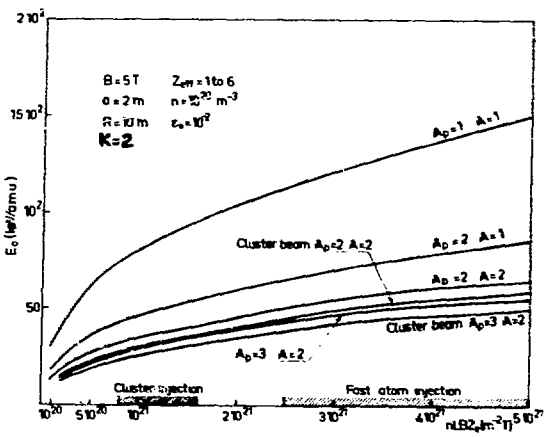

Fig 10 ENERGY PER A.M.U (E_o) VS $nLBZ_e$ FOR INJECTION IN A RIPPLE OF B

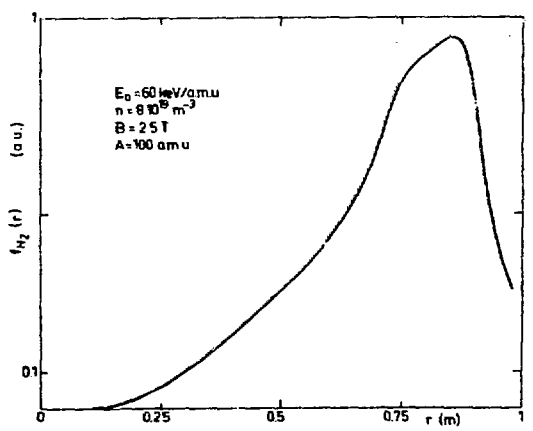

Fig. 7. HISTOGRAM OF H_2 DEPOSITED IN A PLASMA BY CLUSTERS

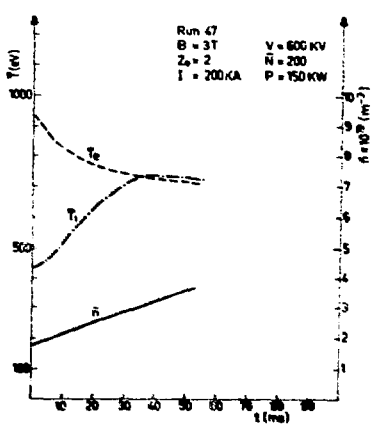

Fig 11 COMPUTED EVOLUTION OF $\bar{T}$, $\bar{T}_e$, $\bar{n}$ FOR CLUSTER INJECTION INTO TFR

REACTOR REFUELING BY USING CLUSTER IONS

S.H.BE, K.OKAMOTO, H.ENJOJI, K.YANO
RIKAGAKU KENKYUSHO
(The Institute of Physical and Chemical Research)
Wako-shi, Saitama,351 JAPAN

Summary. We propose to use a neutral deuterium beam produced from the negative ion source using cluster ions for refueling into TCT material test reactor. After estimating necessary plasma parameters and geometry dimensions of the reactor, we dicuss the feasibility of using the high energy deuterium beam produced from the negative ion source using cluster ions for refueling

1. Introduction

Injection of cluster ion beam into a steady state plasma is considered to be one of possible methods for heating and/or for refueling that plasma.Actually cluster ion accelerators intented for use in heating and refueling experiments with toroidal devices are presently under construction in the Federal Republic of Germany[1] and France[2].We also have been studying fundamental aspects[3] of cluster ion source.On particular we are interested in the interaction between cluster ions and electrons or other particles to understand the break up mechanism of the cluster ions.

According to the calculations of Bottiglioni et al[4], the penetration distance of a cluster of 100 atoms/cluster accelerated up to 1 MV (10 keV/atom) into a plasma of $n=1\times10^{14}$ cm^{-3} is about 30 cm. With such a short penetration distance the cluster ions can not be used for refueling. Furthermore, at 10 keV/atom, charge exchange is an important loss mechanism for ions.

We propose to use the high energetic neutral beam produced from negative ion source[5] using cluster ions for refueling into TCT material test reactor taken up here as a model reactor. After estimating necessary plasma parameters and geometry dimensions of the reactor, we discuss the feasibility of using the high energy atomic beam produced from negative ion source using cluster ions for refueling. However the refueling of the tritium must be supplied by other source such as pellets.

2. Plasma Parameters and Geometry Dimensions

The data and equations with which we need to estimate plasma parameters of the reactor and geometry dimensions are mainly quoted from the review paper by Jassby[6].

2.1 Beam injection energy

In the case of the neutral beam injection into reactor, the neutrals must penetrate adequately before ionization, whereas all the energetic particles must be trapped in the plasma. For a trapping length $\lambda_t \simeq (1/4)a_p$, the neutral beam energy W_{inj} to satisfy these requirements is determined by

$$W_{inj} \simeq 4.5\times10^{-15} n_{ec} a_p Z_{eff} \qquad (1)^6$$

where a_p is plasma radius, n_{ec} electron density at the center and Z_{eff} effective charge of impurity ions. If Z_{eff} and $n_{ec}a_p$ are chosen to be 3 and 1.5×10^{16} cm^{-2} respectively, the injection energy of 200 keV is obtained from eq.(1). For the parabolic profile of the electron density, the electron mean density $\bar{n}_e$ is $n_{ec}/2$, so that $\bar{n}_e=9.4\times10^{13}$ cm^{-3} by giving $a_p=0.8$ m.

2.2 Fusion power density

The relation between fusion power density P_f and wall loading P_w is given by

$$\pi a_p^2 P_f = 2\pi a_w P_w \qquad (2)$$

where a_w is wall radius. If a_w and P_w are chosen to be 1.1 m and 1 MW/m^2 respectively, $P_f=3.4$ MW/m^3 from eq.(2).

2.3 Hot-ion density and τ_p/τ_s

Fusion power density P_f is defined by

$$P_f = n_d n_t \langle\sigma v\rangle_{th} E_f + n_h n_t \langle\sigma v\rangle_h E_f \qquad (3)$$

where $\langle\sigma v\rangle_h$ and $\langle\sigma v\rangle_{th}$ are fusion reactivities of TCT (D-T) and thermonuclear plasma respectively, n_h is hot-ion density and $E_f = 17.6$ MeV. If we assume T_e, W_{inj} that $n_d + n_h/n_e = 0.4$ and $n_t/n_e = 0.6$, then $n_h = 1.8\times10^{13}$ cm^{-3} and $n_d = 2\times10^{13}$ cm^{-3} as $\langle\sigma v\rangle_h$ and $\langle\sigma v\rangle_{th}$ are 1.1×10^{-15} and 0.1×10^{-15} cm^3/sec respectively, from Fig. 1. For $T_e = 10$ keV, $W_{inj} = 200$ keV. Since a beam injection power density $P_{inj} = n_d/\tau_p \times W_{inj} = n_h/\tau_s W_{inj}$, $\tau_p/\tau_s = n_d/n_h$ and its value is 1.1, where τ_p and τ_s are the particle confinement and the thermalization time of injected high energy respectively.

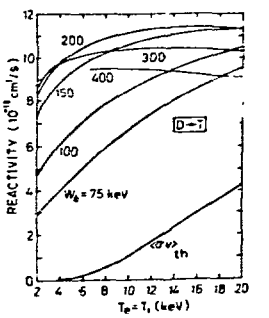

Fig.1 Fusion reactivities in D-T for TCT and thermonuclear plasmas.

(From Ref, 6)

2.4 Energy confinement time

Power balance is represented as follows :

$$\frac{3n_e T_e}{\tau_E} = P_{inj} + P_\alpha \qquad (4)$$

where τ_E is the energy confinement time (we have assumed $T_e=T_i$), and P_α is the power deposition of charged fusion-reaction products. The radiation loss power density P_r is much smaller than the other power density, so that P_r is neglected in this case.For $P_\alpha = 0.2F_\alpha Q \times P_{inj}$, where $Q=P_f/P_{inj}$ is the fusion power multiplication factor and F_α is the fraction of fusion-alpha energy deposited in the plasma (we have assumed $F_\alpha = 1$), eq.(4) becomes

$$\frac{3n_e T_e}{\tau_E} = \frac{n_h}{\tau_s} W_{inj} + 0.2P_f \qquad (5)$$

For $T_e=10$ keV and $W_{inj}=200$ keV, τ_E becomes 142 msec from Eq. (5) as the ratio of τ_s to τ_E is 1.62 from Fig. 2.

Furthermore, Q is 1.4.

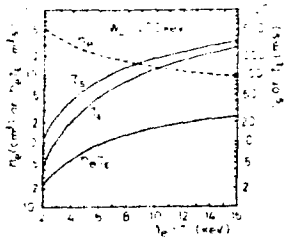

Fig.2 values of n_e, τ_s and τ_E for maximum P_f

(From Ref, 6)

2.5 Injection beam current and power

The injection particle rate per unit volume $P_{inj}/W_{inj} = n_h/\tau_s = n_d/\tau_p = n_a/\tau_p = 7.8\times10^{13}$ cm^{-3} sec^{-1}. For the plasma volume $V_p = 4.7\times10^7$ cm^3, the total injection current and power are 560 A and 112 MW, respectively.

The process of calculations for obtaining the plasma parameters and obtained parameters are summarized in Tables I and II.

TABLE I PROCESSES OF CALCULATION FOR OBTAINING PLASMA PARAMETERS

Equations	Given values	Obtained values	Assumptions
$W_h \approx 4.5\times10^{-5} n_{ec} a_p Z_{eff}$	$n_{ec} a_p = 1.5\times10^{15} cm^2$, $Z_{eff} = 3$	$W_h = 200$ keV	
$n_{ec} a_p = 1.5\times10^{15} cm^2$	$a_p = 0.8$ m	$\bar{n}_e = 9.4\times10^{13} cm^3$	$\bar{n}_e = \frac{n_{ec}}{2}$
$\pi a_p^2 P_f = 2\pi a_w P_w$	$a_w = 1.1$ m, $P_w = 1$ MW/m²	$P_f = 3.4$ MW/m³	
$P_f = n_D n_T \langle\sigma v\rangle_{DT} E_f + n_h n_T \langle\sigma v\rangle_{hT} E_f$	$\bar{T}_e = 10$ keV	$n_h = 1.8\times10^{13} cm^3$, $n_D = 2\times10^{13} cm^3$	$\frac{n_T}{n_e} = 0.6$, $\frac{n_h + n_T}{n_e} = 0.4$
$P_{inj} = \frac{n_p}{\tau_p} W_{inj} = \frac{n_h}{\tau_s} W_{inj}$		$\frac{\tau_p}{\tau_s} = 11$	
$\frac{3 n_e T_e}{\tau_E} = P_{inj} + P_\alpha = \frac{n_p}{\tau_p} W_{inj} + 0.2 P_f$		$\tau_E = 142$ msec	
$Q = \frac{P_f}{P_{inj}}$		14	
$I_{inj} = \frac{P_{inj}}{W_{inj}} V_p = \frac{n_p}{\tau_p} V_p$	$V_p = 4.3\ m^3$	560 A	

3. Neutral Beam Injector System

Total beam current of 560 A and the injection power of 112 MW are required for the proposed material test reactor. The neutral beam may be supplied by 4 injector each giving 140 A and 28 Mw. The system of the injector module is shown in Fig.3. It consists of the cluster ion source, the negative ion source and the neutralizer for converting of D^- ions into D atoms.

A cluster is a condensed aggregation of molecules held together by the van der Waals forces. A cluster beam is obtained by expansion of gas under moderate stagnation conditions through a nozzle into vacuum.

The cluster beam of mean constituent atoms (D) of 5×10^3 has been obtained under the conditions that stagnation pressure and temperature are 4.5 atm and 110 K respectively, using throat diameter of 0.14 mm (Fig.4)[7].

TABLE II. PLASMA PARAMETERS AND GEOMETRY DIMENSIONS

Major radius	R_0	3.4	m
Plasma radius	a_p	0.8	m
Wall radius	a_w	1.1	m
Plasma volume	V_p	43	m^3
Effective Z of impurity ions	$Z_{eff}(M_0)$	3	
Impurity fraction	α	1.3×10^{-3}	
	$\bar{n}_e\tau_E$	1.3×10^{13}	cm^3sec
Energy confinement time	τ_E	142	m sec
Electron mean density	$\bar{n}_e$	9.4×10^{13}	cm^{-3}
Electron mean Temperature	$\bar{T}_e$	10	keV
Injection energy	W_{inj}	200	kev(D°)
Injection current	I_{inj}	560	A
Injection power	P_{inj}	112	MW
Power Production			
Fusion power multiplication factor	Q	1.4	
Fusion power density	P_f	3.4	MW/m^3
Wall loding	P_w	1	MW/m^2

If a slit throat of $0.14^{mm}\times7.8^{mm}$ is used, 2,800 A equivalent current of 5×10^3 atoms/cluster may be obtained. The reason why we choose the cluster equivalent current of 2,800 A will be cleared later on. The portion of cluster beam amounts to about 5 % of the nozzle mass flow. Therefore about 20 times of the mass flow must be disposed of by cryopump and it corresponds to 5.6×10^3 Torrl/sec. The rate of the liquid helium consumption is 400 l/hr

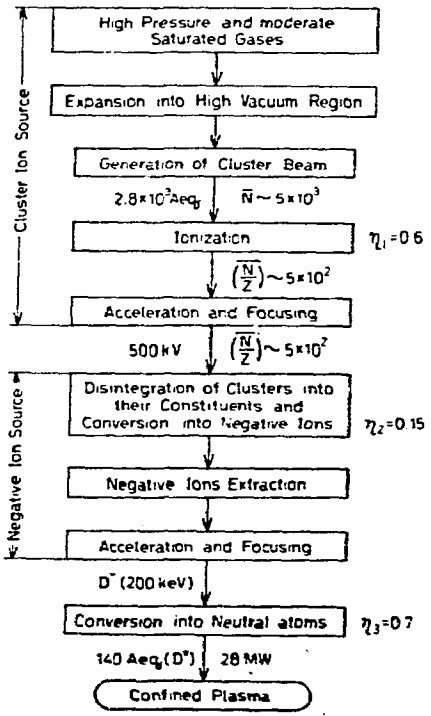

Fig.3. Neutral beam injector system

The cluster can be multitudinously ionized by electron impact and the cluster mean size can be controlled by the stagnation conditions and the nozzle geometry, so that the mean value of $\overline{N/Z}$ of about 5×10^2 may be obtained, where N and Z are the number of constituent atoms and the electric charge respectively. The ionization efficiency of the ionizer is chosen to be 60 %. One experimental result[8] of tailoring of $\overline{N/Z}$ is shown in Fig.5. The figure shows that the clusters of

$\sim 10^5$ molecules are tailored into $\overline{N/Z}$ $\sim 10^4$ with the efficiency of about 60%. The experimental results[9] at Karlsruhe also show that the original clusters of about 4×10^4 atoms are tailored into $\overline{N/Z} \sim 5 \times 10^2$ with the ionization efficiency of about 70 %. In either case it shows that original clusters may be tailored into small one by one order of magnitude.

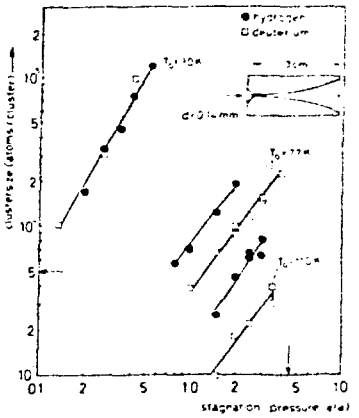

Fig.4 Cluster size as a function of stagnation pressure for three different nozzle temperatures in the case of H_2 and D_2. The used nozzle is also plotted in this figure.

(From Ref, 7)

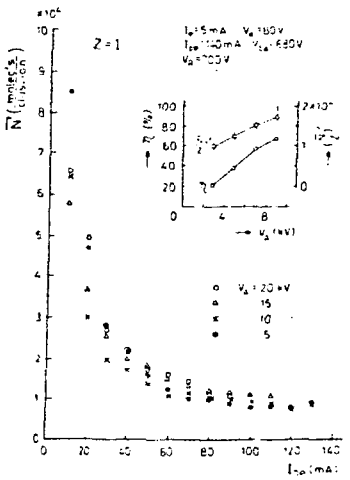

Fig. 5

To obtain mean energy of about 1 keV per constituent atoms, cluster ions of about 5×10^2 must be accelerated up to 500 kV because the equilibrium fraction[10] of cesium vapor as a function of proton energy has maximum values at about 1 keV (Fig. 6). A conversion of cluster ion beam into negative atomic ion beam has been described in detail by Becker et al[5]. Henkes[11] has calculated an efficiency for conversion of cluster ions into negative ions and obtained that of 28 % for clusters of the mean size of 10^3 atoms/cluster accelerated by 1 MV, but we assume the efficiency is 15 %.

We assume the neutralization efficiency for the conversion of D^- at 200 keV into D is 70 %, which corresponds to the lowest value of the range of values estimated by Sweetman et al[12] (Fig.7) and the other overall efficiency of this injector except those stated above 80 %. Thus the total beam efficiency of one module injector becomes 5 % and the cluster equivalent current required to obtain 140 A is 2,800 A.

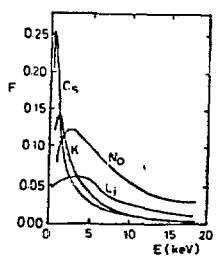

Fig 6 Negative hydrogen component of the total equilibrated beam in alkali metals as a function of proton energy

(From Ref, 10)

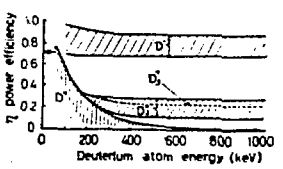

Fig 7 Efficiency versus neutral beam energy for neutralization of D^-, D_2^-, D_3^- and O^- on hydrogen.

(From Ref, 12)

4. Conclusions

We proposed to use the high energetic neutral beam produced from the negative ion source using cluster ions for refueling into the TCT material test reactor.

After estimating plasma parameters and geometry dimensions of the reactor, we also discussed the feasibility of using the beam for refueling. We are not sure at present time that the requirements in the Fig.3 may be fulfilled by techniques of present day. However those would be satisfied by the further development of techniques at present. The problems relating to : (a) the cluster beam generation by the slitshaped nozzle, and the gas efficiency, (b) the flux intensity with a moderate cluster size, (c) the ionization efficiency for extracting the cluster ions with $\overline{N/Z}$ required, (d) the dissociation of D_2 into D and the conversion efficiency of D into D^-, (e) the extraction efficiency of D^- ions and the spreading of D^- ion beam, and (f) the structure of alkali vapor cell should be investigated further hereafter.

Acknowledgements

We wish to thank Mr K. Okazaki for helpful discussions. We also thank the members of our laboratory for valuable discussions and suggestions. The assistance of Mr T.Usuda in preparation of this manuscript is gratefully acknowledged.

References

1. E.W.Becker,H.Falter,O.F.Hagena,W.Henkes,R. Klingelhofer,K.Korting,F.Mikosch,H.Moser,W. Obert, and J.Wust : KFK 2016 (Inst.Kernverfahrenstechnik Karlsruhe 1976).
2. F.Bottiglioni,J.Coutant and M.Fois : EUR-CEA-FC-884 (Assoc.EUratom-CEA 1974)P.127.
3. H.Enjoji,S.H.Be,K.Yano and K.Okamoto : Proc. 9th Symp. on Fusion Tech. (Pergamon Press Oxford and N.Y 1976) P.891.
4. F.Bottiglioni,J.Coutant and M.Fois : Nuclear Fusion 14 (1974) 365
5. E.W.Becker,H.Falter,O.F.Hagena,W.Henkes,R. Klingelhofer,H.O.Moser,W.Obert and I.Poth : Nuclear Fusion 173 (1977) 617.
6. D.L.Jassby : Nuclear Fusion 172 (1977) 307.
7. W.Obert : 10th rarefied gas dynamic Conf. in Snowmass/USA, July (1976).
8. H.Enjoji,S.H.Be,K.Yano and K.Okamoto : contributed for publication in J.J.A.P.
9. W.Henkes,V.Hoffman and F.Mikosch : Rev. Sci. Instrum. 48 (1977) 675.
10. O.B.Morgan :Pro. 2nd Sym. on Ion Source and Formation of Ion Source, Berkely 1974 (Lawrence Berkely Lab.) P.V.I-1-1.
11. W.Henkes : private communication.
12. D.R.Sweetman,A.C.Rivier,H.C.Cole,E.Thomson, D.P.Hammond,J.Hugill,and C.M.McCRacken : Proc. 4th Conf. on Plasma Physics and Controled Nuclear Fusion Research, Madison 1971 IAEA Viena 3 (1971) 393.

SUMMARY OF FUELING BY CLUSTER BEAMS

G. Schilling
Princeton Plasma Physics Laboratory
Princeton, N. J. 08540

The authors of the first paper, "Cluster Beam Injection", Bottiglioni et al., discuss the present status of cluster formation and penetration into a plasma. First, large neutral clusters, 10^3-10^8 a.m.u., are formed as condensates of the expansion of H_2 gas at 20-40° K. These clusters are then fragmented into 50-500 a.m.u. sizes and ionized. Single gap electrostatic acceleration up to 1.2 MV, in present experiments, then gives a beam of many amperes equivalent particle flux at particle energies of 1-10 keV per atom. Neutralization of the cluster beam is possible in gas with 90% efficiency, but is not always required due to the 10^{-2} charge to mass ratio of the cluster ions.

Cluster penetration into a plasma is dominated by ionizing collisions resulting in asymmetric cluster fragmentation. The larger fragment penetrates deeper into the plasma because of its low charge to mass ratio, while the smaller fragment remains trapped near the point of collision and is broken up through further collisions. Calculations based on present knowledge indicate that clusters with energy up to 10 keV per atom will adequately penetrate the plasma of present-day tokamaks. Experiments are being prepared for cluster injection into TFR and ASDEX to study both plasma heating and fueling. Cluster penetration into a large reactor plasma appears inadequate with reasonable technologies, but ripple injection may bring the required energy into the range of 50-70 keV per atom.

The authors of the second paper, "Refueling Into Reactor by Neutral Beam from Negative Ion Source Using Cluster Ions", Be et al., propose to refuel a Two Component Torus materials test reactor with 200 keV neutral deuterium atoms obtained from negative ions. The negative ions are produced from single electron capture by 1 keV deuterium atoms, which, in turn, are the result of the breakup of cluster ions with mass $5 \cdot 10^2$ which have been accelerated to 500 keV. The use of clusters as the source of low energy neutral atoms for electron capture conversion to negative ions avoids the difficulty of producing a low energy positive ion beam with high current density and low divergence. The drawback is the increased technological complexity of cluster production and acceleration to 500 keV.

The resulting 200 keV D° beams will have a total injected particle current of 560 A and total injected power of 112 MW. These particles will heat and refuel the test reactor for a Q of 1.4 although the tritium component must be refueled separately by, for example, pellets.

NEUTRAL BEAMS

Chairman: F. R. Scott
(Electric Power Research Institute, U.S.A.)

BEAM PENETRATION - THEORY AND PREDICTIONS*

James A. Rome
Oak Ridge National Laboratory
Oak Ridge, Tennessee 37830

Summary

A review of the theory of beam penetration and deposition in tokamaks shows that large neutral energies are required to penetrate reactor plasmas. On the other hand, for good efficiency, positive ion sources must operate below ~80 keV (H^+). Thus innovative start-up and heating scenarios are required. Design of an injection system is discussed. Fueling by means of high energy beams appears to be inefficient and may lead to "blow out" or to a lack of central heating.

1. Introduction

Neutral beam injection has proved to be very successful at heating the moderate sized, moderate density tokamaks of today and is now the prime candidate for heating the next generation of tokamaks. It is thus appropriate to consider the conditions under which injection heating can be applied to the larger, denser tokamaks of the future.

Extrapolation into the future is not immediately obvious because the regime of applicability of injection is about to change. There are at least three reasons for this: (1) Beam penetration is becoming increasingly difficult. In machines like ATC, ORMAK, and TFR, even low (20-30 keV) energy beams might not be fully absorbed in the plasma. But, for DIII, TFTR and ALCATOR-C, even 80 keV beams (H) barely get to the center. (2) Injection power is increasing by order of magnitude. So far, injection power has only been up to three times greater than the ohmic heating power. At such a level, significant heating can be observed but no possible deleterious effects of injection have been observed. With proposed levels of injection at about 10 times the ohmic heating power, any limit to injection should be observable. This can be most easily done on smaller machines like ISX-B because the volume is smaller. (3) Injector efficiency decreases with increasing injector energy. In spite of great improvement in source design (particularly with respect to species yield), overall injector efficiency drops drastically as the energy is raised to achieve good beam penetration. At some level, this inefficiency becomes intolerable, at least for reactor applications.

To shed light on some of these issues, we will first briefly review beam deposition theory and then discuss strategies for injection and some implications of high power injection.

2. Beam Deposition in a Tokamak

Energetic neutrals (as opposed to ions) are used for injection in order to penetrate the large toroidal mangetic field of the tokamak. Thus, we must first decide where these fast injected neutrals will become ionized.

There are several ionization processes to consider. At low energies (<30 keV/nucleon), resonant charge exchange with the hydrogen ions is the dominant process. Since this process exchanges a high energy ion for a low energy ion (which can leave the plasma since it becomes a low energy neutral), ions created by charge exchange do not necessarily provide new plasma particles and hence are not a good source of fuel. But, with high power injection at energies below 30 keV, the increase in neutral density may be important and can lead to plasma cooling and increased gas recycling at the walls.

At injection energies over 30 keV/nucleon, ionization by impact on protons (or deutrons) is dominant. Electron impact ionization occurs but is negligible except at very high energies.

Recently, it has been discovered that the injected fast neutrals can charge exchange and/or impact with impurities in the plasma. Since both of these processes seem to go like $Z_j^{1.4}$, they could be dominant in some situations. Adding over all impurity species of density n_j gives an effective enhancement of the proton impact ionization cross-section:

$$\sigma_i \simeq \sigma_{i_{proton}} [n_p + \Sigma_j n_{z_j} Z_j^{1.4}]/n_e \qquad (1)$$

The (non-resonant) charge exchange on impurities cross-section also seems to scale like $Z_j^{1.4}$ but is about five times smaller than the impurity impact cross-section.

Since the injected neutrals go in a straight line, we may treat the beam as being composed of many beamlets each of which traverses the plasma on a different straight line path. Along this path, s, the neutral beam density, N_B, decays by

$$N_B(s) = N_B(0) \exp\left\{ - \int_{-\infty}^{s} K(s') n_e(s') ds' \right\} \qquad (2)$$

where

$$K = \frac{n_i}{n_e} \langle \sigma_{cx} v_{bi} \rangle + \sigma_i V_b [n_p + \Sigma_j n_{z_j} Z_j^{1.4}]/n_e \qquad (3)$$

$N_B(0) I_B$ is the particle source rate of the beamlet of current I_B, v_{bi} is the relative velocity between the beam and the plasma ions, and the averages are over the plasma ion and electron distributions.

Once the fast ions are born, the ions go onto tokamak orbits which are determined by the injection geometry. This process is treated in detail in Ref. 1 for tangential injection.

The point to make here is that the geometrical peaking of the fast injected ion density can occur

*Research sponsored by the Department of Energy under contract with the Union Carbide Corporation.

because the orbit drift surface area can shrink to zero for certain orbits, called "stagnation orbits." This can be easily seen by regarding tokamak orbits as a competition between $\vec{B} \times \nabla B$ are curvature drifts, and motion along field lines. The two drifts are vertical in a low β tokamak. On the equator, there is a poloidal component of $v_{\parallel}$ which is also vertical and of opposite signs on the two sides of the magnetic axis. Thus, there is some radius for which these two velocities precisely cancel and the orbit shrinks to a circle in the equatorial plane centered on the symmetry axis. All other orbits are toroidal shells with finite surface areas.

The result of this shrinking is that neutrals which are ionized near the stagnation point spread over a smaller area and hence the fast ion density is peaked by this geometric effect. The result of many computer calculations shows that this allows the fast ion density to be centrally peaked (instead of decaying exponentially) for a/λ_0, the ratio of minor radius to mean-free path in the center of the plasma, up to 4.

Figure 1 was developed by H. C. Howe and shows the plasma opacity ($n_e(0)a$) versus energy/nucleon for for various values of Z_{eff} under the condition that $a/\lambda_0 = 4$, for a parabolic dnesity profile and tangential injection. Basically, this graph gives an ideal of how much injection energy is needed for a given plasma.

Perpendicular injection can slightly enhance penetration since the path length to the center of the plasma is shorter. On the other hand, perpendicularly injected particles cannot have stagnation orbits and hence do not benefit as much from the geometric peaking (they can however have very small orbits). Also perpendicularly injected particles can get trapped in the ripples in the toroidal field caused by the descreteness of the coils and drift vertically out of the machine. Thus, practically, if perpendicular injection is used, the injectors are tilted about 12° from the true perpendicular so as to avoid this trapping region.

However, the preceeding "back of the envelope" treatment of injection deposition must be revised for several reasons. The $a/\lambda_0 = 4$ criterion is insufficient to assure centrally peaked plasma heating. To do this requires that the deposition profile be more peaked than the plasma density profile. It is becoming increasingly apparent that the highest values of β can be achieved in elongated cross-section plasmas; at high β values, the flux surfaces also become non-concentric. Finally, with long beam lines becoming common, the beam divergence, focusing and cross-section must be taken into account.

For these reasons, D. Post of PPPL developed a new Monte-Carlo beam deposition code which correctly treats the injector geometry. This code was then modified by R. H. Fowler of ORNL to use numerically generated solutions of the MHD equilibrium equation to correctly treat the plasma geometry. Finally, this code is being coupled into the 1½ D transport code of J. T. Hogan which recomputes the plasma equilibrium during the simulation.

3. Injection Strategies

Given that you wish to heat a large, dense tokamak with beams, a quick look at Fig. 1 is very discouraging. For example, typical TNS parameters of $n_e(0) = 1 \times 10^{14}$, $a = 1.25$ m yield a marginal penetration energy of 80 keV (H) for $Z_{eff} = 1.5$. Raising the density or Z_{eff} makes penetration impossible for reasonable injection energies. Once the required injection energy goes above 80 keV (H), more complicated injection scenarios must be used.

One example of this is a low density start-up scenario such as proposed for the ORNL TNS.[2] At low densities, beam penetration is no problem; and the central density must then be increased with, say, pellet injection while heating is continued. As β increases, the magnetic axis shifts outward and fusion reactions begin to occur in the central region. A combination of this α-particle heating and the shortened distance to the center may allow the now marginally penetrating beam to be sufficient.

Table 1

ORNL Source 45A into Neutralizer

Energy	Percent Power	Current into Neutralizer	Neutraliz. Effic	Neutral Current	Power Delivered	
80 keV	85%	38.2A	25%	9.6A	717 kw	
40 keV	10%	9.0A	60%	5.4A	216 kw	1.06 MW total
27 keV	5%	6.75A	70%	4.7A	127 kw	

Berkeley Source 50A into Neutralizer

Energy	Percent Power	Current into Neutralizer	Nutraliz. Effic.	Neutral Current	Power Delivered	
80 keV	60%	30.0A	25%	7.5A	600 kw	
40 keV	30%	30.0A	60%	18.0A	720 kw	1.60 MW total
27 keV	10%	15.0A	70%	10.5A	280 kw	

An alternative scenario proposed for JET is the expanding limiter start-up. If the plasma is started with high denisty but with a small radius, the initial plasma could be heated with moderate energy beams. Then, cold plasma would be added to the outside and would be heated up by the beams which now no longer penetrate.

In order to carry out these scenarios, it may be necessary to use more flexible injector power supply systems which will ramp up the beam energy during a discharge. If the full-bore, full density injection energy were to be used just after start-up in the above scenarios much of the beam would go all the way through the plasma and hit the far wall, wasting power and releasing impurities. Also, the density "window" for effective penetration is very narrow, only about a factor of 3-4 increase in the density will go from a non-absorbed beam to a non-penetrating beam. Since injection seems to be required to attain high density operation in low B-field tokamaks, it seems to be essential that the fast neutral energy be increased as the density builds up.

A further important consideration arises in the selection of an injector system. If penetration of the full energy beam component is marginal, penetration of the half energy component is poor and these particles will heat the outside of the plasma. This may be deleterious because a thick, cool edge region prevents energetic particles from hitting the wall. Also, energy deposited near the plasma edge leaves faster and is thus less effective in heating the plasma.

To emphasize this point, consider typical projected performance values for 80 keV ORNL and Berkeley sources (Table 1). Although the ORNL source only delivers 2/3 the power of the Berkeley source, it is better for heating the center of the plasma since it has more power in the high energy component and much less in the two low energy compoments.

The total beam power/unit volume deposition profiles for tangential injection into the top half of Doublet III are shown for four cases in Figures 2 and 3. The innermost point of Fig. 3 is artifically high due to the large (compared to the beam width) size of the first flux surface. It will be noted that the profiles for the 80 keV Berkeley source and the 50 keV Oak Ridge sources are essentially identical and that the only source that is really peaked on axis is the 80 keV Oak Ridge injector. The conclusion from this is that it is essential to have a very high atomic hydrogen fraction in the source in order to heat the center of large dense tokamaks.

4. Fueling by Neutral Injection

Neutral injection should first be regarded as a source of energy, next, a source of momentum (for tangential injection), and finally as a source of particles. Although beams could be used for fueling, this is not a very energy efficient way to go and may in fact prevent plasma heating.

In order to penetrate a burning reactor, a very high beam energy ($\sim$200 keV D) would be required. This large energy per particle would imply a very large number of very high power injectors to supply the desired number of particles. Operation of burning reactors at such high injection energies has been studied by McNally, et al[3] who showed that with trapped ion losses, the plasma "blows out." Under these conditions, the ion temperature runs away and the density falls towards zero. Also, if the only ions in the plasma are those near the injection energy, a 10% β limit would require densities below $\sim 10^{13}$ cm^{-3}.

In some sense, injection can be regarded as a competition between heating and fueling. Depending upon the models chosen for density transport and recycling at the wall, the plasma density will either increase or reach a level high enough to shield out future beam particles. Once the beam can no longer penetrate to the center, any further heating must be supplied by α-particles. Thus, there must be a very delicate balance between the beam energy, power, and the particle confinement time to achieve the desired density and temperature at the ignition point before the beam is shielded out of the plasma. For this reason, a divertor may be a very desirable "knob" to use to control particle flow at the plasma edge.

Conclusions

For positive ion sources, an upper limit of 80 keV (H) exists for reasonable efficiency. Given this constraint, as much current as possible must be concentrated in the H^+ component of the accelerated ions. For large tokamaks, small radius and/or low density start-ups are required to obtain adequate plasma heating. Finally, high energy neutrals do not appear to be suitable for fueling reacting tokamaks.

References

1. J. A. Rome, J. D. Callen and J. F. Clarke, Nucl. Fusion 14, (1974) 141.
2. J. A. Rome, Y-K. M. Peng and J. A. Holmes, ORNL/TM-5931 (July 1977).
3. J. R. McNally, Jr., J. F. Clarke, R. H. Fowler, T. Hiraoka, R. D. Sharp and D. Steiner, IAEA-CN-33IG1-3, "Plamsa Physics and Controlled Nuclear Fusion and Research, "Vol. III (1974), Tokyo meeting.

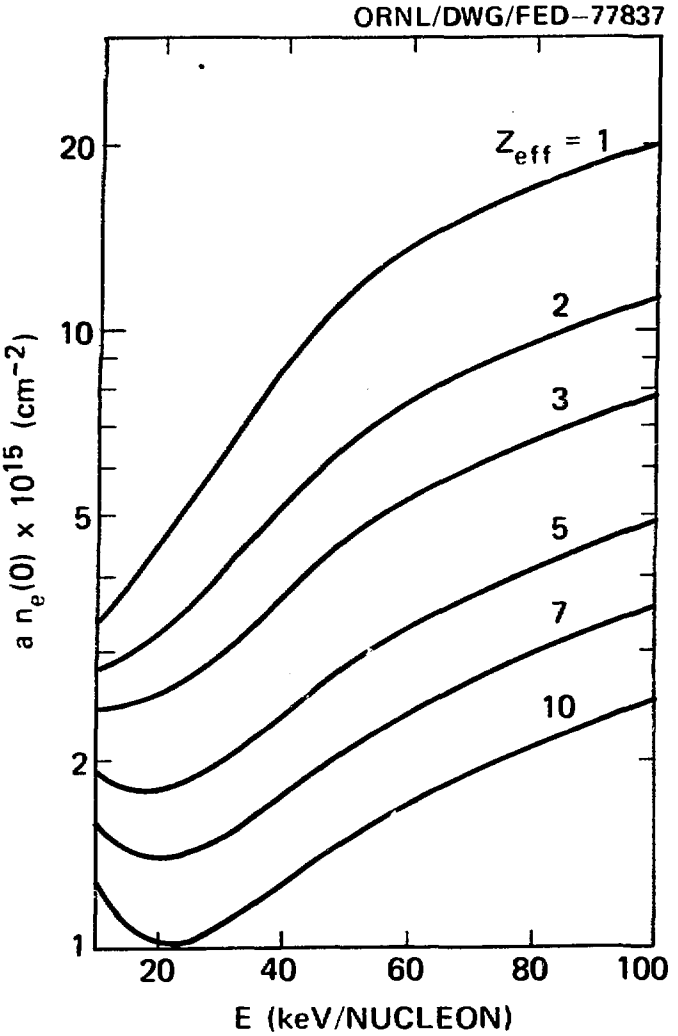

Fig. 1. Plasma opacity ($n_e(0)a$) for various Z_{eff} values assuming parabolic density profiles and uniform Z_{eff}.

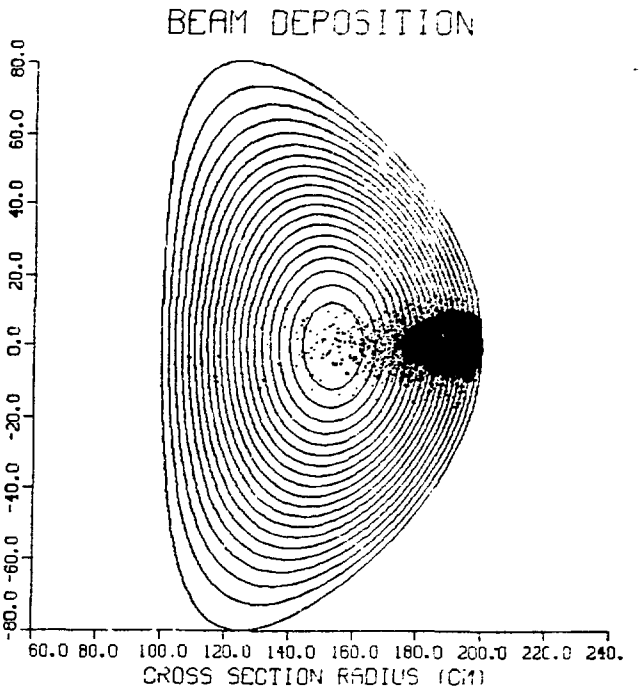

Fig. 2. Deposition profile for one lobe of Doublet III calculated using Monte-Carlo code.

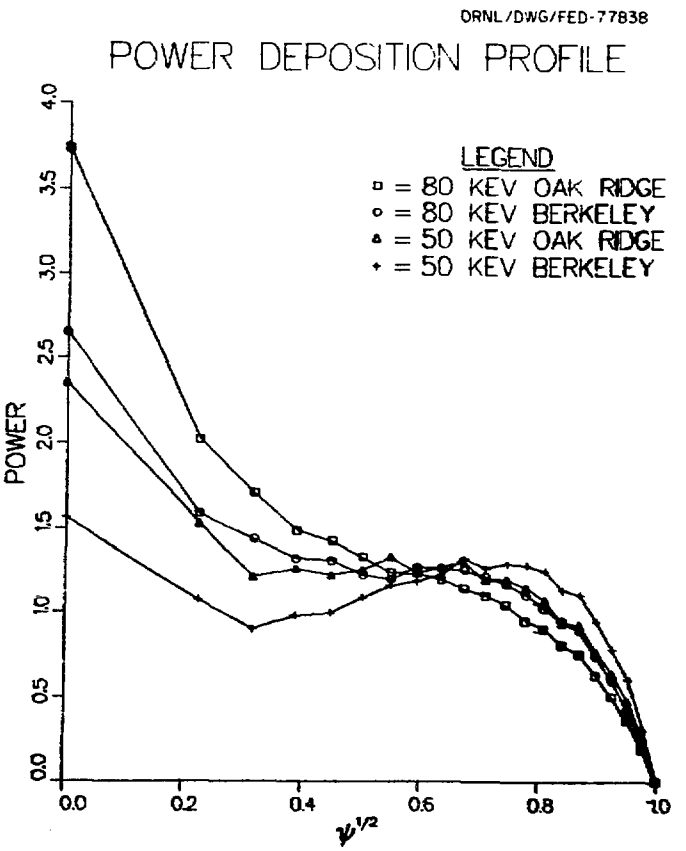

Fig. 3. Beam deposition in Doublet III for the parameters of Table 1.

FUELING WITH NEUTRAL BEAMS*

J. H. Fink†

Lawrence Livermore Laboratory, University of California
Livermore, California 94550

Summary

Neutral beams, which effectively heat and fuel mirror reactors, provide high-energy particles that readily cross magnetic fields to penetrate, heat, and fuel confined plasmas. The potential reliability, efficiency, and cost of large neutral-beam injectors make them desirable components of an operating mirror reactor. Because neutral beams are a poor source of low-energy particles, some other means of fueling large Tokamaks is needed.

Introduction

During the past five years, some of the most important advances in magnetically confined fusion research have resulted from progress in neutral-beam technology. Neutral beams have proven to be capable of heating and fueling plasmas, as well as contributing to plasma buildup without initiating instabilities that adversely affect confinement. So successful have neutral beams been in experiments, that their participation in power-producing fusion reactors is almost assured.

At this work shop, we are concerned with the techniques of fueling a fusion reactor; i.e., the introduction of deuterium and tritium ions into a magnetically confined plasma. However, fueling involves more than ion transport. To sustain the fusion process, we have to bring these ions up to reactive densities and temperatures within the region of magnetic confinement. In addition, to produce maximum power, these ions must be uniformly distributed throughout the entire reactor volume at a rate approximating their loss.

In this paper, I briefly discuss those characteristics of neutral beams that make them particularly suited for reactor fueling; i.e., their capability for particle transport from the ion source into the reactor and for penetrating and heating the plasma. In addition, I discuss the potential capabilities of future neutral-beam injectors; i.e., their reliability, efficiency, and cost. The injectors described come from a series of conceptual studies conducted at Lawrence Livermore Laboratory on neutral-beam injection into mirror reactors. Finally, I note that, while neutral beams are effective for fueling and heating in mirror reactors, some other means of fueling is required for large Tokamaks.

Required Neutral-Beam Current

Fueling can be described by the ion-transport equation

$$\frac{dn}{dt} = S - L - R, \tag{1}$$

where n represents the density of deuterium plus tritium ions, S the ion-fueling rate per unit volume, L the ion-loss rate per unit volume from the magnetically confined plasma, and R the rate per unit volume at which ions are consumed by fusion.

The burn fraction,

$$f_b = R/S, \tag{2}$$

is small. Thus, for steady state or quasi-steady state operation,

$$S = L. \tag{3}$$

With neutral current I^0 injected into a reactor of volume V, the fueling rate becomes

$$S = \frac{I^0 f_t}{eV}, \tag{4}$$

in which f_t represents the fraction of neutral beam that gets trapped as ions. For efficient injection, f_T must approach 100%.

Meanwhile the loss rate of ions from the magnetically confined plasma can be described in terms of the particle-confinement time, τ:

$$L = \frac{n^2}{(n\tau)}. \tag{5}$$

Equating ion loss with injection rate, the required neutral-beam current becomes

$$I^0 = \frac{n^2 eV}{(n\tau)}. \tag{6}$$

*Work performed under the auspices of the U.S. Energy Research and Development Administration under contract No. W-7405-Eng-48.

†On loan from Westinghouse Electric Corporation.

Beam Properties

By definition, a beam consists of a group of particles traveling together at near-parallel trajectories. To become part of a beam, each particle had to receive an added component of energy, directed along the beam path, that was significantly greater than the particle's original, random, thermal energy. Accordingly, as shown in Fig. 1, a neutral beam originates as ions extracted from an ion source. These ions are accelerated and focused by an accelerator comprising a configuration of grids; they are then neutralized in a special cell while en route to the reactor. As a consequence, neutral beams convey both particles and energy.

In some applications, the beam's energy is more significant than its particle content. In a continuously driven reactor such as a mirror, neutral beams simultaneously provide energy and fuel to sustain the fusion reaction. In an ignited reactor, such as a Tokamak, neutral beams provide energy to heat the plasma to ignition temperature. The injected particles are of little importance. For fueling any reactor, beam current is critical because it represents the rate at which particles are supplied to the plasma. Injected energy is also significant because it forms the beam and makes neutral-beam fueling effective.

Beam Transport

One advantage of neutral-beam fueling results from the very high currents of neutrals that can be made to pass through a relatively small aperture in the reactor wall. With a focused beam, aperture dimensions are relatively independent of beam current and the area of the ion source (Fig. 2). The aperture dimensions are related to the transverse velocity distribution of the beam's neutrals. They are directly proportional to the distance from ion source to aperture and inversely proportional to the square root of the beam energy.

The aperture shape, meanwhile, is a function of grid design. A circular aperture can be obtained with grids made of many round holes; an elliptical aperture results from slotted grids. To inject particles through a narrow aperture, the beam can be made astigmatic, with one line focus in the plane of the aperture and the other line focus, perpendicular to the first, located someplace in the reactor plasma (Fig. 3). Astigmatic beams can be formed by curving a slotted grid to form one line focus perpendicular to the slots at one focal length and displacing the grid slots from grid to grid, to form another line focus, parallel to the slots, at a different focal length. The introduction of fuel by means of beams thus offers great flexibility for shaping the entrance aperture.

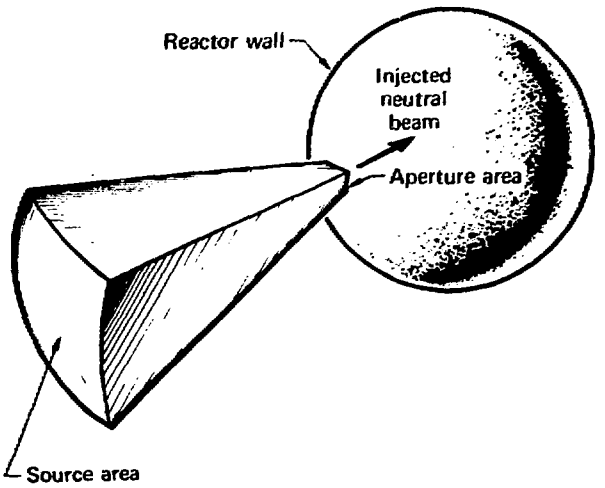

Fig. 2. Injector configuration.

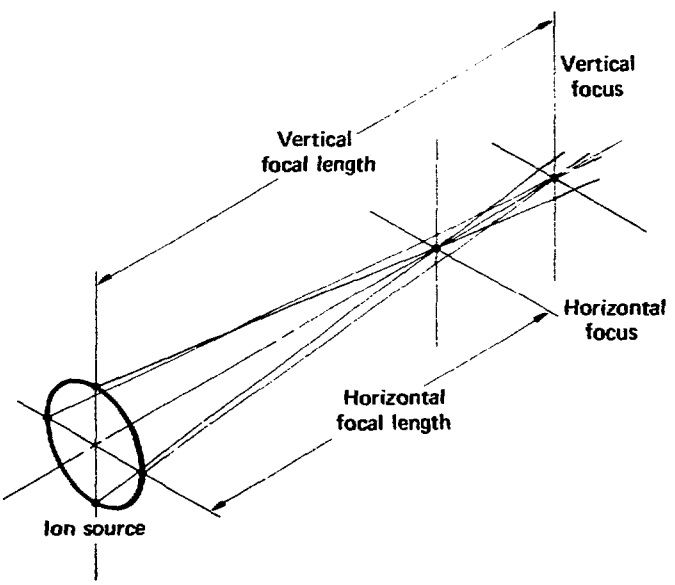

Fig. 3. Astigmatic beam.

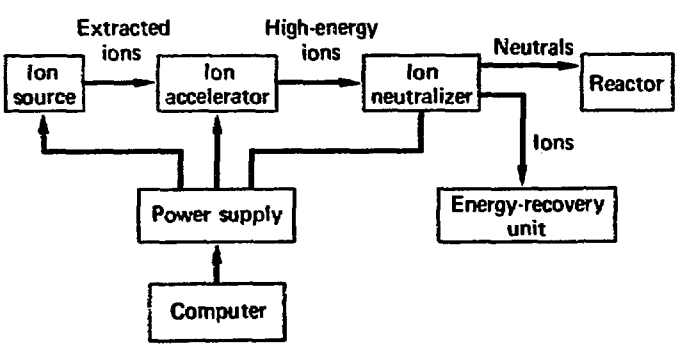

Fig. 1. Formation of neutral beams.

Ion Distribution in the Plasma

To make effective use of the reactor volume, we must introduce ions uniformly throughout. High-energy neutrals passing through the aperture in the reactor wall readily cross magnetic field lines to become ions. This happens either by charge exchange with plasma ions or by ionization on impact with plasma ions or electrons. As a consequence, the neutral beam attenuates as it passes through the plasma, leaving a distribution of trapped high-energy ions in its wake.

After traveling some distance x through a plasma of density n_e, the neutral beam, initially of equivalent current I^0, will decay to

$$I = I^0 \exp\left(-\int_0^x \sigma n dx\right) , \qquad (7)$$

in which σ is the sum of the cross-sections for charge exchange and for impact ionization.[1,2]

As Fig. 4 shows, the magnitude of σ, which is a function of beam energy, gets smaller as beam energy increases. Therefore, to distribute the new ions throughout the plasma, we must adjust beam energy to match reactor size. To be effective, the neutral beam should penetrate the entire plasma and the trapped fraction of ions should be almost 100%.

Now the trapped fraction can be described by

$$f_T = 1 - \exp\left(-\int_0^x \sigma n dx\right) , \qquad (8)$$

so that for f_T to approach 100%,

$$\int_0^x \sigma n dx \geq 3 \qquad (9)$$

The nature of σ is also a function of beam energy, as can be seen in Fig. 4. Accordingly, beams of lower energy are subject to charge exchange. A neutral in the beam, giving up an electron to neutralize a plasma ion, gets trapped as a high-energy ion. If close to the plasma surface, the newly formed neutral may escape confinement or become re-ionized in a subsequent collision. The result of this process is to raise the average temperature of the ions remaining in the plasma. Should beam energy be very low and penetration into the plasma poor, a considerable loss of particles can take place. This makes low-energy beams ineffectual for fueling.

At higher beam energies, in excess of 80 keV, impact ionization prevails. The beam's high-energy neutrals break up into ions and electrons. Thus, high-energy injection tends to raise the electron temperature; low-energy injection results in a large fraction of the injected beam energy going to the plasma ions.

Neutral beams formed from positive ions carry some fraction of half-and one-third-energy neutrals. These result from the components of D_2^+ and D_3^+, which were extracted from the ion source along with the atomic D^+ ions. The molecular ions split up, when neutralized, into the fractional-energy neutrals. These neutrals are not desirable because they do not penetrate the plasma as well as those at full energy.

During startup, advantage can be taken of beam plasma interaction to build up plasma density.[3] Starting with a cold, low-density plasma target, we can use neutral beams to increase plasma temperature and density (Fig. 5). While the target is thin, injected current must be small because only a small fraction of the beam is ionized. The balance of the beam, still neutral, can cause damage to the far wall of the reactor. As plasma density grows, injector current can be increased.

Injector Reliability

In operating reactors, the ion sources will have to be reliable and provide many hours of continuous operation. To achieve this, we need rugged cathodes and heaters. Grids will have to be cooled and consideration

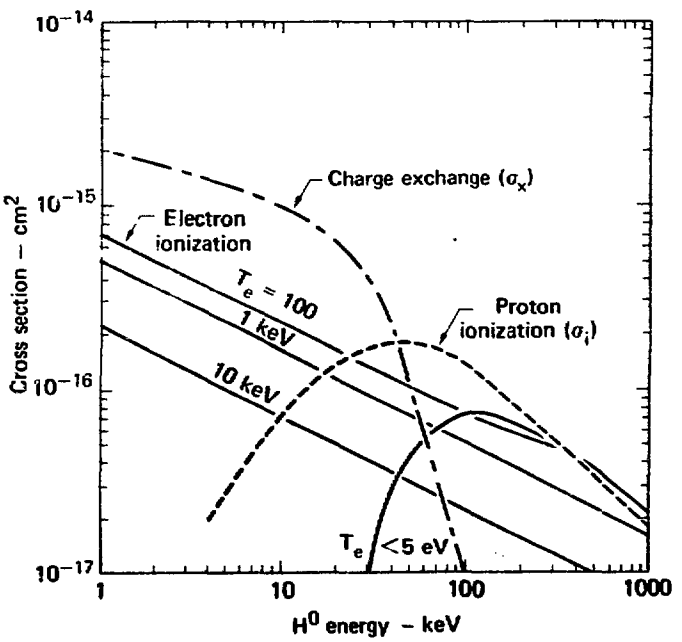

Fig. 4. Separated cross sections for ionization of injected neutral beam vs energy.

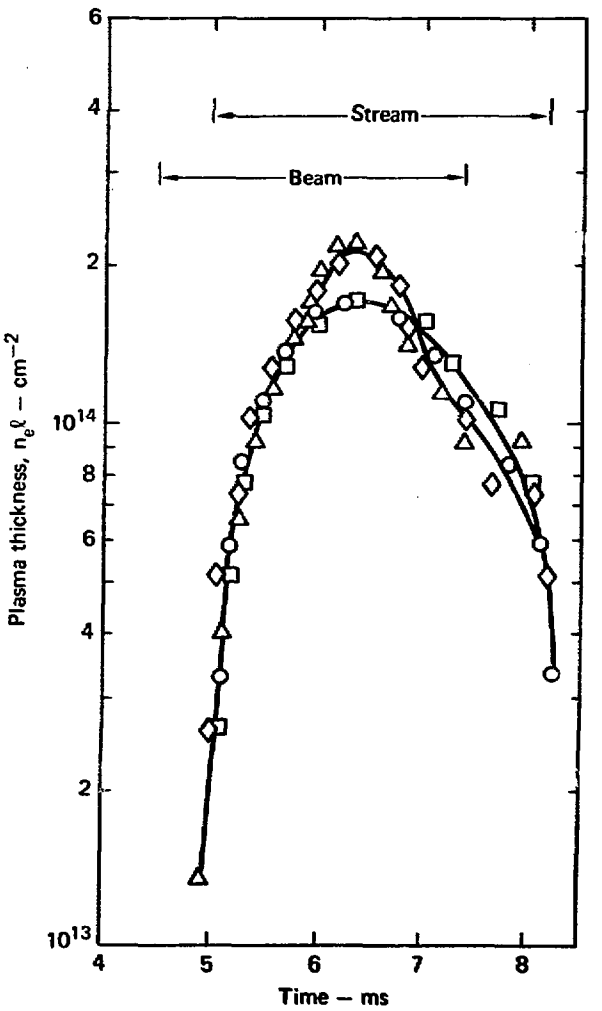

Fig. 5. Plasma buildup in 2XIIB achieved by neutral-beam injection into a streaming plasma.

given to insulators and metals used in the beam lines to protect them from the adverse effects of radiation and neutron bombardment.

Certain features can be employed in present designs to form reliable injectors. For instance, high-voltage insulators can be housed in shielded regions and ion sources can be mounted farther from the reactor, where radiation is less severe.

No matter how conservative a design, high-voltage, low-pressure systems are, and probably always will be, subject to a finite, though small probability of arcing over. In fact, neutral beams are now designed with crowbar and high-voltage interrupt circuits to extinguish spurious arcs. These circuits include arc snubbers as well[4] to dissipate the stored energy of the circuit and to prevent the damage such arcs might cause. As a result, a beam line that had previously arced can be safely reactivated a few seconds after it has been turned off.

With this technology, we can build a reliable neutral-beam injector of many smaller, parallel beam lines. The time constant of the reactor plasma is such that some ripple in the injected beam can be tolerated. Hence, a few of the beam lines can be off for a few seconds without disturbing the reactor. In this way, system reliability can be attained by means of component redundancy.

To create a minimum disturbance as beams are turned on and off, each beam line should contribute a small fraction of the total injected current. This is advantageous in several ways. Smaller components are easier to replace as well as cheaper to make and test. A small ion source entails smaller grids, which are simpler to align and easier to cool. Smaller diameter beams make the design of the neutralizer cell less critical. They are advantageous when attempting energy recovery from the unneutralized fraction of the beam. In addition, small grids improve reliability because the probability of high-voltage breakdown over a small area is less than that over a large one.

Another advantage of an assembly of many small ion sources results from the ease with which the low temperature gas, escaping from each source, can be pumped away through the space between the sources. This is preferable to pumping the gas away, across a broad beam, or letting the excess gas flow down the beam line into regions of lower pressure. A typical array of negative-ion sources might be as shown in Fig. 6. A conceptual design of a neutral-beam injector made of positive-ion sources appears in Fig. 7.

Injector Efficiency

To obtain the most favorable power efficiency from an injector, we have to recover the energy from that fraction of the ion beam that did not become neutralized. This is particularly important in high-energy, positive-ion sources of neutral beams, for which the neutralization efficiency (Fig. 8) falls so drastically at higher beam energies.[6] The energy-recovery system[7] associated with the injector of Fig. 7 is in Fig. 9.

At high beam energies, the greatest gain in efficiency can be obtained with negative ions as a source

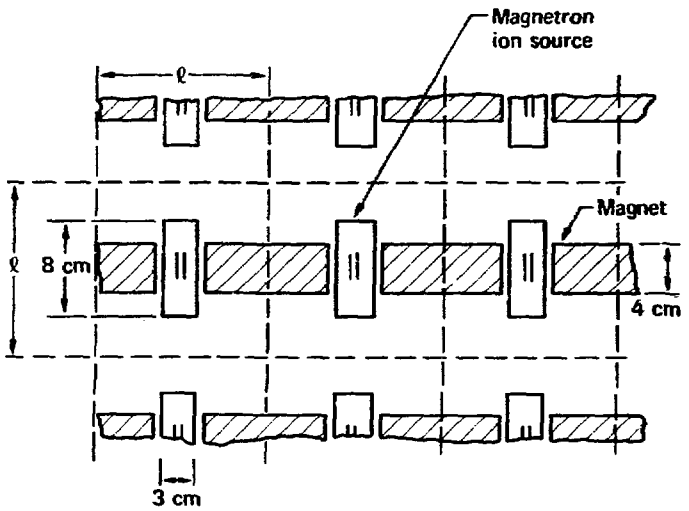

Fig. 6. An arrangement of magnetron negative-ion sources designed to facilitate pumping.

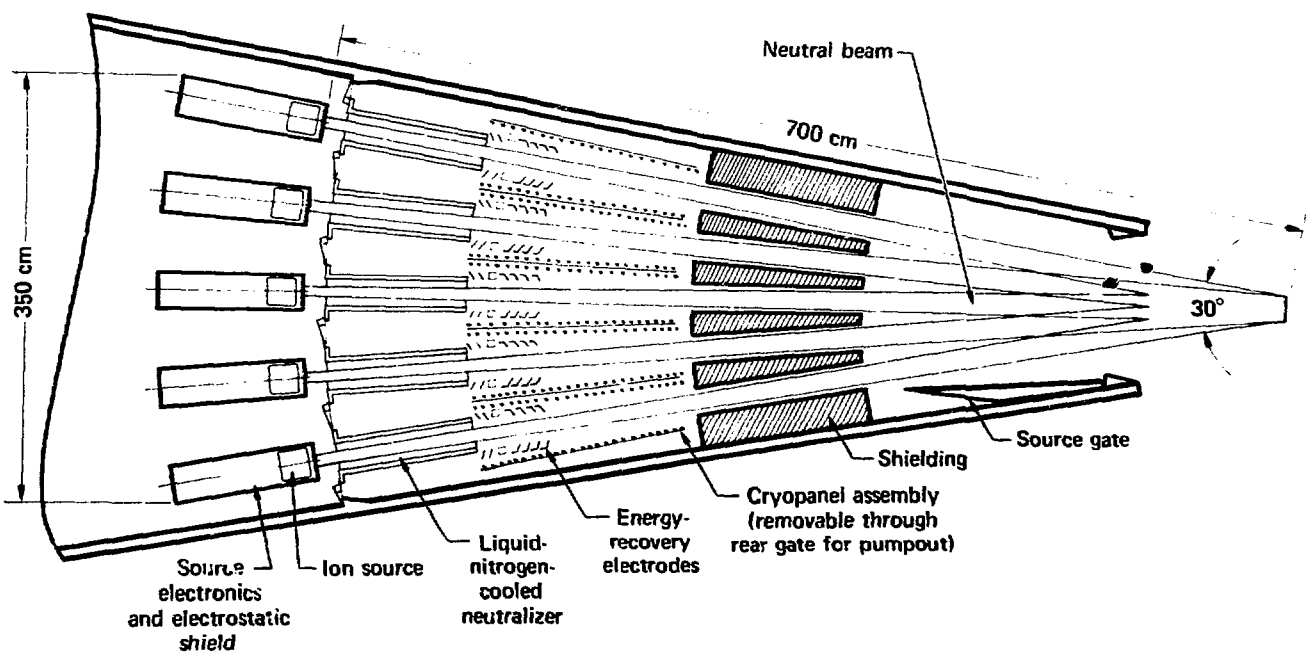

Fig. 7. A 225-MW neutral-beam injector delivering a mixture of 100-keV deuterium atoms and 150-keV tritium atoms.

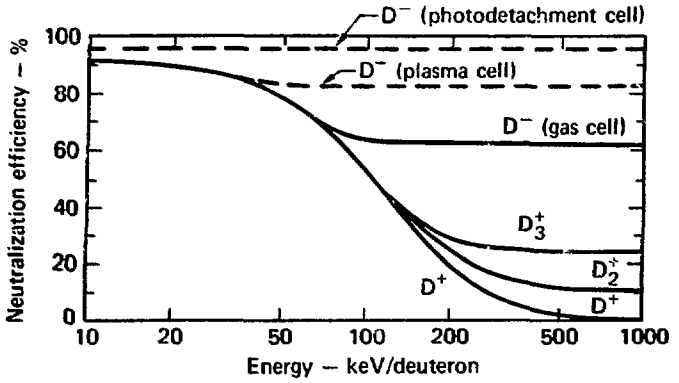

Fig. 8. Optimum neutralization efficiency of a deuterium gas cell as a function of the energy of an incident deuterium atom.

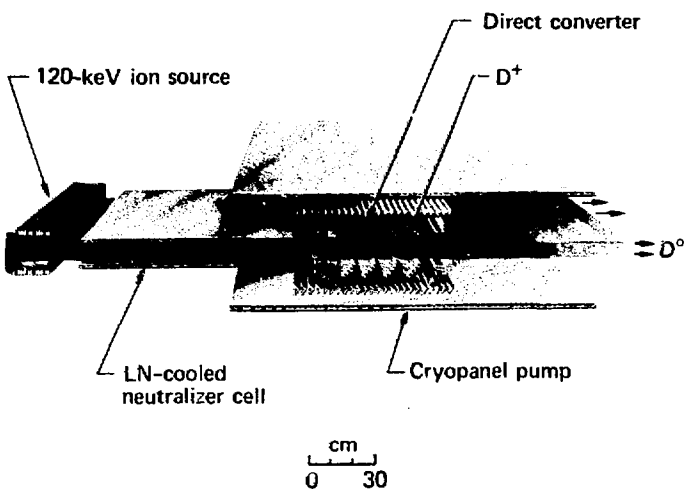

Fig. 9. 100-keV neutral-beam injector system.

of neutral beams. Figure 8 shows that about 62% of a beam of negative deuterium ions can be stripped of their extra electrons in a gas or vapor cell. In a plasma cell, stripping is over 80%; in a photodetachment cell, 95% is possible. Unfortunately, negative-ion sources are not yet available for today's neutral beams.

At present, several techniques of generating negative ions are under development. One involves the magnetron,[8,9] (Fig. 6); in this source, negative ions are born on a hot cesiated tungsten surface. Another uses a double charge-exchange cesium cell in which some fraction of the positive ions is converted to negatives (Fig. 10). With a positive-ion beam energy of about 2 keV, 20% of the incident beam converts to negatives while the remainder of the beam is discarded. This loss is not serious in a high-energy beam when consideration is given to the favorable neutralization efficiencies obtainable with negative ions.

Figure 11 shows a conceptual design of a negative-ion beam line[10]. Positive ions, drawn from a conventional ion source, pass through a cesium vapor double charge-exchange cell with an energy of about 2 keV. The 80% of the beam that does not become negative exits as neutrals to bombard a low-energy target from which some fraction of the energy can be thermally recovered. Meanwhile, the negative ions are accelerated and deflected away from the low-energy neutrals to pass into a stripping cell not shown in this figure.

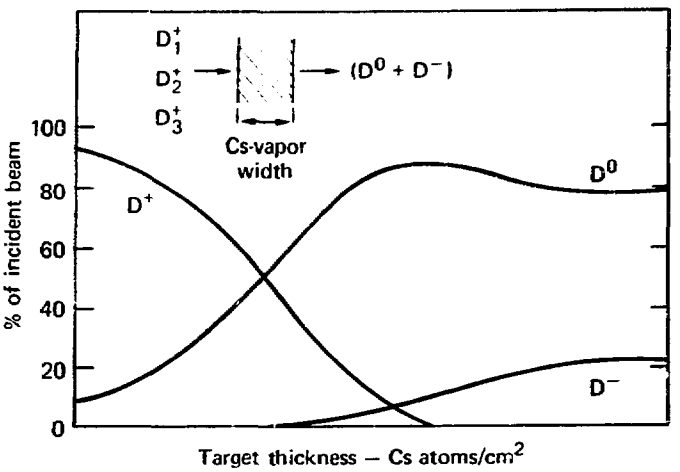

Fig. 10. Conversion of 2-keV D^+ ions to D^- ions in a cesium-vapor cell.

The performance of a 1.2-MeV beam[11] in a gas or vapor cell is compared with a plasma cell in Fig. 12. On penetrating either cell, the negative-ion component rapidly decays, to be replaced by neutrals and positive ions. The plasma cell is preferred because it produces a larger fraction of neutrals in the beam.

A study was made of photodetachment, which has an even higher stripping efficiency.[10] Our analysis shows that with 95% stripping, a neutral-beam power efficiency of 80% is possible. Figure 13 provides a conceptual design of an injector using photodetachment. The technology required for photodetachment, however, requires advanced laser and mirror development. An injector design for the near future will use a cesium-plasma stripping cell with hot tungsten plates similar to that in a "Q" machine. Figure 14 shows a schematic of a 1.2-MeV beam line using such a cell. Our studies indicate that a power of efficiency of 73% is attainable.

Cost

In the final analysis, reactor cost per kW output will determine whether fusion is a practical source of electricity. Consequently, the fueling process can be measured by its impact on reactor costs. As a consequence, the efficiency of neutral beams is critical.

We estimate the cost of neutral beams to be roughly (320/η) dollars per kW output of neutral-beam power, where η represents injector efficiency. At this stage of negative-ion beam development, it is impossible to obtain more reliable cost estimates.

Auxiliary Injection Techniques

Despite the attractiveness of fueling with neutral beams, there is a reactor size beyond which the energy required to penetrate the plasma becomes excessive. The plasma overheats, causing the reaction rate to drop. This problem is of particular importance in an ignited reactor where the fusion process and confinement time are sufficient to maintain the desired ion temperatures without relying on injected energy. In this realm, any technique that reduces the required beam energy will enhance reactor Q and simultaneously make larger reactors creditable. Several techniques are discussed in other papers at this workshop.

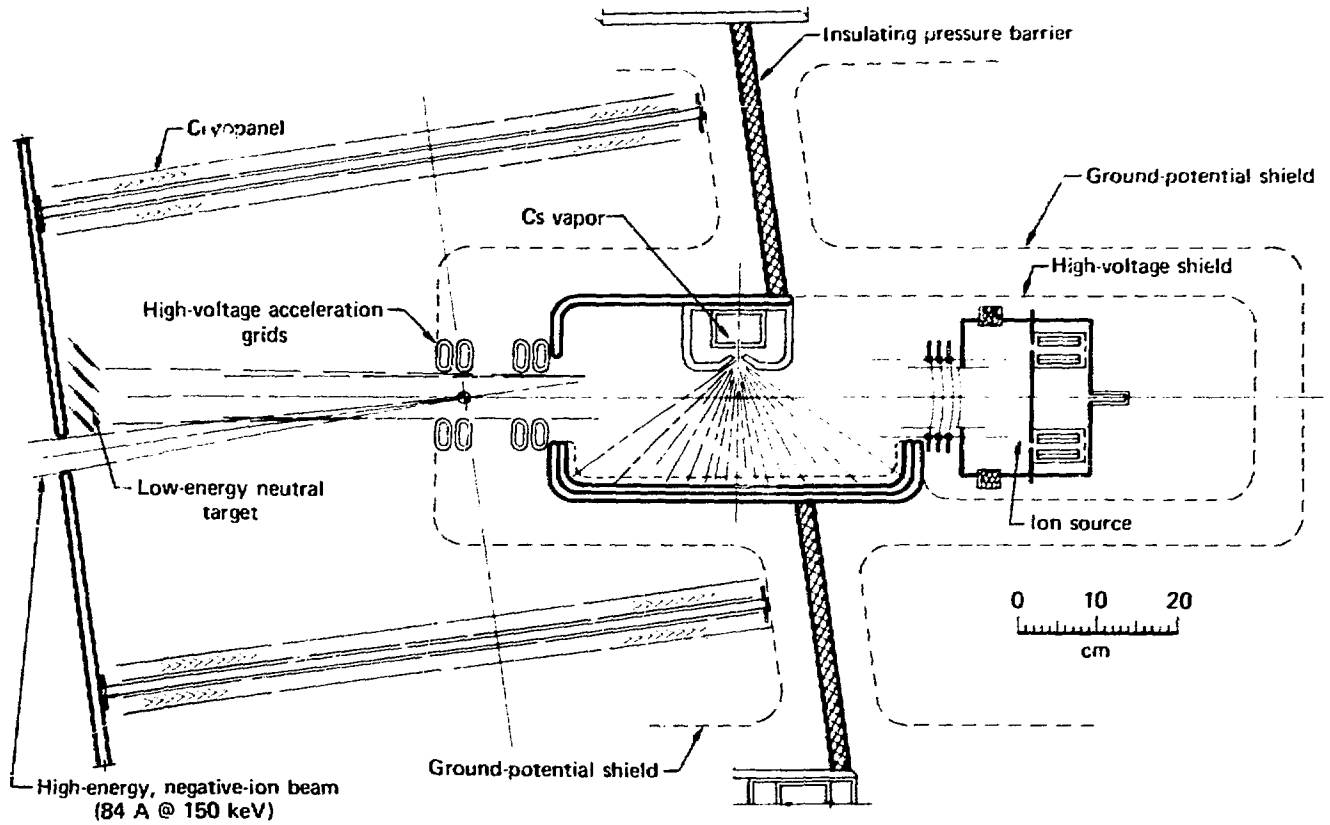

Fig. 11. Negative-ion injection module delivering 84 A of 150-keV D^- ions.

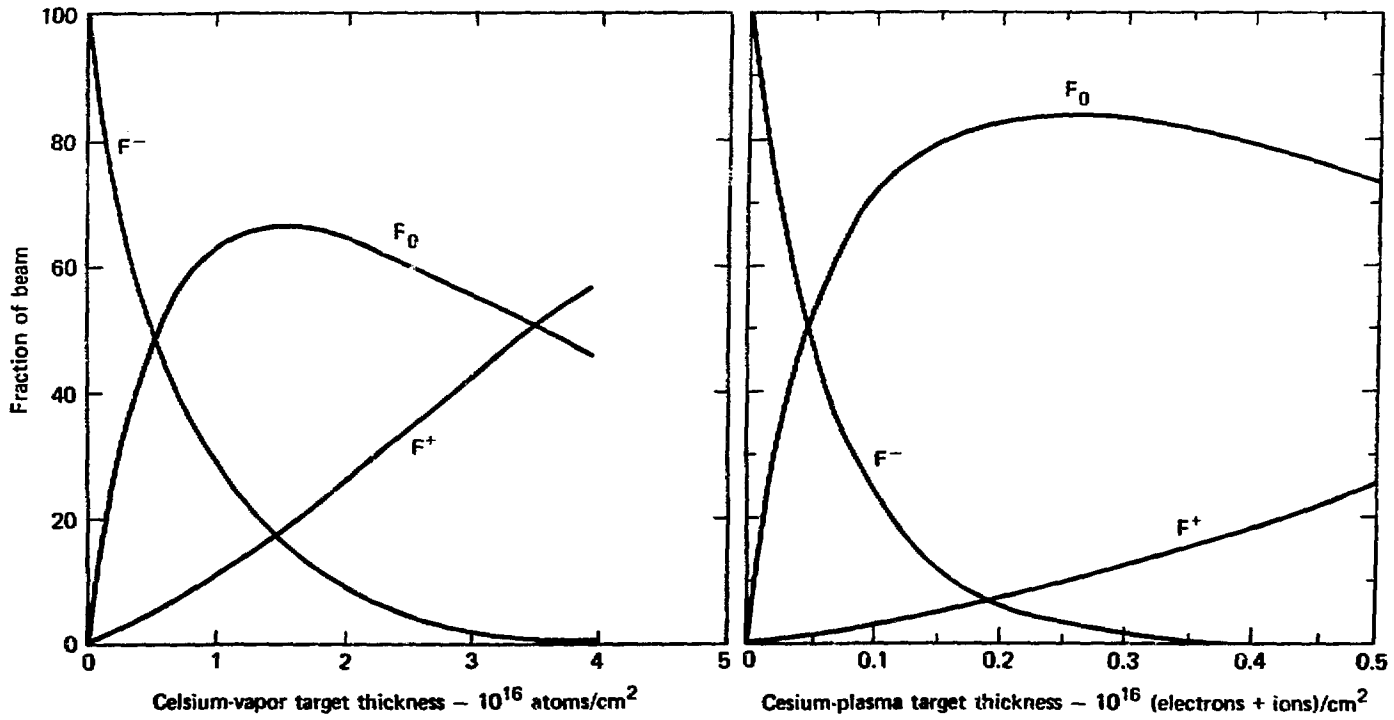

Fig. 12. Comparison of a cesium-vapor target (left) with a cesium-plasma target (right) for a 1.2-MeV D^- ion beam.

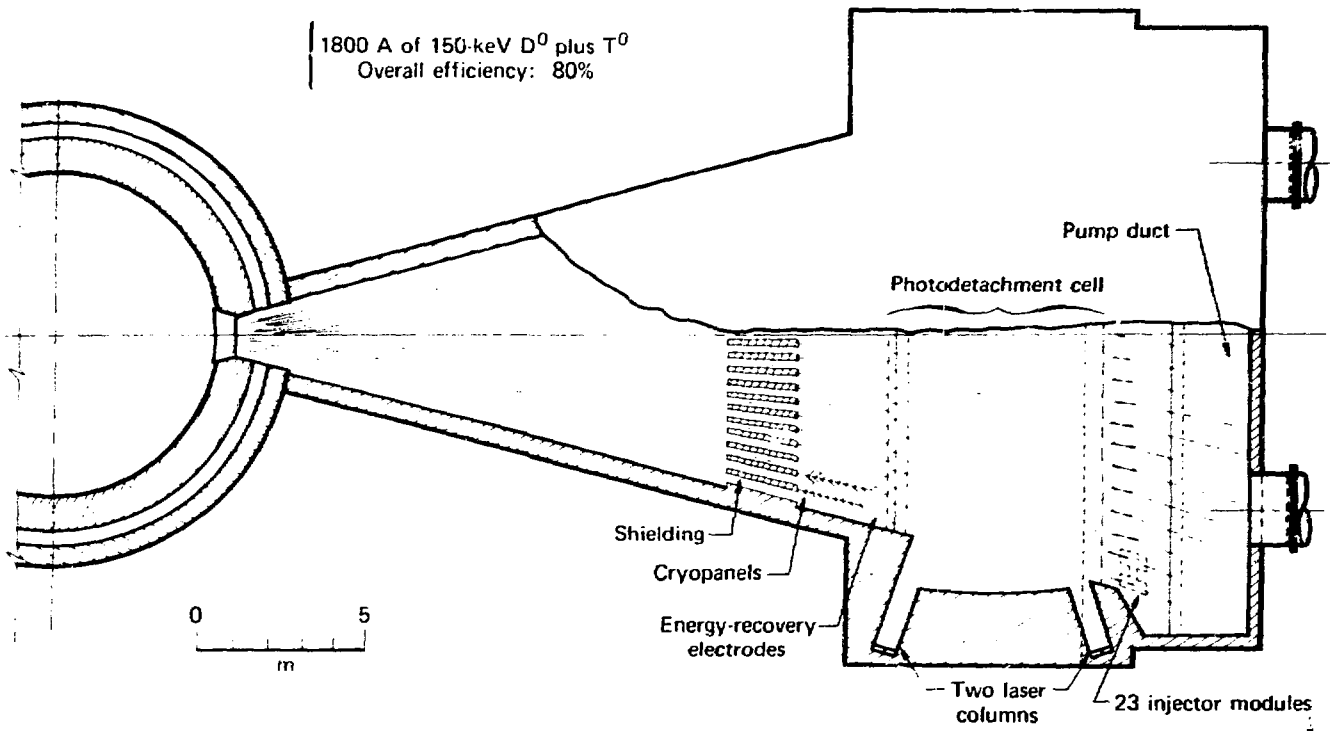

Fig. 13. Neutral-beam injector delivering 1800 A of 150-keV deuterium and tritium atoms.

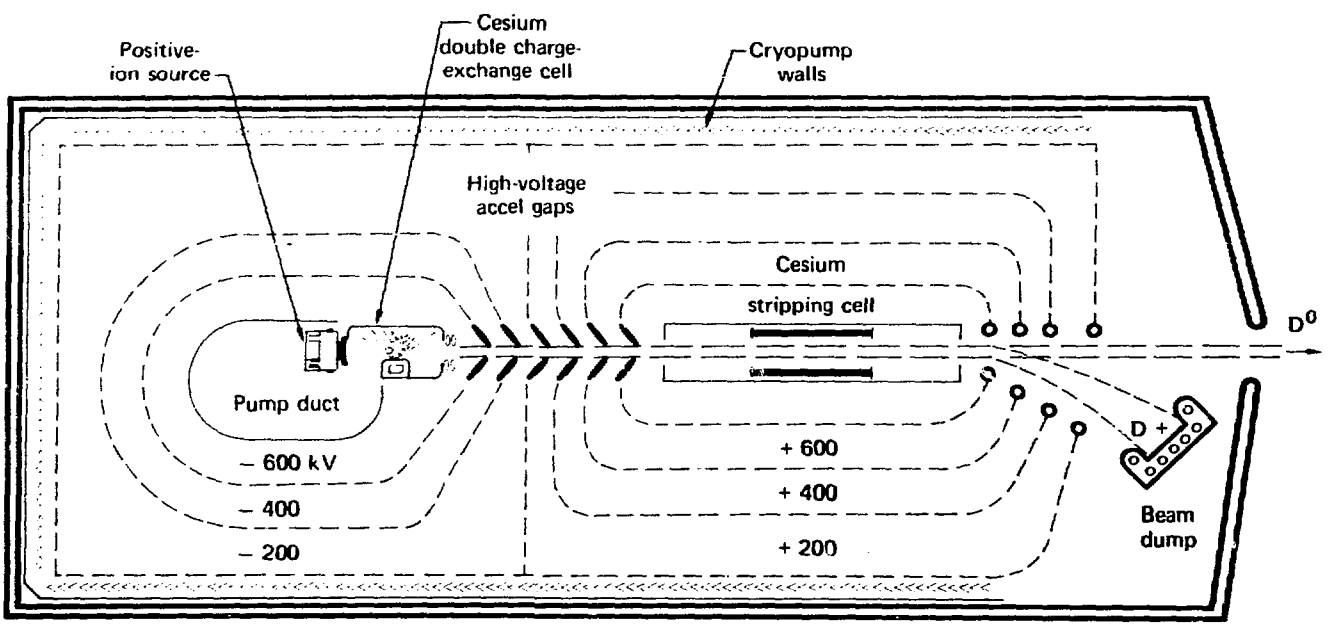

Fig. 14. 1.2-MeV neutral-beam injector.

Conclusion

Neutral beams are effective for high-energy fueling, plasma heating, and plasma buildup in a mirror reactor, but other means are needed for fueling relatively cold ions in a large Tokamak. To fairly evaluate neutral-beam fueling, however, we must consider its future potential. So much stress has been put on development for immediate needs that little has been done to meet the long-term requirements of reliability, efficiency, and cost. We are now reaching the stage in fusion research where higher energy beams are needed. To reduce the cost of experiments using these beams, more efficient neutral-beam injectors must be developed now.

References

1. D. [illegible] Sweetman, "Ignition Condition in Tokamak Experiments and Role of Neutral Injection Heating," *Nucl. Fusion* 13, 157 (1973).

2. A. C. Riviere, "Penetration of Fast Hydrogen Atoms into a Fusion Reactor Plasma," *Nucl. Fusion* 11, 363 (1971).

3. E. W. Stallard, *Radial Plasma Buildup Code for Neutral-Beam Injection into a Mirror Machine*, Lawrence Livermore Laboratory, Livermore, Calif., UCRL-51784 (1975).

4. J. H. Fink, W. R. Baker, and H. M. Owren, "Analysis and Application of a Transformer Core which Acts as an Arc Snubber," UCRL-79016 (1977), submitted to *IEEE Trans. on Plasma Sci.*

5. J. H. Fink, W. L. Barr, and G. W. Hamilton, "A 225-MW Neutral Injection System for a Mirror Fusion-Fission Hybrid Reactor," *Nucl. Fusion* 15, 1067 (1975).

6. K. Bertner, R. V. Pyle, and J. W. Stearns, "Intense, Mixed-Energy Hydrogen Beams for CTR Injection," *Nucl. Fusion* 15, 249 (1975).

7. W. L. Barr and R. W. Moir, "A Review of Direct Energy Conversion for Fusion Reactors," in *Proc. 2nd Topical Mtg. Technology of Controlled Nucl. Fusion, Richland, Washington, 1976*, p. 1181.

8. Yu. I. Bel'chenko, G. I. Dimov, and V. G. Dodnikov, "A Powerful Injector of Neutrals with a Surface-Plasma Source of Negative Ions," *Nucl. Fusion* 14, 113 (1974).

9. K. Prelec and Th. Sluyters, "A Pulsed Negative Hydrogen Source for Currents up to One-Ampere," in *Proc. Particle Accel. Conf., Washington, DC, 1975* (IEEE, New York, 1975), p. 1662.

10. J. H. Fink, W. L. Barr, and G. W. Hamilton, *A Study of Efficient High-Power, High-Energy Neutral Beams for the Reference Mirror Reactor*, Lawrence Livermore Laboratory, Livermore, Calif., UCRL-52173 (1976).

11. J. H. Fink and G. W. Hamilton, "A Neutral-Beam Injector for the Tandem Mirror Fusion Reactor Delivering 147 MW of 1.2-MeV D^0," UCRL-79643 (1977), submitted to *Nucl. Fusion*.

STATUS OF THE LBL/LLL DEVELOPMENT PROGRAM*

K. H. Berkner, W. S. Cooper, K. W. Ehlers, R. V. Pyle and E. B. Hooper, Jr.†

Lawrence Berkeley Laboratory
University of California
Berkeley, California 94720

The status and near-term goals of the LBL/LLL neutral-beam-development program are described. The emphasis in this paper is on the technology of systems based on the acceleration and neutralization of positive ions; this approach will be used in the near term, probably through 1985 at least. For more efficient injection, part of our plan is to develop a negative-ion approach suitable for 200- to 400-kV injectors on confinement experiments in the 1985-90 period. However, the negative-ion based program is still very much in the research phase, and it is difficult to project how it will phase into fusion reactor fueling experiments.

I. Introduction

The LBL/LLL Neutral-Beam Development Group has the responsibility for developing injection systems for mirror experiments and, is one of the two major efforts within DMFE developing systems suitable for tokamak confinement devices. Part of the application will be fusion reactor fueling.

The work proceeds along two lines: The first, based on positive-ion technology, is required for the near-term (perhaps to 1985) applications. The presently identified experiments, 2XIIB, TMX, MFTF, TFTR, and DIII, require injection at energies up to 120 keV, ion currents per module up to 80 A, and pulse lengths to 0.5 sec. Although much work remains to be done, we have achieved 120-kV, 0.5-sec operation of a fractional area (12 A) TFTR prototype source, and are fairly confident about developing useful injectors for the near-term applications, including up-grades for longer pulses. We will go into the present status in some detail to permit the reader to evaluate the work yet to be done.

The second development effort is oriented toward longer term applications requiring efficient neutral-beam systems at energies above 120 keV. These systems will require the production and acceleration of large currents of negative ions. Two of our goals are the demonstration of a 200-kV, 20-A (D^0), ∿ dc system by 1981, and a 400-kV, 20-A (D^0), ∿ dc system by 1983. These achievements will make it possible to have 200- to 400-kV injectors on confinement experiments in the 1985-90 period.

II. The Positive-Ion System Status

The injection of intense, 80-keV H^0- or D^0-beams is planned for the Doublet III-tokamak and the MFTF-mirror experiments for plasma heating; for the Tokamak Fusion Test Reactor (TFTR), 120-keV D atoms (20 MW in 0.5-sec pulses at 5-minute intervals) will be injected into a tritium plasma to produce two-component d-t reactions. The principal components of these neutral-beam injection systems are shown schematically in Fig. 1.

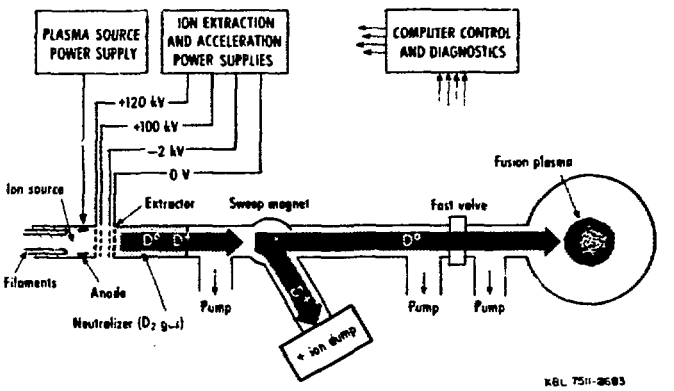

Figure 1. Schematic of a typical neutral-beam injection system.

The system operation is as follows: A deuterium plasma is created in the plasma generator by means of a high-current discharge. Ions from this plasma are accelerated in a carefully designed multi-electrode structure. The ions then pass through a neutralizer containing deuterium gas, and a fraction becomes neutralized by charge-exchange collisions. Remaining ions are removed from the beam by the sweep magnet; otherwise, the various reactor magnetic fields would bend the ions into surfaces near the entrance port, possibly releasing gas bursts or melting the surfaces. The considerable power in this ion beam must be handled by the ion-beam dump. The vacuum pumps distributed along the beam line remove most of the gas emerging from the neutralizer and the ion-beam dump and must maintain the pressure between the sweep magnet and the entrance port at a sufficiently low value that very little of the neutral beam is reionized. Well-regulated power supplies are required to assure good beam optics; to minimize accelerator damage when a spark occurs, the power supplies must also be capable of rapid turn-off with a minimum of stored energy (e.g. in cable capacitance). Optical, mechanical, and electrical sensors determine the condition and performance of the neutral-beam system and permit the control system to adjust the power-supply voltages and to shut down the system if a malfunction occurs.

The LBL 120-keV Neutral-Beam Test Facility[1,2] is used for the development and testing of neutral-beam-system components. It has two beam lines and associated power supplies: (A) a 150-kV, 20-A, 0.5-sec power-supply system[3,4] to test small-area injector modules (plasma source and accelerator), and (B) a 120-kV, 70-A, 30-msec power-supply system to test full-scale modules for short pulses. The beam-diagnostic system for these beam lines is described in Ref. 5.

Long-pulse testing of high-current ion sources will be completed on the High Voltage Test Stand (HVTS) at LLL. This facility is nearing completion in a configuration suitable for testing positive ion sources in

*Work done under the auspices of the United States Department of Energy.

†Lawrence Livermore Laboratory, Livermore, California 94550.

various voltage-current combinations. The initial application will be for TFTR 120-kV, 65-A, 0.5-sec modules. In a year or so, the HVTS will be modified to permit testing of a negative-ion system at 200 kV, 20 A, dc.

Next we describe the operation of a 120-kV, 0.5-sec injector module which, from an 8- x 10-cm accelerator-grid array, produces 14 A of hydrogen ions or 10 A of deuterium ions. This module was used to test the design concepts of the 10- x 40-cm, 120-kV, 65-A, 0.5-sec TFTR module[6-8] which is currently under test.

Injector Module

A cross-section of the 120-kV, 8- x 10-cm injector module is shown in Fig. 2. The ions are produced in a high-current low-voltage discharge with no externally applied magnetic fields. The cathode consists of eighty-four 0.5-mm-diam, 11-cm-long tungsten filaments; the anode is a 10- x 10-cm molybdenum plate shown in the top of the figure. A photograph of the plasma source is shown in Fig. 3; details on this type of plasma generator can be found in Ref. 2.

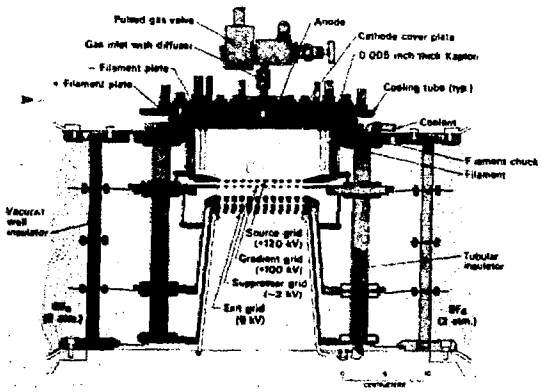

Figure 2. Cross-section of the 120-kV, 0.5-sec source module with an 8- x 10-cm grid array.

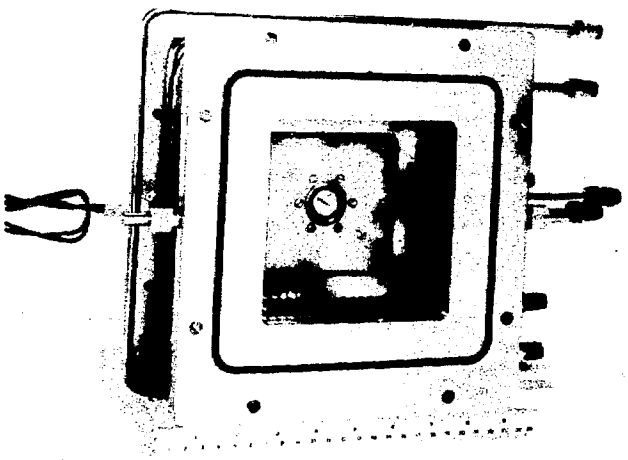

Figure 3. Photograph of the plasma source, illustrating the filament geometry. The flange with the O-ring was used for plasma-uniformity tests; it is not part of the structure shown in Fig. 2.

A four-grid (three-gap) multiple-slot accelerator array (a cross section of a single slot of the array is shown in Fig. 4) is used. Ions are accelerated and electrostatically focused in the first two gaps; the third gap has a weak decelerating field to suppress down-stream electrons. The transparency of the array is 60%; the scale size was set by the desire to limit the maximum potential gradient to about 100 kV/cm (our estimate of the breakdown limit) and resulted in a design ion-current density of 0.31 A/cm^2 for a pure D^+ beam, or about 0.25 A/cm^2 for a beam with a realistic mixture of D^+, D_2^+ and D_3^+. The design shown in Fig. 4 was optimized, using the WOLF code,[9] by varying the shape of the first, beam-forming, electrode and the potential of the second, gradient-grid, electrode. The shapes of all electrodes except the first were chosen to minimize energy deposition in the structure by secondary particles created by ionization of the background gas or by secondary emission from grid surfaces.

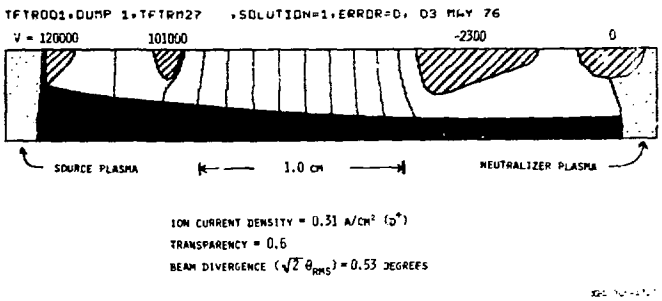

Figure 4. Calculated beam trajectories and equipotentials for a 120-kV accelerator.

The module (Fig. 2) consists of an outer, vacuum-wall insulator that is sectioned to distribute the potential gradients; to keep these insulators reasonably short, the outside of this insulator is pressurized with two atmospheres (absolute) of SF_6 gas. The plasma source and grid assembly are mounted on an inner plug-in structure (Fig. 5). The tubular insulators to which the grid assemblies are mounted also carry de-ionized cooling water to the plates that support the final three grid arrays; cooling for the first (beam-forming) grid is obtained from the plasma-source chamber. The 8-cm long grid rails, arranged in a 10-cm-wide array, are end cooled. The solid molybdenum rails are brazed to a fixed support on one end, forming a comb-shaped structure, and allowed to expand in the long direction to prevent buckling when heated.[7,8] The heat is conducted away in the 1-min interval between pulses.

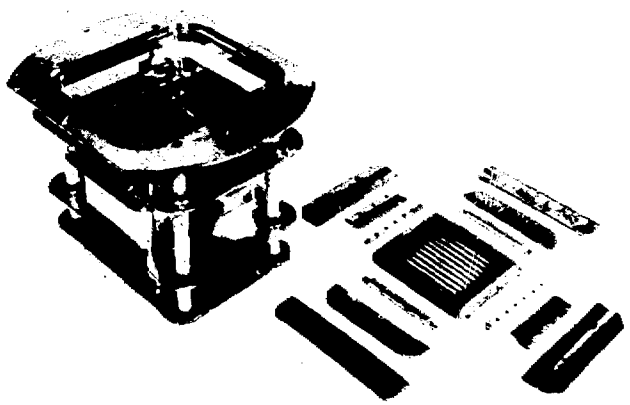

Figure 5. Photograph of the accelerator plug-in structure and one of four multi-slot grids.

The neutralizer to which this structure is attached is constructed of iron to shield the beam from stray magnetic fields. It has an internal cross section of 20 cm x 30 cm and is two meters long. D_2 gas emerging from the plasma generator through the grids produces a line density of $\sim 10^{16}$ molecules/cm^2 ($\sim$0.5 Pa-m) in this section.

The beam is stopped by a copper-plate calorimeter, instrumented with an array of thermistors, located 8.5 m from the grids. The beam divergence is determined from the shape of the heat pattern on the calorimeter[5]; the plate is water cooled in the 1-minute interval between shots.

A deflection magnet, located between the neutralizer and the calorimeter, can be used to sweep the ions out of the beam. An instrumented ion dump, similar to the calorimeter, is used to determine the focusing effects of the magnet (and possibly space charge) on the ions.

Two structures of type shown in Fig. 2 have been operated up to 120 kV with 0.5-sec pulses. In the first (Mark I) the rails of the first two grids, beam-forming and gradient-grid, were curved to an 8.5-m radius to focus the beam in the direction parallel to the slots. The second structure (Mark II) had planar grid arrays.

A typical beam-pulse sequence is as follows: The water to the calorimeter is turned off and the diagnostic computer receives a signal to record the pre-shot thermistor temperatures on the calorimeter. Approximately 5 sec later the filament-power supply is turned on; approximately 2 sec later the filaments have reached their emission temperature and gas is pulsed into the plasma chamber. Within 20 msec the arc-power supply is turned on. When the discharge has stabilized ($\sim$50 msec after the supply has been turned on) the accelerator voltage is applied to the grids by firing the series switch.[3,4] The potential for the gradient grid is obtained from the accelerator power supply by means of a resistive voltage divider; the suppressor supply is slaved to the accelerator supply in that it is gated on by a signal from the high-voltage divider. The rise time of the potentials applied to the three grids is approximately 30 µsec. When any of a number of fault sensors is activated (drop in high voltage below a preset threshold, loss of voltage across the first gap, excessive suppressor current, excessive gradient-grid current, etc.) the series switch is "opened" by firing the shunt switch.[3,4] This removes all high voltage from the grids; the discharge, however, is not turned off. After a preset "interrupt" time, typically 21 msec, the series switch is again fired and the sequence is repeated. At the end of the 0.5-sec pulse all power supplies are turned off. Approximately 5 sec later the final temperatures of the calorimeter thermistor array are recorded by the computer, and the calorimeter water is turned on to cool the plates.

A saturable-core reactor[3,4] dissipates much of the energy stored in the stray capacitance of the power supplies and cables; the stored energy delivered to the grids by a spark is approximately 2 J (the energy stored in the capacitance of the module). We have tried to determine the maximum stored energy allowed without adversely affecting operation of the module by adding capacitance to the source. Very preliminary results indicate that source performance is degraded when more than 7 J are dissipated in a spark.

Operation of the module by interrupting only the grid voltages and leaving the discharge on permits rapid re-starts. It does, however, cause a problem when the potentials are applied to the grids: Without any potential difference between the grids, ions and electrons from the discharge fill the grid region; when the potentials are applied, these ions and electrons must be swept out of the gaps (possibly emitting secondary electrons as they strike the grids) resulting in large currents from the power supply. If the power supply is not capable of providing the extra current this can load down the supply and prevent the required potentials from being applied to the grids -- which in turn gives rise to large currents, and so on. We have found that we can minimize this effect by "step-starting" the discharge: An RC circuit, with a time-constant of about 20 µsec, in series with a thyristor, is connected in parallel with the discharge; when the high-voltage series switch is fired, this thyristor is also fired to shunt the discharge current until the capacitor is charged. Because of the rapid deionization time (sub µsec) of the discharge, this puts a corresponding dip in the plasma density and thus decreases the ion and electron density in the grid region, minimizing the current surge when the voltages are applied to the grids. The recovery time of the plasma density in the discharge is comparable to the RC time of the circuit.

Typical operating parameters for both the Mark I and Mark II structures are given in Table I. The quoted beam widths, $\parallel$ and $\perp$ to the slots of the accelerator grid, were obtained from the temperature profile of the calorimeter located 8.5 m from the grids. The temperature profile was found to be bi-gaussian, i.e. of the form $A \exp-(x/x_0)^2 \exp-(y/y_0)^2$, so that it is possible to characterize the beam width by two parameters, x_0 and y_0; we express these parameters as angles with respect to a point source located at the center of the grid array (no correction is made for the finite size of the source). Since the 8.5-m-radius grids of the Mark I structures focus the beam (in the direction parallel to the slots) at 8.5m, the parallel beam width of the Mark I structure is narrower than that of the Mark II (flat-grid) source.

The parameters given in Table I are for beams tuned for minimum divergence by adjusting the plasma density for a fixed set of grid potentials. The perpendicular beam width, as well as the gradient-grid and suppressor currents, increase drastically if the plasma density deviates from the optimum value by more than $\pm$ 10%.

TABLE I. 120-kV 0.5-sec PERFORMANCE CHARACTERISTICS OF TWO TEST MODULES WITH 8-cm x 10-cm ACCELERATOR-GRID ARRAYS. THE PARAMETERS LISTED ARE FOR BEAMS TUNED FOR MINIMUM DIVERGENCE (SEE TEXT).

	Mark I	Mark I	Mark II
Gas	H_2	D_2	H_2
Gas flow (T-L/sec)	4	7	7
Accelerator Current (A)	13	10	14
Gap 1 voltage (kV)	23	23	19
Gradient-grid current, electrons to grid (mA)	10	10	40
Suppressor Voltage (kV)	2.8	2.8	2.3
Suppressor Current (A)	1.0	0.9	1.2
1/e beam width[a] measured at 8.5 m:			
$\perp$ to slots	$\pm$1.34°	$\pm$1.28°	$\pm$1.24°
$\parallel$ to slots	$\pm$0.42°	$\pm$0.42°	$\pm$0.76°
Arc power (kW)	25	19	23
Filament power (kW)	18	18	18

[a] SEE TEXT

Operation with deuterium was limited because of the large neutron fluxes produced by d-d reactions between the energetic deuterium ions of the beam and deuterium atoms buried in the copper calorimeter. The reaction rate built up gradually as the copper was loaded with deuterium from successive beam pulses. After approximately one-hundred 120-keV beam pulses the neutron-production rate reached an asymptotic value -- approximately 10^{11} neutrons/sec during a beam pulse.

Topics such as reliability, grid heating, molecular-ion composition of the beam, and improvements in beam optics are being investigated.

Based on the R and D effort described above, LBL/LLL engineering groups have designed and started construction of complete prototype injection lines for the PPPL TFTR tokamak[10] and the GA DIII tokamak.[11] Testing of these prototypes is scheduled to start in a little over a year.

Summarizing the positive-ion based program, we note that enormous progress has been made in the last five years, and experimental modules are operating in an energy range that may be suitable for fueling some fusion devices. However, there is a great deal of work to be done before the present systems can be described as reliable components on which reactor engineers can base designs and cost estimates. In addition to emphasizing reliability and gas/electrical efficiency, we will work toward dc operation, and perhaps higher voltages, during the next few years.

III. The Negative-Ion System Status

As mentioned earlier, negative-ion based systems, whether predicated on direct extraction of negative ions from sources, or conversion of positive ions to negative, is still in the R and D stage and will not be discussed here. Our efforts are mainly directed toward experimental and theoretical studies of methods of producing, transporting and accelerating negative-ion beams. The main investigation at present is based on implementation of a conceptual design for a 200-kW, $\geq$ 5-A D^0, dc (1-MW) system. Negative ions are being produced by double charge exchange of $\sim$ 1 keV. The demonstration of the 200-kV, 1-MW dc D^0 beam is presently scheduled for about 1980.

References

1. J. M. Haughian et al., Proc. Sixth Symp. on Engineering Problems of Fusion Research, San Diego, Ca., 1975, (IEEE Nuclear and Plasma Science Society, 1975), p. 53.

2. K. W. Ehlers et al., Proc. 9th Symp. on Fusion Technology, Garmisch, Germany, 1976, (Pergamon Press Oxford, 1976), p. 795.

3. D. B. Hopkins et al., Proc. 9th Symp. on Fusion Technology, Garmisch, Germany, 1976, (Pergamon Press, Oxford and New York, 1976), p. 897.

4. H. M. Owren, W. R. Baker, D. B. Hopkins, and R. C. Acker, "The Lawrence Berkeley Laboratory Power Supply System for Neutral Beam Source Development," Proc. Seventh Symp. on Engineering Problems of Fusion Research, Knoxville, Tenn., 1977.

5. C. F. Burrell et al., "Calorimetric and Optical Beam Diagnostics on the LBL 120-keV Neutral Beam Test Facility," ibid.

6. K. W. Ehlers, "Rectangularly Shaped Large Area Plasma Source," ibid.

7. J. A. Paterson et al., "The Design and Fabrication of an Ion Accelerator for TFTR-Type Neutral Beam Systems," ibid.

8. L. A. Biagi and J. A. Paterson, "On Fabrication and Brazing of 120-kV, 65-A, 0.5-Sec Accelerator Grid Assemblies," ibid.

9. W. S. Cooper, K. Halbach, and S. B. Magyary, Proc. of the Second Symposium on Ion Sources and the Formation of Ion Beams, Berkeley, Ca, 1974, p. II-1.

10. "TFTR Neutral Beam Injection System Conceptual Design," Lawrence Berkeley Laboratory Report LBL-3296.

11. A. P. Colleraine et al., "The Doublet III Neutral Beam Injection System," Seventh Symp. on Engineering Problems of Fusion Research, Knoxville, Tenn., 1977.

NEUTRAL BEAM INJECTION EXPERIMENTS AT ORNL: FUELING ASPECTS*

G. H. Neilson and J. F. Lyon

Oak Ridge National Laboratory
Oak Ridge, Tennessee 37830

Summary

The Oak Ridge National Laboratory (ORNL) neutral beam injection program, beginning with the Oak Ridge Tokamak (ORMAK) and continuing with the Impurity Study Experiment (ISX), is reviewed. The emphasis of these experiments has been on plasma heating, but some insights into the fueling issue have been provided as well. However, there is no conclusive evidence as yet for any significant impact of injection on the plasma particle balance.

I. Introduction

Experiments on ORMAK and other devices have established neutral beam injection as a viable scheme for plasma heating in tokamaks.[1,2] From perturbation levels of 45 kW in 1972, injection power into ORMAK was increased to 360 kW in 1976, providing the first demonstration of injection-dominated ($P_{inj} > P_{OH}$) tokamak operation. The program will continue in 1978 with the installation of 1.8 MW injection on ISX. This device is expected to produce high-$\bar{R}$ plasmas by means of very intense neutral injection ($P_{inj} >> P_{OH}$).

In Section II of this paper we review the major results of injection experiments on ORMAK, which were concerned primarily with ion and electron heating and with the effects of injection on other plasma properties (density, confinement, Z_{eff}, etc.). Specific results which bear upon the fueling issue are also discussed. In Section III, we briefly summarize the experimental plans for ISX-B, which include a test of ripple injection. In Section IV, we discuss the applicability of injection to plasma fueling.

II. The ORMAK Injection Program

The ORMAK device had provision for four tangential injectors, two parallel and two antiparallel to the plasma current, as shown in Fig. 1. These were initially 25-kV, 4- to 6-A sources developed at Oak Ridge. Through optimization and upgrading, we ultimately obtained as much as 360 kW of delivered power from two injectors operating near 30 keV.[3]

Ion temperature was found to increase roughly linearly with injected power, as Fig. 2 shows.[2] Within the uncertainties in the measurement, the scaling is consistent with our theoretical understanding of beam trapping and slowing down and of ion heat conduction.

In all of these scaling studies, ohmic heating was the primary source of plasma energy. At the high power end of Fig. 2, the injection contribution to the power balance becomes significant, to the extent that the temperature of the ions exceeds that of the electrons. As Fig. 3 shows, the power flow between electrons and ions is reversed under such conditions. Finally, we enter another important regime by reducing I_p so that $P_{inj} > P_{OH}$. Here, we find that (after

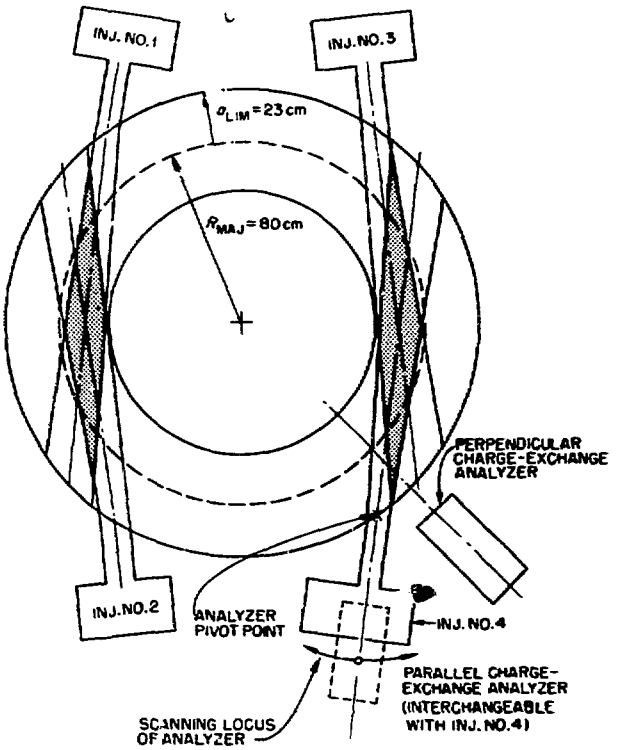

Fig. 1. ORMAK injector layout. ORMAK had provision for two co- and two counterinjectors.

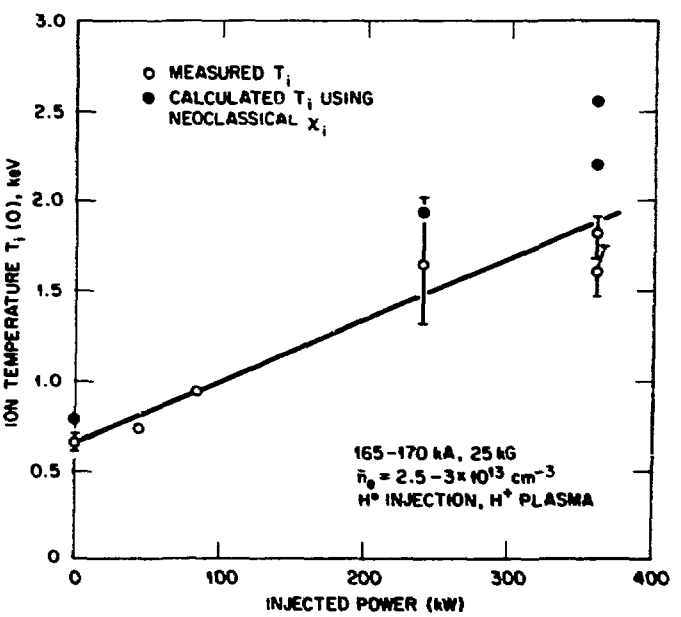

Fig. 2. Ion temperature scaling was roughly linear with power in ORMAK, consistent with neoclassical calculations. Error bars and scatter indicate uncertainties in determining ion temperature from charge-exchange neutrals in the presence of injection.

*Research sponsored by the Department of Energy under contract with Union Carbide Corporation.

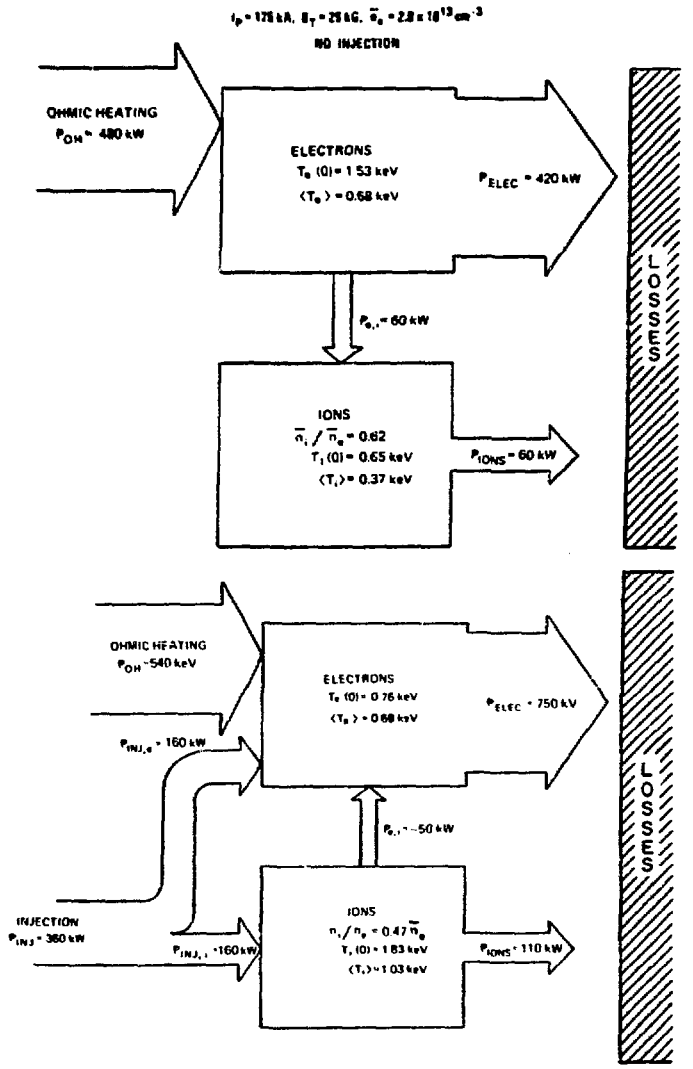

Fig. 3. Injection drastically alters the power balance in the plasma from that obtained with ohmic heating alone. The figure shows 360 kW (2/3 co-, 1/3 counterinjection), $T_i < T_e$, and power flows from ions to electrons; electron energy losses are also greater.

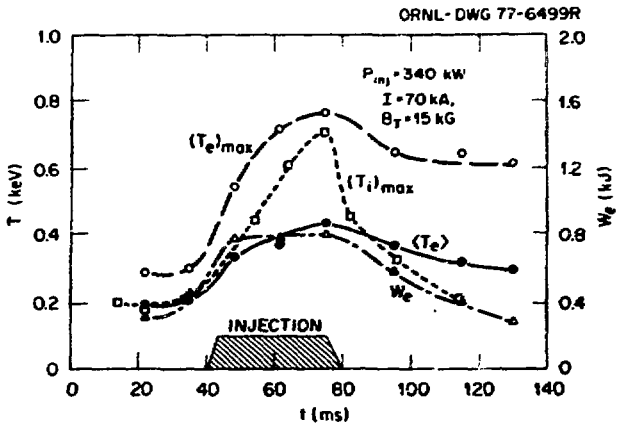

Fig. 4. Electron heating by injection is observed when $P_{inj} > P_{OH}$ and impurities are reduced (from Ref. 4).

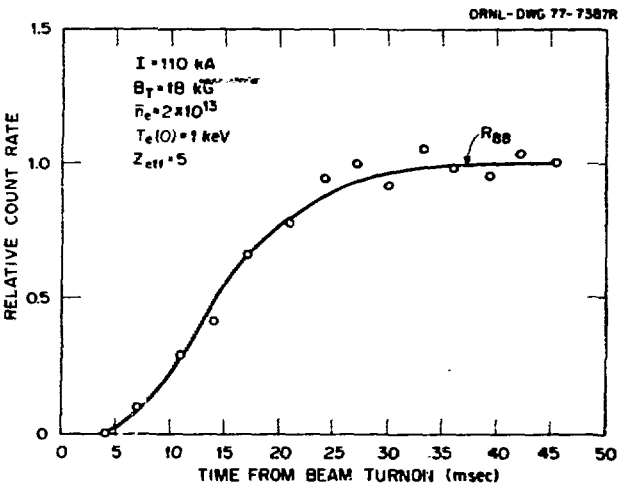

Fig. 5. Neutron production rates measured and calculated from a deuterium beam slowing down in a hydrogen plasma. Beam deuterons react with already trapped slowing-down deuterons (from Ref. 6).

impurity levels are sufficiently reduced) it is possible to obtain beam heating of electrons as well as of ions; the time dependences of ion and electron temperatures for this experiment are shown in Fig. 4.[4]

The results of these experiments on ORMAK imply that injection can be a dominant power source, greatly exceeding ohmic contributions, in future tokamak experiments. It is then appropriate to ask whether it might be an important particle source as well. In the 360-kW ORMAK case, the total injected beam current from the three energy constituents was about 19 A. This corresponds to a volume-averaged gross particle deposition rate, $\dot{\bar{n}}_b$, of 1.2×10^{14} cm^{-3} s^{-1}; for $\bar{n}_e \approx 2 \times 10^{13}$, the replacement time $\bar{n}_e/\dot{\bar{n}}_b$ is 170 ms. Since the beam pulse lengths were only about 50 ms, and since other sources such as cold gas from the drift tubes and enhanced impurity stripping were attendant with injection, it was not possible to determine any net contribution of beam particles to the bulk population.

A number of experiments were done in which we observed the slowing-down fast ion population. Figure 5 shows the neutron production rate from injected deuterium atoms interacting with already trapped deuterons in hydrogen plasma.[5] The observed temporal behavior is consistent with calculations which assume that the primary beam reacts only with other fast deuterons that have scattered in angle but have not lost much energy. However, it is inconsistent with any buildup of "stopped" beam particles joining the bulk plasma. In Fig. 6, relative perpendicular charge-exchange spectra in the fast ion band are plotted comparing co- and counterinjection cases in low current discharges. Coinjected fast ions are better confined and are more likely to survive the slowing-down and scattering process to a 90° pitch angle as this figure indicates. Both of these observations are consistent with particle orbit and Fokker-Planck calculations, supporting the conclusion that beam trapping and slowing-down phenomena are well understood at this time.

To complete the picture for an understanding of beam refueling requires knowledge of particle confinement mechanisms and how they are affected by injection. Local background replacement rates computed from neutral densities [$n_0(0) \approx 10^8$ cm^{-3}] in ORMAK are quite low, suggesting long effective particle lifetimes. The rapid uniform density increase observed with gas puffing suggests the presence of a strong inward plasma transport mechanism, and we note that density

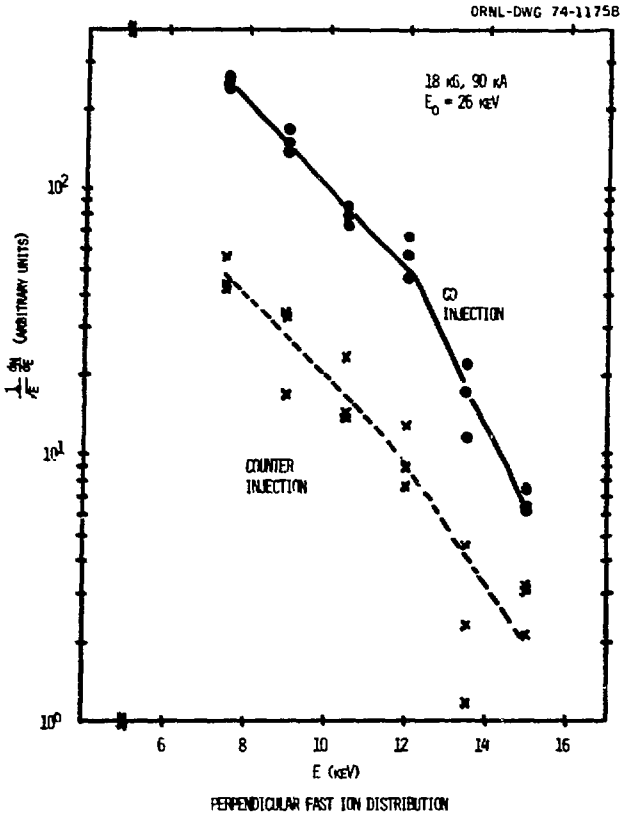

Fig. 6. In low current discharges, coinjected ions are better confined than counterinjected ions. This is predictable from particle trajectory calculations.

limits with gas puffing are apparently raised by injection, as Fig. 7 indicates. However, beyond such evidence there is as yet no coherent understanding of particle confinement and transport.

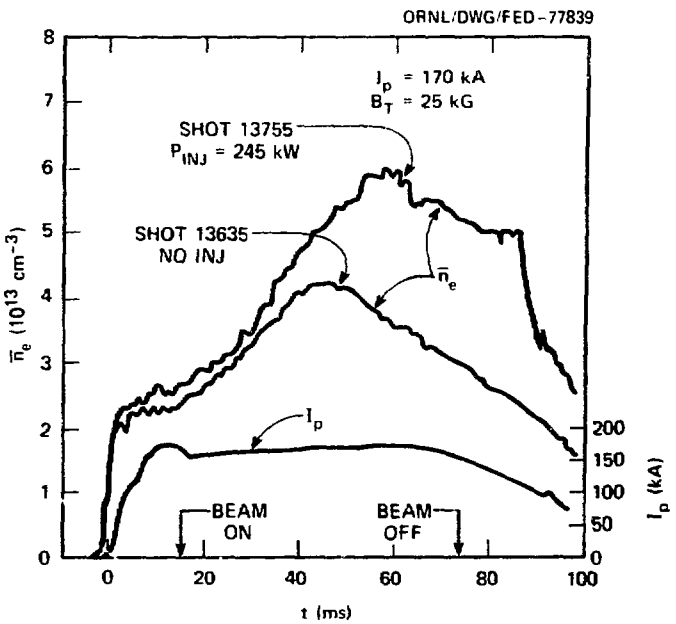

Fig. 7. Injection apparently raises the disruptive limit on density obtainable with gas puffing.

III. The ISX Injection Program

In 1978, the ISX device will be upgraded by the installation of a new heavy-duty liner, a more sophisticated poloidal field system, and two neutral beam injectors. The injectors are 40-kV, 60-A sources of the type developed for the Princeton Large Torus (PLT) and will deliver up to 1.8 MW of total coinjected power to the plasma (a planned source upgrade will increase this to 3 MW). Table I summarizes the parameters of this device, designated ISX-B.

Table I. ISX-B parameters

Device	
Major radius, R_o	92 cm
Minor radius, a	27 cm
Elongation, ε (b/a)	1.5
Volume	2.3×10^6 cm^3
Maximum toroidal field, (B_T/R_o)	1.8 T
Maximum plasma current, I_p	200 kA
Iron core	0.9 V-s
Injectors	
Number	2
Type	Coinjection
Beam energy, E_{inj}	40 keV
Beam power, P_{inj}	1.8 MW[a]
Beam species	40:20:13.3 keV
Beam power	85:12:3 = 100%
Beam current	38:11:4 = 53 A
N_b	23:0.7:0.3 = 3.4×10^{20} s^{-1}

[a] To be upgraded to 3 MW at a later date

The injection program on ISX-B is in some ways an extension of work begun on ORMAK. With P_{inj}/P_{OH} of up to 10, ISX-B will operate as a device which is clearly injection-driven. We plan, as a major aspect of the program, to test the β limits of such a device; average values of β exceeding 5% have been predicted. Impurity and surface work has already started on ISX-A and will continue in the upgraded machine as well.

An experimental test of ripple injection is also being prepared in collaboration with Princeton Plasma Physics Laboratory (PPPL). This scheme would reduce the energy requirements for beam penetration[6] and is thus important to the feasibility of beam fueling.

A layout of this experiment is shown in Fig. 8. An ORMAK 10-cm source located between TF coils beneath the device will produce up to 5 A of neutrals injected vertically at energies variable between 15 and 40 keV. At high densities ($\bar{n}_e \approx 10^{14}$ cm^3) and low beam energies ($E_{inj} \lesssim 20$ keV), beam trapping occurs near the edge of the plasma. A vertically asymmetric ripple produced by a pair of coils adjacent to the injector should enhance the upward transport of the trapped fast ions toward the plasma center. The effect will be measured in terms of increased central fast ion population, as inferred from charge-exchange neutrals when the ripple is turned on.

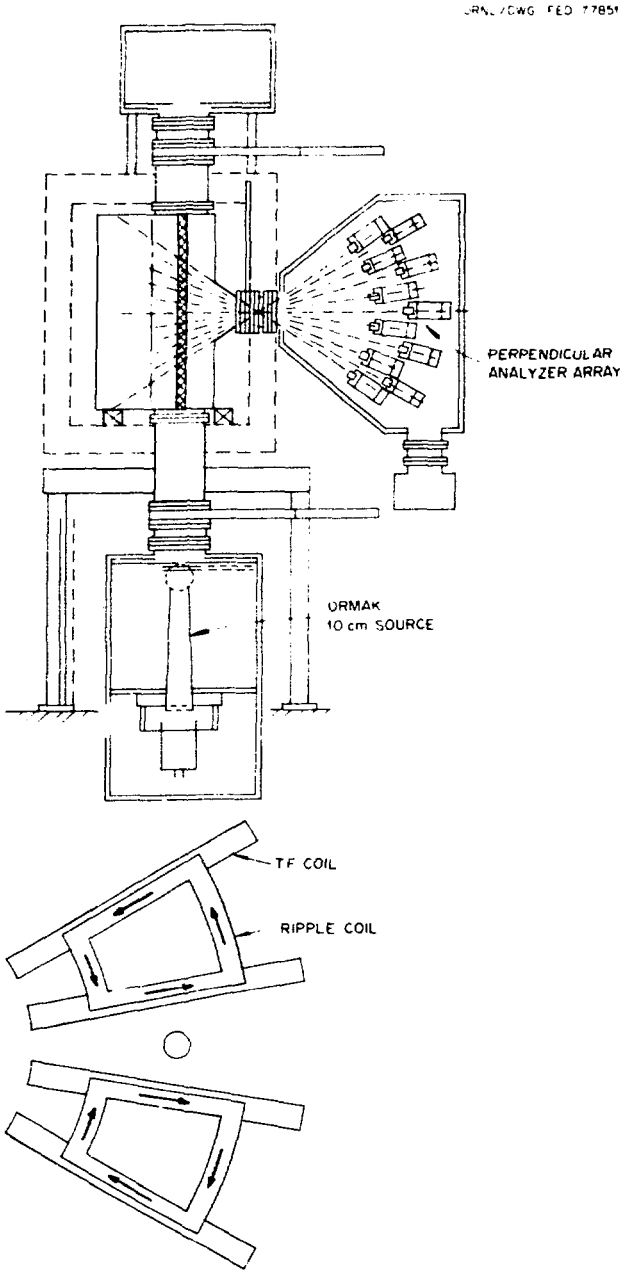

Fig. 8. Schematic layout of ripple injection experiment.

As one means of studying the particle deposition and confinement, ISX-B will employ mass-resolved neutral diagnostics. Ions introduced by puffing, injection, or pellets may then be identified by using a hydrogen isotope (H or D) different from that of the bulk plasma, and analyzing the resulting charge-exchange neutrals by both mass and energy. This feature will be especially valuable in the ripple injection experiment where the test beam deposition will be overwhelmed by that of the primary injectors.

IV. Conclusion

The ORNL injection program has been directed toward the goal of injection-driven tokamak operation. Emphasis has been on ion and electron heating with attention to the effects of injection on confinement, impurities, and bulk drifts. The results to date indicate that injection can serve as the primary power source to a tokamak plasma; this assumption will be further tested on ISX-B.

While injection can be a dominant power source, it does not necessarily represent a significant particle source in these experiments. The reason is that since injection energies are high for penetration requirements, beam currents $I_{inj} = P_{inj}/E_{inj}$ are correspondingly small. For example, we estimate the volume-averaged particle deposition, $\bar{n}_b$, for ISX-B with 1.8 MW of injection to be $\sim 1.4 \times 10^{13}$ cm^{-3} sec^{-1}. For this to sustain a density $\bar{n}_e$ of only 5×10^{13} requires effective bulk particle lifetimes of ~350 ms; there will very likely be observable local effects due to the peaked beam deposition profile, however. Injection would appear to offer the advantage of fueling the center of the discharge; however, results to date suggest that cold gas puffing does this just as well. For these reasons, the desirability of injection as a particle source would seem to depend on some or all of the following developments in the future:

1. Particle lifetimes turn out to be long enough that little replacement is needed.

2. It becomes necessary as a means of fueling the plasma center directly.

3. Energy requirements for penetration become reduced (e.g., by ripple injection), thereby permitting larger beam currents for a given power.

Acknowledgments

This report is a summary of work done on ORMAK and ISX. As such, it represents contributions from the entire staff of the Tokamak Experimental Program.

References

1. L. A. Berry et al., "Plasma Confinement in the ORMAK Device," *Plasma Physics and Controlled Nuclear Fusion Research* 1974, Vol. I, p. 101 (1975).

2. L. A. Berry et al., "Confinement and Neutral Beam Injection Studies in ORMAK," *Plasma Physics and Controlled Nuclear Fusion Research* 1976, Vol. I, p. 49 (1977).

3. O. B. Morgan et al., "The Development of Neutral Injection Heating for Large Tokamaks and Reactors at ORNL," paper presented at the Third Symposium and Workshop on Plasma Heating in Toroidal Devices, International School of Plasma Physics, Varenna, Italy, September 6-17, 1976.

4. M. Murakami et al., "Electron Heating by Neutral Beam Injection in the Oak Ridge Tokamak," *Phys. Rev. Lett.* 39(10), 1977.

5. A. C. England, H. C. Howe, J. T. Mihalczo, and R. H. Fowler, Neutron Time Behavior for Deuterium Neutral Beam Injection into a Hydrogen Plasma in ORMAK, ORNL/TM-6035, Oak Ridge National Laboratory, Oak Ridge, Tennessee (October 1977).

6. D. L. Jassby and R. J. Goldston, *Nucl. Fusion* 16(4), 613 (1976); R. Goldston, paper presented at this workshop.

Development of the TFTR Neutral Beam Injection System*

B.A. Prichard, Jr.
Plasma Physics Laboratory
Princeton University
Princeton, New Jersey 08540

ABSTRACT

The TFTR Neutral Beam Lines are designed to inject 20 MW of 120 keV neutral deuterium atoms into the plasma. This is accomplished using 12 sources, 65 amperes each, mounted in 4 beam lines. The 120 kV sources are being developed by LBL and a prototype beam line which will be tested at Berkeley is being developed as a cooperative effort by LLL and LBL.

The implementation of these beam lines has required the development of several associated pieces of hardware. 200 kV switch tubes for the power supplies are being developed by Eimac and RCA for modulation and regulation of the accelerating supplies. A 90 cm metallic seal gate valve capable of sealing against atmosphere in either direction is being developed for separating the torus and beam line vacuum systems. A 70 x 80 cm fast shutter valve is also being developed to limit tritium migration from the torus into the beam line. Internal to the beam line a calorimeter, ion dump and deflection magnet have been designed to handle three beams, and optical diagnostics utilizing the doppler broadening and doppler shift of light emitted from the accelerated beam are being developed by LBL.

The control and monitoring of the 12 sources will be done via the TFTR computer control system (CICADA) as will other parts of the machine, and software is being developed to condition and operate the sources automatically.

The prototype beam line is scheduled to begin operation in the fall of 1978 and all four production beam lines on TFTR in 1982.

I. INTRODUCTION

The goal of TFTR is to achieve reactor grade plasmas with significant D-T fusion reaction rates. To realize this goas will require the attainment of T_e, T_i ~5-10 keV, a maximization of plasma density, energy confinement times corresponding to $n\tau_E \sim 10^{13}$ to 10^{14} sec./cm^3 and the ability to utilize deuterium and tritium as plasma components. The TFTR will have a standard limiter aperture of a=85 cm, at R=248 cm. The toroidal magnetic field is B_t=5.2T and the available plasma currents are I=1.0-2.5MA. The standard discharge duration is 1 sec, but this can be extended to 4 sec. with B_t=4.5T.

The neutral beam injectors are designed to deliver 20MW of 120 keV neutral deuterium atoms to the plasma. In addition, 12-15MW of 60 keV and 40 keV beams will be injected also. The beam pulse length is presently .5 sec.

II. BEAM PARAMETERS

The TFTR neutral beam lines are being designed to utilize 65 ampere, 120 kV ion sources [1,2] which are being developed by Lawrence Berkeley Laboratory. These sources employ a magnetic field free plasma generator and slotted accelerating grids. There are four grids; the transparency of the accelerating grid structure is approximately 60%. The average current density produced by the plasma generator is .3 amperes/cm^2 and the emitting area is 10 cm x 40 cm. The sources produce an elliptical beam and the measured 1/e half width divergence[3] is ~1.3° perpendicular to the slots and ~.4° parallel to the slots. The area of the source is chosen to give the desired current of 65 amperes when accelerating a deuterium beam to 120 keV. If one were to run hydrogen, the area of the source would be reduced to limit the current to the desired level.

To provide 20 MW of full energy neutrals, 12 sources will be used on TFTR. They will be mounted in four beam lines. Six injection ports are available on the TFTR, four are for co-injection and two for counter-injection. This allows for balanced injection of the four beam lines (2 co- and 2 counter) or all four co-injecting. Also, if necessary, an additional 2 beam lines could be mounted on the machine at a later date. One of these possible arrangements is shown in Figure 1.

*This work performed under the auspices of the U. S. Department of Energy

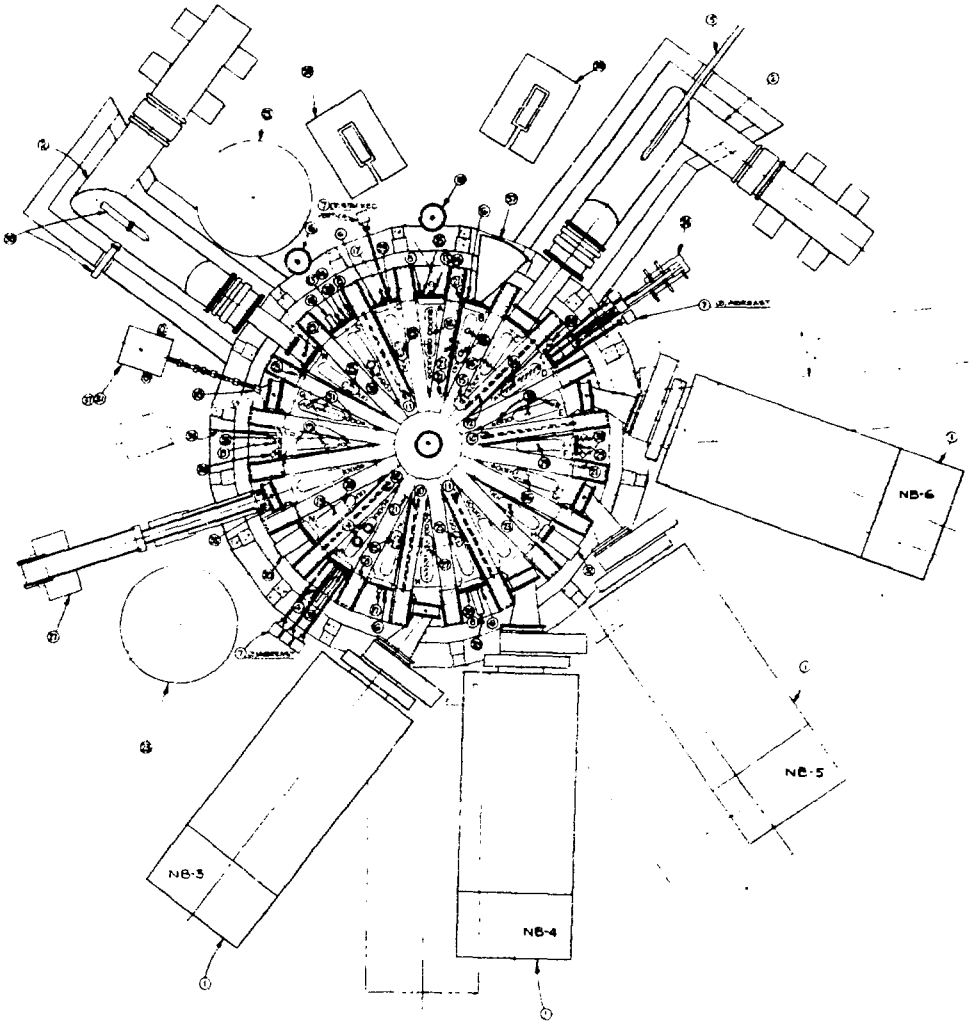

Figure 1 Plan view of TFTR showing various diagnostics positioned about the tokamak and four beam lines mounted for tangential co-injection. The beam lines can be pivoted to any angle between the position shown and perpendicualr injection.

The injection ports are nearly rectangular in shape, 40 cm wide and 80 cm tall. The connecting duct between the beam line and the torus vacuum vessel contains a flexible joint. This joint allows the beam line aiming angle to be changed by 10° without opening either vacuum system. Adapters can be installed to change the aiming angle beyond the 10°, and the injection port is sized such that the injection angle can be changed from perpendicular injection to a tangential injection at a radius of 265 cm, or a total movement of 37°, without restricting the 40 x 80 cm^2.

The large injection port is taken advantage of to reduce the peak beam power density. This is done by eliminating source focusing, or using flat grids, so the emitting surface is flat rather than concave. This reduces the central power density of the beam from 40 kW/cm^2 to 22 kW/cm^2 with only a small increase in the beam size. The calorimeters and ion dumps are angled to reduce this power density to 1-3 kW/cm at the surface.

Using inertial beam dumps at power densities of ~2 kW/cm^2 allow pulse lengths of ~3 sec. The present sources are specified for .5 sec pulses, but it is hoped that this can be extended to 1-3 sec.

III. SOURCE R & D

LBL has successfully operated a 1/4 area test source[4] at 120 kV. This source features a 10cm x 10cm extraction area. The grids used in the test source are identical to those used in a full size source; they are constructed of molybde-

num rods machined in specific shapes. They are brazed at one end to a header, and the other end is free to move to accomodate thermal expansion.

The internal insulators on the test source are alumina surrounded by SF_6 (2 atm). The SF_6 is contained in fiberglass vessel which is the external insulator of the source. The ceramic insulators for the full area source are under development and are proving to be somewhat difficult due to their large size and rectangular shape. Both alumina and machineable glass ceramic are being considered for this purpose.

IV. MECHANICAL BEAM LINE

A TFTR beam line is shown in Figure 2. The vacuum chamber is 4.5 m tall, 5.7 m long and 3 m wide. Both sides of the beam line are covered with 4.5°K cryocondensing panels. Their area is ~34 m^2 and the expecting pumping speed is ~3 x 10^6 l/s. All of the components of the beam line are mounted on large flanges and can be removed with the flange to facilitate remote handling requirements. The 3 ion sources and neutralizers mount on a common flange at the rear of the beam line; however, each source has its own isolation valve and can be removed individually without disturbing the vacuum. The three aperture bending magnet and ion dump are mounted from a large flange in the top center of the beam line, and the calorimeters on a similar flange at the front of the beam line. The cryopanels are suspended from the lid of the beam line vacuum chamber, which is removeable, allowing one to lift the entire cryopanel array out of the beam line.

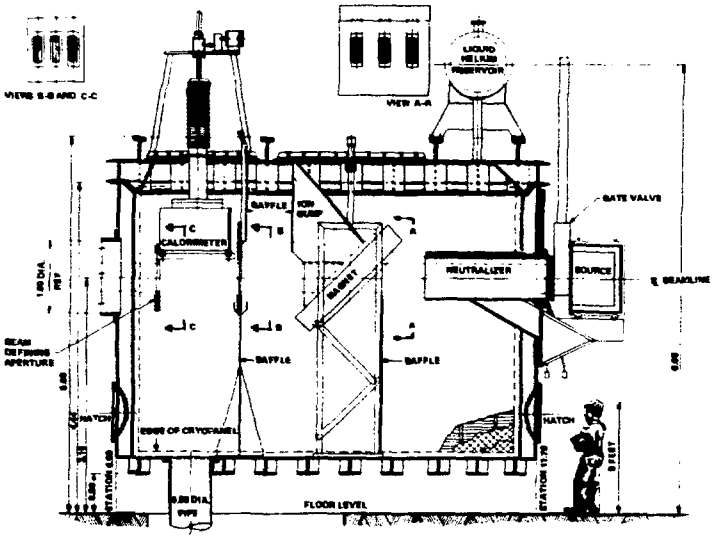

Figure 2 Side elevation of a TFTR Neutral Beam Line. Unspecified dimensions are given in meters. Three sources are mounted side by side at the rear of the beam line, and seperate neutralizers, magnet apertures and calorimeter sections are provided for each beam.

The cryopanels are constructed from 2 sheets of stainless steel which are edge welded and spot welded at regular intervals across the area of the sheets. The unit is then pressurized to inflate the sheets into a quilted pillow-like form. The back of the LHe filled panel is shielded by a similar structure at 77°K and the front is shielded by blackened copper chevrons also at liquid nitrogen temperatures.

The beam dumps are the inertial type and are constructed of 3/4 in. copper plates with cooling lines brazed to the back side. They are angled with respect to the beam to decrease the incident power density by a factor of ~7.

The ion deflection magnet is a transmission magnet angled at 45° to the beam. The full energy ion component is deflected upward at an angle of 60°. The three apertures are angled with respect to one another to accomodate the 3 converging beams and the field in each gap can be controlled independently. Field clamps are used to reduce the effects of the fringe fields. Edge focusing gives a crossover in the beam near the exit of the magnet and the beams are diverging strongly as they enter the ion dump.

The ion sources are located ~8.5 m from the torus vacuum vessel, and a duct nearly 3m long joins the beam line and torus vacuum systems. In addition to the flexible joint, this duct contains an absolute gate valve, a fast shutter valve, and remotely operable connecting joints. Each of these items are a subject of research and development efforts.

The absolute gate valve is an all metal, bakeable to 250°C, valve capable of sealing against atmosphere in either direction. The specified maximum leak rate is 10^{-9} Torr·l/s and minimum life is 800 closures. It employs a radial or belville spring sealing mechanism and features dual gates with interstitial pumping. The diameter of the aperture is 90 cm.

The fast shutter valve has an aperture 70cm wide and 80cm tall. The purpose of the valve is to minimize the amount of tritium that would drift from the torus and be condensed on the beam line cryopanels. The time required from when the valve aperture begins to be obscured to when the aperture is covered is 50 msec, however, 50 msec are used to

start the gates moving and 50 msec are used to decelerate the gates to a stop. Therefore, the total cycle time is 150 msec. The leakage conductance past the shutter valve when in the closed position is 10 l/s. The gates are constructed to prevent eddy current problems and allow free movement in the stray field of the TFTR. They can also withstand a differential pressure of 200 Torr.

V. NEUTRAL BEAM POWER CONVERSION SYSTEM

Each ion source will be powered independently. The arc and filament supplies float at high voltage and are tailored to the Berkeley Ion Source (4000A, 60V arc and 6000A, 13V filaments). The accelerating supplies[5] will employ a series modulator-regulator tetrode, as shown in Figure 3. This is a 200 kV 65 ampere tube being developed by RCA[6] and Eimac[7]. The anode, located in the center of the tube and surrounded by the cathode guns, is capable of dissipating 2MW and is cooled by high velocity high pressure water. The anode segments are angled with respect to the electron beam so that the peak power density is 700W/cm^2.

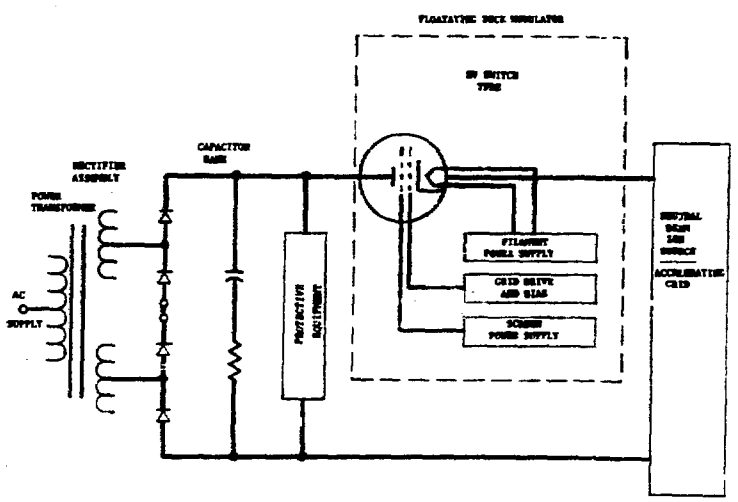

Figure 3 A simplified diagram of the TFTR Neutral Beam Power Conversion acceleration supplies. Modulation and regulation is accomplished by a 200kV, 65 A series tetrode presently under development.

In addition to the 120 kV, the supply also provides ~100kV for the gradient grid of the ion source. A separate supply is used for the suppressor grid and the fourth grid is maintained at ground potential. To increase the flexibility of the accelerating supplies, they will be capable of running with either a positive or negative ground. The supplies are capable of 5.0 sec pulses at a duty cycle of .033.

The plasma source supplies will be located in the basement directly under the ion sources. The distance from these supplies to the source is ~20 ft. The accelerating supplies will be located in a building adjacent to the test cell at a distance of ~100 ft. from the ion sources. This arrangement minimizes the stored energy in the capacitance of sources, supplies and transmission lines within the constraints imposed by buildings and availability for maintenance. This stored energy, if not kept to a minimum, can seriously damage a source during a spark-down.

To additionally protect the source, a series impedance in the form of a transformer core snubber[8] will be employed near the source. By passing all source leads through such a core stack, the stored energy can be absorbed in the cores during a spark and damage to the source prevented. The volt seconds of the core should be large enough to accommodate the stored energy than can be delivered to the source in the event of a spark.

Some of the most difficult problems to eliminate in a neutral beam power supply are fast transients which occur during source sparks. It has been found that after running a supply satisfactorily on a dummy load the interactions with a source reveal new problems which must be solved. Likewise, the problem of cross-talk between adjacent supplies and sources complicate this problem.

VI. CONTROLS AND DIAGNOSTICS

The TFTR Neutral Beam Lines will be computer controlled by the TFTR control system, CICADA. The beam line devices interface with local CAMAC hardware, and where needed local microprocessors will be provided. The CAMAC crates in turn are linked to subsystem computers of which one (or more if needed) will be dedicated to the neutral beam lines. The subsystem computers in turn are linked to four large central computers. The subsystem computers handle real time monitoring and control; the central computers provide servicing for the operating consoles and off line data analysis and program preparation. One of the four, the operations computer supervises the activities of the total system. A shared memory will be used with the central computers for the data pool and for intercomputer communication.

In addition to controlling and monitoring the beam line subsystems, a number of beam diagnostics will be processed by CICADA. These include arrays of thermistors embedded in the calorimeters and ion dumps for measuring beam

power and profiles, and optical diagnostics[9] for determining beam divergence, aiming and species. The divergence can be determined by measuring the doppler broadening of D_α light emitted by the beam. Similarly, the doppler shift can be used to separate the differnet energy components of the beam and the relative light intensities coupled with the proper cross sections can be used to calculate the ratio of D^+ to D_2^+ to D_3^+ contained in the beam.

These systems provide redundant means of measuring the beam properties and will provide valuable information for beam injection experiments on TFTR.

VII. SUMMARY

The TFTR beam lines, which are scheduled to operate in 1982, will employ a large number of items which are presently in the research and development stage. These include, but are not limited to, the sources themselves, 200 kV switch tubes, 90cm metal seal gate valves, fast shutter valves, beam dumps and various types of beam diagnostics. To a large extent, future beam lines will be affected by the problems and promises of the TFTR neutral beam injection system and the development projects it is based on.

One can assume that future beam lines will look for greater power and higher energies as TFTR in itself is a significant extrapolation over existing machine beam capabilities. The operating experience with the prototype beam line and then the production units will provide valuable information as to what future beam lines may be like.

REFERENCES

1. L.C. Pittenger, R.R. Stone, L.E. Valby, L.R. Pedrotti, to be published in Proceedings of Seventh Symposium on Engineering Problems of Fusion Research, Knoxville, October, 1977.

2. K.W. Ehlers, to be published in Proceedings of Seventh Symposium on Engineering Problems of Fusion Research, Knoxville, October, 1977.

3. K.H. Berkner, W.S. Cooper, K.W. Ehlers, R.V. Pyle, to be published in Proceedings of Seventh Symposium on Engineering Problems of Fusion Research, Knoxville, October, 1977.

4. K.W. Ehlers, K.H. Berkner, W.S. Cooper, J.M. Haughian, W.B. Kinkel, B.A. Prichard, Jr., R.V. Pyle, and J.W. Stearns, Proceedings of the Ninth Symposium on Fusion Technology, Garching, 1976, (Pergamon Press, Oxford, 1976), Vol. 1, page 795.

5. A. Deitz, H. Murray, and R. Winje, to be published in Proceedings of Seventh Symposium on Engineering Problems of Fusion Research, Knoxville, October, 1977.

6. J.T. Mark, and J.A. Eshlemen, Proceedings IEEE International Pulsed Power Conference, 1976, (IEEE, New York, 1976), IC5-1.

7. D.H. Priest, IEEE Conference Record of 1976 Twelfth Modulator Symposium, (IEEE, New York, 1976).

8. J.H. Fink, W.R. Baker, and H.M. Owren, "Analysis and Application of a Transformer Core Which Acts as an Arc Snubber" Lawrence Livermore Laboratory Report UCRL-79016 (1977).

9. C.F. Burrel, W.S. Cooper, and W.F. Steele to be published in Proceedings of Seventh Symposium on Engineering Problems in Fusion Research, Knoxville, October, 1977.

SUMMARY OF FUELING BY NEUTRAL BEAMS

D. L. Jassby
Princeton Plasma Physics Laboratory
Princeton, NJ 08540

General Considerations

Injected neutral beams supply energy, particles, and momentum to a plasma, while the thermalizing fast ions also increase the fusion reactivity by beam-target or hot-ion reactions. Magnetic mirror machines take advantage of all of these features, with the exception of the momentum input. Neutral-beam injection into toroidal plasmas has been proposed – and has so far been utilized – mainly as a source of heat, and secondarily as a source of increased neutron production. Nevertheless, fueling by injected beams can also play an important role in toroidal plasmas, especially in the start-up phase of ignited plasmas, or for the quasi-steady maintenance of low-Q plasmas where the average ion energy may exceed the electron energy by a large factor.[1]

For steady-state fueling of a Maxwellian plasma where the particle-averaged temperature $\bar{T}_i = \bar{T}_e$ is maintained by beam injection and fusion alpha particles, the beam energy E_b must satisfy the requirement

$$E_b = \frac{\tau_p}{\tau_E} \frac{3\bar{T}_i}{1 + 0.2Q\, F_{alpha}} \qquad (1)$$

where τ_E and τ_p are the energy and particle confinement times, respectively, Q = (fusion power/injected power), and F_{alpha} is the fraction of fusion alpha energy deposited in the plasma. For tokamak plasmas, $\tau_p \lesssim 4\,\tau_E$. Thus even if $F_{alpha} = 0$, it is evident that E_b must be within an order-of-magnitude of $\bar{T}_i$. Hence the fundamental problem of steady-state fueling is to insure the penetration of low energy beams into the hot central plasma region. Figure 1 shows the maximum Q-value that could be obtained in a beam-fueled and beam-heated thermonuclear D-T plasma as a function of F_{alpha}, when $E_b = 6\times T_i$, and $T_i = T_e$.

Even when penetration is adequate – for example, in expanding-plasma start-up schemes,[2] or in ripple-assisted injection[3] – a lower limit to E_b is set by the following considerations:

(i) The required access area for injecting a large fueling current increases as E_b decreases.

(ii) Charge-exchange loss of fast ions decreases as E_b increases above 30 keV (D°).

(iii) If ripple injection is used,[3] the large ripple required at smaller E_b enhances radial diffusion of the faster members of the bulk-ion population.

Thus the practical *minimum* injection energy for fueling tokamaks of TFTR size or larger would seem to be $E_b \approx$ 60 keV, for both D° and T°. Hence the range of beam energy for fueling can be defined as 60 to 150 keV (D°) for large toroidal devices.

Several aspects of beam fueling were discussed in the formal presentations. J. Rome (ORNL) examined the problems of neutral beam penetration into large, dense plasmas. J. Fink (Livermore) emphasized the need to insure efficiency, reliability, and long life, especially when the beams must perform a variety of functions in steady-state operation, as in mirror machine plasmas. R. Pyle (LBL) discussed the directions of beam-injector development at LBL/LLL, particularly in the energy range of interest for fueling. G. Neilson (ORNL) described the beam-injection experiments on ORMAK (completed) and ISX-B (planned), with special emphasis on beam fueling. B. Prichard (PPPL) described the TFTR injector system, and indicated the extent of plasma fueling by the beams.

Beam Penetration Aspects

In his discussion of beam fueling of tokamak plasmas, J. Rome emphasized that perpendicular injection is essential to insure reasonable penetration of low-to-medium energy beams. At larger values of poloidal beta, the magnetic axis shifts outward and the flux surfaces of the plasma are compressed, thus easing the penetration problem. It is also generally easier to provide access for perpendicular (rather than tangential) injection. When toroidal-field ripple $\gtrsim$ 1% is present near the outside of the plasma, it is necessary to inject at 10 to 15° from the normal, in order to avoid the trapping of fast ions in local magnetic wells, with consequent vertical drift out of the plasma.

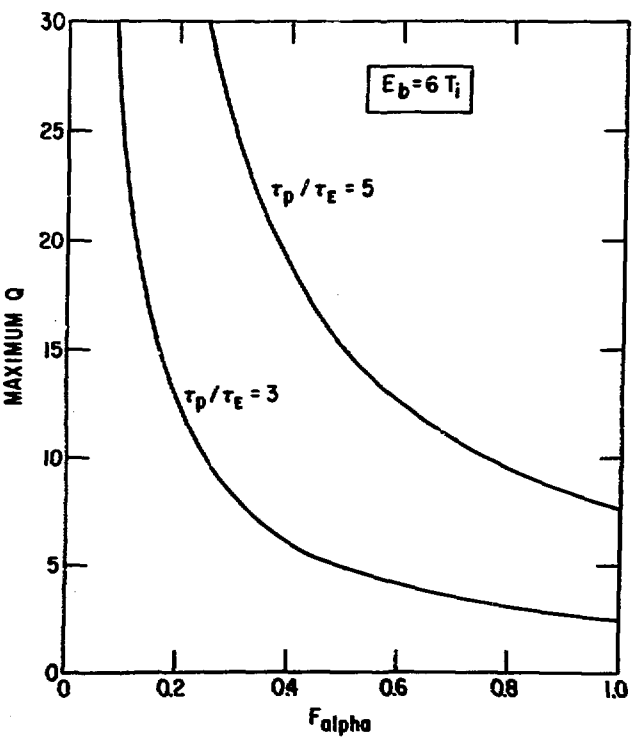

Fig. 1. Maximum possible fusion power multiplication Q in a D-T plasma fueled by beams with energy $E_b = 6\,T_i = 6\,T_e$. F_{alpha} is the fraction of fusion-alpha energy deposited in the bulk plasma. (776191)

Until about 1 year ago, it was thought that the impact-ionization cross section for hydrogenic atoms on impurity ions of charge Z_j varied as Z_j^2, and that the charge-exchange cross section also increased substantially with Z_j. However, recent theoretical and experimental results[4] indicate that the total trapping cross section on impurity ions varies as $Z_j^{1.2}$ to $Z_j^{1.4}$, so that the penetration length of neutral beams should vary only weakly with Z_{eff}.

Efficiency and Reliability

In the range of beam energy relevant to fueling toroidal devices (60 to 150 keV, D° or T°), neutral beams can in principle be produced with 50% efficiency; however, energy recovery techniques must be perfected to insure 50% efficiency at the upper end of this range.[5] In his presentation, J. Fink emphasized that reliability can be increased by stacking many smaller beam sources in one beam line in order to focus large beam currents through a relatively small area. With independent control of each source, one or more sources can be turned off in the case of a one-time arc, or serious fault, without disturbing neighboring sources. Redundant sources should be provided to increase reliability. Both the TFR and 2XII-B devices have already used 5 or 6 sources per beam line, in the 20 to 40 keV range, with acceptable overall reliability. The 120-keV TFTR injectors presently under development will have 3 sources per beam line.

J. Fink also reviewed certain mirror-machine concepts that call for the use of very high energy beams (E_b > 200 keV) for fueling as well as for heating, and for these applications negative-ion beams must be developed.

To insure a satisfactory beam penetration profile during start-up, when the plasma density varies continuously with time, it is desirable to vary E_b during a single pulse. Beam developers from ORNL and LBL expressed the belief that present injector accelerator structures could be adopted for varying E_b by as much as a factor of 3 during a single pulse (say 40 to 120 keV), while maintaining ion current and small divergence. Another possible approach, espoused by ORNL, is to tune the fractional content of D^+ and D_2^+ in the ion beam. If the concentration of either species could be varied from 0.2 to 0.8, for example, then for the same accelerator voltage, E_b is in effect varied by about a factor of 2.

Injector Improvements

R. Pyle discussed how positive-ion-based development work in the 40 to 120 keV range is leading to more reliable and efficient injectors — and hopefully to less costly injectors, once large-scale production will have begun. Some outstanding problems with positive-ion based injectors are the following:

(1) The D^+ fractional content in the plasma generator must be increased toward 1.0. Great strides have been made this past year with the 22-cm modified duopigatron source at ORNL, producing a monatomic yield ~ 0.85 in hydrogen, and probably larger in deuterium.[6]

(2) Spark damage in the accelerator structure can still be a serious problem.

(3) More effective electrode cooling systems must be demonstrated, to insure that multi-second or steady-state beams can be produced.

(4) Switching and regulation systems have been made to work reliably by going to complicated protection systems, whose costs must now be reduced.

(5) Techniques for direct energy recovery of unneutralized ions must be perfected, both to economize on power supply requirements, and to ameliorate the beam-dump heat load and sputtering problems.[5]

(6) Gas choking in the drift tube between the neutralizer and the plasma chamber, as evidenced in PLT operation, for example, must be minimized by effective pumping systems in this region, as planned for the TFTR beam injectors.

The development of negative-ion-based higher energy beams, which would be required for fueling certain types of mirror machines, is proceeding slowly but steadily, with a goal of producing by 1981 a 10-A, 200-kV, dc D^- beam, formed by the double charge-exchange process.

Fueling in Present-Day Tokamaks

G. Neilson described the build-up in plasma density by gas puffing during the high-power beam-injection experiments in ORMAK. However, the beam particles themselves increased the density by no more than 25%. In the ATC, TFR, and now the PLT experiments with intense beam injection, large increases in density have been obtained, but in each case most of the increase has been due to cold gas streaming from the beam ducts. (In PLT at the 0.5-MW level, the injected beam ions contribute perhaps 1/3 of the total density increase, but in the center of the plasma, most of the density increase is due to the injected beam ions, including those thermalized.[7])

With the planned 3-MW neutral-beam injection on ISX-B in 1979, at a nominal E_b = 40 keV, the beams will be able to sustain an average plasma density of 5×10^{13} cm^{-3}, if τ_p = 175 ms. It is conceivable that in ISX-B, and also in the forthcoming PLT experiment with 3 MW injection for 0.3 s, the plasma density will build up to a level that will impede beam penetration. This phenomenon will be aggravated if there is also significant gas influx from the beam ducts, as in the early PLT experiment.[7] Hence in present experiments there is actually a need to restrain beam fueling, in order to limit n_e to a level that permits adequate beam penetration and hence maximum heating. The most effective means of controlling n_e for a given E_b and beam power is to reduce to a very low value the fractional recycling of outflowing plasma and neutrals. This reduction can be accomplished either by active gettering, which is being used successfully in the present PLT experiment, and also proposed for beam-fueled reactors,[8] or by a magnetic divertor, which will be used in PDX and in DITE for this purpose.[9,10]

TFTR Injectors

In his presentation, B. Prichard indicated how all the above aspects impinge on the design, development, and use of the 120-keV TFTR injectors. Each of the 4 injectors can be oriented for tangential or near-perpendicular injection, as desired, and will focus up to 0.4 A/cm^2 into the torus, with at least 60% of the 32 MW input power at E_b = 120 keV, and most of the remainder at 60 keV. After 0.5-s of injection, a time comparable to the expected τ_p, the change in density produced by the beams alone is 6×10^{13} cm^{-3} averaged over the 85-cm plasma volume. If the filling density is half this value, then at the end of injection, the beam trapping profile is just barely peaked on axis. In a proposed upgrade of the TFTR beam system, it is proposed to use

6 injectors with improved ion sources delivering a total of 45 MW, with 77% of the power at 120 keV. Figure 2 shows the time evolution of plasma density.[11] The increase in density during the beam pulse (t = 0.2 to 1.2 s) is due almost entirely to beam fueling. At t > 1 s, the neutral beam cannot penetrate to the central plasma region, but the temperature in that region should become sufficiently large so that strong alpha-particle heating would be observable.

Hence in all tokamak devices up to at least TFTR size, it appears that the beam injectors themselves can provide sufficient fueling, if one stipulates that the maximum desired density is that at which the beams no longer penetrate. Indeed, a more significant problem that may arise during the present and next generations of intense heating experiments is the need to actively restrict the degree of beam fueling.

Ripple-Injection Fueling

The limitation on E_b given by Eq. (1) when Q is relatively small can be accommodated for practically any plasma opacity, $\bar{n}a_p$, if the ripple-assisted penetration technique proves successful.[3] In this method, a ripple with significant top-bottom asymmetry is created in the toroidal magnetic field. When neutral beams are injected vertically from the side of stronger ripple, energetic ions formed from the beams are trapped in the ripple magnetic well, and drift upward to the central plasma region, where the ripple becomes small and the fast ions are detrapped. However, a serious difficulty arises from a basic feature of ripple injection. While the fast ion VB-drifts into the plasma core, the electron is left near the flux surface where the injected neutral is ionized, so that a strong radial field tends to develop. For the relatively modest injection currents needed for heating, the electric field and resulting plasma rotation are expected to be damped by the toroidal-field ripple. When the beams must provide most of the plasma fueling, however, electric fields resulting from the large injection currents could cause severe effects on the plasma.

The first test of ripple injection will take place on the ISX-B device at ORNL in late 1978 or 1979. However, the injection current will be rather small (< 10 A), so that potentially deleterious effects such as electric field build-up may not be observed.

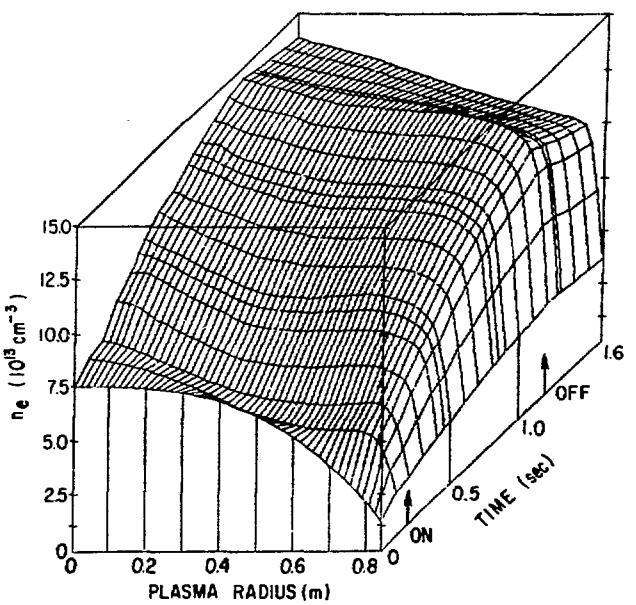

Fig. 2. Evolution of electron density in the TFTR plasma during high-power beam injection.[11] Beams are injected from t = 0.2 s to t = 1.2 s. Injection current = 290 A at 120 keV (35 MW) and 165 A at 60 keV (10 MW). Plasma recycling at the wall is 96%.

Beam Fueling of Expanding Plasmas

Dynamic start-up techniques have been proposed for heating toroidal plasmas to ignition, in which the plasma density is built up, layer by layer, by deceleration of injected energetic ions with energy in the range of 20 to 100 keV.[2] Present and planned mirror-machine plasmas are started-up in this fasion.[13] If such schemes were viable for toroidal plasmas, they would solve simultaneously the problems of initial fueling and heating of an ignition-sized plasma. For example, if a plasma containing 10^{22} ions at an average temperature of 7 keV must be formed in 2 s, the beam requirements are 1700 A at 20 keV, or 34 MW. In practice, some of the plasma would be formed prior to beam injection and some of the heat input would be lost, so that larger beam voltages and smaller currents could be utilized – and indeed must be utilized because of access and charge-exchange problems at low E_b.

This type of beam-fueled start-up offers a potential means of reaching both the density and temperature conditions for ignition in toroidal plasmas with state-of-the-art neutral beams, but it is accompanied by two serious problems. First, D° or T° beams in the 40 to 80-keV range introduce large numbers of neutrals into the plasma by charge-exchange trapping. The fast ions experience charge-exchange loss on these neutrals, and also on the neutral population that is likely to be present in any event at the edge of the expanding plasma where the beams are being deposited. Second, a potentially more disastrous effect is that sputtering of the vacuum vessel wall or liner by hot neutrals escaping from the beam-maintained edge region may result in an intolerable influx of impurities into the plasma. Experiments on PDX, TFTR, and other machines should determine whether or not beam fueling can be accomplished in a safe manner when no means is provided for penetration of fast neutrals deep into the plasma.

Prospects and Problems of Beam Fueling

- In the present and next generation of tokamak and mirror-machine experiments, the plasmas can be fueled by the high-power beams specified for heating, in the energy range 40 to 120 keV (D°). In fact, 'overfueling' by the beams, which might inhibit bulk-plasma heating, could be a serious problem during long pulses.

- Medium-energy beams can be used to fuel (and heat) quasi-steady low-Q reactor plasmas ($Q \lesssim 3$), provided that the plasma opacity $\bar{n}a_p \leq 10^{16}$ cm^{-2}, or that some means is devised for ensuring beam penetration into the hot central core. These plasmas tend to be characterized by $E_{ion} >> T_e$.

- The requirements for start-up fueling and heating of ignition-sized plasmas can be accomplished in principal by medium-energy beams (40 to 120 keV D° and T°) in an expanding-plasma scenario, but the charge-exchange and impurity-influx problems associated with edge heating have been insufficiently analyzed. Initial fueling and heating with good penetration could be achieved in principle by ripple-assisted injection, but this method faces potentially serious problems of electric field build-up and velocity-space instabilities, and in any

event has not yet been tested experimentally.

- In certain mirror-machine concepts, fueling is to be accomplished by beam energies greater than 200 keV. The negative-ion beams required for high efficiency in this range are being developed only slowly at this time.

- Present neutral-beam development programs are rapidly perfecting injectors in the energy range required for fueling toroidal devices (60 to 150 keV, D^0 or T^0), but work on direct recovery techniques requires much greater emphasis to ensure that highly efficient beams can be obtained at the upper end of this energy range.

References

1. Jassby, D.L., Nucl. Fusion 17 (1977) 309-365, Sections 1.1, 2.1, 5.2, 6.2.1.
2. Sheffield, J., in Theoretical and Experimental Aspects of Heating of Toroidal Plasmas (Proc. 3rd Int. Mtg., Grenoble, 1976) 2, 205. Falther, H.D., Henkes, W., in Controlled Fusion and Plasma Physics (Proc. 6th Europ. Conf., Moscow, 1973) 385.
3. Jassby, D.L., Goldston, R.J., Nucl. Fusion 16 (1976) 613. Jassby, D.L., Trans. Am. Nucl. Soc. 26 (1977) 13.
4. Olson, R.E., Salop, A., Phys. Rev. A, 16 (1977) 531.
5. Stearns, J.W., Berkner, K.H., Pyle, R.V., in The Technology of Controlled Nuclear Fusion (Proc. 2nd Top. Mtg., Richland, WA, 1976) IV, 1221-1231.
6. Tsai, C.C., et al., Bull. Am. Phys. Soc. 22 (1977) 1081.
7. Fubank, H.P., Strachan, J.D., private communications (1977).
8. Bromberg, L., Jassby, D.L., Princeton Plasma Physics Lab. Rep. PPPL-1396 (1977).
9. Proc. 6th Sym. on Engin. Problems of Fusion Research (San Diego, 1975), pp. 496-523.
10. Paul, J.W.M., et al., in Plasma Physics and Controlled Nuclear Fusion Research (Proc. 6th Int. Conf., Berchtesgaden, 1976) 2, 269-285.
11. Calculations by Post, D.E., and Schmidt, J.A., November 1977.
12. Goldston, R.J., et al., Princeton Plasma Physics Lab. Rep. PPPL-1398 (1977).
13. Coensgen, F.H., et al., Phys. Rev. Lett. 37 (1976) 143.

GAS BLANKETS AND NEUTRAL-PLASMA INTERACTIONS

Chairman: R. Hancox
(Culham Laboratory, U.K.)

GAS INJECTION IN PLT - EXPERIMENTAL OVERVIEW

G. L. Schmidt, N. I. Bretz, R. J. Hawryluk, J. C. Hosea, D. W. Johnson
Plasma Physics Laboratory, Princeton University
Princeton, New Jersey 08540

Cold gas injection serves both the obvious role of a particle source at the surface of the plasma and a more subtle role as one element in the process by which the relative impurity concentration and the MHD activity of a discharge are determined. In this paper we consider evidence offered by PLT experiments in support of these two widely recognized roles.

Effects of Programmed Gas Feed

Deuterium

Following the initiation of low power discharge cleaning procedures in PLT to remove low Z impurities, relatively pure deuterium discharges have been produced. To date, central electron density and temperature of 7×10^{13} cm^{-3} and 1.5 keV have been reached. These discharges, because of their reduced low Z impurity levels, serve to illustrate the subtle role played by cold gas injection. Electron temperature profiles - hence the plasma current distribution - and high Z impurity levels are both found to depend strongly on the level of the working gas present at breakdown and that introduced during the formation of the current channel. Fig. 1 indicates the dependence on these gas levels of the total plasma current,

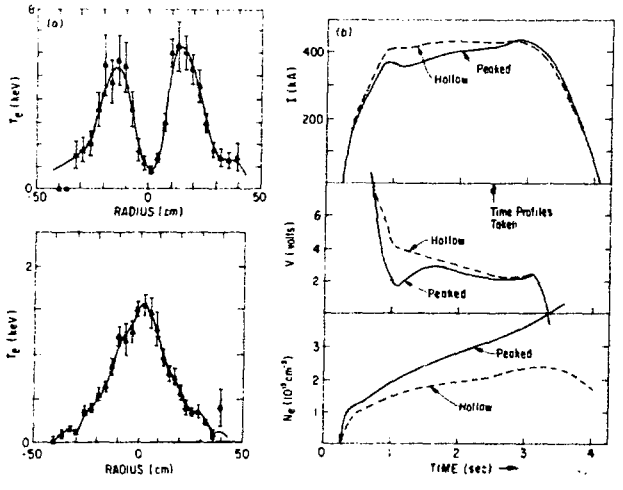

Fig. 1. Comparison of hollow and peaked deuterium discharges. Peaked discharges are produced following an increase (≲ 5%) in initial gas levels.

and the electron temperature profile in discharges having low oxygen levels following low power discharge cleaning. At the lower gas level, low temperature discharges are produced, with a sustained rate of current rise in the initial phase. Hollow electron temperature profiles are observed. At intermediate gas levels, the rate of current rise is seen to decrease following the initial discharge formation. Increased central electron temperatures are also observed with some evidence of MHD activity during the latter part of the current rise. At this point further increases in gas levels (< 5%) produce a factor of ~ 2 increase in electron temperatures. A decrease in m = 2 activity and an increase in m = 1 or sawtooth activity during the discharge flattop is also observed. It is found, that maximum density increase is achieved by gas injection in such discharges. Still further increases in gas levels lead to unstable (disruptive) discharge of short duration.

Tungsten Concentrations

Concurrent with increased gas injection levels and central electron temperatures, a reduction is observed in tungsten levels in the discharge as measured by line radiation near 50 Å.[1] This reduction has been correlated with an increase in low Z (oxygen and carbon) impurity concentrations and a decrease in edge ion and electron temperatures.[2] Tungsten levels remain low so long as high levels of gas injection can be sustained. At present however, such levels of gas injection cannot be sustained during the entire discharge (> 0.5 sec) in hydrogen or deuterium. Although this evidence suggests that gas injection levels, low Z influx, high Z influx and edge plasma temperature are strongly interdependent, the casual relationship and precise role of the injected gas is yet to be firmly established.

Helium

Similar effects are seen using helium as the working gas.[3] In this case, however, the helium radiation itself suppresses the tungsten levels. Oxygen influx is also low and is observed to decrease during some discharges. Relatively pure (Z ~ 2) helium plasmas can therefore be produced, with the additional advantage that continued high levels of gas injection can be sustained. At present, highest densities are achieved in helium. A rate of increase in central density from 1 to 2×10^{14} cm^{-3} sec^{-1} can be sustained throughout the discharge, leading to peak density in excess of 1.5×10^{14} cm^{-3} in discharges of 40 cm minor radius. For these discharges we address the question of density buildup within the discharge core - whether the process occurs by local ionization or inward particle flow. In order to answer this question several calculations have been performed based on the PLT experimental results.

Density Buildup

Neutral Density

Neutral density within the discharge core provides a local ionization source. In the absence of significant recombination[4], penetration by repeated charge exchange collisions is the process by which such neutral density is established. The dominant charge exchange reaction is that between Helium neutrals and He^{++}. Because of its size, substantial attenuation of charge exchange neutral flux can occur in the PLT device at the moderate electron densities reached in helium discharges. A Monte Carlo technique[5] has been used to calculate this attenuation.

Two separate neutral fluxes are modeled in calculating the neutral density - a flux of cold neutrals corresponding to those introduced directly by gas injection, and a flux of warm neutrals, corresponding to particles recycling at the limiter. A rather high average neutral energy of 30 to 40 eV is observed throughout the density rise by Doppler broadening measurements of neutral helium.[2] A Maxwellian velocity distribution with this average energy is therefore assumed for the warm neutrals at the plasma boundary in this calculation. In an effort to fix an upper limit on the helium neutral density within the core of the discharge, all neutrals escaping from the plasma volume are assumed to reflect at the wall with no loss of energy.

The absolute magnitude of the neutral density is determined by a normalization of the Monte Carlo

results. The Monte Carlo procedure in conjection with Thomson scattering profiles of density and temperature is used to calculate the radial dependence of the neutral density, f(r). The volume integral of the source function associated with f(r) is then computed. In the case of cold neutrals, this integral is normalized to the measured increase in the particle content of the discharge. In the case of warm neutrals, the integral is normalized to the measured particle replacement losses. Azimuthal asymmetries during the density rise, limit the accuracy with which particle replacement losses are known for the discharges considered here. Measurements at a single location indicate that replacement times are less than 10 ms and nearly constant in time.[6] An average value of 10 ms is more consistent with the energy input to the discharge, and this value is used here. Note that this value of the particle replacement time is significantly less than the discharge energy confinement time indicating that strong recycling of low temperature edge plasma occurs during build up. Such recycling leads to enhanced levels of neutral density throughout the discharge. Since the recycling flux dominates the problem, the neutral density scales linearly with replacement time.

Fig. 2 displays the results of neutral penetration calculations at three points in time during the density rise. A steady drop in central neutral density occurs as electron density increases. At 825 ms ($n_e(0) = 1.5 \times 10^{14}$ cm^{-3}):

$$R = \frac{n_o(0)}{n_o(a)} = 3 \times 10^{-6} .$$

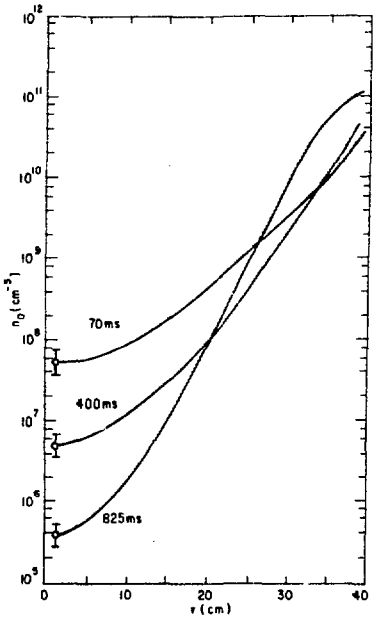

Fig. 2. Neutral density profiles calculated assuming cold neutrals at 0.5 eV, warm neutrals at 40 eV, and a 10 ms particle replacement time. Central electron densities and temperatures were: (70 ms) 3.7 x 10^{13} cm^{-3}, 730 eV; (400 ms) 9.0 x 10^{13}, 1200; (825 ms) 1.5 x 10^{14}, 940.

Local Source

The source term associated with the calculated neutral density is given by the electron continuity equation. In the absence of impurities, this equation can be obtained from the continuity equations for He^+ and He^{++}:

$$\frac{dn_+}{dt} = \frac{1}{r}\frac{d}{dr}\left(rD\frac{dn_+}{dr}\right) + \frac{1}{r}\frac{d}{dr}\left(rn_+ V_{pinch}\right) + n_e (n_o S_o - n_+ S_+) , \quad (1)$$

$$\frac{dn_{++}}{dt} = \frac{1}{r}\frac{d}{dr}\left(rD\frac{dn_{++}}{dr}\right) + \frac{1}{r}\frac{d}{dr}\left(rn_{++} V_{pinch}\right) + n_e n_+ S_+ , \quad (2)$$

where recombination has been ignored. The helium ionization terms dominate Eq. (1), which may be approximated by:

$$n_o S_o = n_+ S_+ .$$

The neglect of the He^+ flux to the limiter, which such an approximation implies, was found to underestimate the electron source term by at most 10%. The electron continuity equation is then:

$$\frac{dn_e}{dt} = \frac{1}{r}\frac{d}{dr}\left(rD\frac{dn_e}{dr}\right) + \frac{1}{r}\frac{d}{dr}\left(rn_e V_{pinch}\right) + 2 n_e n_o S_o . \quad (3)$$

The last term on the right is the electron source term. The second term is due to the neoclassical pinch.

Fig. 3 compares the calculated electron source term on axis to the measured change in central density during the discharge, with increasing density (time in the figure), the source term is decreased to a value more than an order of magnitude less than the observed rate of density increase, and cannot alone account for the observed rate.

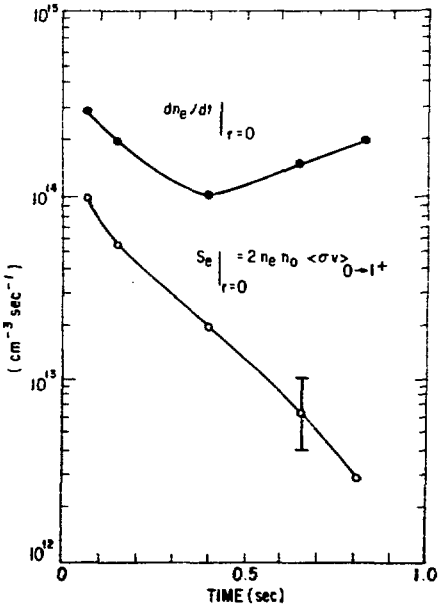

Fig. 3 Comparison between measured changes in central electron density and the computed electron source term near the discharge magnetic axis. Density increases were obtained from Thomson scattering measurements.

Low Z Impurities

Ionization of low Z impurities (principally oxygen) does provide an additional electron source term. However, in these discharges the concentration of oxygen is low and its influx rate is decreasing with time. Preliminary estimates of the source function associated with this flux indicate its magnitude to be comparable to the helium source function within the core of the discharge. The central core of the discharge must be supplied by an inward particle flow.

Neoclassical Pinch

Since a large fraction of the discharge is in the plateau regime, consideration of the neoclassical pinch is warranted. The inward neoclassical pinch velocity, V_{pinch}, is calculated by numerically evaluating the results of Hirshman and Sigmar.[7] In these calculations, the surface voltage used is obtained from the vacuum vessel loop voltage. An inductive voltage correction is included to obtain the surface voltage. A one dimensional magnetic field diffusion calculation is used to obtain the electric field, $E_z(r)$, the poloidal field, $B_p(r)$, and Z_{eff} from this surface voltage, the measured electron density and temperature profiles and the plasma current. Z_{eff} is assumed to be independent of radius. The calculation is only weakly dependent on the radial variation of E_z for fixed surface voltage and total plasma current. The dependence on Z_{eff} is also weak. Fig. 4 illustrates the radial dependence of the dn/dt, source, and pinch terms in Eq. (3) over the inner 20 cm of the discharge. The pinch is sufficient in this discharge to account for the observed density rise on axis; however, the radial extent of the pinch is seen to be limited.

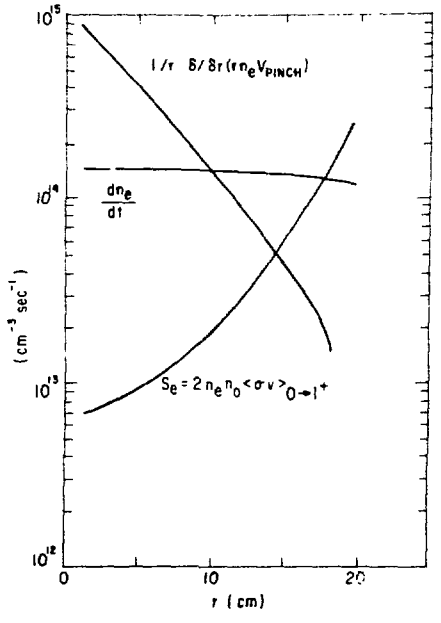

Fig. 4. Radial dependence of terms in the electron continuity Eq. (3) at 650 ms excluding diffusion.

Diffusion

An understanding of the observed rate of density buildup requires, ultimately, a knowledge of the magnitude and radial variation of the particle diffusion coefficient across the discharge. Any proposed mechanism requires a complementary diffusion coefficient. The shape and magnitude of that diffusion coefficient reflect the validity of the mechanism proposed. However, such a diffusion coefficient is meaningful only to the extent that the mechanism proposed dominates the buildup process. In this case, the neoclassical pinch could produce the measured density rise, if the particle diffusion coefficient were to have the radial dependence shown in Fig. 5. Strong diffusion at radii less than 10 cm could be consistent with the $q < 1$ condition: however, the minimum in the region from 15 to 20 cm is not so easily understood. At late times, this minimum value approaches its neoclassical limit indicating the marginal character of V_{pinch} at that point. Note, however, that any anomalous increase in the magnitude of V_{pinch} or the source function would reduce the required radial variation in the diffusion coefficient. Results from earlier helium discharges produced prior to the onset of low power discharge cleaning suggest that a factor of two enhancement in V_{pinch} may be required in some cases to explain the rate of density buildup.

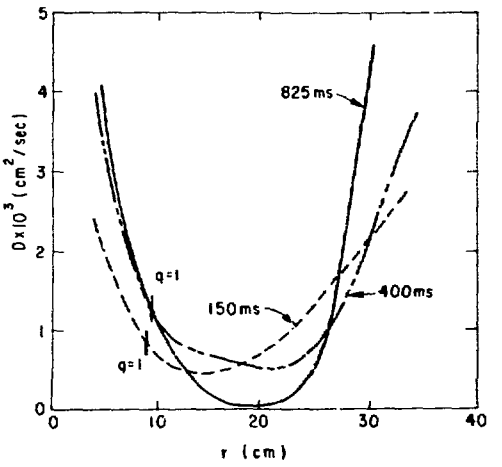

Fig. 5. Diffusion coefficients required to complement the neoclassical pinch term.

In summary, calculations based on PLT helium discharges ($n_e(0) = 1.5 \times 10^{14}\ cm^{-3}$) indicate that neutral penetration by multiple charge exchange collisions cannot account for the observed density build up. The neoclassical pinch, possibly with some enhancement, could provide a substantial density increase within the discharge core, but does not in itself account for the observed profile shape. A self-consistent diffusion coefficient and a strong source term are also required. Diffusion within the interior of the discharge remains the major unknown in determining whether or not the pinch is the mechanism by which density build up occurs.

Acknowledgements

We are very grateful to J. A. Schmidt for many stimulating discussions as well as his participation in the calculations. We are also especially grateful to E. Hinnov and S. Suckewer who very generously provided the spectroscopic data. P. Efthimion was responsible for the edge electron temperature measurements. M. Hughes and D. Post provided the Monte Carlo neutral transport code which was extensively used in this work, and S. P. Hirshman provided recent analytic approximations for the neoclassical pinch.

This work was supported by U.S.D.O.E. Contract EY-76-C-02-3073.

References

1. E. Hinnov et al, Bull. Am. Phys. Soc., 22, 1075 (1977).
2. S. Suckewer et al, Bull. Am. Phys. Soc., 22, 1076 (1977).

3. R. J. Hawryluk et al, Bull Am. Phys. Soc., 22 , 1076 (1977).
4. In helium a two step recombination process is required to form neutral helium within the core of the discharge - this process is assumed negligible.
5. M. H. Hughes, D. E. Post, Princeton Plasma Physics Laboratory Report, PPPL 1375, (1977).
6. E. Hinnov provided the measured values of helium and oxygen flux.
7. S. P. Hirshman, D. J. Sigmar, Phys. Fluids, 20, 418 (1977).

FUELING AND SHIELDING BY GAS-PLASMA BLANKETS IN ALCATOR

Ronald Parker, Kim Molvig, and Louis Scaturro
Plasma Fusion Center and Francis Bitter National Magnet Laboratory
Massachusetts Institute of Technology
Cambridge, Massachusetts 02139

I. Introduction

The Alcator tokamak routinely operates in a regime in which the plasma is opaque to neutrals, the ratio of mean free path ℓ_n to radius a being $\ell_n/a \sim 0.1$. There are two important consequences for high density tokamak operation. First, the plasma fueling, i.e., the buildup and maintenance of high density (in excess of $10^{15}\,cm^{-3}$ at the center) cannot be the result of neutral ionization, and second, the plasma shields the wall from the harmful effects of energetic neutrals.

In the case of the fueling problem, it appears that an inward convection of plasma is required in order to increase the density to the observed levels[1]. Simulations show that the Ware pinch coupled with anomalous particle transport near the edge is capable of mocking up the density rise, however, the time scale in the present model is about a factor of 2 longer than the experimental time scale. More realistic modeling of the edge anomalies may improve this. The observations indicate that fueling an ignition device with a neutral gas blanket may be feasible. However, the physical processes involved are not entirely understood.

The plasma shield is the result of multiple ionization and charge exchange of neutrals which occurs when $\ell_n < a$. Not only do energetic neutrals become reabsorbed before hitting the wall, but the background neutral density falls rapidly as ℓ_n decreases; hence the intensity of the source of energetic neutrals diminishes. The effect has been clearly observed experimentally and is in qualitative agreement with computations of the neutral gas dynamics. This is significant because it greatly reduces the impurity flux which can be sputtered from the wall as a result of bombardment by energetic neutrals created by charge exchange both with the hot ion and beam components. This method of impurity control is important since it may eliminate the need for a divertor on ignition and reactor devices.

II. Fueling

Experimental Observations

Alcator discharges[2] are produced by first establishing a low density equilibrium ($\bar{n} \leq 5 \times 10^{13}\,cm^{-3}$) and subsequently injecting gas so as to produce an increase in density up to operating levels of $\bar{n} = 6 \times 10^{14}\,cm^{-3}$. (See Fig. 1.) The rate of plasma increase is, within a factor of 2, equal to the throughput of the gas valve used for admitting gas to the plasma volume. The exact correspondence depends on wall conditions: the higher the recycling coefficient, the larger the rate of density rise for a given gas admission rate. Under low recycling conditions, most of the recycled gas appears at the limiter; with high recycling, most of the recycled gas comes from the wall. These conclusions are based on the relative intensity of H_α light at each of the four toroidal locations allowed by the port configuration; more quantitative evaluation is difficult because it is not possible to measure $H_\alpha(\varphi, \theta)$ where φ and θ are the toroidal and poloidal angles.

This first question to be asked concerning the plasma buildup is whether the density rise could be due to direct ionization of neutral gas. Numerical simulations (which will be discussed later) show that this is not possible since the central neutral density drops to very low levels in the high density regime. This conclusion is supported by direct experimental evidence, which shows that the energetic neutral flux drops by about 2 orders of magnitude as the plasma density increases from $\bar{n} = 1.5 \times 10^{14}\,cm^{-3}$ to $\bar{n} = 6 \times 10^{14}\,cm^{-3}$. At the same time the rate of density rise remains unaffected. Consequently, we must look for other plasma ingestion mechanisms.

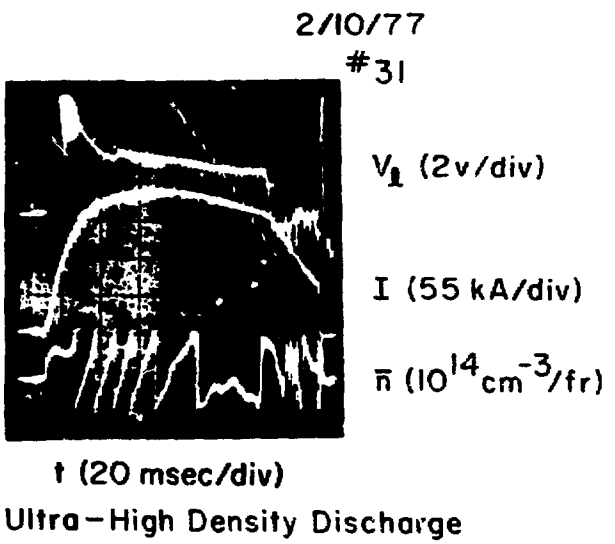

Fig. 1. A high density discharge in Alcator showing loop voltage, current, and density. The discontinuities in the density trace are due to resets in the fringe counter and should be ignored.

By locating valves at 0°, 90° and 180° from the limiter, we have determined that there is no toroidal dependence on poloidal angle, although this has been tested by placing valves only at the top and bottom of the machine.

Also, by reversing the toroidal field, no dependence (less that 5%) on the direction of the toroidal drift relative to the gas valve location has been found, although this has been shown to have an effect in the diffusion of light impurities. The only parameter which has been found to have an effect on the ingestion efficiency is dI/dt. Positive dI/dt tends to increase efficiency and negative dI/dt decreases it. The effect is especially significant near the termination of the current pulse where large, negative dI/dt, on the order of -2.5 kA/msec results in rapid pump-out of the plasma density. There is also a related broadening and contracting of the temperature profile according to whether $dI/dt > 0$ or $dI/dt < 0$. In the case of $dI/dt > 0$ this may place more particles in trapped collisionless regimes, making them susceptible to inward convection by the Ware pinch.

Theoretical Modeling

The computer model consists of a one dimensional (radial) plasma transport code and a Monte Carlo algorithm for calculating the neutral density. These can be run concurrently.

The plasma code[3] evolves the usual transport equations for density, electron and ion temperatures, poloidal magnetic field, and toroidal electric field using the neoclassical fluxes plus anomalous contributions from current driven drift wave fluctuations. The neoclassical coeffi-

cients used are accurate throughout the banana and plateau regimes, which covers the parameters explored experimentally. Since the experimental observations show transport in excess of neoclassical (except possibly at the extreme upper limit of density), some type of anomally must be included if reasonable agreement is to be expected. The current driven drift wave contributions we have used are dominant at all plasma radii for average densities below $\bar{n} \sim 1.5 \times 10^{14}\,cm^{-3}$, and at all densities in the radius range $0.75 < r/a < 1$. Because of the achievement on Alcator of substantially pure, $Z_{eff} \sim 1$, plasmas, we exclude any consideration of impurity transport.

The neutral algorithm[4] uses a numerical Monte Carlo scheme to compute the neutral profiles, given the plasma density, temperature profiles, and the incident neutral flux. Ionization of the pulsed gas (molecular hydrogen) near the plasma edge provides an isotropic source of 3 eV hydrogen atoms. The profile of these is determined from the Monte Carlo scheme. A second source of neutrals due to recycling is treated separately. Our recycling model is as follows. It is assumed that lost plasma ions acquire an electron on the limiter or the wall and return to the plasma as a neutral. The energy and angular distributions of the reflected neutrals are taken from Behrisch[5]. Emergent charge exchange neutrals behave similarly. All particles are returned to the plasma; there is some degradation of their energy.

The combined code is run using the experimental values of toroidal field, current and pulsed gas. It begins from a previously computed low density, $\bar{n} = 0.64 \times 10^{14}\,cm^{-3}$, equilibrium. If the inward Ware pinch effect is turned off in the code, one finds that on a very short, 20 msec time scale the density profile inverts (which is not seen experimentally) and even after 100 msec the central plasma density has not changed appreciably. This is simply due to the small ionization rate resulting from the plasma's opacity. The implication is that some kind of inward plasma flow accounts for the observed density rise. Including the Ware pinch does result in density buildup in the center. Peak densities exceeding $8 \times 10^{14}\,cm^{-3}$ have been obtained computationally without profile inversions. However, the time to achieve this peak value is 112 msec as compared to the observed 60 msec. Also the final density profile obtained is broader than those seen in the experiment.

It is important to note that although, in these high densities, the transport coefficients are predominantly neoclassical over most of the radius, the outer anomalous region nonetheless plays a significant role. The basic difficulty in accounting for the inward flow is that the region where both the Ware pinch and the plasma source (neutrals) exist is very small. The Ware pinch speed falls to the outside due to an increased collisionality. At some point the flux changes sign and is outward. The neutral density decays exponentially toward the center. In fact a negligible number of the 3 eV neutrals from the pulsed gas can penetrate to points of inward flow. One thus arrives at a picture in which the pulsed gas atom is ionized at the edge, heated as an ion to the edge temperature, lost to the wall by diffusion and finally, now as a hot (~ 50 eV) neutral, penetrates to a radius where the pinch can operate. It is accordingly necessary to have high (anomalous) loss rates at the edge to provide a large recycled neutral flux.

With this comes the suggestion that modifying the assumed edge anomally to increase the recycling rate might reproduce the observed density rise rates while maintaining the Ware pinch as the principal mechanism. Such a modification is also suggested by the computed density profiles which are broader than those observed.

III. The Boundary Plasma

Important to both the problem of fueling and wall-plasma interactions is the boundary plasma, that is, the plasma extending from about 1 cm in front of the edge of the limiter to the vacuum chamber wall 2.5 cm behind the limiter.

Langmuir probe measurements have been made within the magnetic shadow of the limiter and typical results are shown in Fig. 2. In addition to the main molybdenum limiter, there are 8 virtual limiters each extending 1 cm from the chamber wall, a few cm to each side of the four diagnostic flanges. As the probe is moved into the shadow of these virtual limiters, an abrupt decrease in density is observed. Although the mean free path for ion-electron collisions is smaller than the machine circumference, it is larger than the distance between virtual limiters. Therefore axial losses result in a precipitous fall of density as the position of the virtual limiter is crossed.

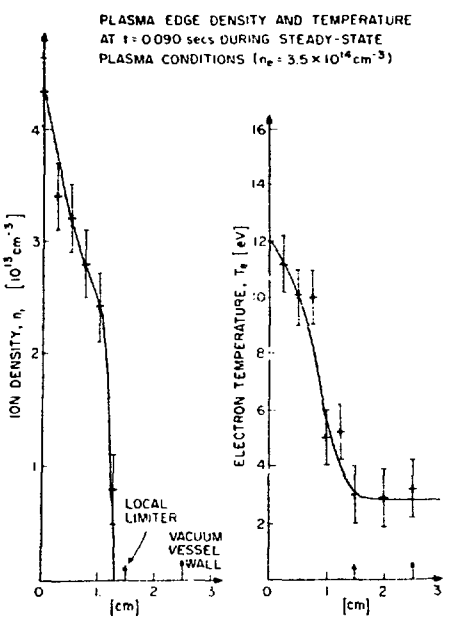

Fig. 2. Plasma edge density and temperature from electric probe measurements vs distance from the edge of the limiter. (0 cm corresponds to a minor radius of 10 cm.)

There are several indications that the transport in this region is non-classical. Neglecting ionization in the limiter shadow, we can estimate the perpendicular diffusion coefficient $D_\perp$ by balancing the divergence of the perpendicular flow against the parallel flow to the limiter. Then, $D_\perp \sim \ell_\perp^2/\ell_\parallel^2 D_\parallel$ or $D_\perp \sim \ell_\perp^2/\ell_\parallel C_S$ depending on whether the parallel flow is limited by diffusion or effusion. Here $\ell_\perp$ and $\ell_\parallel$ are density scale lengths and C_S is the ion sound speed. The parallel ion-electron mean free path in the limiter shadow is comparable with the circumference of the machine, and both estimates give $D_\perp \sim 10^4\,cm^2/sec$, many orders of magnitude greater than classical. A second argument is based on the particle confinement time τ_p which has been estimated by gas injection experiments to be about 50 msec. Using $\tau_p \sim nV/(AD_\perp \nabla_\perp n)$ where V and A are the plasma volume and surface area, we get $D_\perp \sim 2 \times 10^3\,cm^2/sec$. Strong turbulence $\delta n/n \sim 1$ has been observed in this region using both the Langmuir probe itself and CO_2 laser scattering[6]. It is also interesting to note the value of the Bohm diffusion coefficient,

$D_B \sim 10^3$ cm^2/sec is comparable to the estimate based on particle confinement time.

The significance of these estimates is that they appear to rule out energy transport by charged particles as a mechanism for recycling energy to the wall or limiter. Taking the upper bound of $D_\perp \sim 10^4$ cm^2/sec we place a maximum power flux of ~ 1 W/cm^2 compared with typical measured values of 30 W/cm^2. Thus, other mechanisms for convection of energy to the wall, either due to the neutral flux or radiation must be examined.

The probe experiment has also shown that the plasma edge parameters are insensitive to the location of the pulse gas injection. Figure 3 shows the time history of the ion edge density for three locations of gas injection: one directly over the probe (microwave port), one 90° away in the toroidal direction (CO_2 port), and one 180° away (limiter port). It can be seen that the edge density rises in time until the pulse gas valve closes, then slowly decreases until the end of the discharge. The later peaking of the density at the CO_2 and limiter ports is indicative of the smaller conductance of the gas injection system at these locations.

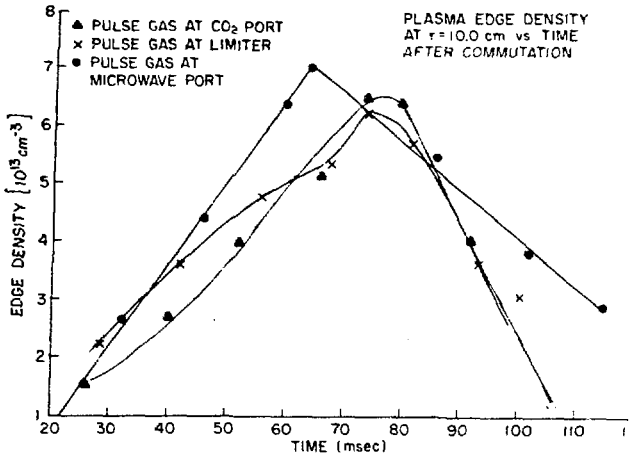

Fig. 3. Edge ion density from electric probe measurements vs time for three toroidal locations of pulse gas injection.

IV. Neutral Flux Cutoff

Experimental Observations

As the density is increased in Alcator, the emitted neutral flux with energies greater than 200 eV first increases up to the density $\bar{n} = \bar{n}_C \simeq 1.5 \times 10^{14}$cm^{-3}, and then decreases abruptly as $\bar{n}$ is raised above $\bar{n}_C$. (See Fig. 4.) This effect is due to the shortening of the neutral mean free path, which results in a simultaneous reduction in the central neutral density and attenuation of the emitted neutral charge-exchanged flux. Since the density at which the neutral signals first decrease is independent of energy, it is believed that the effect is initially due to a decrease in central neutral density. At higher densities, the emitted flux is also severely attenuated and the energy spectrum is then no longer characteristic of the central ion distribution function.

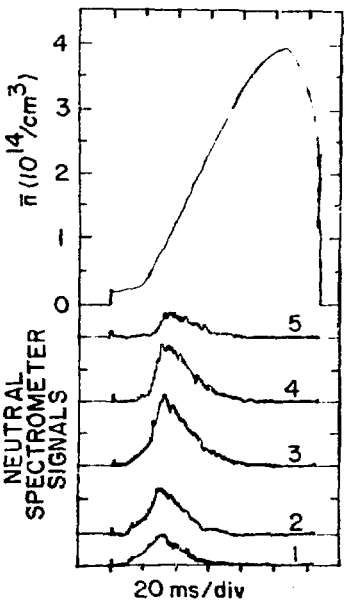

Fig. 4. Cutoff of energetic neutral flux during a high density discharge. The top trace is line average electron density obtained from the 119 μm laser. The lower traces are unnormalized signals from the 5 analyzer channels: 1) 500 eV, 2) 685 eV, 3) 974 eV, 4) 1321 eV, and 5) 1947 eV. Note the decrease in the flux for average densities in excess of 1×10^{14} cm^{-3}.

Theoretical Calculations

As expected, the code results show that the flux of high energy neutrals attenuates as the density increases to values in excess of about 1×10^{14}cm^{-3}. Figure 5 shows a plot of the average energy of emitted neutrals as a function of the central plasma density. Two cases are shown: one for a central ion temperature of 1 keV and a plasma radius of 10 cm, the other for a central temperature of 10 keV and plasma radius of 100 cm. In the first case the average energy drops by nearly an order of magnitude, as the central density is increased from 1×10^{14} to 1.6×10^{15}. The flux of heavy impurities sputtered from a stainless wall by this neutral flux drops by a factor of 50. The case of 10 keV central temperature and 100 cm radius shows that an equivalent reduction in neutral flux capable of sputtering a stainless steel wall occurs even under reactor conditions. Consequently the effect of impurity production by physical sputtering due to charge-exchanged neutrals does not appear to be serious in sufficiently opaque plasma regimes. Two words of caution should be added: this calculation does not include the effects of charge exchange with energetic ions arising from neutral beam heating, nor the effects of recombination. The latter effect has been estimated to give a central neutral density $n_o \sim 10^{-7}$cm^{-3}, whereas the code used here allows the neutral density to drop to arbitrarily low values.

The edge neutral density has been estimated to be $1\text{-}3 \times 10^{11}$cm^{-3} by measurement of H_α emission using a calibrated monochromater. It would be difficult to support an edge neutral density significantly larger than this since influx of neutral gas would then be larger than the plasma outflux. The neutral particle calculation then shows that at $n(o) \sim 10^{15}$, the average energy of neutral outflux is 40 eV and the flux is $0.6\text{-}2 \times 10^{17}$/cm^2/sec, resulting in a power flow of 0.15-0.5 W/cm^2. The tentative conclusion is that power flow to the wall by low energy charge-exchanged neutrals is a negligible part of the total power flow. A more definitive measurement of the actual neutral edge density is required to confirm this assertion.

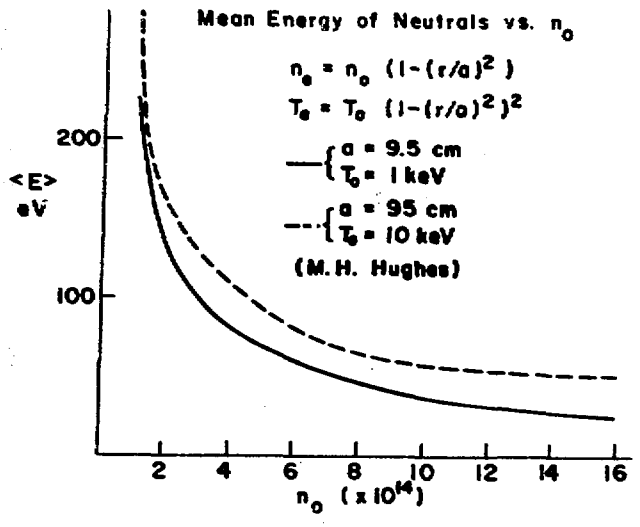

Fig. 5. Mean energy of effluent, charge-exchanged neutral flux vs central plasma density, n_o.

V. Conclusions

From this work it is concluded that a mechanism exists for fueling tokamak plasmas in opaque regimes by maintenance of a gas-plasma blanket at the plasma edge. Theoretical models show that a combination of strong anomalous particle transport in this region together with the Ware pinch is capable of simulating the fueling effect, but the time scale is about a factor of 2 longer than in the experiment.

It is further concluded that the combination of dense plasma and gas blanket is capable of shielding the vacuum wall from the deleterious effects of energetic charge-exchanged neutrals. However, neither the charged particle nor neutral particle fluxes arising from the blanket appear to be capable of transporting the recirculating energy to the wall. For this to occur the gas density would have to be on the order of $10^{13}cm^{-2}$, and at this level the ionization and plasma ingestion rate would probably disrupt the discharge.

Acknowledgment

We would like to acknowledge the substantial contributions of M.H. Hughes in developing the model and performing the numerical computations.

References

1. K. Molvig, Bull. Amer. Phys. Soc. 21, 1125 (1976)
2. M. Gaudreau et al., Phys. Rev. Letters 39 (1977) (to be published)
3. D.E. Post, A. McKenney, P.H. Rutherford, G. Lister, and M.H. Hughes, Bull. Amer. Phys. Soc. 21, 1108 (1976)
4. M.H. Hughes and D.E. Post, Princeton Plasma Physics Laboratory Report 1335 (1976)
5. R. Behrisch, paper presented at Summer School of Tokamak Reactors for Breakeven; Erice, Italy (1976)
6. R.E. Slusher and C.M. Surko, Bull. Amer. Phys. Soc. 22, 1091 (1977)

EFFECTS OF FUELING PROFILES ON PLASMA TRANSPORT*

W. A. Houlberg, A. T. Mense, S. E. Attenberger, and S. L. Milora
Oak Ridge National Laboratory
Oak Ridge, Tennessee 37830

Summary

The effects of cold particle fueling profiles on particle and energy transport in an ignition sized tokamak plasma are investigated in this study with a one-dimensional, multifluid transport model. A density gradient driven trapped particle microinstability model for plasma transport is used to demonstrate potential effects of fueling profiles on ignition requirements. Important criteria for the development of improved transport models under the conditions of shallow particle fueling profiles are outlined. A discrete pellet fueling model indicates that large fluctuations in density and temperature may occur in the outer regions of the plasma with large, shallowly penetrating pellets, but fluctuations in the pressure profile are small. The hot central core of the plasma remains unaffected by the large fluctuations near the plasma edge.

1. Introduction

The evaluation of particle fueling mechanisms is an important step in the assessment of the behavior of future large tokamak plasmas. This paper is devoted to showing how cold particle fueling profiles in general and pellet ablation profiles in particular may affect the thermal behavior of an ignition size plasma. A set of TNS parameters, given in Table 1, is used as representative of an ignition device. An assumed particle source profile, linearly decreasing in intensity from the plasma edge, is used in Sect. 3 to demonstrate the potential effects on the plasma thermal behavior of varying the particle source penetration depth. The effects of a discrete pellet ablation model on the fluid transport are discussed in Sect. 4.

Table 1. TNS Parameters

Major radius	$R = 500$ cm
Minor radius in midplane	$a = 125$ cm
Plasma elongation	$b/a = 1.6$
Toroidal magnetic field	$B_T = 4.3$ T
Toroidal current	$I = 4 \times 10^6$ A

Density and temperature boundary conditions:

$$\left(-\frac{1}{n}\frac{\partial n}{\partial r}\right)^{-1} = \Delta_{n_{\alpha,i}} = 10 \text{ cm}$$

$$\left(-\frac{1}{T_e}\frac{\partial T_e}{\partial r}\right)^{-1} = \Delta_{T_e} = 5 \text{ cm}$$

$$\left(-\frac{1}{T_i}\frac{\partial T_i}{\partial r}\right)^{-1} = \Delta_{T_i} = 10 \text{ cm}$$

2. The Multifluid Transport Model

A one-dimensional fluid transport model is used for the thermal components of the plasma.[1] Two ionic species, including a 50-50 D-T component and a thermal alpha component, are modeled. The electron density is treated as a dependent variable by requiring charge neutrality. Fluid energy equations are used for the thermal ions, alphas, and electrons. The thermal ion and alpha energy equations are added to obtain a "lumped ion" energy balance with the same local temperature for both ions and alphas.

Classical and neoclassical expressions are used as a base for all collisional processes. Thermalization of fast beam ions and fusion alphas is by classical Coulomb collisions. The fast charged particles are assumed to deposit their energy in the background plasma locally on a time scale short compared with radial conductive and convective processes. The parallel electrical resistivity is modeled with neoclassical corrections to Spitzer resistivity.

The particle and energy transport expressions consist of three basic models which are considered additive in effect: the neoclassical model of Hinton and Moore[2] for a multispecies plasma in the banana-plateau regime, a pseudoclassical model for anomalous diffusion and electron conduction, and a trapped particle microinstability model based on expressions given in WASH-1295.[3] The anomalous diffusion and conduction losses for the trapped particle microinstability model become dominant at low collisionality and are driven primarily by density gradients. The model for the anomalous transport yields a diagonal matrix of transport coefficients which assumes that the ion and thermal alpha diffusion are down their respective density gradients, while the electron and ion thermal conduction are down their respective temperature gradients. The neoclassical transport model includes all off-diagonal transport terms except the Ware pinch term. Further discussion of the transport model is contained in Ref. 4.

The one-dimensional fluid equations are solved with the transport code WHIST, which uses conservative spatial differencing for the particle and energy fluxes on a nonuniform spatial mesh and a variable implicit time treatment.[5] Gradient boundary conditions which are given in Table 1, are used for the densities and temperatures to simulate divertor behavior.[6]

3. Effects of Continuous Fueling Profiles on Plasma Transport

For this phase of the study, an assumed analytic particle source profile is used which linearly decreases in intensity from the plasma edge:

$$Sp(r) = \begin{cases} Sp(a)\left[1 - \dfrac{(a - r)}{r_p}\right] & r > (a - r_p) \\ 0 & r < (a - r_p) \end{cases}$$

where a is the plasma minor radius in the midplane and r_p is a penetration length measured from the plasma edge. A feedback scheme is used on the source amplitude to maintain constant average density with a feedback response time of 10 msec used in all cases. In order to determine whether the full-size plasma will ignite 2 sec of beam heating is used. For those cases which do ignite, the beam power is reduced to determine the minimum power for which the plasma does ignite. The relative level of power required gives an indication of the relative ease or difficulty of ignition. No attempt is made to optimize the start up scenario and thus produce a minimum power requirement.

An average density of 10^{14} cm^{-3} is considered. For adequate penetration (12° from perpendicular) 200 keV D° beams are required. Even though the alpha den-

*Research sponsored by the Department of Energy under contract with Union Carbide Corporation.

sity balance is included in the analysis, the alphas do not account for more than a few percent of the total density. The evolution of the plasma is followed only long enough to determine if it has ignited; at this time only a relatively low number of fusion reactions have occurred.

ORNL/DWG/FED-77595

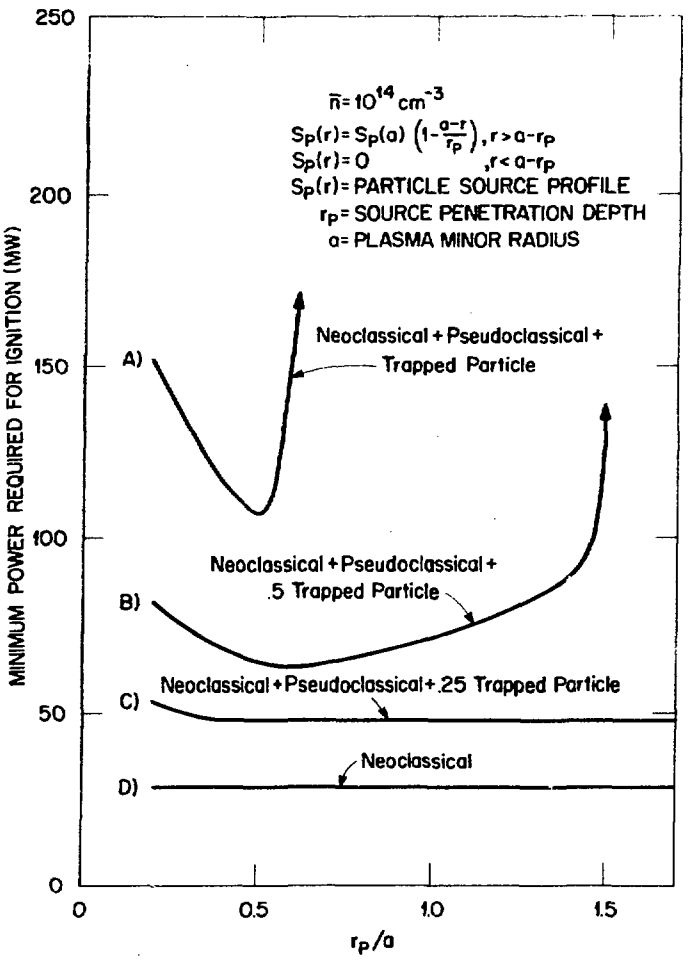

Fig. 1. Minimum required beam power for ignition using 200 keV D° beams for 2 seconds. No fueling was required for the neoclassical case during the beam heating phase since the beam furnished adequate fueling.

Figure 1 indicates the effect of varying the particle source penetration depth and degree of anomalous transport on the minimum power for igniting an $\bar{n} = 10^{14}\ cm^{-3}$ plasma. Model A includes trapped particle and pseudoclassical and neoclassical transport as additive in their effects. For shallow penetration $r_p/a \leq 0.5$, the power requirements are increased because of convective losses associated with fueling so close to the plasma edge. Decreasing penetration decreases the distance particles have to diffuse from the system and causes a very sharp gradient in density near the plasma edge (see Fig. 2). The sharp gradient is in part due to anticipated divertor action.[6] These results indicate that a shallowly penetrating particle source (e.g., cold gas) may not be a wise choice with a divertor if density gradient driven trapped particle modes dominate the transport.

In model B of Fig. 1, the magnitude of the trapped particle transport coefficients is reduced by a factor of two, while pseudoclassical and neoclassical expressions are retained. Convective losses at very small penetration depths still increase the power requirements as in model A. It takes much deeper fuel penetration to increase the density gradient and thus turn on the density gradient driven trapped particle modes. Note that the minimum in the curve is only about a factor of two greater than pure neoclassical losses (model D). For $r_p/a > 1.5$ [$S_p(0) > S_p(a)/3$] no ignited cases were found. Figure 2 illustrates the behavior of the density for shallow penetration ($r_p/a = 0.2$) which corresponds to a penetration depth of 25 cm on the plasma midplane. The strong cooling effect of the particle source at the edge of the plasma can be seen in Fig. 3. Several effects not

ORNL/DWG/FED-77745

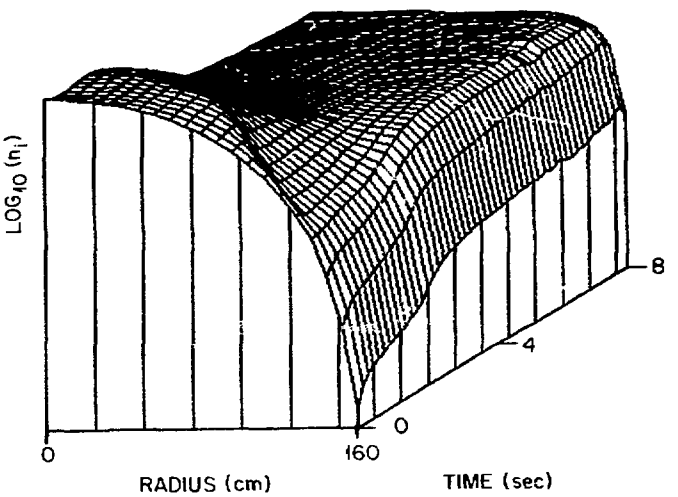

Fig. 2. Time evolution of the plasma ion density for $r_p = 25$ cm, $r_p/a = 0.2$. In the first second, the profile adjusts from the assumed initial conditions. (Transport model B with 85 MW of neutral beam power.)

ORNL/DWG/FED-77743

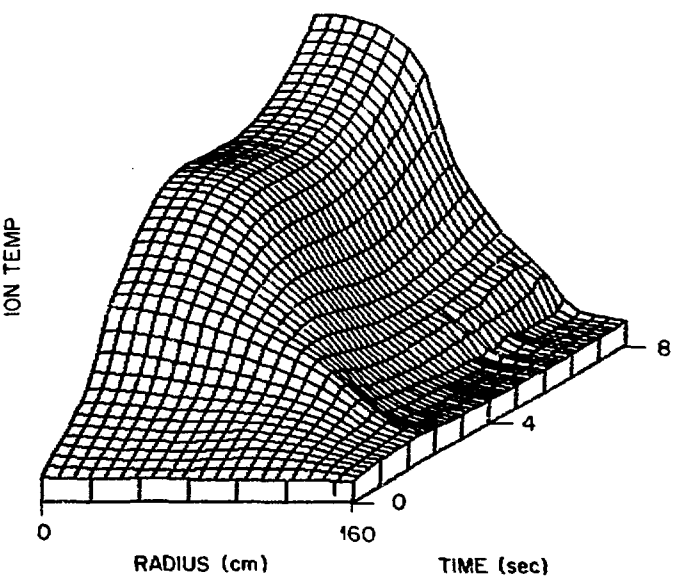

Fig. 3. Time evolution of the ion temperature for $r_p = 25$ cm (see Fig. 2). Note the low edge temperature due to the strong cooling effect of edge fueling.

in the model would be expected to broaden the temperature profile; among them are finite orbit effects and diffusion of fast alphas.[6] The density profile is nearly flat in the central region (Fig. 2) where no fueling takes place; hence, the anomalous transport due to the trapped particle model used is very small. A model for residual modes driven by temperature gradients and magnetic drift effects would be more appropriate under these circumstances.[7,8] Off-diagonal diffusion terms (i.e., Ware pinch and Nernst terms) arising from anomalous transport could also modify the flat density central region.

The transport coefficients of the trapped particle modes are further reduced in model C of Fig. 1 by a factor of four from model A. A very slight increase in losses is noted at low penetration, while no increase is found at deeper penetration for the range considered. Figures 4 and 5 show the plasma behavior for a deep penetration case ($r_p/a = 1.6$). The density and temperature profiles (Figs. 4 and 5, respectively) are both centrally peaked. The temperature profile smoothly transforms from the beam heating profile to the alpha heating profile.

ORNL/DWG/FED-77711

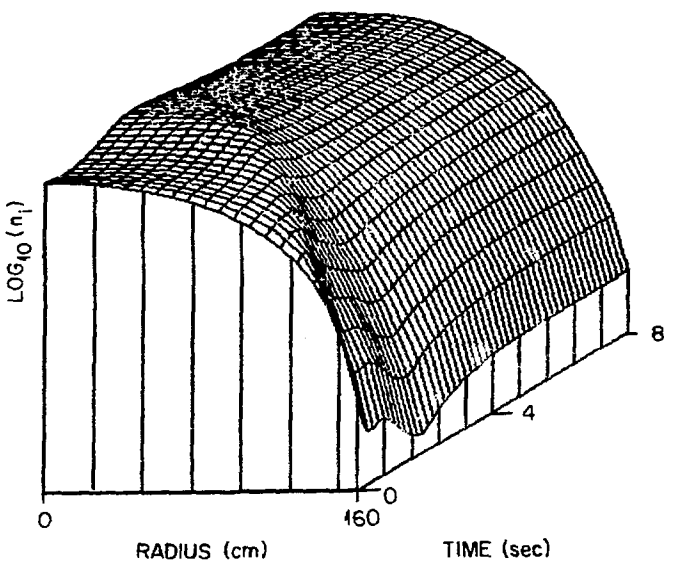

Fig. 4. Time evolution of ion density profile for deep penetration case $r_p/a = 1.6$.

Model D of Fig. 1 is included as a base case with only neoclassical transport. The beams provide more than enough particles to fuel the plasma, and no additional fueling is required during the 8 sec the plasma evolution is followed. The density builds up during the 2 sec the beam is on, then decays very slowly.

In general, the power requirements are reduced as the plasma density is reduced because the amount of plasma to be heated decreases and the penetration of the neutral beams is improved. However, in models A and B the increase in trapped particle losses is more abrupt at deeper penetration than for the corresponding cases run at higher average densities because of the lower collisionality. ($C \propto$ density.)

4. Effects of Discrete Pellet Fueling on Plasma Transport

One of the most interesting aspects of this study centers on initial investigations of the effects of discrete pellet fueling on the fluid transport equations. The model employed to describe the evaporation of solid hydrogen pellets injected into the tokamak plasma is based on the recent theory of Parks, Turnbull, and Foster[9] with the modifications proposed by Milora and Foster.[10] The inclusion of the pellet deposition model in the transport code is an important step toward a realistic treatment of a fueling model. In the following scenario, pellets shot into hot plasmas are found to ablate completely near the plasma edge, thereby cooling the edge and raising the edge density.

The low edge temperature may tend to reduce sputtering by charge-exchanged neutrals, but more work remains to be done in this area. Parameter variations involving pellet sizes and velocities have not been carried out here. (Most cases were run with 2 mm diameter pellets traveling at 10^3 m/sec.

The discreteness of the pellets poses special problems. In particular, strong temperature and density gradients arise on a fast time scale which taxes the transport theory for a fluid plasma. Local kinetic effects due to perturbation of the local distribution function by the cold pellets should be further investigated by experiment and theory to determine whether pellet sizes must be limited. However, the following observations can be made with some confidence: (1) The alpha power generated by a low velocity, pellet fueled reactor is fairly steady, since the temperature and density fluctuations are confined to the edge region. (2) The pressure profile fluctuates very little, since the stored energy is not changed much by the introduction of a pellet.

ORNL/DWG/FED-77709

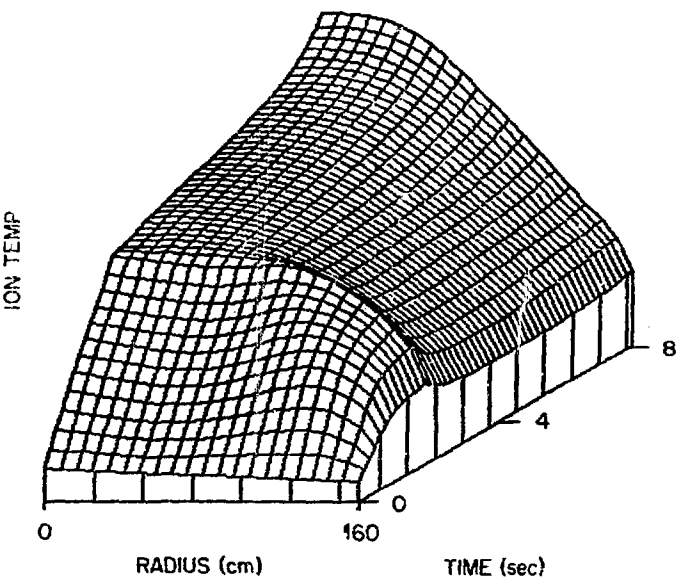

Fig. 5. Time evolution of ion temperature for $r_p/a = 1.6$ case. Note that the edge did not undergo as drastic a cooling as in the $r_p/a = 0.2$ case.

Figure 6 shows a 100-msec segment of the evolution of a typical plasma density profile. At about 75 msec, the plasma density has relaxed to a monotonically decreasing function of radius with an average density of 3×10^{13} cm^{-3}. At that time, a 3-mm pellet is injected into the plasma at a velocity of 10^3 m/sec. The pellet ablates almost instantaneously (<1 msec) leaving a spike in the plasma density near the edge. Figure 7 shows the corresponding effect on the ion temperature. Initially the edge temperature is depressed by the presence of cold plasma from the previous pellet. As the edge warms, the particles diffuse out of the edge region. At 75 msec the

ORNL/DWG/FED-77778

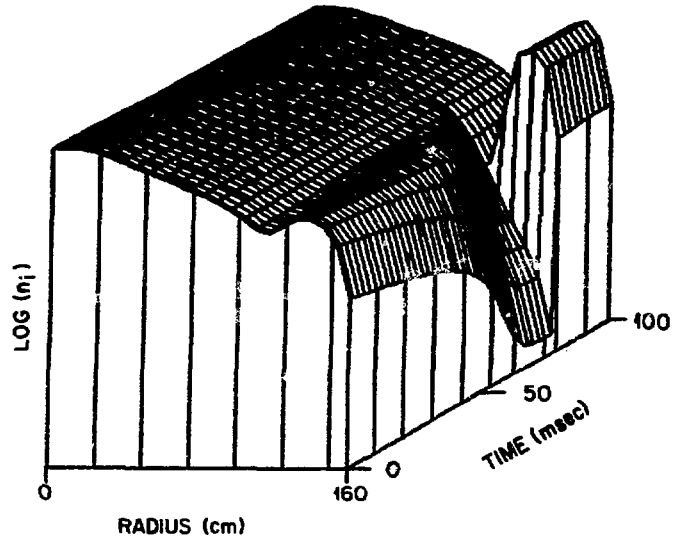

Fig. 6. 100 msec segment of plasma evolution. A low density ($\bar{n} \approx 3 \times 10^{13}$ cm^{-3}) plasma and large (3mm) pellets were used here to illustrate clearly the pellet ablation spike. Pellet velocity = 10^3 m/sec.

ORNL/DWG/FED-77779

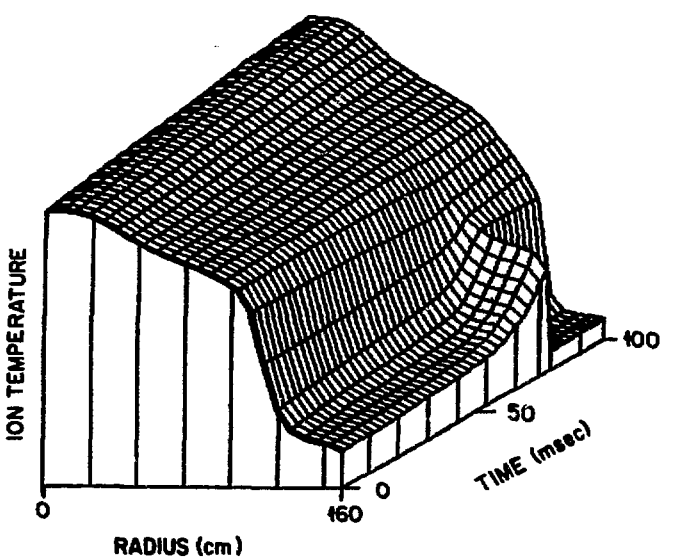

Fig. 7. Ion temperature evolution corresponding to density profile in Fig. 6. Note abrupt drop in T_i at edge due to pellet.

temperature drops sharply due to the injection of another pellet. Except for a short interval, the edge temperature remains at ~ 0.5-1.0 keV. This is true despite the fact that the beam is on during this segment of the simulation. The edge temperature is relatively high due to the divertor-type boundary conditions which neglect recycling of cold gas and exclude impurities.

Figures 8 and 9 show a complete simulation of a typical TNS case using smaller pellets in a more dense plasma. Most of the detail of the discrete pellets is washed out in these figures, due to the fact that 177 pellets were injected during the 8 sec, but only 45 profiles were used in the creation of these 3-D plots. A 2-mm radius pellet is injected whenever the

ORNL/DWG/FED-77780

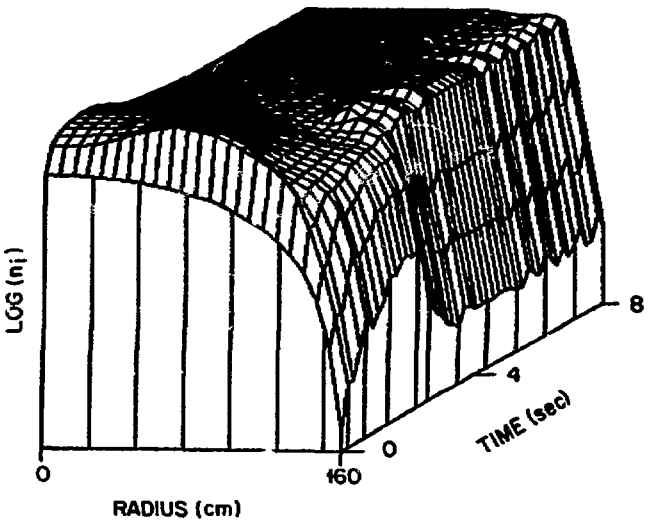

Fig. 8. Temporal evolution of ion density. Most detail of discrete pellets is not shown clearly due to the fact that 177 pellets were injected over 8 sec period. $\bar{n} \approx 10^{14}$ cm^{-3}.

ORNL/DWG/FED -77781

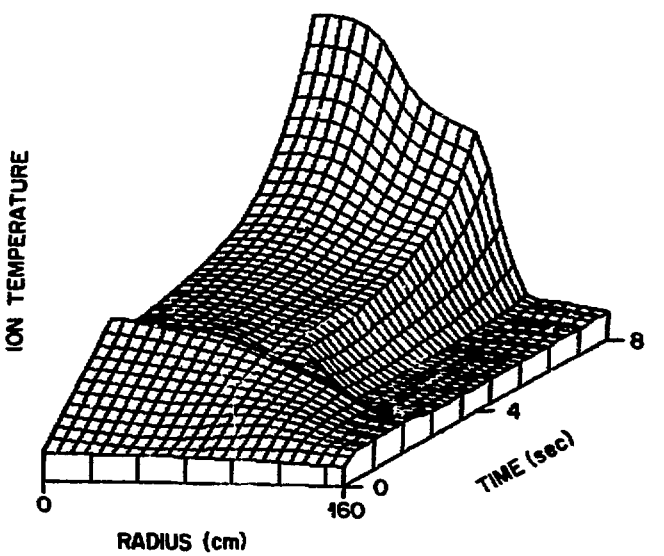

Fig. 9. Temporal evolution of ion temperature corresponding to case shown in Fig. 8. $\bar{T}_i$(8 sec) = 13.6 keV. Note low edge temperature.

average density falls below 1.0×10^{14} cm^{-3}. The pellet is injected at 10^3 m/sec. For the first 2 sec, 80-MW of 200 keV neutral deuterium beam is applied. The simulation is terminated at 8 sec, at which time the plasma is well ignited and the temperature is rising rapidly. At 8 sec, the following values are obtained: average ion temperature = 13.6 keV, average electron temperature = 15.0 keV, peak ion temperature = 35.1 keV, peak electron temperature = 35.4 keV, average density = 1.03×10^{14} cm^{-3}, peak

density = 1.27×10^{14} cm^{-3}, average beta = 6.4%, and peak beta = 19.4%. Similar behavior is seen at lower densities with the obvious modifications which show deeper beam penetration and somewhat deeper pellet penetration.

These reactor-like conditions were reached in spite of the inclusion of the full trapped particle mode diffusion as described in WASH-1295.[3] The one-dimensional treatment allows us to see the flattening of the density profile which occurs with shallowly penetrating pellets. The reduction of the density gradient diminishes the effect of the trapped particle mode diffusion terms as observed in Sect. 3.

ORNL/DWG/FED-77783

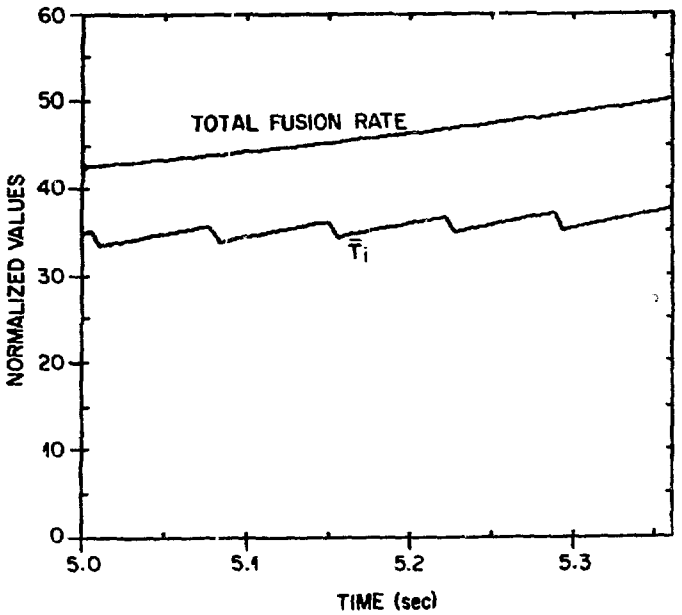

Fig. 10. Normalized values of alpha power (top curve) and density averaged ion temperature (lower curve) as function of time. Edge density and temperature fluctuations do not cause oscillation in fusion power.

Figure 10 shows normalized values of the density-averaged ion temperature and alpha power as a function of time for a typical case. The irregularity of the temperature curve is due to fluctuations in the edge region from pellet injection. Note that the alpha power curve is relatively smooth, since the alpha power comes mostly from the center, where the temperature and density are not fluctuating. For the same interval, Fig. 11 shows the evolution of the β (pressure) profile. Since β is proportional to the density temperature product (i.e., the stored energy density), and since a pellet carries very little stored energy, the β fluctuations are quite small.

Figure 12 illustrates the effect of plasma density on the power required to ignite the plasma.[3] Fueling is with 2-mm pellets at a velocity of 10^3 m/sec in all cases. The ordinate is the minimum beam power required to ignite a TNS plasma in 2 sec with a 200-keV deuterium beam. The general trend is that higher density requires higher beam power to maintain a similar power per particle. However, at very high densities the beam is unable to penetrate and the curves approach a limiting density asymptotically. At low densities, if the trapped particle modes are not too severe, the ohmic heating reduces the required beam power. However, if the trapped particle losses are severe, then there is minimum density which will not ignite at any temperature for the pellet parameters used here.

The most important point is that the spread in the data, which includes cases run with negligible trapped particle contributions (mainly neoclassical) and cases run with full WASH-1295 trapped particle contributions, is only about a factor of two in beam power. This is a clear indication that the trapped particle mode diffusion coefficients given in WASH-1295[3] can be very nearly turned off by shallowly penetrating pellets.

ORNL/DWG/FED-77784

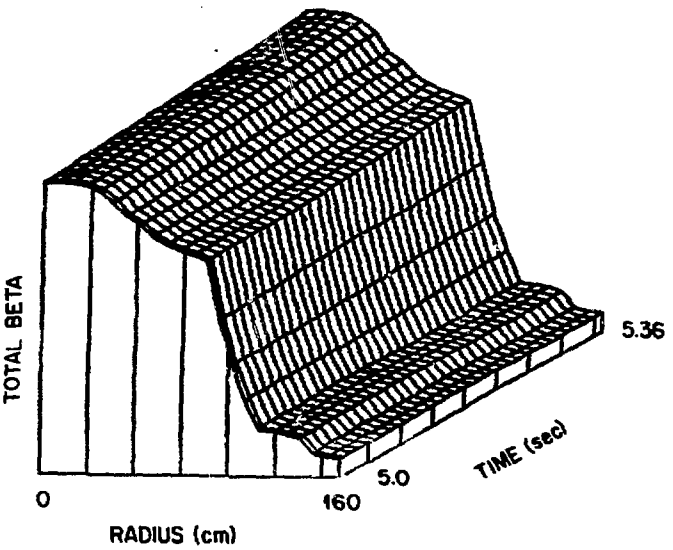

Fig. 11. Total Beta profile $\propto p(r)/B_T^2$. Note that edge n and T fluctuations offset one another and therefore $\beta \propto nT$ stays sensibly constant.

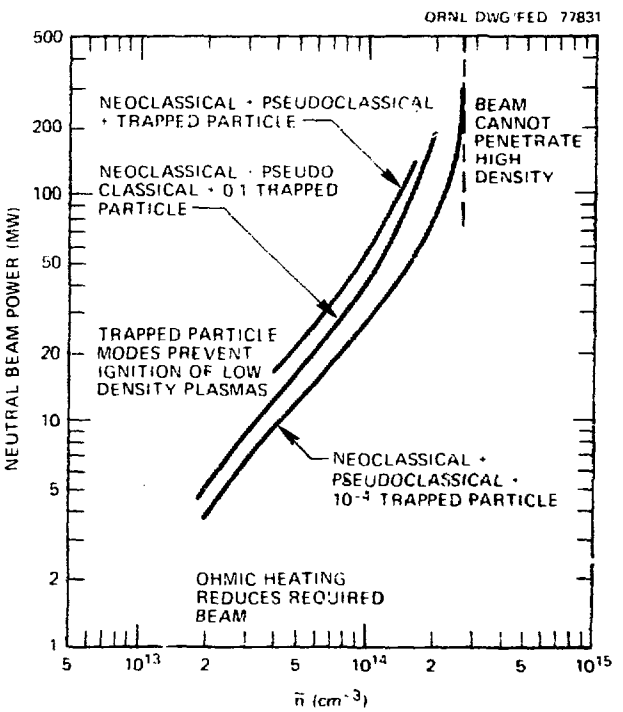

Fig. 12. Minimum beam power for ignition (200 keV beams on for 2 sec). Note only factor of ~2 in required beam power between full trapped particle and neoclassical.

5. Conclusions

Initial investigations of the effects of particle fueling profiles on plasma transport and plasma behavior have been reported here. In general, a controllable particle source profile may provide a significant amount of control over dynamic behavior.

A controllable particle source may be used to add external control over the plasma behavior during heating to ignition. Very low penetration is easy to accomplish (e.g., gas puffing) but may increase losses near the plasma edge. Very deep penetration to the plasma center would be very difficult and may be undesirable if density gradient driven trapped particle modes dominate the transport. Intermediate penetration depths appear to provide an optimum in the heating-to-ignition power requirements for the model studied here.

The discrete pellet fueling model provides very encouraging results. Fairly large fluctuations can occur in the density and temperature near the plasma edge with large pellets, but pressure fluctuations are very small. The central density and temperature do not fluctuate with shallowly penetrating pellets; therefore, power production in a reacting plasma should be continuous and not oscillatory. No significant increased beam attenuation is observed even in fairly large ablation spikes in the edge density. All of the above considerations allow fairly large, low velocity pellets to be used if kinetic effects do not invalidate the assumptions of fluid behavior.

Much further theoretical and experimental work needs to be done to adequately assess the effects of varying fueling profiles, and the transport model certainly needs improvement. The ordering of scale lengths in determining the growth rates of the trapped particle modes under the conditions of edge fueling should be examined more fully. For any transport model, the existence of pinch and Nernst terms in the diffusion equation can be important when density profiles become flat. In addition, because fueling of the central region is accomplished by inward diffusion when the fuel deposition is limited to the plasma edge, relative diffusion rates of deuterium and tritium must be further assessed for reactor conditions.

Experimental verification of the pellet ablation model is needed for higher density and hotter plasmas. Pellet injection experiments may also provide added insight in experimental determination of the transport coefficients.

References

1. J. T. Hogan, Meth. in Comput. Phys. 16, 131 (1976).
2. F. L. Hinton and T. B. Moore, Nucl. Fusion 14, 639 (1974).
3. S. O. Dean et al., "Status and Objectives of Tokamak Systems for Fusion Research," WASH-1295, USAEC, Washington, D.C. (1974).
4. A. T. Mense, W. A. Houlberg, S. E. Attenberger, and S. L. Milora, Effects of Fueling Profiles on Plasma Transport, ORNL/TM-6026, Oak Ridge National Laboratory, Oak Ridge, Tennessee (September 1977).
5. W. A. Houlberg and R. W. Conn, Nucl. Sci. Eng. 64, 141 (1977).
6. A. T. Mense, Ph.D Thesis, Nucl. Eng. Department, University of Wisconsin (1977).
7. J. C. Adam, W. M. Tang, and P. H. Rutherford, Phys. Fluids 19, 561 (1976).
8. W. M. Tang, J. C. Adam, and D. W. Ross, Phys. Fluids 20, 430 (1977).
9. P. B. Parks, R. J. Turnbull, and C. A. Foster, Nucl. Fusion 17, 557 (1977).
10. S. L. Milora and C. A. Foster, ORNL Neutral Gas Shielding Model for Pellet-Plasma Interactions, ORNL/TM-5776, Oak Ridge National Laboratory, Oak Ridge, Tennessee (May 1977).

EQUILIBRIUM AND STABILITY FEATURES OF GAS BLANKET SYSTEMS

D. Ohlsson

Royal Institute of Technology, S-10044 Stockholm, Sweden

Summary

The equilibrium properties of gas blanket systems will be reviewed. In particular, steady state solutions of the balance equations, compatible with the neutral gas blanket concept, are presented. The stability properties of gas insulated plasmas are discussed in some detail. It is shown that the joint effect of plasma neutral gas interaction and resistivity introduce strong stabilizing effects for a large class of MHD modes. This applies however only within specific parameter ranges.

Introduction

The gas blanket concept[1,2,3,4] offers unique possibilities for fueling and controlling the impurity influx in a thermonuclear reactor. The surrounding neutral gas could act as a fuel reservoir, provided the transport processes are such that deuterium and tritium can diffuse inwards and helium ions outwards. Further, the boundary regions will act as a shield for highly energetic charge exchange neutrals, if the product of characteristic ion density n_c and characteristic dimension L_c exceeds a certail critical value[2,4] for hydrogen $n_c L_c > 10^{15}$ cm^{-2}. Thus the flux of charge exchange neutrals impinging on the vessel walls and the associated sputtering becomes strongly reduced. The condition $n_c L_c > 10^{15}$ cm^{-2} also implies that the hot core becomes impermeable for cold neutrals penetrating from the outside thus assuring that the heat losses due to charge exchange are kept at a tolerable level. However only when the ion density is chosen well within the impermeable density regime, for magnetic field strengths and characteristic dimension typical for present day confinement devices, the main plasma body is insulated from material walls by a neutral gas blanket.

The main purpose of this communication is to elucidate the main equilibrium and stability features of gas blanket systems. Solutions of the balance equations, assuming classical transport, are presented. The stability properties of the boundary regions becomes of particular importance for two reasons. First large pressure gradients are likely to arise across the boundaries in gas insulated plasmas[3]. Second minimum-$\bar{B}$[5] and shear are expected to become less effective on account of insufficient line tying and the small localization regions of the modes considered respectively.

Equilibrium

The existence of a gas blanket system depends on whether steady state solutions of the balance equations exists with the proper boundary conditions imposed by the surrounding neutral gas. The particular form of the solutions depends on the specific transport mechanisms prevailing in different parts of the plasma. We will restrict ourselves in what follows to classical transport processes, for the simple reason that most work done so far has been limited to such processes. We recognize that this is a severe restriction. The transport in a future reactor is very likely to be anomalous. Consequently several of the conclusions drawn from the physical models discussed could be subject to alterations.

Central Regions

Detailed analysis of the ion and impurity density profiles in cylindrical arc discharges have been made. Assuming collisional transport and vanishing particle flux, the latter condition being also a good approximation for reactor conditions[4], it was found that the ion density n becomes related to the electron temperature T_e by the relation[6]

$$nT_e^{(2\delta-Z_i)/2(\delta+Z_i)} = \text{const} \qquad (1)$$

Here Z_i = charge number of plasma ions, $\delta = T_i/T_e$, T_i = ion temperature. Further the density of impurities n_I, assuming vanishing impurity flux, $n_I/n \ll 1$, $\delta = 1$ and $Z_i = 1$, becomes related to the ion density by[4]

$$n_I n^{-3Z_i(2M-1)-4} = \text{const} \qquad (2)$$

$$M = (m_I - m/Z_i)/(m_I+m) \qquad (3)$$

Here m = ion mass and m_I = impurity mass. Similar analysis have been made in toroidal geometry assuming boundary temperatures of the order of a few eV[4,7]. Assuming neoclassical transport the density temperature relations become

$$nT^{-0.28} = \text{const in the banana regime} \qquad (4)$$

$$nT^{1.46} = \text{const in the plateau regime} \qquad (5)$$

$$nT^{0.58} = \text{const in the Pfirsch-Schlüter regime} \qquad (6)$$

$$nT = \text{const in the highly collisional regime} \qquad (7)$$

Here $T = T_i$, $\delta = 1$. Schematic plots of the density and impurity profiles for a bell-shaped temperature profile are shown in Fig.1. The profiles calculated are consistent with the neutral gas blanket concept.

Verboom and Rem[8] investigated the possibility of a gas blanket reactor in straight cylindrical geometry. A balance was assumed between the thermonuclear power production and the heat losses due to bremsstrahlung, heat conduction and heat convection. Steady state solutions, where deuterium and tritium diffuse inwards and helium ions outwards, was found with a power production up to 1GW/m for axial magnetic field between 3-10 T and plasma radius of the order of a few meters.

Boundary Regions

The balance of the partially ionized boundary regions has been investigated by several authors[2,9,10,11,12]. The general structure is illustra- in Fig.2. There are essentially three subregions[2,12]. First, a rather narrow ionization region where the main part of the ionization processes occurs. Second, a diffusion region where the outflux of charged particles is balanced by an equal and opposite influx of neutral particles. Third, a wall near cool neutral gas region. The particle and momentum balance in the diffusion region, assuming density gradient effects more important than temperature gradient effects, can be expressed in plane slab geometry as follows[2,12]

$$\frac{dN}{ds} = \frac{1}{N} + N + N_n \quad (8)$$

$$\frac{dN_n}{ds} = -2(N+N_n) \quad (9)$$

Here $N = n/n_B$, $N_n = n_n/n_B$, $n_B = k_B B$, $k_B = [\eta_\perp m m_n \xi_{in}/(m+m_n)]^{-1/2}$, $s = m m_n \xi_{in} \Gamma x / 2kT_m(m+m_n)$, ξ_{in} = effective collision frequency for ion-neutral collisions, n_n = neutral particle density, m_n = neutral mass, B = magnetic field strength, k = Boltzmann's constant, $\eta_\perp$ = perpendicular resistivity, Γ = outflux of charged particles from the internal plasma region, T_m = average value of the temperature, x = spatial coordinate. These equations have been solved analythically and numerically by Lehnert[2,12]. The asympthotic solutions of the normalized densities $N_b = n_b/n_B$ and $N_{no} = n_{no}/n_B$ on either side of the diffusion region becomes related by

$$N_{no} = \frac{2}{3} N_b^3 \ll 1 \quad (10); \qquad s_b = \frac{1}{2} N_b^2 \quad (11)$$

$$N_{no} = 2N_b \gg 1 \quad (12); \qquad s_b = \ell n 2 \quad (13)$$

Here $s_b = s(x=x_b)$, x_b = boundary layer thickness.

Stability

Fully Ionized Region

The global MHD stability of gas blanket systems has been investigated by several authors.[13,14,15] Murty[13] showed that the neutral gas could in many cases be accounted for by introducing an enlarged mass. Since the growth rate of MHD modes are typically proportional to the Alfvén velocity, this results in reduced growth rates. The general picture is as follows. Stability limits for modes localized to central parts are typically unchanged as compared to vacuum insulated plasmas. The growth rates however could be considerably reduced, in particular when the density of the surrounding neutral gas is much larger than the plasma density. It should be pointed out that there are exceptions, for instance in cases when force free currents are induced in the partially ionized boundary regions thus improving the stability properties[16].

Partially Ionized Boundary Region

A neutral gas blanket indirectly affects the stability properties by modifying the equilibrium pressure profiles. This effect becomes of particular importance in the boundary regions where the neutral gas tends to "pump up" the density profiles over limited distances, thus large pressure gradients inevitable builds up. The stability of the boundary regions therefore becomes essential for the whole neutral gas blanket concept. This problem becomes particularly important since conventional stabilizing mechanisms are expected to become less effective as was discussed in the introduction. We make a localized perturbation analysis in cylindrical geometry assuming all quantities to vary as $\exp[i(k_r r+m\theta+2\pi nz/L-\omega t)]$. The main magnetic field is in the axial direction. The equilibrium properties depend on the radial coordinate only. In this simplified analysis we disregard effects due to shear. The main purpose of this analysis is to investigate whether complementary or alternative stabilization mechanisms exist, which are particular for gas blanket systems. A standard type analysis assuming $\omega_n \ll \omega \ll \omega_{ci}$ yields

$$\left[(\omega+i\omega_\mu)(\omega+i\omega_{\eta p}+i\omega_{\mu p})+\omega_g^{*2}\right]\tilde{\phi} - \left[\frac{(\omega_A^2-\omega_{dj}^2)(\omega+i\omega_{\eta p}+i\omega_{\mu p})}{k_\parallel}\right]\tilde{A}_\parallel = 0 \quad (14)$$

$$\left[1+\frac{i}{\omega+i\omega_{\eta p}+i\omega_{\mu p}}\left(\frac{\omega_n\omega_\mu}{\omega_{ci}^*} - \frac{\omega_j\omega_r\omega_{ci}^*}{\omega_A^2}\right)\right]\tilde{\phi} - \left[\frac{\omega}{k_\parallel} + i\frac{\omega_r}{k_\parallel}\right]\tilde{A}_\parallel = 0 \quad (15)$$

$$\omega_\mu = \frac{\mu_c k_\perp^2}{n m_c} \quad (16)$$

$$\omega_n = \frac{\gamma k_b T}{neB}\frac{dn}{dr} \quad (17)$$

$$\omega_g^{*2} = \left(1 - \frac{\omega}{\omega_{ci}^*} - i\frac{\omega_\mu}{\omega_{ci}^*}\right)\omega_g^2 \quad (18)$$

$$\omega_g^2 = \frac{4k_b e\omega_n}{m_c k_\perp^2}\frac{dB}{dr} \quad (19)$$

$$\omega_{ci}^* = \frac{mk_b\omega_{ci}}{m_c k_\perp^2 n}\frac{dn}{dr} \quad (20)$$

$$\omega_r = \frac{\eta_\parallel k_\perp^2}{\mu_0} \quad (21)$$

$$\omega_{\eta p} = \frac{2\gamma nkT\eta_\perp k_\perp^2}{B^2}\left[1 - \frac{3(\gamma-1)}{4\gamma}\right] \quad (22)$$

$$\omega_{\mu p} = \frac{\gamma kT\mu_c k_\perp^4}{ne^2B^2} \quad (23)$$

$$\omega_A = k_\parallel \frac{B}{(\mu_0 n m_c)^{1/2}} \quad (24)$$

$$\omega_{dj}^2 = \frac{k_b k_\parallel B}{n m_c k_\perp^2}\frac{dj_\parallel}{dr} \quad (25)$$

$$\omega_j = \frac{3(\gamma-1)k_\parallel j_\parallel}{2ne} \quad (26)$$

Here $k_\perp = (k_b^2+k_r^2)^{1/2}$, $k_b = 2\pi n B_\theta/LB - mB_z/rB$, $k_\parallel = mB_\theta/rB + 2\pi nB_z/LB$, $\mu_c = \mu_i+\mu_n$, $m_c = m(1+n_n m_n/nm)$, L = length of plasma column, $\delta = 1$, γ = ratio between specific heats, B_θ = azimuthal magnetic field, B_z = axial magnetic field, $B = (B_\theta^2+B_z^2)^{1/2}$, $j_\parallel$ = current density along lines of force, μ_i = viscosity coefficient due to ion-ion collisions μ_n = neutral gas viscosity coefficient[5], ω_{ci} = ion cyclotron frequency, e = electric charge, $\eta_\parallel$ = resistivity parallel to the lines of force, $\tilde{\phi}$ = perturbed scalar potential, $\tilde{A}$ = perturbed magnetic potential along the lines of force.

Kink and Balooning Modes

The stability criterion for the high frequency electromagnetic branch can be found from Eqs. (14)-(15). After making the appropriate approximation we arrive at the following criterion

$$\omega_g^2 + \omega_{dj}^2 - \omega_r\omega_\mu - \omega_A^2 < 0 \quad (27)$$

The first term is associated with the driving force for balooning modes i.e. "bad" curvature of the lines of force. The second term corresponds to the driving force for kink modes i.e. the torque arising from the gradient of the current density along the lines of force. The term $\omega_r\omega_\mu$ corresponds to a stabilizing effect particular for gas insulated plasmas which arises due to a joint resistive-viscous effect (quite different from the joint viscous-resistive-pressure effect discussed in connection with flute modes[5]). The viscous effects are strongly enhanced on account of plasma neutral gas interaction effects in certain parameter ranges. The last term ω_A^2 corresponds to the stabilizing effect which arises due to the bending of the lines of force. Let us first consider kink like modes neglecting effects associated with ω_g^2. The critical current density gradient$(dj_\parallel/dr)_c$ for stability is given by the following expression

$$\left(\frac{dj_\parallel}{dr}\right)_c = 2\frac{k_\perp^4}{k_b\mu_o}(\mu_c n_\parallel)^{1/2} \qquad (28)$$

It is quite easy to show that the most difficult modes to stabilize correspond to modes with the largest scale. Consequently we put $k_\perp = \sqrt{2}\,?\,/x_b$. We further use the previously derived expressions for the density of neutrals and boundary layer thickness given by Eqs. (10)-(11). We further assume that the particle flux Γ depends on ion density and magnetic field strength in the following way

$$\Gamma \sim n^\alpha B^{-\beta} \qquad (29)$$

Here α and β equal constant. In the following analysis we will assume a near classical scaling i.e. $\alpha \sim 2$, $\beta \sim 2$. We thus find

$$\left(\frac{dj_\parallel}{dr}\right)_c \sim n^{3\alpha-5}B^{5-3\beta} \qquad (30)$$

Consequently as the plasma density increases or the magnetic field strength decreases the stability properties improves. The stabilizing effect associated with plasma neutral gas interaction effects enters through the term ω_μ. One would of course expect these effects to become increasingly important as the plasma density increases or magnetic field decreases since $n_n/n \sim n^2B^{-2}$. In an analogous way we find that the critical pressure gradient for exciting balooning modes ∇p_c^b neglecting effects associated with ω_{dj}^2 is given by the expression

$$\nabla p_c^b = \frac{Bk_\perp^2}{4\mu_o k_b^2}(\eta_\parallel\mu_c k_\perp^4 + \frac{B^2}{q^2R^2})(\frac{dB}{dr})^{-1} \qquad (31)$$

Here $q = rB_z/RB_\theta$, $R = L/2\pi$. In a similar way as for kink modes we can derive the scaling of ∇p_c^b with n and B. The conclusions are essentially the same. For datas typical of the partially ionized boundary layers of gas insulated plasmas, for example $n \sim n_n \sim 2 \times 10^{15}$ cm^{-3}, T ~ 5eV, $x_b \sim 1$ cm, B ~ 1T, we find, indeed, that plasma neutral gas interaction effects and resistivity modify the stability criterions for kink and balooning modes and introduce strong stabilizing effects. It must, however, be emphasized that for datas typical of present day tokamaks, plasma neutral gas interaction processes plays only a minor role.

Flute, Current Convective and Drift Modes

Considering the low frequency electrostatic branch, including finite Larmor radius and diamagnetic drift effects we arrive at the following stability criterion

$$\omega_g^2 + \omega_j\omega_{ci}^* + \omega_\Lambda^2 - \omega_\Lambda\omega_n - \omega_\mu\omega_{\eta p} - \frac{\omega_{\eta p}+2\omega_{\mu p}}{\omega_r}\omega_A^2 < 0 \qquad (32)$$

$$\omega_\Lambda = \frac{2\omega_n\omega_A^2/\omega_r + \omega_n\omega_{\eta p} + \omega_j\omega_\mu + \omega_g^2\omega_\mu/\omega_{ci}^*}{\omega_{\eta p} + \omega_\mu + \omega_A^2/\omega_r} \qquad (33)$$

The first term in the inequality (32) corresponds to the driving force for flute modes, i.e. the curvature of the lines of force. The second term $\omega_j\omega_{ci}^*$ corresponds to a destabilizing effect and arises due to the joint action of the current along the lines of force and the pressure gradient. The third term ω_Λ^2 corresponds to the driving force for drift modes. The term $\omega_\Lambda\omega_n$ corresponds to a stabilizing effect associated with finite Larmor radius effects in the ion pressure tensor. The term $\omega_\mu\omega_{\eta p}$ represents a stabilizing joint viscous-resistive-pressure effect previously discussed by Lehnert in connection with flute modes[5]. The last term $\omega_A^2(\omega_{\eta p}+2\omega_{\mu p})/\omega_r$ finally corresponds to a stabilizing effect which arises due to a joint resistivity-cross diffusion effect, particular for modes propagating along the lines of force. Note that the last two terms arise due to the simultaneous effects of plasma neutral gas interaction and resistivity. Proceedings in a similar way as in the previous section it is easy to show that the stability conditions improve for increasing ion densities due to enhanced plasma neutral gas interaction effects. Considering flute modes we found that the critical pressure gradient ∇p_c^f is given by the expression

$$\nabla p_c^f = \frac{\gamma nkTk_\perp^6\eta_\perp\mu_c}{2Bk_b^2}\left[1 - \frac{3(\gamma-1)}{4\gamma}\right](\frac{dB}{dr})^{-1} \qquad (34)$$

Using the same type of scaling as in the previous section we arrive at a critical density limit n_ℓ^f above which the system becomes flute stable. Here n_ℓ^f scales as

$$n_\ell^f \sim B^{\beta-1/(\alpha-1)} \qquad (35)$$

Similarly for current convective modes

$$j_\parallel^c = \frac{4}{3}\frac{n^2m_ck_\perp}{(\gamma-1)Bk_b}\left[\frac{B^2}{\eta_\parallel nm_c}(2\omega_{\mu p}+\omega_{\eta p})\omega_{\eta p}\omega_\mu\right]^{1/2}(\frac{dn}{dr})^{-1} \qquad (36)$$

The critical density limit n_ℓ^c for these modes scales as

$$n_\ell^c \sim B^{2\beta-1/2(\alpha-1)} \qquad (37)$$

Drift modes can be treated in an analogous way. If one includes also ionization effects in the analysis one finds that there exists an upper density limit n_u^i common for all electrostatic modes discussed, corresponding to the onset of an ionization type instability. Here

$$n_u^i = \frac{2(\gamma-1)}{\gamma+3}\frac{B^2n_n}{k\eta_\perp k_\perp^2}\frac{d\xi}{dT} \qquad (38)$$

where $n_n\xi$ = ionization frequency. The upper density limit scales in the following way

$$n_u^i \sim B^{2-\beta/(3-\alpha)} \qquad (39)$$

For data typical of the partially ionized boundary regions we find that the stability criterion given by the inequality (32) can be satisfied within specific density limits for given magnetic field strength, current density etc. The lower density limit which has to be surpassed in order for plasma neutral gas interaction effects to be important has not yet been reached in present day tokamaks.

Conclusions

The equilibrium properties of gas insulated plasmas, including the boundary regions, has been reviewed. Steady state solutions exists, compatible with the neutral gas blanket concept, at least for classical and neoclassical transport processes. Several of the results obtained could,however,be subject to alterations since the transport in a thermonuclear reactor is expected to be anomalous.

Concerning the MHD stability it is found that the stability limit for modes localized to central regions are typically unchanged as compared to a vacuum insulated plasma. The main effect of the surrounding neutral gas is thought to be a reduction of the corresponding growth rates. The stability limits for modes localized to the boundary regions can however be drastically changed. The stability of the boundary regions is of particular importance, since it seems inevitable that large pressure gradients will arise across the boundaries in gas insulated plasmas. General stability criteria for high frequency kink and balooning modes as well as low frequency flute, drift and current convective modes have been derived neglecting shear. The present analysis indicates that the joint effect of plasma neutral gas interaction and resistivity introduces strong stabilizing effects. Considering all effects simultaneously it seems possible that complete stabilization of electromagnetic as well as electrostatic modes can be achieved within specific parameter ranges. Present tokamak experiments are typically performed at ion densities and magnetic field strengths where plasma neutral gas interaction effects on stability are of minor importance.

Acknowledgements

The author is indebted to Prof. B. Lehnert for fruitful and enlightening discussions.

This work has been supported by the European Communities under an association contract between Euratom and Sweden.

References

[1] ALFVÉN, H., SMARS, E., Nature 188, (1960), 801.

[2] LEHNERT, B., Arkiv Fysik 18, (1960), 251 and 38(1968)499; Nuclear Fusion 8, (1968)173 and 11(1971)485;Roy.Inst. of Technology,Stockholm, TRITA-PFU-77-03, updated September 1977.

[3] LEHNERT, B., Roy.Inst. of Technology, Stockholm, TRITA-EPP-72-26; Third International Symposium on Toroidal Plasma Confinement, Garching, (1973),C7.

[4] ENGELMANN, F., GOEDHEER, W., NONCENTINI, A., SCHÜLLER, F., International Symposium on Plasma Wall Interaction at Jülich, (1976); Comments on Plasma Physics and Controlled Fusion III, No.2(1977)63.

[5] LEHNERT, B., Plasma Physics and Controlled Nuclear Fusion Research (1974)IAEA, Vienna,II (1975), 717.

[6] VENUS, G., Z. Physik 259,(1973), 437.

[7] ENGELMANN, F., NONCENTINI, A., Sixth International Conference on Plasma Physics and Controlled Nuclear Fusion Research, Berchtesgaden(1976), IAEA-CN-35/B7.

[8] VERBOOM, G., REM, J., Nuclear Fusion 13,(1973), 958.

[9] WIENECKE, R., Zeitung für Naturforschung, 18a, (1963)1151.

[10] VERBOOM, G., Plasma Physics 11,(1969),903.

[11] REM, J., Nuclear Fusion 10,(1970),95.

[12] LEHNERT, B., Nuclear Instruments and Methods 129(1975),31.

[13] MURTY, G., Arkiv för Fysik 19,37,(1961)511.

[14] TALWAR, S., TANDON, J. Plasma Physics,(Journal of Nuclear Energy, Part C)5, (1963)243.

[15] WILHELM, H., Proceedings 5th International Conference on Ionization Phenomena in Gases, Munich(1961)2233.

[16] GOEDBLOED, J.P., Workshop on Cold-Blanket Research, Rijnhuizen Report, 77-103(1977).

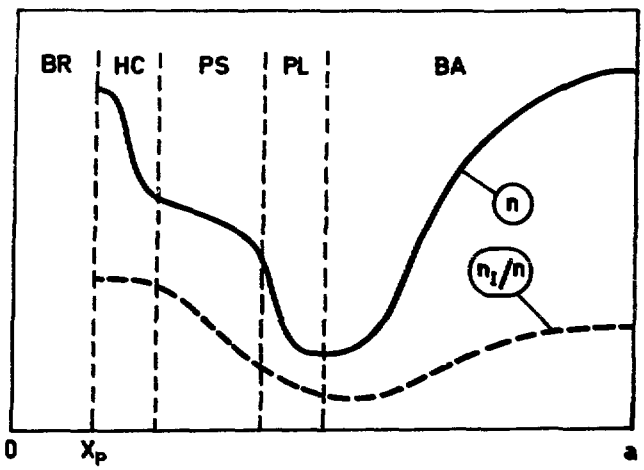

Fig.1. Schematic plots of density and impurity profiles in toroidal geometry. Temperature profile is assumed bell shaped. Regions: BR=Boundary, HC=Highly collisional, PS=Pfirsch-Schlüter, PL=Plateau, BA=Banana[4,7].

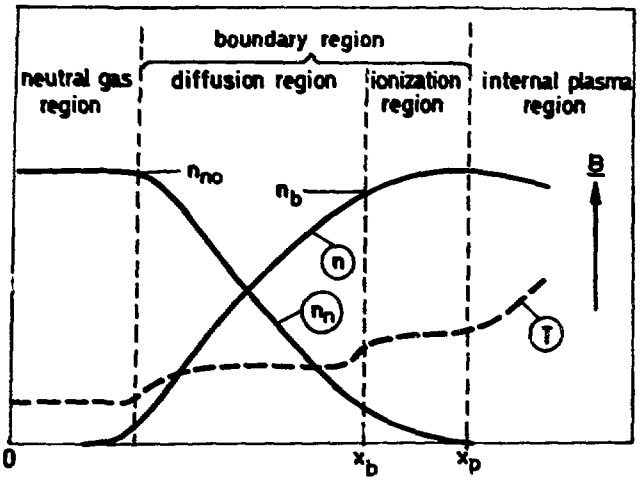

Fig.2. Schematic plot of boundary structure of gas blanket systems[2,12].

GAS BLANKET FUELING OF A TOKAMAK REACTOR†

S. L. Gralnick
Princeton Plasma Physics Laboratory
Princeton, NJ 08540

I. Introduction

The purpose of this paper is a speculative investigation of the potential of fueling a Tokamak by introducing a sufficiently large quantity of gaseous deuterium and tritium at the vacuum wall boundary. It is motivated by two factors: current generation tokamaks are, in a manner of speaking, fueled from the edge quite successfully as is evidenced by pulse lengths that are long compared to particle recycling times[1], and by rapid plasma density increased produced by gas puffing [2], alternative, deep penetration fueling techniques that have been proposed [3] possess severe technological problems and large costs.

The term "Gas Blanket" which has become synonymous with this approach to the boundary region of a fusion reactor was first introduced by Alfven and Smars [4] who were concerned with the problem of isolating the plasma from the surrounding vessel walls by the thermal insulation provided by a dense layer of fully ionized, but cool, plasma; they proposed this technique as an alternative to requireing a vacuum region between the plasma and the wall. Subsequent, more detailed calculations, based on this proposal were performed by Falthammar [5] and independently by Alikhanov [6], and an experimental test of this proposition was later reported by Smars and Johansson [7].

Consideration of the effect of neutral gas in the boundary region of the device was first undertaken by Lehnert who has subsequently investigated many aspects of this problem [8]. We will discuss Lehnert's model of a gas-blanket system and its utilization in a tokamak below.

While the work referenced above has focused on equilibrium solution to the particle, energy, and momentum balance equations, Oliphant [9] has considered the time dependent problem in the context of devising a means of rapidly cooling or quenching a pulsed, high β (ratio of energy density to magnetic field energy density) device. His analysis is conceptually quite different from that of the previously cited work, but is still quite relevant to the problem at hand. In fact, the case that Oliphant has considered is one that we should like to avoid, namely the quenching of the plasma due to the introduction of neutral gas. This will occur when the energy source provided by fusion reactions and ohmic dissipation within the core of the plasma is not adequate to ionize and heat the incoming neutral gas as well as support the radiation losses from the plasma.

Perhaps the most detailed analysis of the fully ionized, reacting core-plasma is that of Verboom and Rem [10] who have considered the problem of determining the temperature profile in a reactor under the supposition that the fuel supply and ash removal occur via diffusion through a gas blanket. The experimental program at Jutphass aimed at testing these hypotheses is described by F. C. Schuller et al., [11].

Recently Bhadra and Gross [12] have proposed a cold flowing plasma blanket as a means of isolating the central core plasma from the wall, relying on the excitation of a current-convective instability to provide desired heat conduction properties. Although the authors do not specifically draw upon the previous studies of fully ionized plasma blankets, it would appear that their analysis provides an interesting extension of this earlier work.

We shall be principally concerned with consideration of a gas-blanket model somewhat similar to that of Lehnert, which will be described in the next section of this article. Specific reference to the analysis of fully-ionized plasma blankets will only be made as they bear on the content of the present analysis.

The plan of presentation of the remainder of this article is as follows: In Section 2, Lehnert's gas-blanket model is reviewed and its applicability to tokamak fueling studies is evaluated. Section 3 is then devoted to a discussion of the physical mechanisms of neutral gas fueling and the evaluation of conditions under which these mechanisms appear to be adequate to provide required fuel supplies.

II. Lehnert's Gas-Blanket Model

Lehnert's model is illustrated in Fig. 1 [8]. A one-dimensional analysis is performed. The region of space $\chi > o$ is occupied successively by a region of weak ionization in which charged and neutral matter counterdiffuse, a region of narrow extent in which full ionization is achieved and a fully ionized plasma core region. Between $\chi = o$ and the boundary of the system at $\chi < o$ is found neutral gas. A system of magneto-fluid-static equations are employed in analyzing this model, and the solution of these equations under various assumptions yields profiles of plasma density, neutral gas density and a common temperature for all species present.

Several caveats must be observed and are discussed at some length by Lehnert [8]. The model depicted in Fig. 1 breaks down if the plasma density falls below a certain critical denisty, n_c. The case illustrated is that of an impermeable plasma for which $n \gg n_c$, where n_c is determined by

$$L = \frac{5 \times 10^{18}}{n_c}, \quad \text{[MKS units]} \qquad (1)$$

and L is the characteristic dimension of the system. When $n \sim n_c$ the partially ionized plasma region extends to the system wall and energetic neutrals produced by charge exchange permeate the body of the plasma while the colder source neutrals are absorbed (by ionization and upscatter, i.e. charge exchange), near the boundary. This parameter range is characteristic of current tokamak experiments. At still lower densities both low energy and high energy neutral particles will be found throughout the volume of the plasma.

Some question exists of the validity of applying a fluid analysis to the neutral gas component of this model. At the lowest density values this cannot by justified, as has been pointed out by Lehnert [8]. At the density characteristic of todays experiments and at high densities (impermeable plasmas) the author asserts that the plasma denisty is sufficiently high so that a fluid analysis is valid.

Analyses performed by Lehnert and others indicate that it is possible to find solutions in which the flow of energy outward from the plasma is sufficient to ionize and heat the incoming neutral gas as well as to balance the radiation losses from the plasma; this is a prerequisite to maintaining a gas blanket system. The problem of determining the plasma equilibrium has been treated by including a viscous like drag term that arises from the counter streaming of the plasma and gas components. Finally some investigations of the stability of these systems have been performed [13].

Although a qualitatively correct description of the neutral gas plasma interaction is given by the fluid model described above, the application of this analysis to the gas component is not, in a rigorous sense, justified. In plasmas for which the product of the characteristic length, (the boundary layer thickness), and the plasma density exceeds 5×10^{18}, ionizing collisions are very frequent as are charge exchange events and consequently the plasma is very absorbing. In the optical sense it is opaque. No consideration is given however to the frequency of neutral-neutral collisions which can be very small (less frequent than neutral plasma interactions) if the neutral density is moderate. The validity of the results stems from the fact that after many plasma-neutral collisions the neutral particle distribution function closely resembles the plasma distribution function at each point in space. If the plasma is Maxwellian the neutral particles will also have this distribution function. Calculations based on the moment description (fluid model) can be used to determine gross properties. They will not suffice, however, for the determination of phenomena that depend on the angular and energy distribution of the neutral particles or for consideration of plasmas that are nonopaque or have nonMaxwellian distributions.

The establishment of a neutral gas region is not assured by the existence of equilibrium solutions. As it is difficult to achieve ignition at higher densities, it is likely that the discharge will be initiated at lower densities and then fueled to achieve the final operating density. The time dependent introduction of a gas fuel source at the edge of a tokamak plasma must then be considered, and the desired solution is a graceful transition to the final operating state. In the course of these events the variation of the plasma properties will mean that a wide range of plasma opacities will be encountered. This problem will not be amenable to analysis by the previously described fluid theory.

III. Physical Mechanisms of Neutral Gas Fueling

First, let us consider the relevant phenomena observed in todays experiments. In these devices pulse durations are typically much longer than the particle confinement times, consequently, if a straight forward diffusion analysis were performed based on the assumptions of very weak sources in the plasma interior and recycling at the edge, one would expect a marked flattening of the profile to occur. This is not consistent with the experimental evidence, and in devices such as Alcator [2] in which neutral gas is introduced at the boundary, the rate of increase of the axial density is far an excess of that which is consistent with simple diffusion theory. The implication of these results is that either neutral particles are penetrating to a much greater depth requiring some as yet undetermined upscatter mechanism, or that a plasma transport phenomena is responsible. The latter explanation is currently taken to be the correct one, and the mechanism by which the effect occurs is thought to by the Ware pinch [14]. Detailed numerical transport analyses that include such neoclassical effects [15] have been able to qualitatively model the experimental results.

Whatever mechanism is responsible for this data, and it is critically important to understand this phenomenon, the fact remains that todays tokamaks are self edge-fueled devices. It is not known whether this behavior will persist in larger machines. If, in fact, the Ware pinch mechanism is responsible, than it is likely that the mechanism would not be as effective in the collisionality regime of most fusion reactor concepts.

If edge self fueling is present in larger reactor devices, and if the boundary consisted of a dense cold plasma layer, than one could in all likelihood operate a 10 - 100-sec pulse-length device in which the pulse duration would be determined by the alpha particle accumulation rate and consequent fuel depletion. When divertors are used on tokamaks, and the boundary becomes an effective density sink [unload mode of operation], recycling is not a viable means of supporting or increasing the central density [16]. This type of plasma boundary condition will require deep penetration fueling and will not be discussed further here.

We will now consider a rather speculative system in which a sufficient quantity of neutral gas is introduced at the edge of the plasma so as to significantly alter the density profile of the plasma. In particular the condition that we seek to achieve is one in which $n'(r) > 0$ and for which the diffusion current is inward. For small n' this would imply a significant reduction in the transport loss rate and the required fueling rate would be that required to balance the fusion reaction rate. Based on classical understanding the driving forces for the diffusion current would come mainly from the Nernst term with $T'(r) < 0$ and from the frictional force between the alpha particles and the hydrogenic species. A beneficial consequence of this model would be the outward diffusion of the alpha particles and pumping at the plasma boundary either directly or by using a shielding divertor would exhaust these ashes.

In the absence of detailed transport analyses of this model and experimental evidence of inverted profiles, we must once again state that this is a speculation. It is motivated by the apparent simplicity and therefore high utility of the concept that would result.

†Research supported by Department of Energy contract EY-76-C-02-3073.

References

1. J. Hosea, Bull. Am. Phys. Soc. 22, 1057 (1977).

2. R. R. Parker, Bull. Am. Phys. Soc. 22, 1057 (1977).

3. C. A. Foster & S. L. Milora, These Proceedings.

4. H. Alfven & E. Smars, Nature 188, 801-802 (1960).

5. C. Falthammak, Phys. of Fluids 4, 1145-1151 (1961).

6. S. G. Alikhanov et al., Nuc. Fus. 10, 13-18 (1970).

7. E. Smars & R. B. Johansson, Phys. of Fluids 4, 1151-1155 (1961).

8. a) B. Lehnert, Arkiv for Fysik 38, 499-535 (1968).
b) B. Lehnert, Physica Scripta 12, 327-336 (1975).

8. c) B. Lehnert, Nuc. Instruments and Methods, 129, 31-37 (1977).

9. T. A. Oliphant, Nuc. Fusion 13, 521-527 (1973).

10. G. K. Verboon and J. Rem, Nuc. Fusion 13, 69-79 (1973).

11. F. C. Schuller et al., Plasma Physics and Controlled Nuclear Fusion Research, Fifth Conference Proceedings November 1974, Vol. II, p. 725.

12. D. K. Bhadra and L. Gross, Nuc. Fusion 17, 622-625 (1977).

13. D. Ohlsson, These proceedings.

14. A. A. Ware, Plasma Physics and Controlled Nuclear Fusion Research, 4th Conference Proceedings, Vol. I, p. 411 (1971).

15. M. Hughes, PPPL-1411 (1978) to appear.

16. S. L. Gralnick, D. M. Meade, and F. H. Tenney, Trans. Am. Nuc. Soc. 23, 38-39 (1976).

Illustrations

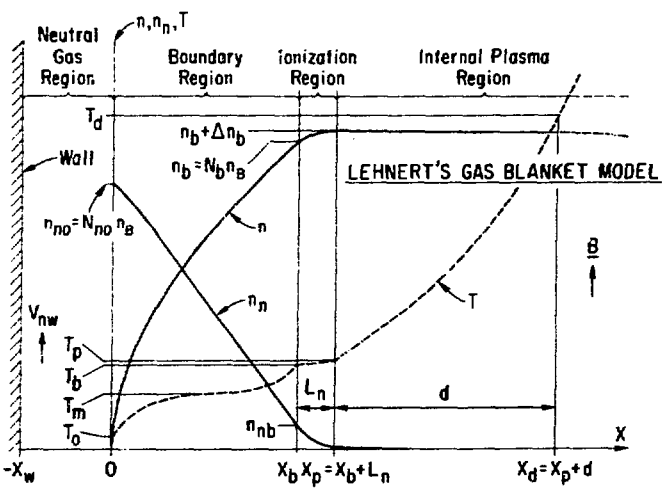

Fig. 1. Model of a Fusion Reactor Gas Blanket After B. Lehnert.

COLD BLANKET STUDIES IN JUTPHAAS

F.C. Schüller, W.J. Goedheer, L.Th.M. Ornstein, F. Engelmann, and T.J. Schep
Association Euratom-FOM, FOM-Instituut voor Plasmafysica
Rijnhuizen, Jutphaas-Nieuwegein, The Netherlands

Summary

An impermeable cold plasma-gas blanket surrounding a hot plasma core reduces the plasma-wall/limiter interaction. Moreover, accumulation of impurities in this blanket can be expected. Fueling from a blanket may be possible as shown by experimental results, though not fully explained by classical transport of neutrals. An anomalous inward flux of protons may be caused by drift-type instabilities.

Experimental studies of a cold impermeable plasma have been done on the tokamak-like RINGBOOG device. Particle diffusion is in agreement with Pfirsch-Schlüter theory and an extension thereof to a higher collisionality. A scaling law for the neutral pressure at the wall as a function of the plasma parameters in the cold blanket has been verified experimentally. The high neutral density, necessary to maintain $n_e \approx 10^{21}$ m^{-3}, causes hydrogen line radiation to dominate the energy balance.

Numerical studies on the transport of neutrals in a cold blanket, including detailed balancing of the various excited states and reabsorption of radiation, are in agreement with the profiles in our resistive arc-discharges. Extrapolations to a blanket around a thermonuclear core are possible.

1. Historical survey

The start of the gas-blanket research programme at Jutphaas was induced in 1966 by publications of Alfvén and Smårs[1] who proposed to balance the pressure of a thermonuclear plasma core by a gas blanket of equal pressure. A magnetic field was to be applied to reduce the radial heat conductivity. It soon became clear that this concept was incompatible with a stationary reactor state. The bremsstrahlung in the cooler outer layers turned out to be much higher than the thermonuclear power generated in the centre and, moreover, diamagnetic effects would cause a magnetic confinement instead of a gas pressure confinement. Rem and Verboom[2] developed a numerical code for a stationary cylindrical reactor model with an axial magnetic field. In this model fueling and helium exhaust took place by collisional diffusion across the magnetic field; the energy transport consisted of contributions by classical heat conduction and bremsstrahlung. Markvoort[3] improved this model by inclusion of impurities, cyclotron radiation and anomalous enhancement of heat conduction. It was found that a parameter window exists in which such a reactor could burn.

The experimental programme around 1970 was directed towards the research into the plasma of the transition layer which might prevail between the fully ionized core of the reactor of the Rem-Verboom type and the wall. Such partially ionized layers of densities between 10^{21} and 10^{22} m^{-3} and temperatures of a few eV could be studied in magnetized arcs as was shown by Wienecke and co-workers[4]. It was understood that end-losses could not be neglected in the Rem-Verboom model unless unrealistically long axial dimensions were envisaged. Therefore it was decided to redirect the programme towards toroidal geometries. At the same time it became clear from tokamak experiments that impurities strongly influenced the plasma behaviour and that the presence of a cool plasma-gas blanket could be of great importance to keep the plasma clean.

The scope of the present programme is mainly dedicated to the study of transport processes in the toroidal highly collisional plasmas of the cold blanket. The rebuilding of the Rem-Verboom model into toroidal geometry requires knowledge on the transport processes in the inner layers together with insight in the problem of toroidal equilibrium and stability, i.e. present-day tokamak physics. A first attempt for such a toroidal model was done by Volkov et al.[5].

2. Advantages of a cool blanket

According to current knowledge the advantages of the application of a cool plasma-gas blanket around a hot thermonuclear core as sketched in Fig. 1 can be centered around two general features:

1. The reduction of the impurity content of the core.
2. The possibility of fueling and helium exhaust.

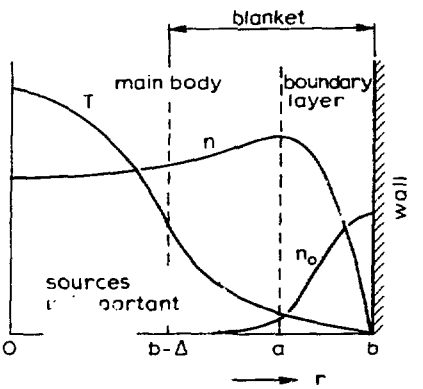

Fig. 1. Schematic plot of a radial profile of a steady-state plasma surrounded by a cold blanket.

2.1. The reduction of the impurity content of the core

Plasma wall interaction. The sputtering of wall material due to bombardment by energetic charge-exchange neutrals from the core is strongly reduced if their energy is moderated by many collisions to values lower than the sputtering threshold ($\sim$ 200 eV). This means that the product of the blanket density and the blanket thickness must be larger than 3×10^{18} m^{-2} (Lehnert's impermeability criterium[6]).

Plasma-limiter interaction. Recent experimental evidence[7,8] proves that the release of high-Z material from the limiter diminishes strongly if the temperature of the plasma in contact with the limiter is kept low ($\lesssim$ 50 eV), for instance by gas "puffing". A cool blanket reduces the probability for the occurrence of unipolar arcs, which may cause plasma contamination by metal impurities, as reported by the DITE-team[7]. Similarly, such a blanket could reduce the bombardment of the limiter by impurity ions accelerated in the sheath potential, which mechanism is proposed by the PLT-team[8].

Transport theory predicts an inverted density profile for the outside region of a thermonuclear reactor with a cold blanket and an accumulation of impurities, including helium, in the blanket (see section 3.2).

2.2. Fueling and exhaust

The fluxes necessary to sustain fueling and helium exhaust are small compared to the various contributions to the fluxes of deuterons and α-particles, caused by

temperature and density gradients. This means that the density and temperature profiles, which are necessary for fueling and exhaust, are only slightly different from the profiles which are necessary for keeping the particle fluxes at zero. Thus, fueling is essentially a consistency problem: how to tailor the energy balance to be consistent with the profiles needed for fueling and exhaust.

The results of Alcator and other experiments with gas "puffing" techniques are favourable. They indicate that it is possible to induce inward fluxes which are even much larger than those necessary for fueling, without disturbing the temperature profile too much. The mechanisms behind these phenomena are not completely understood. In this respect three effects could have some influence:

a. A non-maxwellian high-energy tail on the neutral energy distribution, as has been found in the Pulsator experiment, can explain a density rise up to 5×10^{20} m^{-3} according to the Düchs code[9]. If such a tail is too weak for the fueling of a reactor it can be enhanced by neutral beam injection at relatively low energies ($\sim$ 5 keV) as proposed by Gibson[10].

b. An anomalous inward flux of fuel ions and an outward flow of helium or other impurities can be caused by drift instabilities. This "anomalous Nernst effect" sets in when the ratio of the scale lengths of n and T is sufficiently large (see section 3.4).

c. An inward flux of fuel ions and an outward flux of helium and impurities can be induced by asymmetric particle and energy sources counteracting the torus drift and the compensating fluxes along the field lines. Asymmetric proton sources can be forced on top or bottom of the torus by asymmetric gas puffing and pumping as proposed by Ohkawa and Burrell[11,12,13].

3. Theoretical considerations on transport in plasmas with a cold blanket

A hot discharge surrounded by a cold blanket can exist only on time-scales longer than those characteristic for transport if there exist steady-state solutions for the particle and energy balance equations. The characteristics of these steady states determine the efficiency of the shielding by the blanket and the degree of accumulation of impurities in the blanket.

3.1. The highly collisional regime: an extension of the Pfirsch-Schlüter transport theory

It can be shown that the ratio of the collision frequency, ν, and the bounce frequency, ω_b, must be very high in the cool blanket since the electron density must be high in order to act as a shield for neutrals and the temperature must be low. The plasma must be far in the collision-dominated regime. In this case the usual Pfirsch-Schlüter theory has to be supplemented by the effects of energy transfer between electrons and ions, which affects the temperature gradients within a magnetic surface and, hence, the particle and energy fluxes. For values of:

$$S^2 \equiv 0.61\ (\nu_i/\omega_{bi})^2 (m_e/m_i)^{\frac{1}{2}}$$

larger than $(m_e/m_i)^{\frac{1}{2}}$ but $\nu_e/\omega_{ce} < (\delta_p/\delta_t)^2$ one finds for sufficiently small ion larmor radius (Engelmann, Nocentini[14,15]) that all poloidal and radial fluxes depend on the radial pressure gradient only and that the toroidal enhancement of the total heat flux (electrons and ions added) disappears. The following equations are used in the next sections of this paper. Under the assumptions $T_i \simeq T_e = T$, $n_i \simeq n_e = n$, and $Z_{eff} \simeq 1$, we find that

$$\frac{\partial T}{\partial \theta} = 0.44\ \frac{R}{\omega_e \tau_e}\, q^2\, \frac{\cos\theta}{n}\, \frac{dp}{dr} . \qquad (1)$$

For the charged particle fluxes Γ we find

$$\Gamma_r = \Gamma_{ir} = \Gamma_{er} = -\frac{\eta_\perp}{B^2}\, n \left\{(1+1.3q^2)\frac{dp}{dr} - \frac{3}{2}\frac{n dT_e}{dr}\right\} \qquad (2)$$

and for the heat flux carried by charged particles,

$$q_r^{e+i} = -\left(\kappa_\perp^e + \kappa_\perp^i\right)\frac{\partial T}{\partial r} + 0.32\ \kappa_\perp^e\, \frac{1}{n}\frac{dp}{dr} . \qquad (3)$$

Furthermore,

$$\frac{\partial n}{\partial \theta} \simeq -\frac{n}{T}\frac{\partial T}{\partial \theta} \qquad (4)$$

and

$$\frac{\partial \phi}{\partial \theta} = 1.3\ \frac{R}{\omega_e \tau_e}\, q^2 \cos\theta\, \frac{1}{ne}\frac{dp}{dr} , \qquad (5)$$

in which holds $dp/dr = \vec{j}\times\vec{B}$; the transport coefficients are given by Braginskii (Ref. 16), all other symbols have their usual meaning.

3.2. Relations between n_e, n_i and T for steady states

It is of importance to know the relation of the electron and impurity density profiles, and the temperature profile. At present, only information on collisional transport is detailed enough to study this problem. For a clean toroidal plasma with large β_p and in the absence of particle sources and sinks, one finds from the conditions $\Gamma_r = 0$ (Engelmann et al.[17]):

$$nT^{-0.28} = \text{constant in the banana regime} \qquad (6a)$$

$$nT^{1.46} = \text{constant in the plateau regime} \qquad (6b)$$

$$nT^{0.58} = \text{constant in the PS-regime} \qquad (6c)$$

$$nT = \text{constant in the highly collisional regime} \qquad (6d)$$

The highly collisional regime is discussed in section 3.1. The density profile in case of a gaussian temperature profile is sketched in Fig. 2.

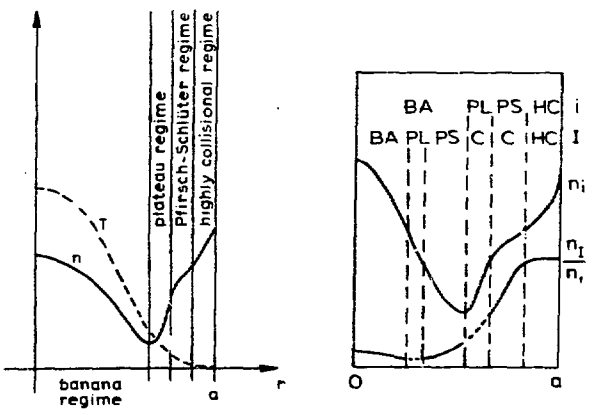

Fig. 2. Schematic plots of the radial proton and impurity density profiles in case of a gaussian temperature profile in the absence of proton sources.

Since the refueling flux is small compared to typical diffusive fluxes, these results apply also to steady states of a burning thermonuclear plasma. These results are expected to be consistent with the existence of a steady-state energy balance all over the fully ionized column (Engelmann et al.[17], Volkov et al.[5]).

For a plasma containing impurities, many combinations of regimes are possible. Relations of the type

$n_I(T)$ depend also on the type and quantity of the impurities present (Engelmann et al.[17], Engelmann and Nocentini[18]). The global result is that no important accumulation of impurities appears at the plasma centre (see e.g. Fig. 2). On the other hand, a certain concentration is expected in the blanket.

The applicability of these n(T) and $n_I(T)$ relations is rather limited because anomalous transport effects often occur in high temperature discharges, possibly with the exception of the outside layer, i.e. the cold blanket.

3.3. Transport of neutrals: relations between n_e and n_n

In a stationary situation and in the presence of particle sources the outward flow of charged particles Γ_r must be equal to the inward flow of neutrals $\Gamma_n = -\Gamma_r$. In the cold blanket Γ_r is given by Eq. (2). The inward flow of neutrals can be found from the momentum balance if it is assumed that the mean free path for neutrals is much shorter than scale lengths of temperature and density. Thus:

$$\frac{\partial p_n}{\partial r} = n_n \sum_j n_j (v_{rj} - v_{rn}) \varepsilon_{jn} \simeq \Gamma_r (n+n_n)(\varepsilon_{in}+\varepsilon_{en}), \qquad (7)$$

in which ε_{jn} are the friction coefficients given by:

$$\varepsilon_{jn} = \frac{8}{3}\sqrt{(2kT/\pi)(m_j m_n/(m_j+m_n))}\,\sigma_{jn}$$

with σ_{jn} = the total cross-section for collisions between neutrals and particles j. Integration of Eq. (7) after substitution of Eq. (2) must be done numerically (see section 4). From the structure of Eqs. (7) and (2) it is clear that the result must follow a scaling law for the neutral density on the wall, n_{nw}, as a function of the electron density in the blanket, n_{eb}:

$$n_{nw} = C\,\frac{n_{eb}^3}{T_b}\,\frac{q_b^2}{B^2} \qquad (8)$$

(the subscript b stands for blanket). A similar result was found by Wienecke[19], Lehnert[6] and Rem[20] for the case of a straight cylinder. The strong dependence on n_{eb} limits the maximum density of a cool blanket. The value of the numerical constant, C (cf. Fig. 7) implies that at $n_{eb} \simeq 10^{21}$ m^{-3} the neutral density n_{nw} becomes comparable in magnitude to n_b!

3.4. Anomalous transport

The particle density in the centre of a tokamak experiment can be increased by bleeding neutral gas into the discharge. Since the maximum values of the density obtained in Alcator and the rate at which this density is reached cannot fully be explained by a classical process, we explore the possibility that collective modes can produce the transport of cold plasma from the edge of the column towards the centre. One expects that the radial influx of cold plasma will cause a local flattening of the density profile, and will steepen the temperature profile. As a consequence, the ratio of the characteristic lengths of density and temperature, L_n/L_T can become large. Therefore, we consider collisional temperature drift instabilities. Adopting a slab model in which the equilibrium magnetic field is $\underline{B} = B_o\{\underline{i}_z + (x/L_s)\underline{i}_y\}$, we may represent the perturbed electric potential by $\tilde{\Phi} = \bar{\Phi}(x)\exp(-i\omega t + ik_y y)$. The modes of interest are found for $v_{ti} < \omega/k_\parallel < k_\parallel v_{te}^2/\nu_c$, where $v_{te,i}$ are the thermal velocities, ν_c is the collision frequency and $k_\parallel = xk_y/L_s$ is the component of the wave vector along the magnetic field. The electron density and temperature perturbations can be obtained from fluid equations (Braginskii[16]). In the case of electrostatic modes we obtain:

$$\frac{\tilde{n}_e}{n} = \frac{e\tilde{\Phi}}{T} - (1+\alpha)\frac{\tilde{T}_e}{T} \quad \text{and} \quad i\chi\frac{k_\parallel^2 T}{m_e \nu_c}\frac{\tilde{T}_e}{T} = \frac{3}{2}\omega_T\frac{e\tilde{\Phi}}{T},$$

where $\omega_T = k_y cT/(eBL_T)$, $L_n = -\{d\ell n\, n/dx\}^{-1}$, $L_T = -\{d\ell n\, T/dx\}^{-1}$ and α and χ are the coefficients of the thermal electric force and the thermal conductivity along the field lines, respectively.

These perturbed quantities lead to the following quasi-linear expressions for the particle and electron thermal energy diffusion coefficients:

$$D_n = L_n < \frac{\tilde{n}}{n}\tilde{v}_{Ex} > = -3\,\frac{1+\alpha}{\chi}\,\frac{L_n k_y^2}{L_T k_\parallel^2}\,\nu_c \rho_e^2 \left|\frac{e\tilde{\Phi}}{T}\right|^2 \qquad (9)$$

and

$$D_{nT} = \frac{\alpha}{1+\alpha}\,\frac{L_T}{L_n+L_T}\,D_n, \qquad (10)$$

where $\tilde{v}_{Ex}$ is the radial component of the $\tilde{E}\times B$-drift and ρ_e is the electron gyro radius. Both diffusion coefficients are negative, hence the corresponding fluxes are directed inward.

Here, we omit the details of the mode structure and of the dispersion relation, and evaluate $k_\parallel$ at $x = x_T$, where $x_T \sim \rho_i (L_s/L_T)^{\frac{1}{2}}$ is the characteristic radial length of the modes of interest, ρ_i being the ion gyro radius. Then, for $L_n = 0.12$ m, $L_s = 1$ m, $L_T = 0.05$ m, $B = 5$ T and $T = 400$ eV (i.e. numerical values for a typical high density discharge in Alcator at half radius, Apgar et al.[21]), we obtain

$$D_n \simeq -\,10^6\,\nu_c \rho_e^2 \left|\frac{e\tilde{\Phi}}{T}\right|^2;$$

We see that for relatively low fluctuation levels the quasi-linear diffusion coefficient, can become locally much larger than the classical one.

4. Numerical calculations

A one-dimensional code has been developed to solve the following set of equations under the assumption that the mean free path for neutrals is much smaller than typical scale lengths:

a. The momentum balance for the neutrals as given by Eq. (7).
b. The charged particle flux as given by Eq. (2).
c. The continuity equation:

$$\frac{1}{r}\frac{d}{dr}\,r\,\Gamma_r = S_e\,. \qquad (11)$$

d. The energy balance

$$\frac{1}{r}\,\frac{d}{dr}\,r\left(q_r^{e+i} - \kappa_o\frac{dT}{dr} + \sum_s h_s v_{sr}\right) = \sigma_\parallel E_t^2 - \mathrm{Rad}, \qquad (12)$$

in which: S_e = the source or sink of the electrons;
κ_o = the heat conductivity of the neutrals, mainly caused by ion-neutral collisions ≃ charge-exchange losses;
$\sum_s h_s v_{sr}$ = enthalpy transport ≃ $(5/2\,kT+\varepsilon_{ion})\Gamma_r$;
Rad = (emission-reabsorption) of radiation,
and q_r^{e+i} is given by Eq. (3).

The source function S_e and the net emitted radiation, Rad, are computed from a set of rate equations obtained from the simplified level scheme of the hydrogen atom as shown in Fig. 3. For a more detailed description of this model see Goedheer[22,23].

The equations are solved in an iterative way as an eigenvalue problem. The choice of the five necessary boundary conditions depends on the problem to be treated.

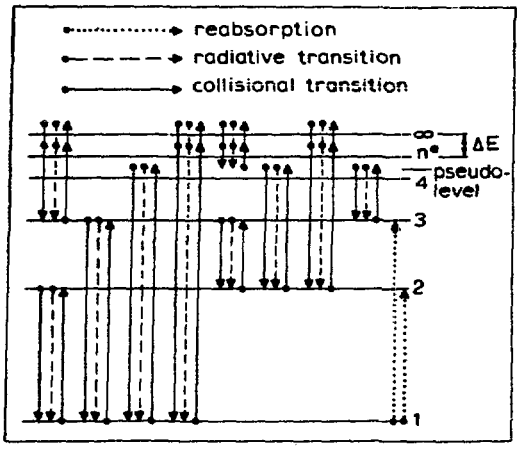

Fig. 3. The level scheme of the hydrogen atom as used in the numerical code with the various excitation and de-excitation mechanisms which are taken into account.

The iteration starts with a trial profile for p_e and T. Firstly, $p_n(r)$ and $\Gamma_r(r)$ are calculated from Eqs. (7) and (11) and from that new p_e- and T-profiles are obtained from Eqs. (2) and (12).

Two cases have been studied:

a. Low-temperature and high-density discharges of the type found in the Ringboog device (see section 5). In this case the eigenvalue is E_t. The boundary conditions: Γ_r (o) = 0, T(b=wall radius) = 0.5 eV, p_n(b), T(o) and p_e(b) are chosen in agreement with experimental values.

The numerical results for low-current discharges (see Figs. 4,5,6) are in good agreement with experimental profiles and will be discussed in section 5. Although the profiles are determined by radiation emission and reabsorption, the contribution to the total heat loss is small, due to the fact that the plasma is optically thick. Convection losses are more important than heat conduction (cf. Fig. 5). The scaling law for the neutral wall density, Eq.(8), is confirmed (cf. Fig. 7).

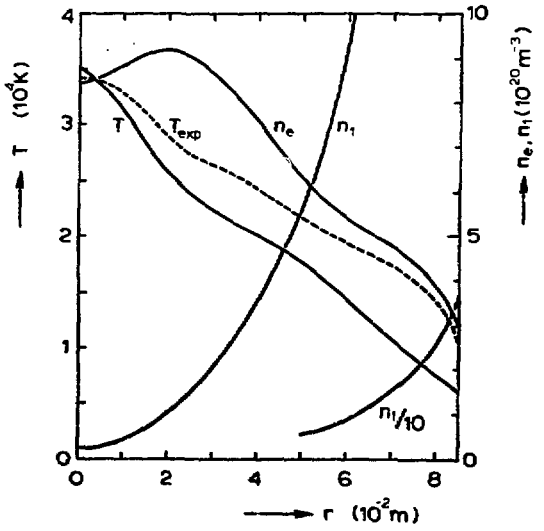

Fig. 4. The temperature, the charged particle density, and the density of neutrals in the ground state n_1, as found by means of the numerical code for I = 4.9 kA, B_t = 1.65 T, p_n(b) = 300 N/m², T(o) = 3.5×10⁴ K and p_e(b) = 25 N/m². The dotted line is the experimental T-profile for I = 8 kA and n(o) = 8×10²⁰ m⁻³ (see section 5.3).

b. The outside layer of a thermonuclear reactor. Here, the following boundary conditions are used: p_n(b), p_e(b), T(b) = 0.5 eV and T(b-Δ) = 50 eV, where Δ is the blanket thickness (see Fig. 1). The boundary condition on p_n is chosen to be $p_n(b-\Delta) = 3p_n^{eq}(b-\Delta)$, in which p_n^{eq} is the value of p_n when S_e = 0.

The results are not very sensitive to the choice of the proportionality constant. In this problem the ohmic input is neglected and the eigenvalue is now $Q^{tot}(b-\Delta)$, i.e. the heat flow necessary to maintain the cold blanket. It is assumed that Δ << b (slab model) and that q is constant over the cold blanket. In Fig. 8 typical results for the profiles are given. In Fig. 9 Q^{tot} is given as a function of n_{eb} for several values of q/B and Δ. It should be noticed that in general the necessary heat flow is moderate.

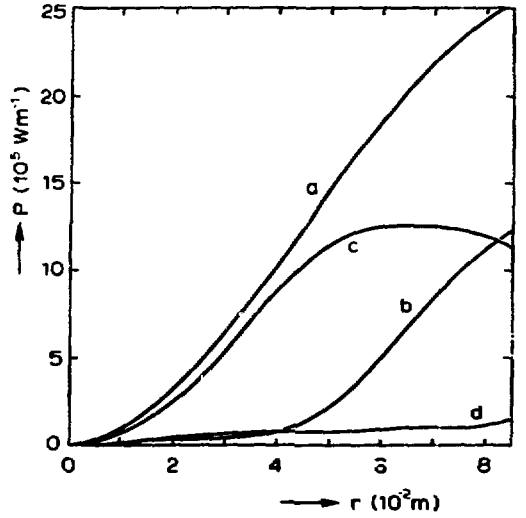

Fig. 5. The power loss per metre length as a function of the radius for the same parameters as Fig. 4. Curve a: the ohmic input power $2\pi\int_0^r \sigma E^2 \rho d\rho$; curve b: the heat conduction flux $2\pi r(q_r^{e+i} - \kappa_o(dT/dr))$; curve c: the convection loss $2\pi r \Sigma_s h_s v_{sr}$; curve d: the radiation flux $2\pi\int_0^\rho Rad\rho d\rho$.

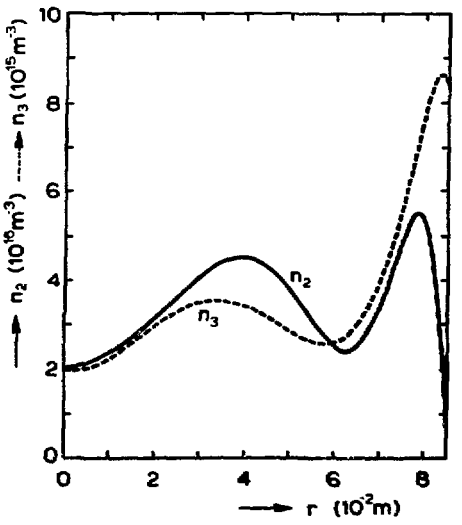

Fig. 6. The density profiles of the first and second excited state of neutral hydrogen for the same parameters. Note the second maximum around r = 4×10⁻² m caused by re-absorption of Ly-α and Ly-β radiation emitted from the centre.

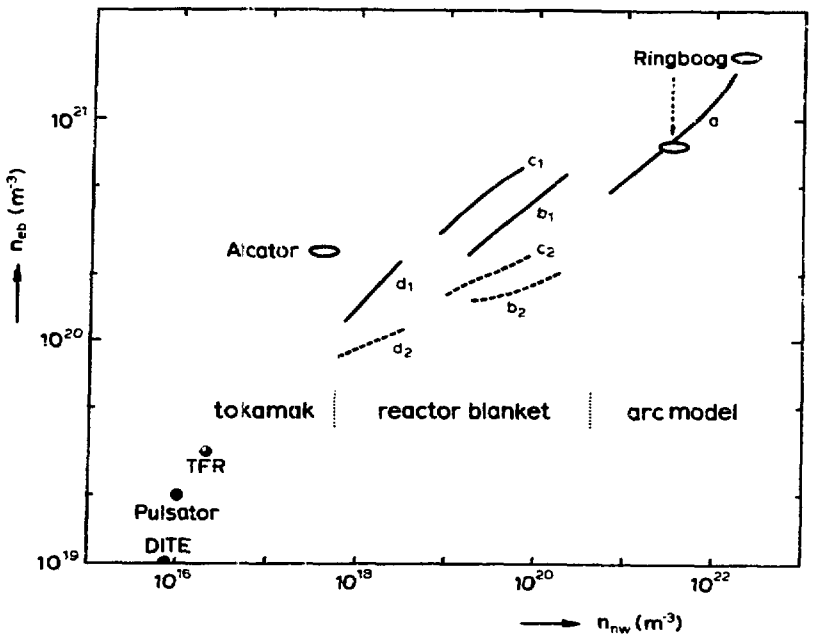

In Fig. 7 n_{eb} is given as a function n_{nw} for several values of q/B and Δ for the reactor blanket as well as for the arc model. The blanket densities at $T = 5\times10^5$ K (dotted lines b_2, c_2, d_2) are lower than those at $T = 5\times10^4$ K (full lines b_1, c_1, d_1). At the higher temperatures the $n_{nw}^{1/3}$ scaling does not hold since the neutrals are burnt out, so that the density profiles at r = b-Δ are not determined anymore by neutral transport. Some experimental points from Ringboog and from various tokamak experiments are shown. As expected, tokamak values deviate to some extent from the scaling law since the neutral fluid model is not valid; moreover in the experiments anomalous loss mechanisms are likely to occur.

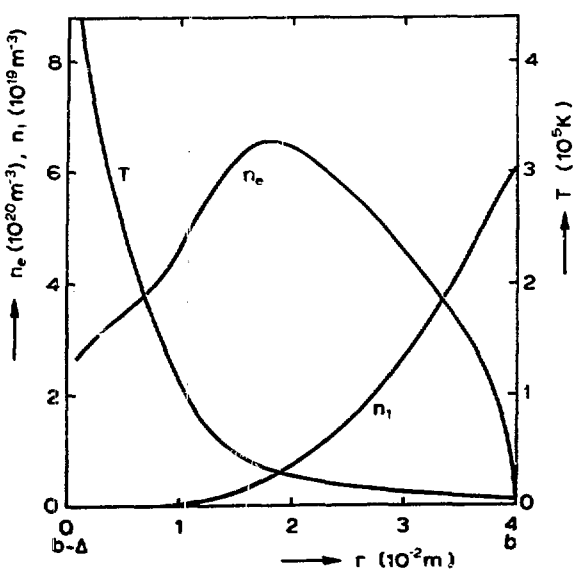

Fig. 8. The profiles of n, T and n_i in a reactor blanket with q/B = 1 T^{-1}, Δ = 4×10^{-2} m and $Q^{tot} = 6\times10^4$ Wm^{-2}.

Fig. 7.
The electron density in the blanket n_{eb} as a function of the neutral density at the wall, n_{nw}, for several values of q/B and Δ.

Curve a: Numerical results for the arc model with q/B = 14 T^{-1}. Here, Δ is taken as the whole radius of the arc. Thus, the value of the electron density on the axis is equal to n_{eb}.

Curves b, c, and d: Numerical results for the reactor blanket with:

curve	q/B(T^{-1})	Δ(10^{-2} m)	T(10^4 K)
b_1	1	4	5
b_2	1	4	50
c_1	2	4	5
c_2	2	4	50
d_1	1	8	5
d_2	1	8	50

Experimental results for some tokamak discharges and for the Ringboog experiment are also shown. For the tokamaks the value of n_{eb} is chosen as the experimental value of n_e at the location when $T = 5\times10^4$ K.

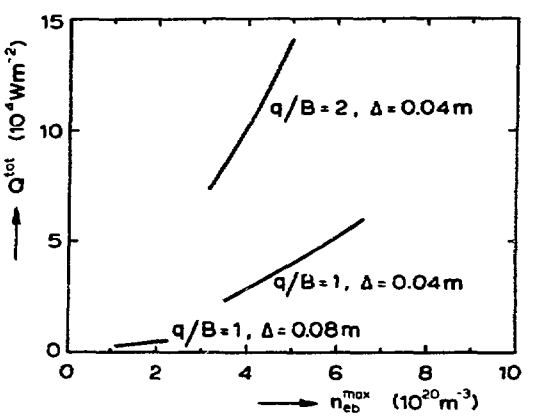

Fig. 9. The energy flux Q^{tot} necessary to maintain a cold blanket as a function of the maximum density in the blanket with Δ and q/B as indicated.

5. Experimental results

The programme of the Ringboog experiment is focussed on the verification of the theory on highly collisional toroidal plasmas (section 3.1), the inward transport of neutrals (section 3.3), and the particle and energy balances as predicted by the numerical calculations (section 4).

5.1. Description of the apparatus

Ringboog is a tokamak-like device with: R = 0.52 m, b = 0.087 m, and B_t up to 3.2 T (Ringboog team[24]). A copper limiter with radius a = 0.08 m is used. The discharge with currents up to 70 kA is struck inside a quartz torus filled with hydrogen gas at pressures between 10 and 100 mtorr. The total flux swing of the iron core is 1.2 Vs. There is no copper shell, equilibrium is maintained by vertical and horizontal magnetic fields (cf. Fig. 10). We shall report on quiescent discharges with low discharge currents (I = 8 kA, B_t = 1.65 T) and on discharges with a strong oscillatory behaviour at higher currents (I = 20 kA, B_t = 1.65 T). At still higher currents the oscillations, to be discussed below, become so violent that it is impossible to take reproducible shot-to-shot measurements.

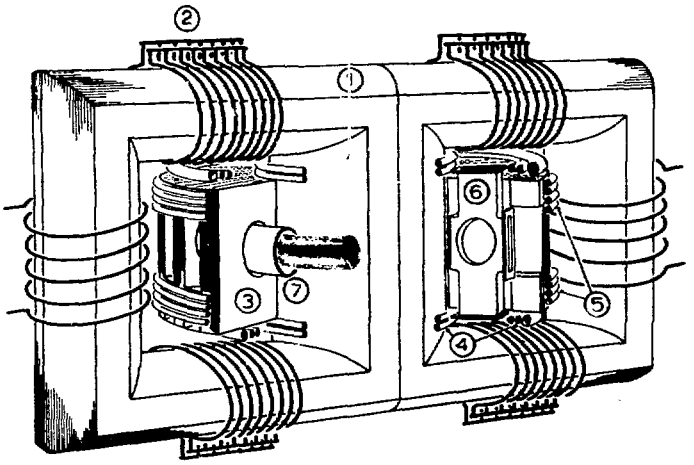

Fig. 10. Cut-away view of the Ringboog experiment.
1. Iron core
2. Primary windings
3. Bitter coils for B_t
4. Vertical field windings
5. Horizontal field windings
6. T-ports
7. Discharge vessel

5.2. Diagnostics

Various radial profiles are studied. In case of strong oscillatory behaviour, values averaged over several periods are presented.

The low plasma temperature causes loop voltages, V_ℓ of several hundred volt. This limits the pulse duration to only a few msec. It is therefore possible to immerse small probes in the plasma. Radial scans in horizontal and vertical directions of $B_p(R,Z)$, $B_t(R,Z)$ and of the floating potential $\phi_f(R,Z)$ are taken. Two dimensional current distributions and floating potential distributions have been inferred from these measurements.

Combination of j_t with the measurement of V_ℓ and $\vec{B}_p \cdot \nabla\phi_f$ yields the radial distribution of the conductivity temperature, T_e^σ, under the assumption that $Z_{eff} = 1$. T_e^σ agrees well with the temperature as measured by Thomson scattering, $T_e^{Ts}(r)$. The ion temperature is measured by Doppler broadening of impurity lines and turns out to be equal to T_e.

Electron density profiles, n_e^{inf}, are obtained by Abel inversion of the fringe pattern of a CO_2-laser-interferometer. At high discharge currents the density is hollow and, consequently, the error after Abel inversion is large in the centre; local values of the density as found by Thomson scattering; $n_e^{Ts}(r)$, are used as reference values for the central region.

Analysis of the Balmer-line intensities gives information on the spatial distribution of neutrals in excited states. VUV spectroscopy is used to detect the contamination level.

Combination of the n_e and T_e-profiles yields a plasma pressure profile which can be compared with the pressure profile derived from integration of $\vec{\nabla}p = \vec{j}\times\vec{B}$. The difference must needs be the neutral wall pressure, p_w.

5.3. Results at low-current discharges

This type of discharge is characterized by the following experimental values: I = 8 kA, B_t = 1.65 T, q(a) = 12.7, filling density $n_f = 1.5\times10^{21}$ m^{-3}, $n_e(o) = 8\times10^{20}$ m^{-3}, $n_{nw} = 3\times10^{21}$ m^{-3}, $T_e(o)$ = 3.0 eV, E_t = 58 V/m. This is in reasonable agreement with the results of the numerical code for the same T(o) and B_t. The code was run several times with increasing n_{nw} until a solution for n(o) was found equal to the experimental value. Then the results are: I = 4.9 kA, q(a) = 20.7, $n_{nw} = 3.6\times10^{21}$ m^{-3}, E_t = 52 V/m.

The experimental T_e^σ-profile is shown in Fig. 4 (as T_{exp}) together wit the numerical profiles. There is a qualitative agreement, but T^σ is somewhat too high as a consequence of the fact that the actual current is 60% higher than the numerical result. The actual energy losses are 60% higher than the losses predicted by the theory of section 3.1.

Good agreement with the theory of highly collisional plasma is found by comparing the measured ϕ_f-distribution (cf. Fig. 11) with the theoretical ϕ-distribution of Eq. (5). The values of ϕ_f can only deviate a few times kT/e from ϕ; this is insignificant compared to the large potential differences consistent with the double vortex convection pattern of the Pfirsch-Schlüter type.

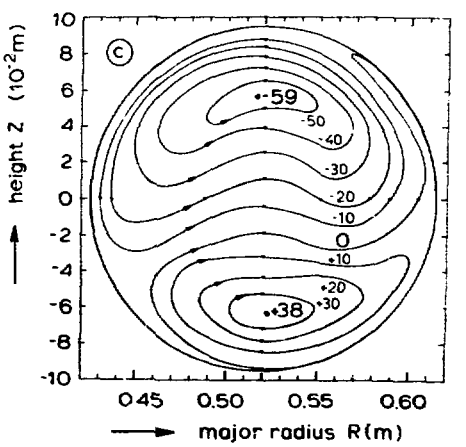

Fig. 11. The distribution of the floating potential, ϕ_f, measured at I = 8 kA, B_t = 1.65 T, $n_f = 1.5\times10^{21}$ m^{-3}. It can be proven that equipotential lines coincides with flow lines.

According to Eqs. (1) and (5) the maximum vertical asymmetry in the temperature distribution, ΔT is given by $\Delta T = 0.44\, e\Delta\phi/1.31k$, in which $\Delta\phi$ is the maximum potential asymmetry, i.e 50 V. This means that ΔT would amount to 16 eV. That is impossible since the temperature averaged over hte magnetic surface is only about 2 eV. This contradiction is due to the fact that the collisionality of the experimental plasma is even higher than allowed by the conditions under which the transport theory of section 3.1 is valid. Experimentally, strong vertical asymmetries in the density are found. As the pressure must be constant over a magnetic service, we may conclude (cf. Eq. (4)) that in fact $\Delta T \simeq 1$ eV.

5.4. Results at high discharge current and high density

An illustrative example of high current, high density type of discharges is given by: I = 20 kA, B_t = 1.65 T, q(a) = 5.1, $n_f = 6\times10^{21}$ m^{-3}, n(o) = 2.5×10^{21} m^{-3}, $n_{nw} = 2\times10^{22}$ m^{-3}, T(o) = 2.8 eV, E_t = 122 V/m. It should be noted that the value of n_{nw} is in reasonable agreement with the scaling law of Eq. (8). The penetration length of neutrals is shortened by the higher density so that the central neutral density is much lower than in the previous case, notwithstanding the fact that the neutral density is much higher at the wall. This means that the radius where the plasma becomes opaque for Ly-α photons, emitted at the centre, shifts to the outside to r/a $\simeq$ 0.7. From Fig. 6, which shows the density profiles of the excited levels n = 2 and 3 for the previous case, it can be seen that the population of excited levels is markedly enhanced over PLTE-values at the radius where the plasma becomes optically thick. This is confirmed experimentally. In this high-density case the excited levels locally become so strongly populated that collisional ionization from these levels considerably enhances the particle source function S_e, i.e. a kind of staged photon-ionization. A stationary solution cannot be found numerically. In the experiment an oscillatory behaviour occurs, which may be described by the following mechanism: the value of S_e is so high that fluxes are not sufficient for transporting the newly formed plasma. Therefore, the density at r/a = 0.7 builds up until the pressure profile becomes inverted to such a degree that it collapses. Cold and hot plasmas are mixed, the surplus on density recombines on the wall and a new cycle starts.

The time-averaged n, T, and p profiles are shown in Figs. 12 and 13. The pressure oscillates between a nearly flat profile and a strongly inverted profile. The strongest variations on all signals are found at r/a $\simeq$ 0.7, whereas all values measured on axis show hardly any oscillations. The mode numbers are m = 0, n = 1 and 2. The observed frequency in the range of 10 kHz agrees with an acoustic propagation in the toroidal direction (Ringboog team[24]).

6. Conclusions

Particle fluxes

1. The charged particle fluxes as predicted by the highly-collisional transport theory have been verified experimentally in the RINGBOOG device.

2. The scaling law found from this transport theory, namely $n_{nw} \propto n_{eb}^3 q^2/B^2$, extrapolated to lower densities, may be applicable to a cold reactor blanket.

3. Fueling from a blanket may be envisaged through the feeding of gas into the outside layers of the plasma; this leads to only slight modifications of the temperature and density profiles.

4. The fueling could be greatly enhanced by anomalous transport due to temperature drift waves. This phenomenon is proposed as the explanation for the density increase to the extreme values in the Alcator experiment.

Energy balance

5. The energy transport as predicted by the highly collisional transport theory has not been verified experimentally, because the resistive arc plasmas of RINGBOOG have a too high collisionality.

6. Atomic effects like emission and reabsorption of hydrogen line radiation completely dominate the energy balance at densities in the range of 10^{20} - 10^{21} m^{-3}.

7. Taking these atomic effects into account, the heat flux needed to maintain a reactor blanket may be comparable to the thermal flux of a thermonuclear plasma.

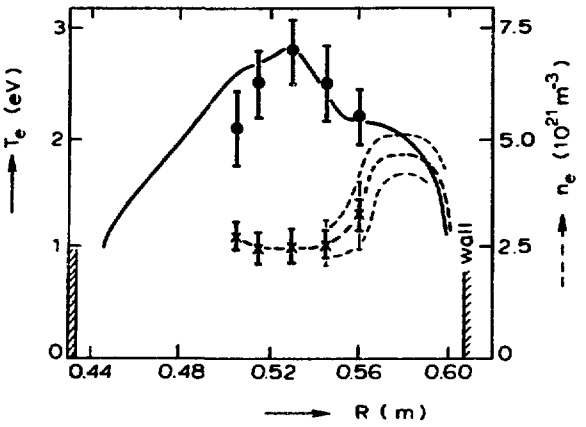

Fig. 12. Experimental density and temperature profiles of discharges with I $\simeq$ 20 kA, B_t = 1.65 T, $n_f = 6.4\times10^{21}$ m^{-3}. The drawn line represents T^{σ}, the broken line n^{inf}. Laser scattering data are given as ϕ and ϕ. Note that due to the local oscillatory behaviour the shot-to-shot variations in the outside region are larger than the measuring errors.

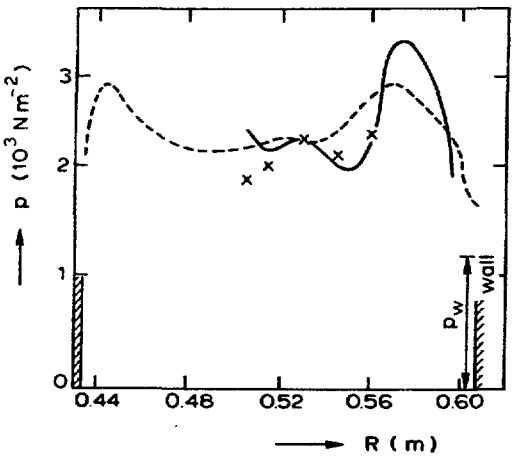

Fig. 13. Radial pressure profiles for the same discharge as Fig. 12. The drawn line represents $p = 2n^{inf}T^{\sigma}$; crosses indicate the pressure according to Thomson scattering data: $p = 2n^{Ts}\cdot T^{Ts}$; the broken line represents: $p = p_w + \int_{r_o}^{R} (\vec{j}\times\vec{B})\cdot d\vec{R}$.

Acknowledgements

This work was performed as part of the research programme of the association agreement of Euratom and the "Stichting voor Fundamenteel Onderzoek der Materie" (FOM) with financial support from the "Nederlandse Organisatie voor Zuiver-Wetenschappelijk Onderzoek" (ZWO) and Euratom.

References

1. Alfvén, H., Smårs, E.A., Nature 188 (1960) 801.
2. Verboom, G.K., Rem, J., Nucl. Fusion 13 (1973) 69.
3. Markvoort, J.A., Rijnhuizen Reports RR 75-90 and RR 75-91.
4. Mahn, C. et al., Z. Naturforsch. 20a (1965) 475; Klüber, O., Z. Naturforsch. 22a (1967) 1599.
5. Volkov, T.F. et al., Proc. 6th Int. Conf. on Plasma Phys. and Contr. Nucl. Fusion Res., Berchtesgaden 1976; Suppl. to Nucl. Fusion (1977) Vol. III, p.359.
6. Lehnert, B., Nucl. Fusion 8 (1968) 173.
7. McCracken, G.M. et al., Proc. 8th Eur. Conf. on Contr. Fusion and Plasma Phys., Prague (1977) 40.
8. Von Goeler, S. for the PLT-team, Invited Lecture 8th Eur. Conf. on Contr. Fusion and Plasma Phys., Prague (1977) Vol. II.
9. Düchs, D.F., Int. Summer School on Theory of Magnetically Confined Plasmas, Varenna 1977.
10. Gibson, A., Watkins, M.L., Proc. 8th Eur. Conf. on Contr. Fusion and Plasma Phys., Prague (1977) 31.
11. Ohkawa, T., Kakuyugo-Kenkyu 32 (1974) 61 and 32 (1974) 67.
12. Burrell, K.H., Phys. Fluids 19 (1976) 401.
13. Burrell, K.H., Ohkawa, T., Proc. Int. Symp. on Plasma Wall Interaction. Jülich (1976) 589.
14. Engelmann, F., Nocentini, A., Nucl. Fusion 16 (1976) 694.
15. Nocentini, A., Engelmann, F., Nucl. Fusion 17 (1977) 761.
16. Braginskii, S.I., in Reviews of Plasma Physics (M.A. Leontovich, Ed.), Consultants Bureau, New York, 1 (1965) 205.
17. Engelmann, F. et al., Proc. 6th Int. Conf. on Plasma Phys. and Contr. Nucl. Fusion Res., Berchtesgaden 1976; Suppl. to Nucl. Fusion (1977) Vol.II p. 19.
18. Engelmann, F., Nocentini, A., Proc. 8th Eur. Conf. on Contr. Fusion and Plasma Phys., Prague (1977) 34.
19. Wienecke, R., Z. Naturforsch. 18a (1963) 1151.
20. Rem, J., Nucl. Fusion 10 (1970) 95.
21. Apgar, E. et al., Proc. 6th Int. Conf. on Plasma Phys. and Contr. Nucl. Fusion Res., Berchtesgaden 1976; Suppl. to Nucl. Fusion (1977) Vol. I, p.247.
22. Goedheer, W.J., Proc. Int. Symp. on Plasma Wall Interaction, Jülich (1976) 665.
23. Goedheer, W.J., to be published as a Rijnhuizen Report.
24. Ringboog-team, Proc. Int. Symp. on Plasma Wall Interaction, Jülich (1976) 647.

GAS BLANKETS AND NEUTRAL PARTICLE INTERACTIONS

SESSION SUMMARY

R. J. Colchin

Oak Ridge National Laboratory*
Oak Ridge, Tennessee 37830

Presentations in the session on gas blankets and neutral particle interactions included a number of rather diverse topics. In summarizing these reports, it seemed best to discuss them from a single point of view and to leave subjects outside the point of view to individual papers. A common thread which ran through all the presentations was that of gas blankets, including their refueling, and that is the subject discussed hereon.

A "gas" blanket is somewhat of a misnomer, since such a blanket is now envisioned as consisting of a cool plasma with $n_i \ell > 10^{15}$ cm^{-2} where n_i is the ion density and ℓ is the characteristic width of the blanket. If the blanket is fed by neutral particles from near the first wall, then it may be thought of as consisting of several regions, as discussed by D. Ohlsson, wherein the neutral gas mixes with cold plasma and is ionized. If a gas blanket were realized, it might have the following beneficial effects:

1. It would cool hot plasma core particles, including neutrals, as they leave the plasma thus shielding walls, limiters, and divertor plates from bombardment by such particles. This, in turn, would reduce the impurity influx from walls and limiters due to sputtering or vaporization.

2. If the density gradient were reversed between the hot plasma and the gas blanket, deuterium and tritium particles would diffuse inward from the gas blanket automatically refueling the plasma. Also, impurities should accumulate in the gas blanket, as might α particle ash from a thermonuclear burn.

3. Evidence from PLT presented by G. L. Schmidt indicates that it is important to keep the plasma near the limiter cool to prevent the influx of limiter material by arcing or plasma-potential-induced sputtering. Gas blankets are ideally suited to keep the plasma-limiter region at low temperature.

Unfortunately, gas blankets have not been realized experimentally, even though tokamaks such as Alcator have approached gas blanket densities ($\bar{n}_e \simeq 2 \times 10^{15}$ cm^{-3}). Since gas blankets do not appear automatically as the consequence of present CTR experiments, the following questions may be raised:

1. How does one form a gas blanket? (This is mainly a problem of both energy and particle sources and sinks.)

2. Once a blanket is formed, does a stable equilibrium exist?

The first question, namely, how does one form a gas blanket, has been considered experimentally and theoretically. Particles may be fed into the plasma-edge region as thermal neutrals from a gas feed, as fast neutrals from plasma refluxing or from guns, and as a distributed feed from pellets. Once ionized in the boundary or blanket region, they may be adsorbed into the main plasma which acts as a sink, or they may be lost to the wall.

The physics of particle injection into the main body of the plasma, or fueling, has been studied experimentally on several tokamaks by gas puffing. In these experiments, neutrals introduced at the plasma boundary appeared quite quickly at the plasma center as added plasma density. This voracious appetite for gas at the edge may explain why gas blankets have not been observed.

The initital gas puffing experiments came as quite a surprise because the theory of penetration of neutral thermal particles precluded such fueling. Attempts by D. Düchs[1] to explain the density increases on Alcator by fast refluxing of neutrals proved inadequate at densities above 5×10^{14} cm^{-3}. It was apparent that another transport mechanism was necessary and H. C. Howe[2] proposed the Ware pinch as a likely candidate for density rises observed in ORMAK and Alcator. This work has been extended in two papers presented at this meeting by G. L. Schmidt for PLT and R. Parker for Alcator. G. L. Schmidt noted that the Ware pinch loses its effectiveness in the outer region of the plasma and that anomalous diffusion or some other mechanism must be invoked to carry ions inward to radii where the Ware pinch can take over. R. Parker discussed the possibility that this could be accomplished by strong turbulence, observed near the limiter radius in Alcator by means of CO_2 laser scattering. F. C. Schüller discussed the derivation of a quasi-linear diffusion coefficient based on collisional temperature drift instabilities which might explain this anomalous diffusion.

On the other hand, R. Parker noted that the time scales for inward diffusion via the Ware pinch are too slow by a factor of 2, and that the densities above 10^{15} cm^{-3} cannot be explained by these calculations. The general feeling one gets is that the Ware pinch is inadequate to explain all of the experimental results, and that a new piece of neutral particle or plasma transport theory is needed. In any case, the rate of gas ingestion in present tokamak plasmas is too high to sustain an inverted density gradient.

Will gas blankets be possible in larger plasma devices such as TFTR (Tokamak Fusion Test Reactor)? S. Gralnick reported on work looking into this question. He noted that gas puffing is the cheapest and easiest method of refueling tokamaks. He indicated that a delicate balance exists between fueling, exhaust, and heating, but if everything goes just right, gas blankets could be a reality. F. C. Schüller and D. Ohlsson described experiments underway on the Ringboog and F1 devices to study the characteristics of gas-blanket-type plasmas. Good agreement between theory and detailed probe measurements has been found on the Ringboog device. W. A. Houlberg has considered the merits of fueling to an arbitrary depth inside the plasma with a distributed neutral source such as that provided by pellet injection. The concept of a controllable particle source profile offers a new host of possibilities. Using a one-dimensional fluid transport code, he found that shallow to intermediate penetration depths were best, based on criteria for stability and heating. This is a new area of investigation with exciting possibilities, both theoretically and experimentally.

*Operated by Union Carbide Corporation for the Department of Energy.

If gas blankets are to be a reality, there must be a possible equilibrium which is stable. The papers presented by F. C. Schüller and D. Ohlsson gave results of calculations which indicate that such an equilibrium is possible. D. Ohlsson addressed the question of edge stability in some detail. The net result of a local stability analysis is that electrostatic and electromagnetic modes can be stabilized within certain parameter ranges within the gas blanket region. W. A. Houlberg found that shallow fueling tends to turn off density-gradient-driven trapped particle modes by flattening the density profile. Unfortunately, these optimistic predictions have not been confirmed experimentally. As noted previously, R. Parker reported on density fluctuations near the plasma edge in Alcator. These density fluctuations increase with increasing density, reaching as high as $\tilde{n}_e/n_e \simeq 1$.

The appeal of gas blankets is great. The associated problems are complex and all of the important pieces of physics may not yet be in hand. Although an interesting start has been made, much work remains, both experimentally and theoretically, to ascertain whether or not gas blankets can be realized in thermonuclear reactors.

References

1. D. F. Düchs and D. Pfirsch, Bull. Am. Phys. Soc. 21, 1125 (1976).

2. H. C. Howe, Bull. Am. Phys. Soc. 21, 1170 (1976).

PELLET INJECTION

Chairman: S. L. Gralnick
(Princeton Plasma Physics Laboratory, U.S.A.)

REVIEW OF PELLET FUELING

Robert J. Turnbull
Department of Electrical Engineering
University of Illinois
Urbana, Illinois 61801

Abstract

Fusion reactors based on the Tokamak concept (possibly mirrors, too) will require a low energy method of fueling. Refueling by using solid pellets of hydrogen isotopes appears to be the most promising low energy technique. The main issue in assessing the feasibility of pellet fueling is the ability of the pellet to penetrate into the central region of the reactor. A review is presented of the various theories predicting the lifetime of the pellet and their regions of applicability. Among the phenomena considered are neutral ablation of the solid, ionized ablation of the solid, shielding of the pellet by neutral molecules and electrons and ions, flow of the ablation cloud, distortion of the magnetic field by the flow of an ionized ablation cloud, and charging and electrostatic shielding of the pellet. A brief summary of results of experiments done by the University of Illinois - Oak Ridge and Riso groups is presented. The results of these experiments indicate that, at least at the low temperatures and densities used, a neutral ablation - neutral shielding model is correct. Finally, since all indications are that in order for pellet fueling to be successful, high velocity pellets will be needed, a brief discussion of possible acceleration techniques is presented.

I. Introduction

The use of solid pellets of hydrogen isotopes to refuel fusion reactors was first suggested by Spitzer et al.[1] The advantage of using pellets is the possibility of depositing fuel in the center of the reactor with the expenditure of modest amounts of energy. In order to design a pellet fueling system the following questions must be answered:

1. How can pellets be generated?
2. What is the evaporation rate and lifetime of a pellet in a fusion plasma?
3. What is the effect of the pellets on the plasma? (What size pellets can be used?)
4. To what velocities can pellets be accelerated? By what techniques?

The first question has essentially been answered and much progress has been made both theoretically and experimentally toward answering the second question. The last two questions are just beginning to be addressed. Therefore, this paper will deal primarily with the first two questions.

II. Pellet Generation

Two methods have been developed for generating solid hydrogen pellets. In the first technique,[2] liquid hydrogen is formed into a jet which is broken up into uniform sized drops. The drops are frozen by lowering the pressure below the triple point pressure. Finally, they are injected into vacuum. In the second technique[3,4] solid hydrogen is forced through an orifice. The resulting ribbon of solid hydrogen is cut either thermally or electrically into pellets. Either of these methods could be incorporated into a pellet refueling system so the pellet generation problem can be considered to have been solved.

III. Theory of Pellet Evaporation in a Plasma

The first theoretical consideration of this problem was in the paper by Spitzer et al.[1] In that paper they discuss a number of the physical phenomena which have been developed more extensively by later investigations. Rose[5] considered the possibility of the ionized ablation cloud deforming the plasma magnetic field to reduce the incident energy flux to the pellet. Chang[6] concluded that magnetic field deformation is unlikely to be important. Gralnick[7] calculated the shielding effect of an ionized ablation cloud. Parks et al[8] concluded that neutral molecules would be ablated from the pellet. (This is supported by experiments.[9,10]) They then calculated pellet lifetimes using the shielding effect of the neutral gas. Vaslow[11] gave scaling laws based on a neutral shielding model. Parks and Turnbull[12] improved on the neutral shielding model by more accurately solving for the flow of the gas.

The basic mechanism for pellet ablation is that neutral molecules are ablated from the pellet by the electron energy flux.[8,12] The neutral ablatant then flows away from the pellet. The resulting neutral gas cloud absorbs most of the incident electron energy flux, lengthening the pellet lifetime. In this paper this neutral shielding model will be discussed first and then it will be shown when other effects (shielding by an ionized ablation cloud, distortion of the magnetic field, and electrostatic shielding) become important.

Since the energy needed to ablate a molecule from the solid is so small (~ 0.01 eV) the cloud around the pellet will be dense enough to almost completely shield the pellet. The energy is deposited in the ablation cloud and mostly becomes heat energy resulting in a flow which is simultaneously being heated and expanded. Near the pellet the heating dominates and the flow is subsonic. The flow then goes through a subsonic-supersonic transition and becomes supersonic farther from the pellet where the expansion dominates. Using this model an expression for the pellet evaporation rate is[12]

$$\frac{dr_p}{dt} = -1.58 \times 10^{-8} r_p^{-2/3} n_{eo}^{1/3} T_{eo}^{1.64} \quad \text{cm/sec} \qquad (1)$$

where r_p is the pellet radius in cm, n_{eo} the plasma electron density in cm^{-3} and T_{eo} the plasma electron temperature in eV. The above result is for deuterium, as are all numerical results given here unless otherwise stated. In order to determine the pellet lifetime, Eq. (1) should be integrated over the pellet trajectory taking into account the varying plasma conditions.

In order to determine the conditions for which the shielding of the pellet is predominantly due to ions and electrons rather than neutrals, we look at the neutral shielding results and determine when they break down. Reference 12 shows that about two thirds of the incident electron energy is deposited in the

region near the pellet where the flow of the ablatant is subsonic. Therefore, a rough criterion to determine the type of shielding is to see if the ablatant is predominantly ionized before it reaches the sonic radius. Equations (2) and (3) are expressions for the temperature and density of the ablation cloud at the sonic radius assuming it is still composed of neutral molecules.[12]

$$T_s = 1.88 \times 10^{-8} r_p^{2/3} n_{eo}^{2/3} T_{eo}^{-0.14} \quad \text{eV} \qquad (2)$$

$$n_s = 2.2 \times 10^{12} r_p^{-1} T_{eo}^{1.68} \quad \text{cm}^{-2} \qquad (3)$$

As a typical example for T_{eo} = 20 keV, $n_{eo} = 10^{14}$ cm^{-3} and r_p = 1 mm the fractional ionization at the sonic radius given by the Saha equation and Eqs. (2) and (3) is 16.5%. Increasing the electron density by an order of magnitude would result in essentially complete ionization. Actually the temperature at the sonic radius is less than that calculated from Eq. (2) because that portion of the incident energy flux which goes into ionization and dissociation is not available to heat the ablation cloud. The cross sections for neutral and ionized deuterium are about equal for high energy electrons (> 1000 eV). However, an ionized cloud would be more effective in shielding a pellet if instead of expanding spherically it expanded preferentially along the magnetic field. In most cases the plasma pressure will be so large that the ablation cloud would still expand almost spherically. In conclusion, the principal difference between neutral and ionized shielding is that energy is used to dissociate and ionize the ablation cloud thereby increasing the shielding effect of the cloud.

In order for the ablation cloud to distort the magnetic field away from the pellet and thus deflect the hot electrons away from the pellet, two conditions must be satisfied. The pressure of the ionized portion of the ablation cloud must be larger than the magnetic field pressure and the magnetic Reynold's number must be greater than 1. If we take the same case as before ($n_{eo} = 10^{14}$, T_{eo} = 20 keV, r_p = 0.1 cm) and look at the sonic radius we find for a magnetic field of 40 kG

$$\beta = \frac{nkT}{B^2/8\pi} = 22.4 \qquad (4)$$

We conclude that the pressure is high enough to deflect the magnetic field. Next the magnetic Reynold's number is given by

$$R_M = \frac{4\pi\sigma r_p v}{c^2} \qquad (5)$$

where σ is the electrical conductivity and v the velocity of the ablation cloud. For the conditions given above the magnetic Reynold's number at the sonic radius is about 0.2. Both the numbers in Eqs. (4) and (5) are actually too high since the energy going into ionization has not been accounted for. In order for magnetic field distortion to be important the plasma density or pellet size would have to be raised by about an order of magnitude. If the magnetic field distortion was the dominant effect in determining the pellet lifetime, the ablation rate of the pellet would be that needed to maintain the magnetic Reynold's number at a large enough value to deflect the magnetic field.

Another phenomenon which could increase the lifetime of the pellet is charging of the pellet due to the incident electrons. Since the pellet is evaporated by an electron flux if there is not a return current the pellet will charge negatively and thereby shield itself electrostatically. Solid deuterium has a secondary emission coefficient which falls below one for incident electrons of energy greater than a few hundred electron volts.[13] However, since the ablation cloud is partially ionized, it will tend to short out any voltage. To get an estimate let us again use the neutral shielding model to estimate the conductivity of the cloud and then determine the voltage needed to make the return current equal to the incident current. Let us consider secondary electrons due only to direct ionization by plasma electrons and neglect thermal ionization. The ionization cross-section is[8]

$$\sigma_i \approx 10^{-14}/T_{eo}^{0.823} \quad \text{cm}^2 \qquad (6)$$

where T_{eo} is in eV. The recombination cross-section due to dissociative recombination (assuming 1 eV secondaries) is 6.4×10^{-16} cm^2. Now referring to Reference 12, we assume that the incident electrons retain their energy and that the incident energy flux and therefore the incident current varies as $[(r/r_p) - 1]^{1/2}$ for $r_p < r < 2r_p$. We also assume that the neutral density decays as $1/r^3$. This results in a conductivity (assuming 1 eV electrons and our same plasma conditions again) of

$$\sigma = 7.6 \times 10^{11} \left(\frac{r}{r_p}\right)^{3/2} \left(\frac{r}{r_p} - 1\right)^{1/4} \quad \text{sec}^{-1} \qquad (7)$$

Combining this with the incident current shows that a voltage of about 2000 volts is sufficient to provide the return current and therefore electrostatic shielding does not appreciably increase the pellet lifetime. The actual voltage needed is somewhat less because thermal ionization will reduce it. A larger pellet or higher plasma density would reduce the electrostatic shielding effect still more. A more detailed consideration of electrostatic shielding is given in Reference 14.

In summary, a neutral shielding model is valid for the conditions specified (r_p = 0.1 cm, T_{eo} = 20 keV $n_{eo} = 10^{14}$). For larger pellets or densities the effects of ionizing the ablation cloud and possible magnetic field distortion need to be considered.

IV. Experiments on Pellet-Plasma Interaction

There have been two sets of experiments done studying the interaction of hydrogen pellets with plasmas. In the first set a pellet of linear dimension 0.25 mm was injected into a rotating plasma.[10] The amount of mass ablated from the pellet was measured and the results were consistent with a neutral shielding model. More details of this experiment will be given in a later paper in these proceedings.[15]

In the other experiment a hydrogen pellet of diameter $\sim$ 0.2 mm was injected into a Tokamak discharge and the lifetime of the pellet measured.[9] The experimental results correlated with the neutral shielding model. Again the details will be presented later in this conference and will not be repeated here.[16]

V. Prospects for Pellet Fueling

Once we know the lifetime of a pellet, we can calculate the velocity needed for a given size of pellet to reach the center of a reactor. For example, if we take the Experimental Power Reactor designed by General Atomic,[17] a pellet of radius 3 mm would contain 10% of the reactor mass. From Eq. (1) and the parameters of the reactor the velocity is 2×10^5 cm/sec. It is possible that distortion of the magnetic field will reduce this requirement somewhat but in any case a velocity of about 10^6 cm/sec will be necessary to reach the center with this pellet. For larger reactors the pellet sizes go up but the velocities are about the same. If it is possible to reach these kinds of velocities with large pellets then pellet refueling will be realizable. If it is not possible then pellet refueling can be used if the reactors will tolerate larger pellets or refueling nearer the plasma edge. Another possibility is that nature may look fondly on us and produce pellet lifetimes longer than predicted.

In order to achieve the velocities required, various acceleration schemes have been proposed. We will look briefly at three types of acceleration here, mechanical, electrostatic, and ablation.

In mechanical acceleration schemes the pellet is accelerated by contact with a high velocity solid. One mechanical technique accelerates the solid linearly using magnetic forces.[18] This technique will not be considered further except to say that many difficult technological problems must be solved before it can be considered feasible. The other mechanical acceleration scheme, for which a prototype is now being constructed[19] uses a high speed rotating arm to accelerate the pellet. The pellet velocity is limited to $\sqrt{2}$ times the velocity of the tip of the arm. The limitations for this acceleration are due to the strength of both the rotating arm and the pellet. It does not appear feasible to rotate an arm at a velocity greater than $2\text{-}3 \times 10^5$ cm/sec so pellet velocities of 10^6 cm/sec are probably not attainable. The limitation due to pellet strength can be calculated as follows. A pellet experiences a maximum force due to the arm of

$$f_{max} = \frac{m_p v_m^2}{2r_a} \tag{8}$$

where m_p is the mass of the pellet, v_m the maximum pellet velocity and r_a the radius of the arm. For a cubic pellet with side of length ℓ, the maximum pressure experienced by the pellet is

$$p_{max} = \frac{f_{max}}{\ell^2} = \frac{\rho \ell v_m^2}{2r_a} \tag{9}$$

where ρ is the density of the pellet. Since the yield strength of hydrogen is about 10^6 dynes/cm^2, a velocity of 10^6 cm/sec for a pellet with $\ell = 2$ mm requires an arm of radius 8000 cm.

Electrostatic acceleration is limited by the charge which can be placed on a pellet due to the strength of hydrogen. The maximum charge-to-mass ratio because of this limitation is

$$\frac{q}{m} = \frac{5 \times 10^{-3}}{r_p} \text{ kg/coul} \tag{10}$$

with r_p in cm. Thus for a pellet radius of 1 mm a voltage of 10^9 volts is necessary to accelerate the pellet to 10^6 cm/sec.

The last technique for accelerating pellets which we will consider is ablation acceleration. This includes all techniques for which atoms, molecules, electrons, or ions are used to accelerate the pellet. The reason for this is that more momentum is transfered to the pellet from the molecules ablated off due to incident particle flux than results from direct momentum transfer (assuming mostly inelastic collisions). Laser acceleration also falls into this category. If we want a velocity of 10^6 cm/sec we need to heat one side of the pellet very hot ($\sim$ 1 eV) while the rest of the pellet remains cold. Thermal conductivity for solid hydrogen is so small that the thermal diffusion time for a pellet of radius 1 mm is about 0.1-1 sec. Therefore an acceleration pulse of less than 1 msec should be fast enough to prevent the pellet from evaporating by heat conduction. Another restriction occurs since the desired directional energy is about 100 times the energy needed to evaporate the pellet. This restriction is that very little energy should go into acoustical waves in the solid because this acoustical energy will eventually degrade into heat. For an acceleration with constant force the fraction of energy which goes into acoustical energy is about equal to

$$\left(\frac{\tau_t}{\tau_f}\right)^2 \tag{11}$$

where τ_t is the transit time for a sound wave in the pellet and τ_f is the total time the force acts. For our 1 mm pellet $\tau_t \approx 10^{-6}$ sec. Therefore the acceleration pulse should be longer than about 10 μsec. To see the conditions necessary to accelerate a pellet of 1 mm radius to 10^6 cm/sec with an electron beam we use the neutral ablation theory discussed previously. We assume that the electrons are incident on only one side of the pellet. The net force transferred to the pellet is equal to

$$f = \pi r^2 (p + \rho v^2) \tag{12}$$

evaluated at some radius. If we use the sonic radius to evaluate this expression, the result for deuterium is

$$\frac{dv_p}{dt} = -121\, r_p^{-2/3} n_{eo}^{1/3} T_{eo}^{-0.1} \frac{dr_p}{dt} \tag{13}$$

where v_p is the pellet velocity in cm/sec and the rest of the quantities have the same definitions as before. If the final pellet radius is half the initial pellet radius we have as the final pellet velocity

$$v_p = 75\, r_p^{1/3} n_{eo}^{1/3} T_{eo}^{-0.1} \text{ cm/sec} \tag{14}$$

We also can derive the expression for the duration of the pulse from Eq. (1). This becomes

$$\tau_f = 2.6 \times 10^7 r_p^{5/3} n_{eo}^{-1/3} T_{eo}^{1.64} \text{ sec} \tag{15}$$

If we set the pulse time to 20 μsec we have for the beam conditions

$$\begin{aligned} n_{eo} &= 2.7 \times 10^{14} \\ T_{eo} &= 3000 \text{ eV} \end{aligned} \tag{16}$$

Needless to say it is extremely difficult to get such an electron beam. However, a high energy ion beam may be useful for providing the necessary energy flux.

References

1. L. Spitzer, D. J. Grove, W. E. Johnson, L. Tonks, and W. F. Westendorp, USAEC Report NYO-6047 (1954).

2. C. A. Foster, K. Kim, R. J. Turnbull, and C. D. Hendricks, Rev. Sci. Instrum. 48, 625 (1977).

3. A. F. D. S. Taylor, J. of Physics E 2, 696 (1969).

4. F. R. Jarboe and W. R. Baker, Rev. Sci. Instrum. 45, 431 (1974).

5. D. J. Rose, Culham Laboratory Technology Division Memorandum 82 (1968).

6. C. T. Chang, Nuclear Fusion 15, 595 (1975).

7. S. L. Gralnick, Nuclear Fusion 13, 703 (1973).

8. P. B. Parks, R. J. Turnbull, and C. A. Foster, Nuclear Fusion 17, 539 (1977).

9. C. A. Foster, R. J. Colchin, S. L. Milora, K. Kim, and R. J. Turnbull, (To be published in Nuclear Fusion, December 1977).

10. L. W. Jorgensen, A. H. Sillesen, and F. Oster, Plasma Physics 17, 453 (1975).

11. D. F. Vaslow, IEEE Trans. Plasma Science PS-5, 12 (1977).

12. P. B. Parks and R. J. Turnbull, (To be published).

13. H. Sorensen, Nucl. Inst. and Meth. 132, 377 (1976).

14. P. H. Miller, P. B. Parks, R. Prater, and D. F. Vaslow, General Atomic Report GA-A14477.

15. C. T. Chang, These proceedings.

16. S. Milora, These proceedings.

17. Experimental Power Reactor Conceptual Design Study, EPRI Report ER-289 (1976).

18. P. H. Miller, Bull. A.P.S. 22, 1064 (1977).

19. C. A. Foster, These proceedings.

EQUILIBRIUM AND LINEAR STABILITY OF GAS FLOW NEAR AN ABLATING PELLET*

P. Parks, F. Felber, P. Miller, R. Prater, D. Vaslow
General Atomic Company
P. O. Box 81608
San Diego, California 92138

The present pellet ablation model is being refined because the feasibility of pellet fueling strongly depends upon the pellet ablation rate. The relevant atomic processes occurring in the ablation, such as thermal dissociation, excitation, and ionization affect the temperature and density of the ablation, and therefore must be included self-consistently. The temperature and degree of ionization determine the conductivity of the ablation, which is necessary to estimate the effect of electrical charging of the pellet on the ablation rate. The space-charge and the energy sinks of the atomic processes reduce the ablation rate.

Nonlaminar flow, or turbulence, near the pellet can have a large effect on the ablation rate. A linear perturbation analysis of the compressible-flow equations, however, shows that the ablation cloud is stable. Several factors contribute to the stability. Because the rate of increase of the pellet surface recession is negligible compared to $\nabla p/\rho$, where p is the pressure and ρ is the mass density, the Rayleigh-Taylor instability will be insignificant. Moreover, convection carries perturbations beyond the sonic point where they can no longer influence flows in the subsonic region of the cloud. Other stabilizing mechanisms are noted.

Introduction

The feasibility of refueling magnetic-confinement fusion reactors by injecting solid hydrogen pellets depends upon the ablation rate of the pellets. Present estimates of the ablation rate indicate that the pellets may have to be accelerated to velocities as high as 10^6 cm/sec to reach the interior of the thermonuclear plasma.

In the following section, we discuss plans to refine our pellet-ablation model to include the effects of various atomic processes occurring in the ablation cloud. Our goal is to estimate the ablation rate more reliably. Towards this end we also consider the question of the fluid stability of the ablation. Clearly, any instabilities growing during the ablation process can affect the ablation rate. However, our analysis shows no evidence for significant growth of any fluid instabilities in the subsonic ablation.

Refining the Plasma-Pellet Ablation Model

Approximate models have been developed to estimate the time for a solid hydrogen pellet to ablate when immersed in a plasma.[1-4] Thus far these models have provided good estimates of experimental ablation times of hydrogen pellets injected into ORMAK[3] and of polystyrene pellets injected into the Texas Tech. theta pinch.[5] In both of these experiments the primary source of energy driving the ablation is the plasma electrons. In another experiment conducted at RISO, hydrogen pellets were injected into a puffatron plasma[6] in which the plasma ions were the primary source of energy driving the ablation. Scaling law estimates of the energy required to ablate one molecule based on the assumed incident power flux at the pellet surface with no ablation cloud shielding, agree well with the experimental values.[1] Although these models have been successful in predicting ablation rates of pellets for a wide range of experimental conditions, they are as yet relatively crude. Present predictions of the ablation rates of pellets immersed in thermonuclear plasmas indicate that high injection velocities ($\sim 10^6$ cm/sec) may be required to fuel the interior.[1-4] If a refined ablation model predicts a factor of two difference in the requisite injection velocity, it would significantly affect demands on accelerator technology.

An important feature of present models is the "self-regulating"[1] or "self-shielding"[2,3] mechanism in which the stopping power of the ablation cloud is a constant related to the range of the incident particles. This mechanism was assumed in the scaling law developed by Vaslow.[1] In the transonic-flow model developed by Parks,[2,4] this mechanism was manifested by the weak dependence of the stopping power on the plasma density and pellet parameters. In order to estimate the stopping power, the Maxwellian plasma electron distribution has been approximated by an equivalent monoenergetic distribution for the energy flux. This simplification gives rise to a stopping power, and hence an ablation time, that is too large by perhaps 25%.[4]

On the other hand the present models do not account for the additional stopping power of the ambipolar electric field. A simplified attempt to account for this effect reduced the ablation rate for a pellet in a thermonuclear plasma by about a factor of two.[4] The main assumptions used were that a resistive electron current balanced the incident fast electron current, that the resistivity was primarily caused by electron-neutral collisions, and that the electron density was primarily regulated by dissociative recombination in the region of interest. While the assumption of electron-neutral particle resistivity may be reasonable near the pellet surface where the degree of ionization is low, the resistivity becomes Spitzer-like (electron-ion friction) farther away. Our assumption of electron-neutral friction throughout probably leads to underestimates of the electrical resistivity, stopping power, and ablation time.

Further refinements which should be included in the pellet ablation model are the following. In the transonic flow model[2,4] a constant fraction of the energy deposited by the incident electrons is assumed converted to heat to drive the expansion of the ablation cloud. In fact this fraction depends on radial position according to the amount of energy converted to radiation and to the potential energies of dissociation and ionization. This fraction affects the temperature and density profiles of the ablation cloud, and must be determined in order to accurately estimate the Spitzer resistivity.

Another assumption of the transonic-flow model is that the ablation rate may be determined from a steady-state solution of the flow equations. The general solution to the flow equations which satisfies all the pellet boundary conditions[7] and simultaneously gives rise to transonic flow is time dependent,[1] even neglecting the recession of the pellet surface. However, the steady-state solution appears to be a good approximation, since the pellet surface recession speed is much smaller than the ablation cloud flow speed[3] and also the same scaling law can be derived from both the

*Work supported by the Electric Power Research Institute under Contract RP-323-2.

steady-state approach and the approximation to the time dependence approach.[1]

We shall now discuss a scheme for determining the effect of the ambipolar electric field including the treatment of the radially-dependent fraction of energy deposited that is converted to heat. This approach is not fully self-consistent since the slow-down of incident electrons is treated as if the ablation cloud consisted of only molecular hydrogen. Furthermore, we continue to treat the ablation cloud as a single-species fluid. The mass of the "gas" decreases as the degree of dissociation increases. All other species of interest including ions and electrons are assumed to acquire the same temperature and flow velocity as the "gas". Consequently, each of these species is described by an equation of continuity with appropriate source and sink terms. The electric field which is included in the equation for the slow-down of incident electrons is obtained from the relation $E = \eta j_e$, where η is the resistivity of the "gas" and j_e is the incident electron-current density.

The species of primary interest are: H_2, H, H_3^+, H_2^+, H^+, H_2^* ($C^1\Pi$), H^* (n = 2), and e. Cross-sections and processes for these species are discussed elsewhere.[4] Dissociation of H_2 occurs primarily as a result of Franck-Condon dissociation, dissociative recombination, and thermal dissociation. Ionization and excitation occur as a result of primary (incident) electron and thermal electron collisions. De-excitation of excited species occurs either radiatively or non-radiatively in the dense, gaseous regions close to the pellet. Each of these many processes is either exothermic or endothermic, and the energy transfer balance determines the fraction of deposited energy that is converted to heat to drive the expansion of the ablation cloud. Some of the source and sink terms in the continuity equations are determined by a modified Monte-Carlo technique discussed in another report[4], and other terms have the familiar $n^2 \sigma V$ appearance.

The refinements proposed here should help us pin down the ablation rate more accurately. We do not expect to have to modify the model to account for the possibility of nonlaminar flow, since the following analysis discloses no significant instabilities.

Linear Stability Analysis of Plasma-Pellet Ablation

In this section, we present the results of an analytic and numerical study of the stability of the ablation of a long, cylindrical fuel pellet surrounded by a thermonuclear plasma. We find no evidence for significant growth of any fluid instabilities in the ablation.

The linear stability analysis was performed upon a system of compressible-fluid equations describing the steady ablation of gas caused by heating by incident thermonuclear electrons. The equations depart from the transonic flow model[2-4] only in their cylindrical geometry. The steady, gas-dynamic profiles are qualitatively similar to those describing spherical flow.

The pellet surface is considered stationary on the hydrodynamic time scale determined by the ratio of sonic radius, r_*, to sound speed at the sonic surface, V_*. The analysis loses validity over longer times, but perturbations generally propagate out of the subsonic ablation on the hydrodynamic time scale anyway.

Several factors contribute to the stability of the ablation. Because the rate of increase of pellet-surface recession is negligible compared to $\nabla p/\rho$, the Rayleigh-Taylor instability will be insignificant. Furthermore, the velocity gradient of the ablation causes a dispersion of propagating perturbation wave packets, thereby reducing their amplitudes before they are convected out of the subsonic ablation altogether. This and other stabilizing mechanisms are noted in the analytic treatment below.

The perturbations are Fourier-decomposed in the longitudinal and azimuthal directions so that their only dependence on z and ϕ is of the form $\exp[i(kz + m\phi)]$. All fluid quantities and perturbations are dimensionless, normalized to their values at the sonic surface. Time is normalized to r_*/V_*, radius to r_*, and the dimensionless Lagrangian coordinate ξ is defined as

$$\xi = -t + \int_1^r dr'/V(r') \quad .$$

The dimensionless perturbed quantities, denoted by a tilde, are scaled as

$$\theta = \tilde{T},\ g = \tilde{\rho}/\rho,\ h = \tilde{q}/q,\ u = \tilde{V}_r/V,\ w_\phi = im\tilde{V}_\phi,\ w_z = in\tilde{V}_z$$

in which $n = kr_*$. The equilibrium temperature is T, density ρ, velocity V, and electron heat flux q. With these transformations the linearized equations become

$$\partial(uV^2)/\partial t = -(T/\gamma)\,\partial g/\partial\xi - (Vr/\gamma)\,\partial(\rho\theta)/\partial\xi \qquad (1)$$

$$\partial w_\phi/\partial t = -Vw_\phi/r + m^2(\theta + Tg)/\gamma r \qquad (2)$$

$$\partial w_z/\partial t = n^2(\theta + Tg)/\gamma \qquad (3)$$

$$\partial g/\partial t = -\partial u/\partial\xi - (w_z + w_\phi/r) \qquad (4)$$

$$\partial\theta/\partial t = \gamma q\Lambda(h - u) - (\gamma - 1)\,[T(w_z + w_\phi/r + \partial u/\partial\xi) - \theta(V/r + \partial\ell n V/\partial\xi)] \qquad (5)$$

$$h = -\lambda_* \int_\xi^\infty g\Lambda\, d\xi'/r \qquad (6)$$

in which Λ and λ_* are the "effective" electron energy flux cross-section and eigenvalue defined in Refs. 2-4. This system of equations has been integrated as an initial-value problem using a finite-difference scheme. The numerical results follow the presentation of several analytic approaches below.

The first analytic approach demonstrates the wave nature of purely radial perturbations ($m = n = 0$). If temperature perturbations are neglected, Eqs. (1) and (4) yield a hyperbolic wave equation in u,

$$\frac{\partial^2 u}{\partial\xi^2} - \frac{\gamma V^2}{T}\frac{\partial^2 u}{\partial t^2} = \frac{\gamma}{T}\left[2\frac{\partial V^2}{\partial t}\frac{\partial u}{\partial t} - \frac{\partial}{\partial t}(V^2 u)\frac{\partial}{\partial t}\ell n\, T + u\frac{\partial^2 V^2}{\partial t^2}\right] . \qquad (7)$$

For radial modes of wavelength much shorter than the scale length of zero-order quantities, the solution of (7) is a superposition of ingoing and outgoing waves, $u(\xi,t) = u^+ + u^-$, where

$$u^{\pm} = C^{\pm} \left(\frac{\partial V^2}{k^2 T} \right)^{1/4} \left[\exp \int_o^t \left(\frac{V}{2} \frac{T'}{T} - 2V' \right) dt \right]$$

$$\times \exp ik \left(\xi \pm \int_o^t \frac{T^{1/2} dt}{\gamma^{1/2} V} \right) , \qquad (8)$$

and a prime denotes $\partial/\partial r$. In the fluid frame, the ingoing and outgoing waves propagate with local velocities

$$d\xi/dt = \pm T^{1/2}/\gamma^{1/2} V \quad .$$

In the pellet frame, the local propagation velocities are

$$dr/dt = V \pm (T/\gamma)^{1/2} \quad ,$$

in which

$$(T/\gamma)^{1/2}$$

is the dimensionless isothermal sound speed.

The first exponential in (8) represents two physical effects. Firstly, the zero-order flow helps transfer more perturbed momentum out of a fluid element than into it since $V' > 0$ everywhere in the ablation cloud. This clearly has a stabilizing effect on the perturbed radial flow velocity u_r. Secondly, the zero-order temperature, T, now acts like an "effective pressure" term since ρ has been absorbed in the expression for the reduced perturbed density g. Since $T' > 0$ an "effective force" exists in the negative radial direction opposing the stabilizing influence of the first effect. The combination of the two effects is stabilizing since at all locations in the ablation cloud $VT'/2T < 2V'$. Solution (8) agrees well with the numerical solution of the equations (1-6) for both $h = 0$ and $h \neq 0$ and $m = n = 0$.

The next analytic approach involves a normal mode analysis in which perturbations of the heat flux are neglected. Perturbation modes having high mode numbers m and n, as well as those near the pellet surface where $T \approx 0$, tend to be convected with the outward flow rather than be propagated as radial waves. Therefore, the gradients with respect to ξ of such modes can be neglected in Eqs. (1-5). The validity of the normal mode analysis also depends upon the oscillation period of the perturbations being short compared to the time during which zero-order quantities change appreciably in the fluid frame. Then the perturbed quantities may be assumed to have a time dependence of the form $\exp(\Gamma + i\omega)t$ in which Γ and ω are real constants.

The resulting dispersion relation is a quintic equation in $(\Gamma + i\omega)$ that indicates that all modes satisfying the conditions above are stable ($\Gamma < 0$). For example, the $m = 50$, $n = 1$ mode gives an oscillation period of $2\pi/\omega = .095$ and a decay rate of $\Gamma = .6$ for the highest frequency mode. Figure 1a

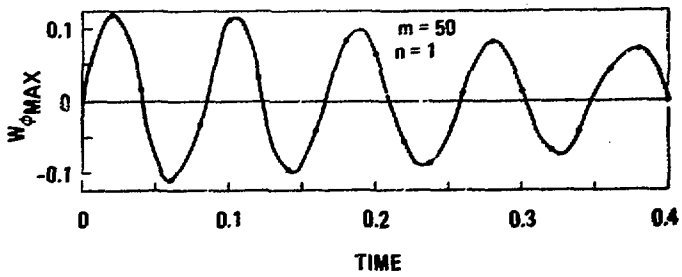

Fig. 1a. Maximum amplitude of the perturbed azimuthal flow velocity, w_ϕ, as a function of dimensionless time. The perturbations are the result of an initial density perturbation.

shows the oscillation period and damping rate of w_ϕ for the same mode found by solving Eqs. (1-6) numerically with an initial density perturbation only.

The stabilizing mechanism in this case is seen from Eq. (5) to be the reduction of perturbed temperature by the compressional work done by a perturbation on its surrounding fluid. The Coriolis force acting on azimuthal flow helps damp perturbed modes as well.

If the perturbed heat flux is not neglected in the normal mode analysis, then an approximate dispersion relation can still be derived from Eqs. (1), (4), (5), and (6), but is valid only for the $m = n = 0$ mode near the pellet surface. The cubic dispersion relation indicates that such a mode is unstable ($\Gamma > 0$) wherever

$$\Lambda > (\gamma - 1)(V' + V/r)/\lambda_* \quad . \qquad (9)$$

This inequality is typically satisfied in the ablation within about one pellet radius of the pellet surface. However, a perturbation convected through the entire unstable region undergoes growth in amplitude by only a factor of about 4.

This instability, although inconsequential, has an interesting physical origin. A region of fluid perturbed by a compression is compressed further by the gradient in perturbed heat flux driving the compressed region against its convective flow. The gradient in heat flux is represented by the left side of (9), while the stabilizing effect of compressional work is represented by the right.

The exact numerical solutions of Eqs. (1-6) confirm that perturbations damp and spread out. Figure 1b

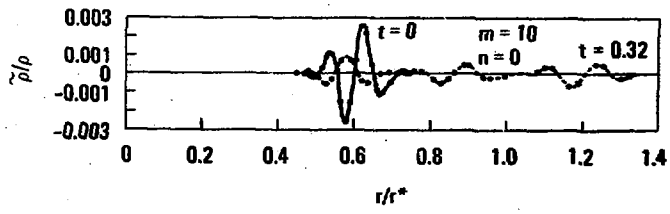

Fig. 1b. Normalized density perturbation at different times for $m = 10$, $n = 0$ mode.

shows the decay of a density perturbation wave packet from its initial configuration. Figure 2 illustrates the time evolution of an axially symmetric ($m = n = 0$) perturbation of the radial velocity. The initial wave packet splits into decaying ingoing and outgoing packets having local velocities in the pellet frame of $V - \sqrt{T}$ and $V + \sqrt{T}$ respectively. With $\theta = 0$ the

numerical solution agrees well with the analytic solution (8), and has the same qualitative behavior illustrated in Fig. 2.

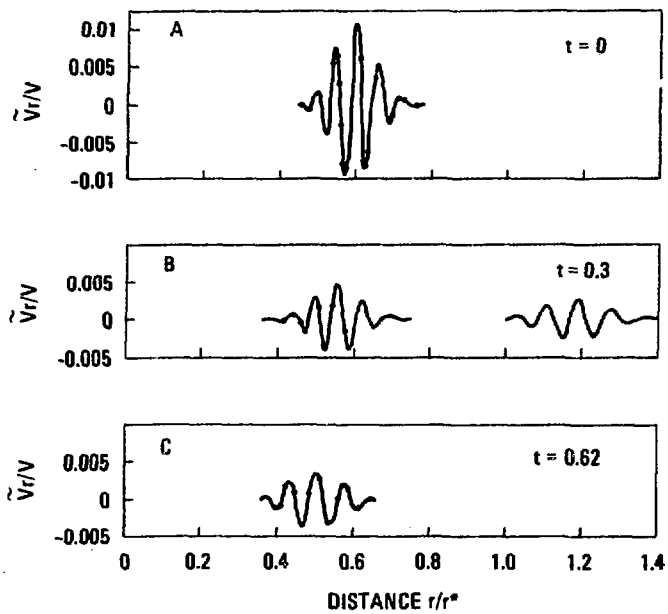

Fig. 2abc. Normalized radial flow velocity perturbation for $m = n = 0$ at three different times. Inward and outward propagating waves travel with velocities $V - \sqrt{T}$ and $V + \sqrt{T}$ respectively. The damping agrees with the short-wave approximation (Eq. 8).

Conclusions

Present models of the ablation of fuel pellets in thermonuclear plasmas have several shortcomings. Areas in which increased understanding can improve our estimates of ablation rates are the atomic processes in the ablation, possible charging of the pellet and ablation, radiation energy losses, and boundary conditions. Our instability analysis shows no evidence for significant fluid instabilities growing in the subsonic ablation. Therefore, we expect no turbulent behavior in that region to affect ablation rates.

References

1. D. F. Vaslow, "Scaling Law for Ablation of a Hydrogen Pellet in a Plasma," IEEE Trans. Plasma Science PS-5, 12-17 (1977).

2. P. B. Parks, "Model of an Ablating Solid Hydrogen Pellet in a Plasma," Ph.D. Thesis, University of Illinois, October 1976.

3. P. B. Parks, et. al., "A Model for the Ablation Rate of a Solid Hydrogen Pellet in a Plasma," Nucl. Fusion 17, 539-556 (1977).

4. P. H. Miller, Jr., P. B. Parks, R. Prater, and D. Vaslow, "Physics of an Ablating Pellet in a Thermonuclear Plasma," General Atomic Company Report GA-A14477, July 1977.

5. D. L. Smith, M. Kristiansen, and M. O. Hagler, "Ablation Rates of Spherical Polystyrene Pellets in a Theta Pinch," IEEE 1977 Int'l. Conf. on Plasma Science, May 1977.

6. L. W. Jorgensen, A. H. Sillesen, and F. Oster, "Ablation of Hydrogen Pellets in Hydrogen and Helium Plasmas," Plasma Phys. 17, 453-461 (1975).

7. D. F. Vaslow, "Hydrodynamic Boundary Conditions at the Surface of an Ablating Material, General Atomic Company Report GA-A14533, July 1977.

MAGNETIC SHIELDING EFFECTS IN PELLET PLASMA INTERACTIONS*

P.A. Politzer and G.E. Thomas, Jr.

Department of Nuclear Engineering
Massachusetts Institute of Technology
Cambridge, Massachusetts 02139

I. INTRODUCTION

The principal goal of the analysis of the interaction between solid D-T pellets and a thermonuclear reactor grade plasma is the determination of the ablation rate, and the pellet lifetime as functions of the reactor plasma parameters and the pellet size. This analysis can be separated into four parts: (1) the shielding of the pellet surface by the ablated material; (2) calculation of the ablation dynamics for the reduced energy flux; (3) analysis of the time evolution of the shielding cloud and ablation rate; (4) analysis of the motion of an ablating pellet across the reactor plasma. The latter two questions have not as yet been considered in any detail. In computations of the fuel deposition profile, the pellet velocity has always been assumed to be constant and equal to the injection velocity. Transients in the time evolution of the cloud of ablated material have also been neglected, generally on the assumption that these transients are short compared to the pellet lifetime, and so a quasi-steady-state situation exists at all times. In this paper we consider the first of these questions, the shielding of the pellet surface by the ablation cloud.

In particular, we are concerned with the case in which the particles in the ablation cloud become ionized while at a pressure sufficient to exclude the external magnetic flux from the region surrounding the pellet.[1,2,3] If this is the case, the high energy particles from the external plasma are constrained to follow magnetic field lines and thus their energy is deposited in the outer layers of the ablation cloud. The only mechanisms available to transport this energy to the pellet surface are thermal conduction and transport by superthermal particles. Transport by superthermal particles becomes important only when the thickness of the ablation cloud is not large compared to the pellet radius, and when the density is low enough to allow these particles to reach the pellet surface. The first condition is required in order to achieve a significant probability that a high energy particle entering the ablation cloud hits the pellet surface. These conditions apply only for restricted ranges of external plasma densities and temperatures. Thus, we are restricted to the use of thermal conduction to transport the energy inward. This immediately implies that the flow velocities in the ablation cloud are subsonic. This condition is consistent with the existence of a field-free region because the flow is strongly retarded at the boundary between field-free and finite field zones.

II. BUBBLE MODEL

A qualitative picture of the density, temperature, and magnetic field profiles in an ablation cloud is shown in Fig. 1. Here, n_s and T_s are the density and temperature of the solid pellet; n_∞, T_∞, B_∞ are the values in the external plasma ($n_e = n_i$; $T_e = T_i$ assumed), r_p is the pellet radius, r_i is the ionization radius, and r_m is the radius of the "field-free" zone.

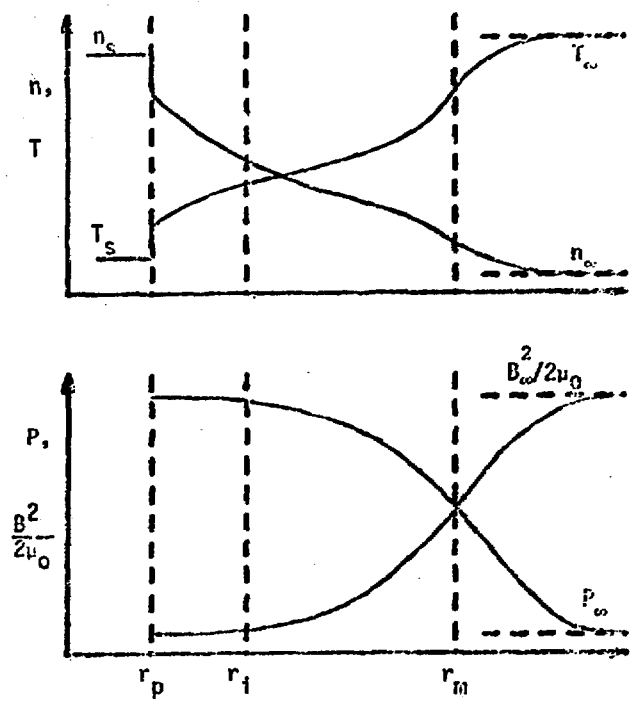

Fig. 1. Schematic radial profiles of density, temperature, magnetic pressure, and kinetic pressure.

Assume that $(r_i - r_p) < r_p$ so that we can take $r_i = r_p$. For simplicity, assume that $B = 0$ for $r < r_m$. We, therefore, have a fully ionized, unmagnetized plasma between $r = R_0 \approx r_p$ and $r = R_1 \approx r_m$. Fig. 2 schematically shows a cross-section of this system.

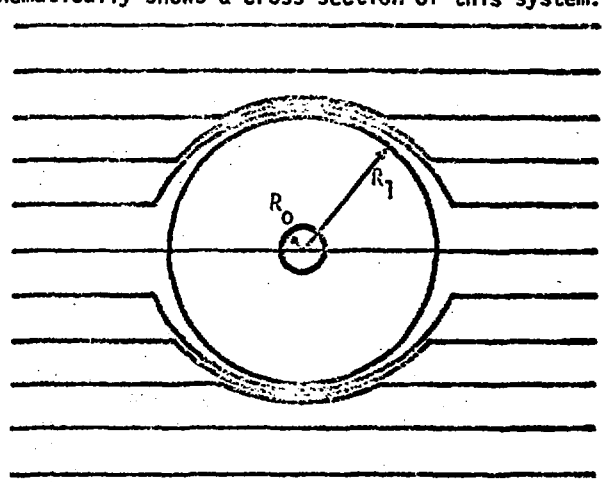

Fig. 2. Cross-section of the model system.

Assume further that this cloud is spherically symmetric. Define the ablation rate as G ions/sec. Conservation of particles gives

$$4\pi r^2 nV = G \tag{1}$$

Conservation of momentum:

$$nm_i V\frac{dV}{dr} = -\frac{d}{dr}(2nkT) \tag{2}$$

(the factor of 2 arises because we must add the election and ion pressures). Conservation of energy gives

$$nV[3kT + \frac{1}{2}m_i V^2] - \kappa\frac{d}{dr}(kT) = -nVk\lambda \tag{3}$$

where λ is the energy per ion going to ablation, ionization, and radiation losses inside $r = R_0$ (we assume $\lambda \approx 18$ eV). Define a dimensionless radius

$$\rho \equiv r/R_1 \tag{4}$$

and

$$M \equiv V\sqrt{\frac{m_i}{2kT}} \tag{5}$$

Eqn. (1) becomes

$$n = \frac{G}{4\pi R_1^2 \rho^2 M}\sqrt{\frac{m_i}{2kT}} \tag{6}$$

Eqn. (2) becomes

$$(1-\frac{1}{M^2})\frac{dM^2}{d\rho} = \frac{4}{\rho} - (1+M^2)\frac{1}{T}\frac{dT}{d\rho} \tag{7}$$

Eqn.(3) becomes

$$\frac{dT}{d\rho} = \frac{G}{4\pi R_1}\frac{1}{\kappa}\frac{1}{\rho^2}[\lambda + T(3+M^2)] \tag{8}$$

The boundary condition at $r = R_0$ ($\rho = R_0/R_1$) is an energy balance condition

$$\kappa\frac{d}{dr}(kT)\Big|_{R_0} - n_0V_0[3kT_0 + \frac{1}{2}m_iV_0^2] = n_0V_0\,k\lambda \tag{9}$$

This condition has already been used in writing Equations (3) and (8). At $r = R_1$ (ρ=1) we require that the plasma-magnetic field boundary be stationary, so that a momentum balance obtains:

$$2n_\infty kT_\infty + \frac{B_\infty^2}{2\mu_0} = 2n_1\,kT_1 + n_1m_i\,V_1^2 \tag{10}$$

There must also be an energy balance at ther outer surface. The energy convected outward crosses this boundary and is dissipated in the external plasma. The remaining balance is between the energy deposited at this surface from the external plasma and the inward thermal conduction. The electron energy flux in the external plasma is

$$\Gamma_{Ee} = (\frac{1}{4}n_\infty\,\bar{V}_{e\infty})\,(2kT_\infty) \tag{11}$$

This energy is transported along magnetic field lines. We assume that the effective area intercepted by the ablation cloud is πR_1^2, giving an incident power of

$$P_e = 2(\pi R_1^2)\,\Gamma_{Ee} \tag{12}$$

The factor of two arises because the flux is incident on both sides of the system. We assume that only a fraction α of this energy is deposited at the surface $r + R_1$, giving finally

$$(\frac{1}{4}n_\infty\bar{V}_{e\infty})\,(2kT_\infty)(\pi R_1^2)(2)\alpha = (4\pi R_1^2)\kappa\frac{d}{dr}(kT)_{R_1} \tag{13}$$

To calculate α, we assume that all of the incident electrons are guided around the cloud by the magnetic field at radius R_1. We, therefore, examine the slowing down and scattering of fast electrons by coulomb collisions in a plasma of density n_1 and temperature T_1. If R_1 is large, the electrons are stopped and give up all of their energy. If R_1 is small, the electrons pass through the outer layer of the cloud, giving up a fraction α of their energy. To a good approximation we find a critical radius,

$$R_{1c} = 6.48\times10^{15}\frac{T_\infty^2}{n_1\ln\Lambda} \tag{14}$$

(here, and in all practical formulae, MKS units are used, except that T is in eV).

For $R_1 > R_{1c}$, $\alpha = 1$. For $R_1 < R_{1c}$

$$\alpha = 4.09\times10^{-17}\frac{R_1n_1\ln\Lambda}{T_\infty^2} \tag{15}$$

Thus α changes discontinuously at $R_1 = R_{1c}$ because an electron is assumed to lose all of its energy if it is scattered through 90°. The only other number required is the electron thermal conductivity[4]

$$\kappa = \hat{\kappa}T^{5/2}$$

$$\hat{\kappa} = 4.558\times10^{23}/\ln\Lambda \tag{16}$$

Two additional boundary conditions are required. At R_0 we set the temperature equal to T_0 and the Mach number equal to M_0. Strictly, these values should be determined by the ablation dynamics and the behavior of the neutral gas layer close to the pellet surface. However, the gas is very dense in this region, and the ionization and recombinatin rates are sufficiently rapid so that the fractional ionization can be determined using the Saha equilibrium relation.

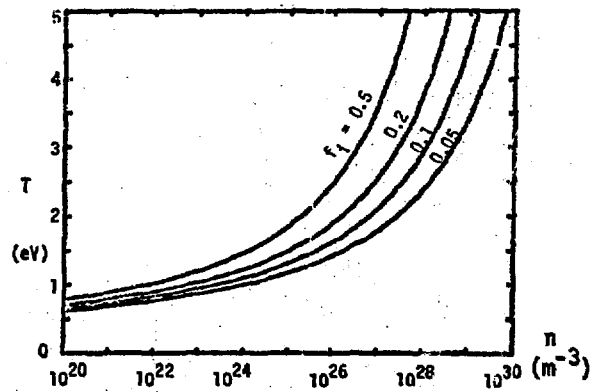

Fig. 3. Saha equilibrium for atomic hydrogen; $n=n_0+n_1$ is the total density; $f_1=n_1/n$ is the fractional ionization.

At the densities considered, significant ionization is obtained for $T_0 \sim 1$-2 eV. We thus choose T_0 in this range. Most of the ablation models which have been considered give a Mach number in the neighborhood of unity, so that the range of values is $M_0 \sim 0.5$-1.5. Since a subsonic solution for M is desired, we write Eqn. (7) in the limit of small M:

$$\frac{1}{M^2}\frac{dM^2}{d\rho} = \frac{1}{T}\frac{dT}{d\rho} - \frac{4}{\rho} \tag{17}$$

This gives

$$M = M_0 \left(\frac{T}{T_0}\right)^{1/2} \left(\frac{R_0}{R_1\rho}\right)^2 \tag{18}$$

In the limit of small M, Eqn. (8) integrates to

$$f(T) = f(T_0) + \frac{G}{4\hat{\kappa}R_0}\left[1 - \frac{R_0}{R_1\rho}\right] \tag{19}$$

where

$$f(T) = \frac{2}{3}\left(\frac{\lambda}{3}\right)^{5/2}\left[\frac{1}{5}x^5 - \frac{1}{3}x^3 + x - \tan^{-1}x\right]$$

$$x = \sqrt{3T/\lambda} \tag{20}$$

III. RESULTS

Define the following coefficients which depend on the external plasma parameters:

$$A_1 = 2.16\times10^{29}\left[B_\infty^2 + 8.05\times10^{-25}\, n_\infty T_\infty\right]$$

$$A_2 = 4.95\times10^{-16}\, n_\infty \ln\Lambda / T^{1/2}$$

$$A_3 = 1.75\times10^{-25}\ln\Lambda$$

$$A_4 = 2.10\times10^{6}\, n_\infty \tag{21}$$

For $R_1 < R_{1c}$ ($\alpha<1$) we obtain

$$R_1 = \left[\frac{M_0 R_0^2 T_1 (3T_1+\lambda)}{A_2 T_0^{1/2}}\right]^{1/3}$$

$$M_1 = \left[\frac{A_2^2 R_0^2 M_0}{T_0^{1/2} T_1^{1/2}(3T_1+\lambda)^2}\right]^{1/3} \tag{22}$$

$$G = \frac{A_1 R_0^2 M_0}{T_0^{1/2}}$$

and

$$0 = f(T_1) - f(T_0) - \frac{A_1 A_3 M_0 R_0}{T_0^{1/2}}\left[1 - \left(\frac{A_2 R_0 T_0^{1/2}}{M_0 T_1 (3T_1+\lambda)}\right)^{1/3}\right]$$

For $R_1 > R_{1c}$ ($\alpha = 1$):

$$R_1 = R_0\left[\frac{A_1 M_0 (3T_1+\lambda)}{A_4 T_0^{1/2}}\right]^{1/2}$$

$$M_1 = \frac{A_4 T_1^{1/2}}{A_1(3T_1+\lambda)}$$

$$G = \frac{A_1 R_0^2 M_0}{T_0^{1/2}} \tag{23}$$

and

$$0 = f(T_1) - f(T_0) - \frac{A_1 A_3 M_0 R_0}{T_0^{1/2}}\left[1 - \left(\frac{A_4 T_0^{1/2}}{A_1 M_0 (3T_1+\lambda)}\right)^{1/2}\right]$$

The density is obtained from Eqn. (6). In the low M limit, the pressure is constant ($n_1 T_1 = n_0 T_0$). Note that the ablation rate G is the same in either case. It depends only on R_0, T_0, M_0, and the total (magnetic plus kinetic) external pressure. If n_s is the density of the solid, the recession rate of the solid surface is

$$4\pi R_0^2 \frac{dR_0}{dt} n_s = G$$

$$\frac{dR_0}{dt} = \frac{A_1}{4\pi n_s}\frac{M_0}{T_0^{1/2}} \tag{24}$$

Thus the pellet lifetime is

$$\tau_p = \frac{4\pi n_s}{A_1}\frac{T_0^{1/2}}{M_0} R_0(t=0)$$

$$= \frac{2.45}{B_\infty^2 + 8.05\times10^{-25} n_\infty T_\infty}\cdot\frac{T_0^{1/2}}{M_0} R_0(t=0) \tag{25}$$

The range of values obtained is shown in Table 1:

Table 1[a]

R_0 (mm)	T_∞ (keV)	N_∞ (m^{-3})	N_0 (m^{-3})	T_1 (eV)	R_1 (mm)	τ_p (μsec)	τ_{tr} (μsec)	τ
0.5	1	1(21)	1.6(25)	41	1.5	130	.023	.48
0.5	10	1(19)	1.6(25)	46	11	140	5.3	.030
0.5	10	1(20)	1.6(25)	46	5.0	130	0.7	.014
0.5	10	1(21)	2.1(25)	48	2.4	110	.081	.0084
2	1	1(21)	1.6(25)	80	170	540	150	1
2	10	1(19)	1.6(25)	78	38	550	9.2	.063
2	10	1(20)	1.6(25)	77	18	540	1.2	.030
2	10	1(21)	2.1(25)	79	8.4	420	.13	.018

[a] For all cases, B = 5 T, M_0 = 0.5, T_0 = 2 eV

The paramters for a specific case are shown im more detail in Table 2:

Table 2

$n_\infty = 1\times10^{20}\ m^{-3}$
$T_\infty = 10$ keV
$B_\infty = 5$ T.
$R_0 = 0.5$ mm
$n_1 = 7.03\times10^{23}\ m^{-3}$ $\quad n_0 = 1.60\times10^{25}\ m^{-3}$
$T_1 = 45.6$ eV $\quad T_0 = 2$ eV
$R_1 = 5.01$ mm
$M_1 = 2.38\times10^{-2}$ $\quad M_0 = 0.5$
$G = 4.93\times10^{23}\ sec^{-1}$
$\tau_p = 134$ μsec
$\alpha = 1.44\times10^{-2}$
$R_m = 7.41$
$\lambda = 18$ eV

For small parameter variations around the conditions shown in Table 2, we find that the pellet lifetime scales like

$$\tau_p = 13.2 \times \frac{R_o T_o^{1/2}}{M_o} \times n_\infty^{-.034} \times T_\infty^{-.028} \times B_\infty^{-1.934} \quad (26)$$

The variations of pellet lifetime and bubble radius with B_∞ are shown in Fig. 4, with all other fixed parameters as given in Table 2.

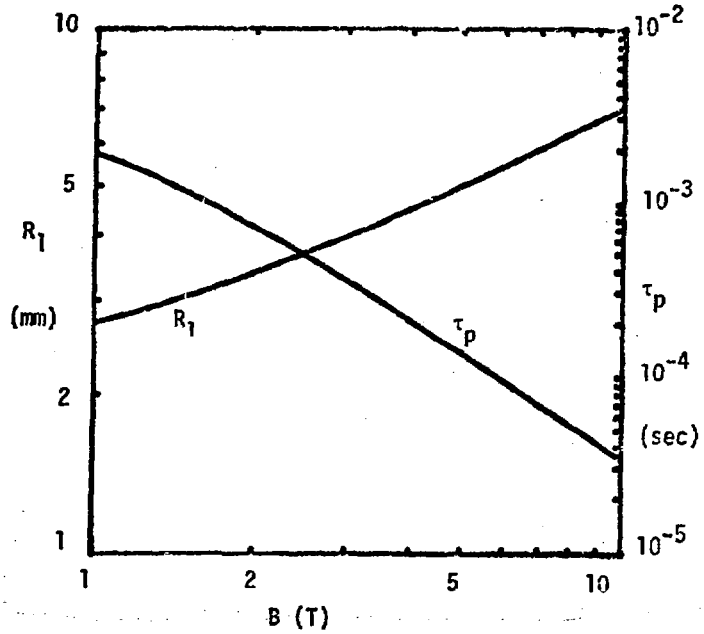

Fig. 4. τ_p and R_1 vs. B_∞; $n_\infty = 10^{20}$ m^{-3}; $T_\infty = 10^4$ eV; $R_o = 0.5$ mm; $T_o = 2$ eV; $M_o = 0.5$.

IV. REGION OF VALIDITY

There are only certain external plasma regimes and pellet radii for which the model assumed here is valid. One obvious condition is that the duration of the initial transient for setting up the magnetic bubble be shorter than the calculated pellet lifetime. We estimate the initial time constant by calculating the transit time for a fluid element across the bubble:

$$\tau_{tr} = \int_{R_o}^{R_1} dr/v$$

$$= \frac{4\pi n_o T_o}{G} \int_{R_o}^{R_1} dr\, r^2/T \quad (27)$$

We require that $\tau_p > \tau_{tr}$. Another related condition is that the total number of ions in the bubble be smaller than the number initially in the pellet.

$$N_{c1} = 4\pi \int_{R_o}^{R_1} dr\, r^2\, n$$

$$= 4\pi n_c T_o \int_{R_o}^{R_1} dr\, r^2/T \quad (28)$$

We require that $N_{c1} < N_o = \frac{4}{3}\pi R_o^3 n_s$. This condition scales identically with the condition on the transit time, but is a factor of three more stringent. A third requirement is that the velocity at $r = R_1$ be large enough to prevent diffusion of the magnetic field into the bubble. In other words, the magnetic penetration distance (skin depth) in a time of the order of τ_{tr} must be small compared to the bubble radius R_1. These requirements are satisfied if we require that an "effective" magnetic Reynolds number of greater than unity at R_1:

$$R_{me} > 1$$

$$R_{me} = V_1 \mu_o \sigma_1 R_1 \quad (29)$$

In Fig. 5, we show n_∞ - T_∞ parameter space for fixed B_∞(5 T) and R_o (0.5 mm).

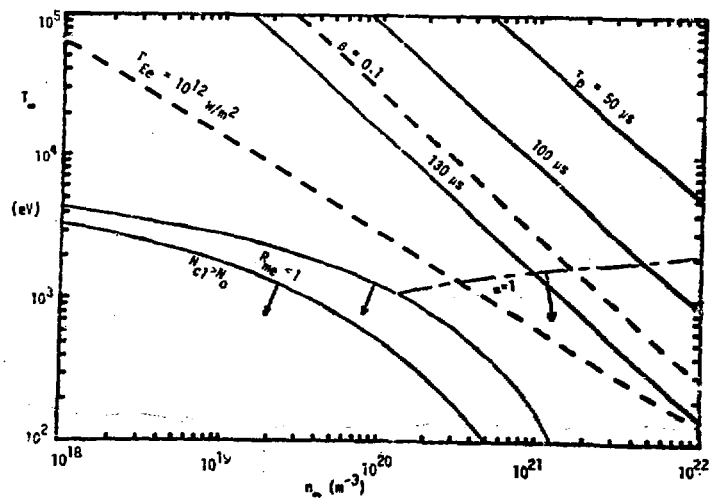

Fig. 5. n_∞- T_∞ parameter space for $B_\infty = 5$T, $R_o = 0.5$ mm, $T_o = 2$ eV, and $M_o = 0.5$.

Indicated on this figure are the regions in which $N_{c1} > N_o$, $R_m < 1$, and $\alpha = 1$. Shown for reference are the lines along which $\beta_\infty = 10\%$ ($\beta_\infty = 2n_\infty kT_\infty / (B_\infty^2/2\mu_o)$), and $\Gamma_{Fe} = 10^{12}$ w/m^2. The lines along which $\tau_p = 50$, 100, and 130 μsec are also shown.

V. CONCLUSIONS

We have developed an approximate model for the magnetic shielding of an ablating pellet in a thermonuclear reactor grade plasma. This model predicts that the pellet lifetime varies linearly with initial pellet radius, and inversely as the total external pressure. For possible reactor conditions and pellet sizes the lifetime falls in the 100-500 μsec range, indicating that the required pellet velocity is of the order of 10^4 m/sec. This model breaks down for either densities or temperatures which are significantly lower than might be found in a reactor plasma. In these regimes, the flow velocity is too small to exclude the magnetic field, and the initial transient time for setting up the shield is too long. Therefore, we expect that a bubble will form only if either the plasma temperature exceeds about 3 keV, or the density exceeds 1×10^{21} m^{-3}. If neither of these conditions is satisfied, magnetic shielding does not occur. This, however, is just the regime in which neutral gas shielding models do apply.[5]

REFERENCES:

1. D.J. Rose, Culham Lab. Tech. Div. Memo. No. 82 (1968).

2. C.T. Chang, Nuclear Fusion, 15, 595 (1975).

3. L.L. Lengyel, IPP Garching Rep. 4/160 (1977).

4. L. Spitzer, Jr., "Physics of Fully Ionized Gases", Interscience, N.Y., 1962.

5. S.L. Milora and C.A. Foster, ORNL/TM-5776 (1977)

*Supported by U.S.E.R.D.A.

CRYOGENIC IMPLICATIONS FOR DT

P. C. Souers
Lawrence Livermore Laboratory
Livermore, CA.

Summary

We are currently compiling cryogenic hydrogen data for magnetic fusion engineering. Many physical properties of DT can be extrapolated from H_2 and D_2 values. The phase diagram properties of the D_2-DT-T_2 mixture are being measured. Three properties which will be greatly affected by tritium should be measured. In order of their perceived importance, they are: 1) solid thermal conductivity, 2) solid mechanical strength, and 3) gaseous electrical conductivity. The most apparent need for DT data is in Tokomak fuel pellet injection. Cryopumping and distillation applications are also considered.

Introduction

The fusion fuel that ignites at the lowest temperature is DT; i.e., a mixture of the two isotopes of heavy hydrogen. The DT may be liquified or frozen at several stages in Tokomak operation. First, a fuel pellet may be fired at high speed through the magnetic field. If not initially solid, passage through the reactor chamber vacuum will freeze it. After the fusion reaction, the DT will be drawn from the reaction chamber by the 4.2 K cold of copper cryopanels. These panels will be periodically cleaned, and the DT will be distilled to D_2 and T_2 so that the proper mix is ready for the next fuel cycle.

The unique aspect about tritium, of course, is that it is radioactive, with a half-life of 12.3 years.[1] The daughter products are He^3, a beta particle, and an antineutrino. The total decay energy is 18 keV, but the beta particle can carry any amount, with 5.65 keV the mean amount.[2] The beta particle travels about 2 μm in liquid or solid, and it leaves a trail of over a hundred ion pairs behind it. Although neutrons have a more obvious ability to damage by billiard-ball collisions, ionizing radiation can cause a surprising amount of damage over time.

Of General Importance: Mixture Effects

The most obvious effect of the radiation is to transform DT into the three-component mixture: D_2-DT-T_2. This is because the tritium beta particle catalyzes the chemical reaction:

$$D_2 + T_2 \rightleftharpoons 2DT \qquad (1)$$

At room temperature and above, a 50% D - 50% T mixture produces about 50% molecular DT; at 20 K, 40%, and at 4.2 K, 9%.[3] Almost nothing is known of the reaction rate. At room temperature, the half-time to equilibrium appears to be on the order of ten minutes.[4,5] At 20 K, the H-T reaction appears to slow down to hours, as shown by the change in total pressure (DT is not sensitive enough for this method).[4] Also of interest are the rotational transitions (ortho-para) of D_2 and T_2, which may react in minutes at 20 K in the presence of a catalyst like the beta particle.[6] At Lawrence Livermore Laboratory, we are readying mass and infra-red spectroscopy to better study these reactions. An infra-red spectrum of 92% T_2 - 8% DT is shown in Fig. 1. The S(0) peak is a measure of the amount of the ground rotational state (para-T_2), and the Q and S(1) peaks measure mostly the first excited state (ortho-T_2). The smaller DT peaks are seen at higher frequency.[4] The infra-red spectrometer is a promising tool for quantitative analysis of all the isotopic and rotational hydrogen species.

There is no way to avoid the D_2-DT-T_2 mixture, because the fusion reaction itself is a near-instantaneous catalyst. Separating the tritium for magnetic fusion will be done by distillation.[5] At 25 K, for example, liquid 50% D - 50% T will fractionate to 55% D - 45% T in the vapor. Corrections of interest in distillation are the several percent deviation from Raoult's Law and the several percent increased volatility caused by the ever-present H impurity.[4,7]

The most serious potential problem occurs in freezing DT. At the 19.8 K triple point, liquid 50% D-50% T freezes to solid 48% D - 52% T. This is a small effect, but it is the accumulated fractionation that matters. The result, then of a slow freeze will be a graded composition, tritium-rich at the surface of

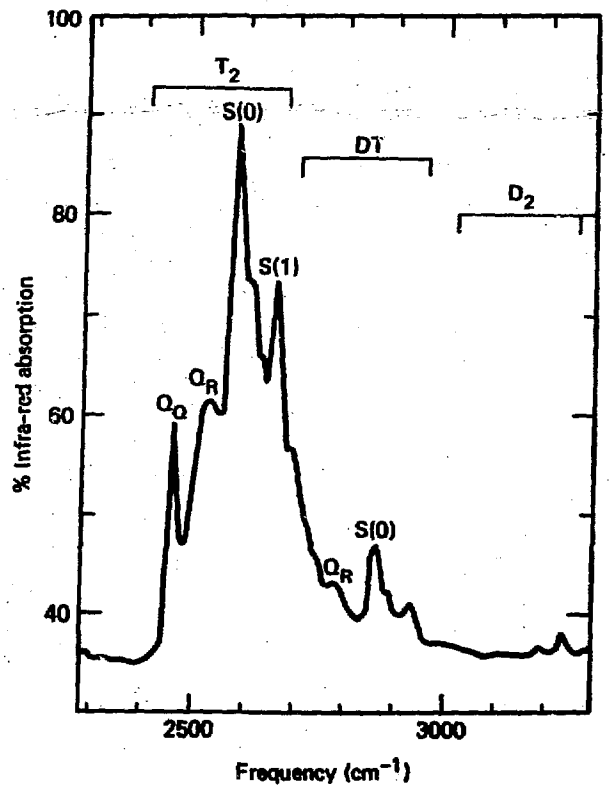

Fig. 1. Infra-Red Spectrum of Liquid 95% T_2 - 8% DT at About 21 K. The S(0) peak represents the ground rotational state; the Q and S(1) peaks measure mostly the first excited state. The Q_Q-Q_R splitting is a measure of the quasi-Debye temperature, Θ_D.

Work performed under the auspices of the U.S. Energy Research & Development Administration under Contract No. W-7405-Eng-48.

first freezing and almost pure D_2 at the end of the freeze. A "slow" freeze is faster than one might think. For the sub-μm DT films in laser fusion targets, the extreme mobility of the liquid hydrogen[8] requires a freeze in less than 20 ms to avoid fractionation. Once frozen, the sample quickly sublimes, redistributing portions of itself to unexpected parts of the containment vessel in a crude distillation.[9] At 4.2 K, solid 50% D - 50% T will chemically equilibrate to 99% D - 1% T in the vapor phase. A final note on the solid is the possible, although unlikely occurrence of phase separation. Early arguments about this effect in solid H_2-D_2 were never quite resolved.[10]

It could be desirable to avoid mixture effects while forming and shooting the fuel pellet. This could be done by taking the center cut of the distillation column and obtaining pure molecular DT. We do not know, however, how stable this compound is (to decomposition by Eq. 1) at low temperatures.

Pellet Injection into Tokamaks

There are three properties, at least, that cannot be accurately estimated from H_2 and D_2 data. Two properties are of prime importance: solid thermal conductivity[11] and solid mechanical strength.[12] We currently lean towards the former as the first one deserving measurement, since it is needed for heat flow calculations in virtually every device that freezes DT. Radiation can only degrade this property, and the only question is how fast. Mechanical properties are important to determine the deformation of the pellet as it is accelerated. Here, there is a choice between using the soft, fresh solid or deliberately making it harder and more brittle by accumulated radiation.

The third property-electrical conductivity of DT gas--is the least important because it is needed only if electrostatic acceleration of fuel pellets is used. The tritium decay is too slow to ever self-charge a DT pellet by escape of the beta particles. The charge will have to be put on by a discharge from a needle.[13] The current and breakdown characteristics of the DT gas, which is subject to constant ionizing radiation, will affect sparking of electrodes and leakage of charge from the pellet.

We shall consider each of these three properties in the current order of importance.

Solid Thermal Conductivity

The reason why most physical properties will probably not be affected by the tritium radioactivity is the length of the half-life. The disintegration rate is 1.072×10^{15} Bq/mol T or only 2 out of 10^9 nuclei per second. At this rate, damage generally must accumulate some time to show up. The damage must also remain frozen in during this time, as in the solid, especially around 4 K. We may expect almost instantaneous annealing in the liquid.

Solid thermal conductivity is a typical solid property in that extensive radiation damage is needed to affect it. It will take hours or days--the time to produce aggregates and bubbles in the solid.

The crucial question is what the D_2-DT-T_2 mixture, plus possible rotational excitation, will do to the thermal conductivity. Data for unirradiated H_2[14] and HD[15] is shown in Fig. 2 (only one good data point exists for D_2[16]). The numbers refer to the percent of molecules in the first excited rotational state. Such excited molecules, along with dislocations and impurity atoms, all scatter phonons and lower the thermal conductivity below 10 K. The presence of the DT mixture will also cause this, and we estimate a value of about 0.2 W/m-K at 4.2 K for fresh DT. This is five orders of magnitude below that expected for a perfect crystal-never yet achieved, although a recently grown pH_2 crystal has set a new conductivity record.[17]

A few hints are to be had from 4.2 K electron spin resonance studies on solid T_2[18] and Co^{60}-irradiated solid H_2 and D_2.[19-20] The number of free electron defects saturates at about 5 ppm after 30 minutes to 30 hours. In DT, we also expect 10^{-4} mole fraction of He^3 atoms every day. Unknown, however, is the extent of local crystal breakup due to the beta particle. Such breakup should be slow to heal, even just below the triple point, as indicated by the slow molecular self-diffusion coefficient of 10^{-18} m^2/s.[21] As a pure guess, then, we estimate that the tritium radiation will lower the thermal conductivity of frozen DT from 0.2 to 0.04 W/m-K after 24 hours, and to 10^{-3} W/m-K

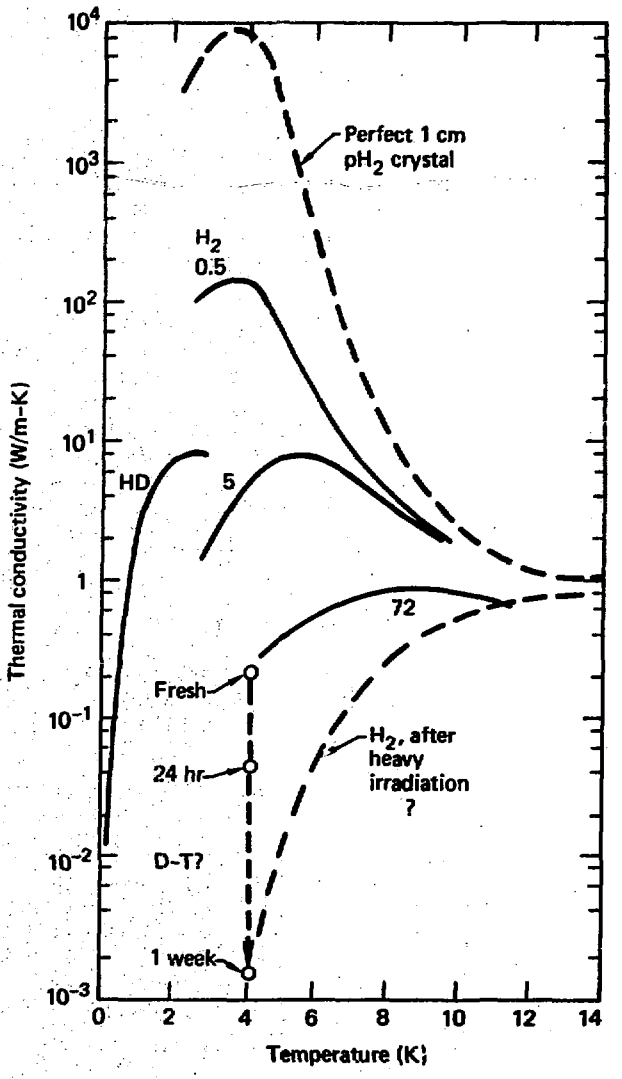

Fig. 2. Solid Thermal Conductivity of the Hydrogens. The dashed lines, which includes all DT points, are estimates. The numbers are the % of molecules in the first excited rotational state.

after a week. These values will produce unacceptable thermal gradients in DT layers thicker than 3 mm, 120 μm, and 4 μm, respectively.

A related property is the heat capacity, which will increase slightly with radiation, and then reverse sign as the radiation damage stores energy, to be released upon heating.

Solid Mechanical Properties

Pure D_2 solid has the strength of cold butter. Just below the triple point, the yield stress is 13 psi and the necking stress (where massive failure occurs) about 35 psi. At 1.4 K, the solid is only slightly stronger: the stresses are about 50 and 80 psi, respectively.[22] If we consider a single measurement on an N_2-O_2 mixture, there is no reason to expect the freshly frozen D_2-DT-T_2 to be much harder than D_2.[23] We may expect radiation hardening, which could be caused by the very first point defects formed. We are again left with a time scale of minutes to hours to ponder.

Electrical Resistivity of DT Gas

This property is instantaneously affected by radiation in all phases. Pure liquid H_2 is a hard dielectric at 10^{16} Ω-m, with charge carriers being produced only by cosmic rays. Even one part T_2 in 10^9 D_2 reduces the resistivity a hundredfold.[24] Our preliminary measurement of 5% DT - 95% D_2 is shown in Fig. 3. Resistivities are now reduced to 10^9 to 10^{11} Ω-m, or to about the range of a soft dielectric. The dashed, voltage-dependent "solid" curves are probably really gas breakdown in the cracks between the shrunken solid and the electrical plates. The efficiency of producing charge carriers drops considerably as the tritium concentration rises from 10^{-7} to 2.5%. This means the charge carriers are recombining quickly and again, the material anneals out the greater part of the damage. In the gas, however, the low density means longer lived charge carriers and perhaps the lowest electrical resistivity of any phase.

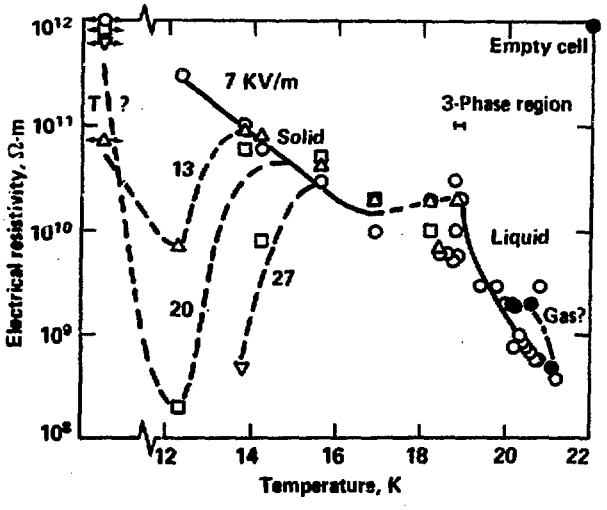

Fig. 3. Preliminary Data for Electrical Resistivity of 5% DT - 95% D_2. The dashed curves are thought to be electric breakdown of gas in shrinkage cracks between the solid and the electrical plates.

Mass Effects: Predicting DT Properties

For most properties, the only expected difference between H_2 and DT is that due to mass. It would take too long to measure all the DT properties, and it is easier to estimate them from data for H_2 (a lot), D_2 (less), HD and T_2 (very little). There is almost nothing for DT itself. Such estimates are empirical, because there is no function or process that converts the value of one isotope to that of another.

There are several excellent compendia of cryogenic hydrogen properties to start from--all but one from the National Bureau of Standards.[25-29] These sources contain little tritium data and no extrapolations (save the fluid H_2 model to 1000 atm).

We are currently preparing a compendium to complement those above. We will further develop the available data and extend estimates to DT itself.[30]

The current program to build a supersonic liquid hydrogen jet has led into little-traveled parts of the nH_2 phase diagram (100 K; 5000 atm).[31] This provides an interesting example of developing current data. We may combine molar volume and sound velocity, whether of the solid or fluid, to obtain a quasi-Debye temperature, Θ_D.[32] This is really a measure of the highest energy "lattice" vibration of a Debye solid, but it is often used as an overall parameter in equation-of-state models.[33-34] Fig. 4 shows a quick plot of available data, including the NBS fluid model.[29,35-40] This kind of plot allows rapid access to vast portions of the phase diagram for persons who must quickly calculate heat capacities. The next step is to use Θ_D to calculate the zero point energy of a molecule in its cell,[41] and from there, to work one's way to the potential energy. As an example, Fig. 5 shows the energies for solid DT at the triple point at 19.8 K.[30] We see that the zero-point energy pushes the DT molecule about half-way up in the classical potential well. Of course, all the DT data is estimated.

We close the circle by returning to the infra-red spectrum of Fig. 1. The splitting between the Q_0 and Q_R lines is a little-used but direct measure of Θ_D.[42] For the T_2 in Fig. 1, we obtain a Θ_D of 85 K for both the solid and liquid near the triple point. This shows that Θ_D is not just a function of molar volume, as is so often assumed.

Cryopumping

All present cryopumps use a 77 K baffle followed by direct condensation of the DT onto a copper panel. The helium goes on to be captured in a second stage by a molecular sieve,[5,43] ion pump,[44] or trapping in a frozen gas.[45] We have already postulated that the solid thermal conductivity and self-heating will not be important unless mm of DT are condensed or the solid layer remains for many hours. The other possible issue with solid DT concerns a possible "anomalous" vapor pressure, caused by the spike of the beta particle. Solid H_2 in the path of gas at 77 to 695 K shows a deviation above the expected vapor pressure only below 3 K and 10^{-9} torr.[46] The effect of the tritium beta particle will probably be no larger, if as great, as this. This has been recently confirmed by a mass spectrometric measurement over a thin DT film at 4.2 K.[44] The observed 10^{-11} torr total pressure compares with the expected 10^{-12} torr by extrapolation from the other isotopes.[47]

The only other possible tritium issues center on the second stage of the cryopump. Helium can be effectively pumped by trapping in an argon gas stream,[45] but H_2 and D_2 are generally ineffective.[44,45] There is a

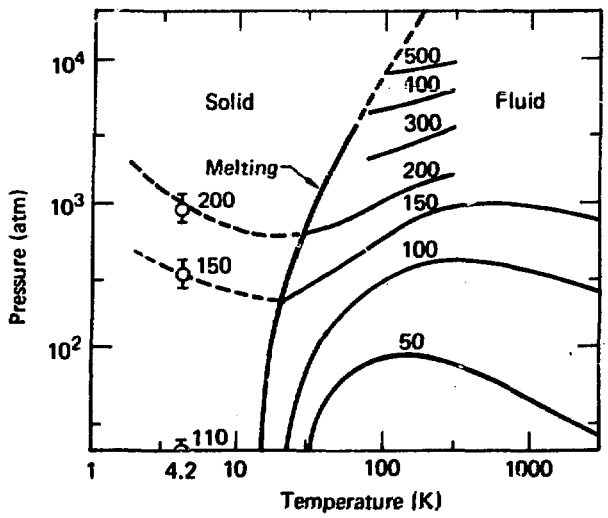

Fig. 4. The Quasi-Debye Temperature, Θ_D, of Super-Critical nH_2. Θ_D is derived from sound velocities, molar volumes, and heat capacities. The high temperature limit for the translational heat capacity is 3R for the solid and 3R/2 for the fluid.

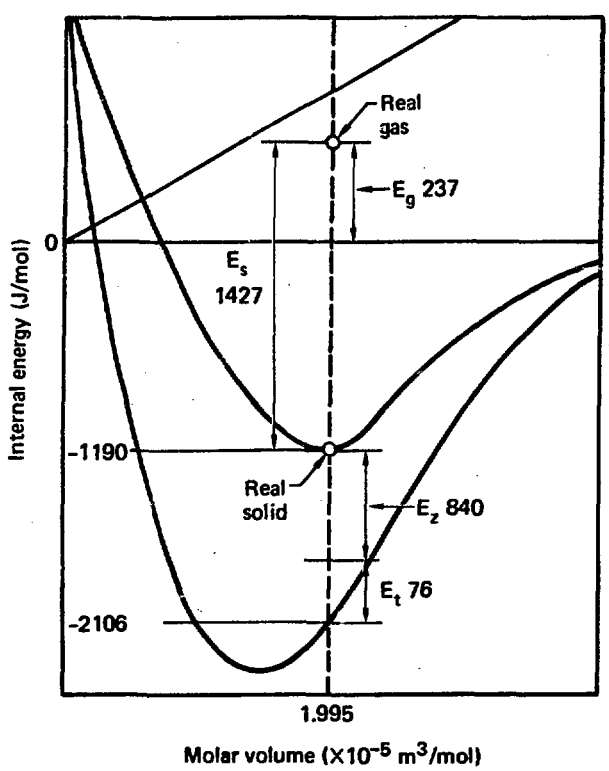

Fig. 5. Potential Energy Diagram for Solid DT at the Triple Point, 19.8 K. All numbers are estimates. The energies are: real gas (E_g), sublimation (E_s), zero-point (E_z), and thermal energy of the solid (E_t). The binding energy is -1190 J/mol, and the classical potential energy, -2106 J/mol.

faint chance that DT or T_2 with their higher mass, might dynamically trap helium, but it is not likely. There is finally the possibility of using a molecular sieve to collect DT, should an unforeseen calamity affect the copper plates. Plans are underway at ORNL to measure the amounts of H_2 and D_2 captured by adsorbents.[43] There is again a faint possibility that tritium radiation could damage the molecular sieves, although a time of days or weeks would probably be needed. A more likely problem might be the beta catalysis of an impurity reaction that poisons the adsorbent.

We see that no obvious tritium problems should affect thin cryopumped DT layers. Should thicker DT layers be used, we are led once again to the solid thermal conductivity as the main property of interest.

The Dominating Implication: Containment

The most important implication of tritium really has nothing to do with property changes. It is, instead, the containment of tritium, so that neither personnel nor environment are injured.[48-51] Time and expense are multiplied by an order of magnitude in the transition from D_2 to DT. One now has to consider glove boxes with inert atmospheres, monitors, and alarms; tritium clean-up systems; and inventory measuring equipment. It is now a world of all-metal seals, x-ray certified welded joints, double-contained transducers, miniaturized lines, and multi-thousand-dollar ballast tanks. All current certified tritium parts are made for room temperature and above. The engineering of cryogenic DT is yet to come.

Acknowledgments

I would like to thank Dr. H. Cullingford and the Division of Magnetic Fusion Energy, Department of Energy, for the support for this paper and the cryogenic hydrogen compendium. The data on the phase diagram and kinetics, including the infra-red spectra, were taken under a grant by the Division of Basic Energy Sciences. The electrical conductivity work was made possible by the Chemistry Research Fund, Lawrence Livermore Laboratory. I should also like to thank J. Pyper for his assistance in describing the cryopumping area.

References

1. K. C. Jordan, B. C. Blanke, and W. A. Dudley, J. Inorg Nucl Chem 29, 2129 (1967).

2. W. L. Pillinger, J. J. Hentges, and J. A. Blair, Phys Rev 121, 232 (1961).

3. J. W. Pyper and P. C. Souers, The Chemical Equilibria Relating the Isotopic Hydrogens at Low Temperatures, Lawrence Livermore Laboratory, Report UCRL 52104 (1976).

4. Our data, to be published.

5. R. Sherman, Los Alamos Scientific Laboratory, Los Alamos, NM, private communication (Sept., 1977).

6. J. W. Pyper and C. K. Briggs, The Ortho-Para Forms of Hydrogen, Deuterium, and Tritium: Radiation and Self-Induced Conversion Kinetics and Equilibria, Lawrence Livermore Laboratory, Report UCRL 52278 (1977).

7. R. H. Sherman, J. R. Bartlit, and R. A. Briesmeister, Cryogenics 16, 611 (1976).

8. D. E. O'Reilly and E. M. Peterson, J Chem Phys 66, 934 (1977).

9. T. M. Henderson, R. B. Jacobs, and R. J. Simms, "Cryogenic Pellets for Laser-Fusion Research-Theoretical and Practical Considerations," preprint, presented at the 1977 Cryogenic Engineering Conference, Boulder, Colo., Aug. 2-5, 1977.

10. D. White and J. R. Gaines, J Chem Phys 42, 4152 (1965).

11. R. J. Turnbull and K. Kim, University of Illinois, Urbana, private communication (Oct., 1977).

12. S. Milora, Oak Ridge National Laboratory, Oak Ridge, TN, private communication (Sept. 1977).

13. J. P. Woosley and R. J. Turnbull, Rev Sci Instr 48, 254 (1977).

14. R. W. Hill and B. Schneidmesser, Z. Phys Chem., Neue Folge 16, 257 (1958).

15. J. H. Constable and J. R. Gaines, Phys Rev 8B, 3966 (1973).

16. R. W. Hill and B. Schneidmesser, Bull. Inst. Int. Froid, Annexe 2, 115 (1956), cited in Ref. 15.

17. J. R. Gaines, the Ohio State University, private communication (Oct., 1977).

18. J. Lambe, Phys Rev 120, 1208 (1960).

19. L. A. Wall, D. W. Brown, and R. E. Florin, J Phys Chem 63, 1762 (1959).

20. D. W. Brown, R. E. Florin, and L. A. Wall, J. Phys Chem 66, 2602 (1962).

21. F. Weinhaus, H. Meyer, and S. M. Myers, Phys Rev 7B, 2960 (1973).

22. D. N. Bol'shukin, Y. E. Stetsenko, and L. A. Alekseeva, Soviet Physics - Solid State 12, 119 (1970).

23. I. C. Trapp, "The Hardness of Solid Nitrogen, Oxygen, Argon, and Nitrogen-Oxygen Mixtures," Schweiz Arch angew Wiss u Tech 24, 191 (1958); cited in Chem Abstracts 53, 21e (1959).

24. W. L. Willis, Cryogenics 6, 279 (1966).

25. H. W. Woolley, R. B. Scott, and F. G. Brickwedde, J. Research Nat Bur Standards 41, 379-475 (1948).

26. R. Prydz, The Thermodynamic Values of Deuterium, National Bureau of Standards, Rept. 9276 (Washington, D.C., 1967).

27. B. N. Esel'son, Yu. P. Blagoi, V. N. Grigor'ev, V. G. Manzhelii, S. A. Mikhailenko, and N. P. Neklyudov, Properties of Liquid and Solid Hydrogen (Israel Program for Scientific Translations, Keter Press, Jerusalem, 1971).

28. H. M. Roder, G. E. Childs, R. D. McCarty, and P.E. Angerhofer, Survey of the Properties of the Hydrogen Isotopes below Their Critical Temperatures, National Bureau of Standards, Tech. Note 641 (U.S. Government Printing Office, Washington, D.C., 1973).

29. R. D. McCarty, Hydrogen: Its Technology and Implications. III. Hydrogen Properties, K. E. Cox and K. D. Williamson, ed. (CRC Press, Cleveland, 1975).

30. P. C. Souers, Cryogenic Hydrogen Data Pertinent to Magnetic Fusion Energy, Lawrence Livermore Laboratory, Report UCRL, to be published (1978).

31. R. Cooper, High Pressure Tokamak Fuel Injector, Physics International, Rept. PIP-1847 (San Leandro, CA., March 1977).

32. W. R. Wanner and H. Meyer, J. Low Temp. Phys, 11 715 (1973).

33. M. Van Thiel and M. Wasley, Compressibility of Liquid Hydrogen to 40,000 Atmospheres and 1100°K, Lawrence Radiation Laboratory, Rept. UCRL 7833 (1964).

34. M. Van Thiel, L. B. Hord, W. H. Gust, A. C. Mitchell, M. D'Addario, K. Boutwell, E. Wilbarger, and B. Barrett, Phys Earth Planet Int. 9, 57 (1974).

35. J. W. Stewart, Phys. Chem. Solids 1, 146 (1956).

36. R. D. Goodwin, Cryogenics 2, 353 (1962).

37. G. Ahlers, J. Chem Phys. 41, 86 (1964).

38. W. Van Dael, A. Van Itterbeek, A. Cops, and J. Thoen, Cryogenics 5, 207 (1965).

39. R. L. Mills, D. H. Liebenberg, J. C. Bronson, and L. C. Schmidt, J Chem Phys 66, 3076 (1977).

40. D. H. Liebenberg, R. L. Mills, and J. C. Bronson, Thermodynamic Properties of Fluid nH_2 in the Range 75-300 K and 2-20 Kbar, Los Alamos Scientific Laboratory, Rept. LA-6645-MS (April, 1977).

41. J. E. Mayer and M. G. Mayer, Statistical Mechanics (John Wiley, New York, 1940), p. 251.

42. H. P. Gush, W. F. J. Hare, E. J. Allin, and H. L. Welsh, Can. J. Phys. 38, 176 (1960).

43. J. Watson, Oak Ridge National Laboratory, Oak Ridge, TN, private communication (Sept. 1977).

44. H. Halama and T. S. Chou, Brookhaven National Laboratory, Upton, L.I., N.Y., private communication (Sept., 1977).

45. T. Batzer, Lawrence Livermore Laboratory, Livermore, CA., private communication (Sept. 1977).

46. T. J. Lee, L. Gowland, and V. C. Reddish, Nature Phys Sci 231, 193 (1971).

47. P. C. Souers, C. K. Briggs, J. W. Pyper, and R. T. Tsugawa, Hydrogen Vapor Pressures from 4 to 30 K: A Review, Lawrence Livermore Laboratory, Rept. UCRL 52226 (1977).

48. T. B. Rhinehammer and P. H. Lamberger, Tritium Control Technology, Mound Laboratory, Rept. WASH-1269 (U. S. Government Printing Office Washington, D.C., Dec. 1973).

49. P. D. Gildea, "Containment and Decontamination Systems Planned for the Tritium Research Laboratory Building at Sandia Laboratories, Livermore," Proceedings International Conference Radiation Effects and Tritium Technology for Fusion Reactors, Gatlinburg, TN, Oct. 1-3, 1975; Rept. CONF-750989 (National Technical Information Service, Springfield, Va., March, 1976), III, 112-128.

50. H. J. Garber, "TFTR Tritium Handling Concepts," reference 49, III, 347-395.

51. R. T. Tsugawa, D. Fearon, P. C. Souers, R. G. Hickman, and P. E. Roberts, "A Secondary Containment System for a High Tritium Research Cryostat," reference 49, IV, 226-235.

PELLET EXPERIMENTS AT ORNL*

S. L. Milora and C. A. Foster

Oak Ridge National Laboratory
Oak Ridge, Tennessee 37830

Summary

A review is given of the results of the recent series of experiments performed on the Oak Ridge Tokamak (ORMAK) in which pellets of solidified hydrogen were injected by a gas dynamic acceleration technique into the warm edge plasma at speeds varying between 90 and 100 m/sec. Pellets of different size, namely 70 μm diam and 210 μm diam, were injected during experiments conducted separately in order to ascertain the functional dependence of pellet ablation rate on pellet size. Optical diagnostic techniques, including line radiation measurements and high speed photography, were employed to monitor the region of interaction of the pellet in the plasma. The evidence strongly suggests that a large (∿1 cm) luminous cloud of neutral hydrogen surrounds the pellet , shielding it from plasma electrons which are degraded in energy as they penetrate the cloud en route to the pellet surface.

In addition to providing a direct measurement of pellet lifetime, the diagnostic techniques mentioned above provided information from which the pellet position, the ablation rate, and the spatial distribution of mass in the hydrogen cloud were inferred. These measured parameters were found to be in good agreement with a recently proposed theoretical pellet ablation model which accounts for the shielding of energetic plasma electrons by neutal hydrogen molecules ablated from the hydrogen ice. The consequences of the pellet lifetime scaling law resulting from this theory and the direction of future pellet experiments at Oak Ridge National Laboratory (ORNL) are discussed.

Introduction

Several of the unique features and advantages of fueling proposed tokamak power reactors by high speed injection of solid fuel pellets have been treated in detail by others within the context of this conference (R. J. Turnbull, P. A. Politzer, P. B. Parks et al., W. A. Houlberg et al., this volume). In this paper we take a brief glimpse at the results of the first hydrogen pellet injection experiments performed on a tokamak (ORMAK) and indicate the course of future experiments at ORNL and elsewhere using the next generation of pellet injection devices currently being developed (C. A. Foster and S. L. Milora, this volume). A more detailed description of this subject matter may be found in the references.

The experiments mentioned above were performed on separate occasions at Oak Ridge in a cooperative effort with the University of Illinois and ORNL[1-3] using the pellet injection apparatus developed at the University of Illinois.[4-5] These initial efforts were important in many respects as they formed the basis for development of the neutral molecule ablation models (P. B. Parks et al., this volume) and stimulated widespread interest in the development of fueling techniques at several U.S. laboratories.

Experimental Procedure

Figure 1 depicts schematically the pellet injector and the diagnostic arrangement employed in the ORMAK experiments. Full details of the pellet injector are given elsewhere[4-5] and only a brief functional description is repeated here. A continuous stream of subcooled liquid hydrogen formed by condensing hydrogen gas in helium-cooled heat exchangers issues from a nozzle and is broken into uniform droplets by the destructive action of capillary waves launched on the free surface of the jet by acoustic vibrations. A series of valves, which are actuated momentarily, admit a pulse of pellets into the 3-m-long drift tube connecting the injector to the tokamak plasma chamber. The pellet size and production rate are controlled by the nozzle diameter, the flow rate of the liquid hydrogen stream, and the frequency of the acoustic driver. Acceleration is accomplished by gas dynamic drag forces acting on the pellet in the 10-cm section of tubing which connects the pressurized region of the injector with the evacuated drift tube. Individual pellets enter the plasma edge (a = 25 cm, R = 80 cm) along a trajectory that makes an angle of 45° with respect to the plasma's minor radius.

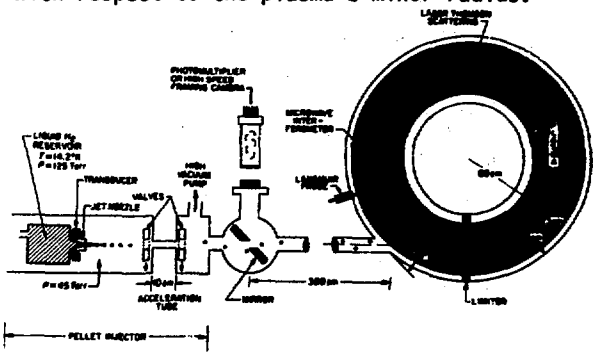

Fig. 1. Schematic of experimental arrangement for pellet injection studies on ORMAK featuring University of Illinois pellet apparatus.

A photomultiplier tube mounted so as to view the injection tube monitored the H_α light emitted from the excited neutrals within the ablation cloud surrounding the pellet. In addition to this diagnostic, a high speed framing camera (to 14,000 frames per second) was used to record the interaction of the pellets with the plasma. Plasma parameters for the series of runs were obtained from the standard complement of tokamak diagnostics. The pellet velocity was inferred from a time-of-flight measurement (time interval between opening of fast valves and initial light burst emanating from the pellet as it entered the plasma).

In the initial experiments,[1] pellets which were nominally 70 μm in diam were injected into the plasma discharge at velocities of about 90 m/sec. The plasma current and toroidal magnetic field values were held at approximately 120 kA and 18 kG respectively. In the latter series of experiments,[2] the pellet diam was a nominal 210 μm, while the injection velocity was increased slightly to 100 m/sec. The plasma current and toroidal magnetic field values were 60 kA and 11 kG, respectively. For the 70 μm series, a line average plasma density of $2.2 \times 10^{19} m^{-3}$ and central electron temperature of about 900 eV were recorded. In the 210 μm series these parameters were $1 \times 10^{19} m^{-3}$ and 650 eV, respectively. The differing experimental conditions permitted a multiparameter check on the

*Research sponsored by the Department of Energy under contract with Union Carbide Corporation.

sensitivity of the ablation process to the key physical parameters.

Experimental Results

The temporal behavior of the ablation rate for individual pellets may be inferred from the luminosity of the ablation cloud since the magnitude of the photomultiplier signal is directly proportional to the pellet ablation rate.[3] This results from the fact that the ratio of the rate of H_α light emission to the rate of ionization by electron impact is nearly constant over the range of electron energies of interest. The reduced data are shown in Figs. 2 and 3 where measurements taken from several shots have been assembled to form composites of the pellet ablation process. The ordinate represents the rate at which the pellet supplies neutral atoms to the plasma. The solid lines are calculations based upon the neutral molecule ablation model of Parks et al.[6] The numerical calculations were performed by following a pellet in time as it traversed the plasma along the known trajectories.[7] Zero time is taken as the instant the pellet enters the plasma edge. The experimental curves have been displaced along the abscissa so as to align with the termination of the ablation process as given by the theory. The scale along the top of Fig. 2 refers to the pellet position projected onto the plasma radius (as inferred from the time, velocity, and known trajectory).

The experimental and theoretical trends show clearly that the ablation process proceeds slowly at first while the pellet is in the tenuous edge plasma within the shadow of the limiter ($r \geq 23$ cm). This is followed by a rapid rise in the ablation rate as the pellet encounters the hotter, more dense plasma outside the limiter. Finally, the ablation rate drops abruptly to zero as the last of the solid pellet matter is consumed by the plasma. The duration of the entire event is in all instances less than one millisecond. This implies that pellets did not penetrate beyond 19 cm from the center of the plasma. At their deepest radial penetration, pellets would encounter a plasma electron temperature of approximately 100 eV and a plasma density in the range of 2-5 x 10^{18} m^{-3}.

The results of the framing camera studies provide a graphic illustration of the ablation process consistent with the above results. The sequence of photographs (negatives) in Fig. 4 shows the evolution of the ablation cloud size and luminosity of a single 210 μm diam pellet as a function of path length into the plasma. The time interval between frames is 140 μsec, and the exposure is 50 μsec. The total lapsed time of 840 μsec is in excellent agreement with the pellet lifetime as measured by the width of the ablation rate curve of Fig. 2. The trends indicated above regarding the gradual increase in ablation rate followed by an abrupt decrease are confirmed by Fig. 4.

The photographs provide additional quantitative information including the size of the luminous cloud and the relative luminosity of the individual images. The latter is subject to direct comparison with the H_α light signals and hence, through proper normalization, with the ablation rate itself. This additional information follows from the sequence of profiles shown in Fig. 5 which depicts the spatial variation of the optical density of the cloud images of Fig. 4. At its greatest size and intensity, the cloud is approximately 3-cm wide (which is more than two orders of magnitude greater than the physical dimensions of the pellet). It is interesting to note that the ionization radius (identified as the distance from the center of the cloud to the point at which the light vanishes) remains constant at roughly 1.5 cm. This is in agreement with the radius that one would calculate for ionization of a neutral (by electron impact ionization) which is being convected away from the pellet by the gas source flow. These data are convincing evidence in support of the argument that a large neutral hydrogen cloud is present. As will be shown in the following section, this cloud is responsible for partially shielding the pellet from the effects of the plasma.

To be consistent with the H_α measurements, the development in time of the total luminosity of the cloud images as measured by the area beneath the densitometer profiles should parallel the photomultiplier results. The agreement is shown in Fig. 2 where the processed photographic data are represented by the triangular marks. The same trends as previously noted are apparent, and it is concluded that the two measurement techniques are equivalent.

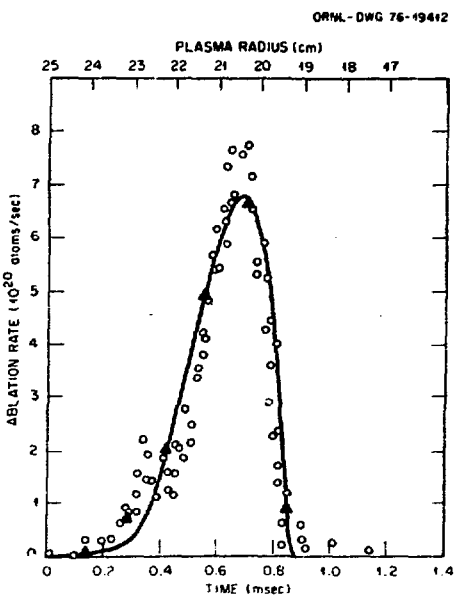

Fig. 2. Composite of ablation rate of 210 μm pellet inferred from H_α data and photographic images (▲). Solid line represents neutral gas shielding model calculation.

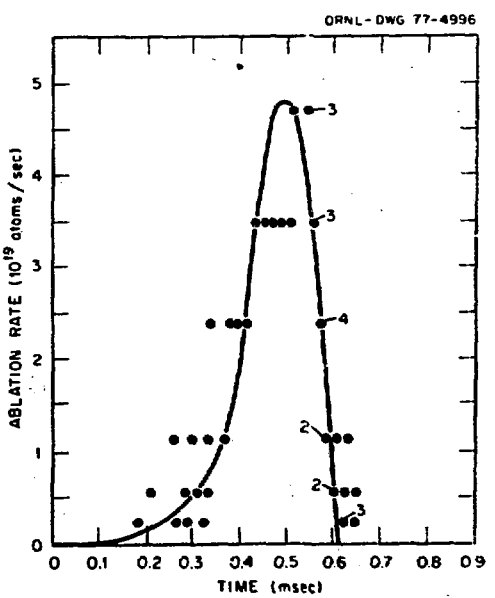

Fig. 3. Composite of ablation rate of 70 μm pellet inferred from H_α data. Solid line represents neutral gas shielding model calculation.

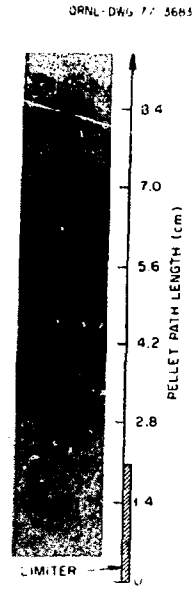

Fig. 4. High speed framing camera photographs depicting evolution of luminous cloud of a single 210 μm pellet. Time between frames is 150 μsec.

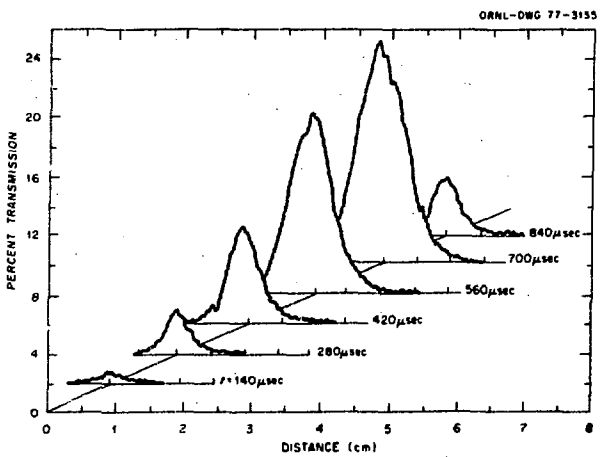

Fig. 5. Densitometer scans of images in Figure 4 — dimensions are full scale.

Comparison with Theory

Several theories have been proposed to describe the behavior of hydrogen pellets in a plasma including those of Spitzer et al.,[8] Rose,[9] Gralnick,[10] Chang,[11] Vaslow,[12] and Parks et al.[6] For convenience they may be grouped into two broadly defined categories; those which rely in effect on the presence of a cold plasma surrounding pellet to partially shield the surface from the plasma heat flux (Group I) and those which postulate that expelled neutral matter serves to limit the rate of heat transport from the external plasma to the pellet surface (Group II). We take a representative model from each of these groups for the purpose of comparison with experiment.

Typically, the problem of the ablation of a pellet is formulated in terms of a simple energy balance applied at the receding pellet surface. We write the resulting rate equation in the following generalized form

$$G = 4\pi n_s r_p^2 \frac{dr_p}{dt} = \frac{n_e \bar{c}_e}{4} \cdot A \cdot \frac{2kT_e}{\lambda} f \qquad (1)$$

where r_p is the pellet radius. G is the ablation rate, λ is the effective energy needed for removal of a single atom (or ion) of fuel from the surface, n_s is the solid atomic number density, n_e is the plasma electron density, T_e is the plasma electron temperature, c_e is the plasma electron thermal speed, and A is the effective area for interception of plasma electrons by the pellet (usually $4\pi r_p^2$). The parameter f(≤1) is a shielding factor, which by definition is the effective normalized plasma energy as seen by the shielded pellet.

In the form which we have written Eq. (1), the factor f may account for shielding by any or all of the following processes: slowing down of plasma electrons by elastic scattering with neutrals, electron flux attenuation by elastic scattering and/or negative charging of the pellet surface, or through large beta effects which may diminish the effective exposed pellet cross section by excluding the magnetic field from the volume surrounding the pellet. Depending on the physical model being considered, f may be a function of the pellet size, the plasma parameters, and perhaps the magnetic field. In general, another equation or set of equations is required to describe f. In the model of Gralnick,[10] which is the cold plasma shielding type (Group I) $f \approx 1/2$ for reactor grade plasmas. In the neutral molecule ablation model of Parks et al.,[6] (Group II) it is a function of plasma temperature and density and pellet size, with greater shielding occurring for larger pellets and the more dense plasmas ($f \sim n_e^{-2/3} r_p^{-2/3} T_e^{0.21}$). Another factor which may differ in the various theories is the parameter λ, which is typically either 32.6 eV for removal of an ion pair (Group I) or 0.005 eV for sublimation of a neutral atom (Group II). When comparing theories, the ratio f/λ is the relevant parameter to be considered.

Agreement of the theory of Parks et al., as is demonstrated in Figs. 2 and 3, is excellent. The theory accurately reproduces the overall shape of the ablation curves and the observed pellet lifetimes for both the 70 μm and the 210 μm series. Similar agreement with still another Group II theory (Vaslow[12]) has recently been demonstrated for the 70 μm series. This result is not surprising in view of the strong experimental evidence favoring the presence of the neutral shielding cloud.

The degree of this shielding by neutrals is demonstrated in Fig. 6 where we have plotted calculated values of the normalized effective plasma energy f as function of time for the 210 μm case.[7] The theoretical variation of the pellet radius is also depicted. During the period of time in which significant ablation occurs ($r_p^2 dr_p/dt$, large) f assumes values in the 20-30% range. High values of f occur at early times primarily because the pellet is surrounded by a weak plasma which cannot sustain a high density ablation cloud. High values of f (less shielding) are present at later times because as the pellet size diminishes, the dilution of its shielding cloud in space is more pronounced (the cloud becomes "optically" thin).

The parameter λ/f is evidently the amount of energy that the plasma must supply in order to remove a single fuel atom from the pellet surface. Taking 0.25 as a representative or average value for f, we find λ/f = 0.02 eV (for λ = 0.005 eV). For the Group I theories this parameter is typically in the tens of electron volts range ($f \approx 0.5$-1, $\lambda \approx 33$ eV) which gives pellet lifetimes far greater than those measured experimentally. The inadequacy of these theories is evident for the warm, tenuous plasma investigated here, but their

validity may yet be demonstrated in the hot, dense plasmas of future tokamak confinement devices.

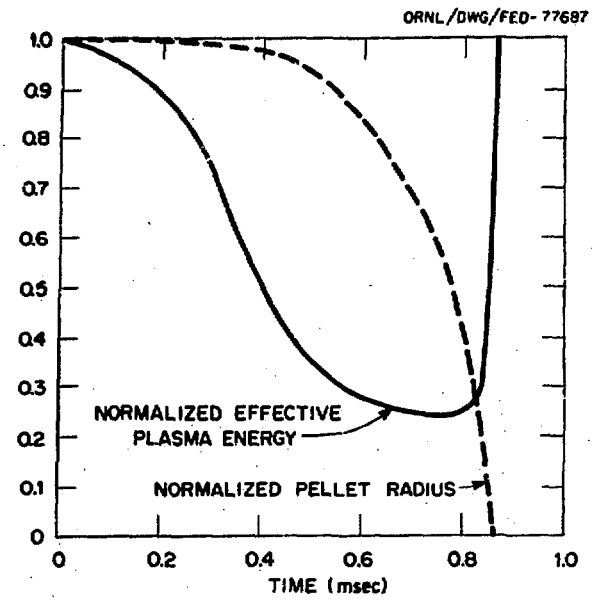

Fig. 6 Calculated values of the normalized pellet radius and normalized effective plasma energy f as a function of time for 210 μm pellet.

Applications to Fueling and Future Tokamak Experiments

Given the initial success of the neutral molecule ablation models in reproducing the experimental results, it is logical to use these models in designing pellet fueling devices and planning future pellet fueling experiments. In investigating pellet injector requirements for various tokamaks, we have[7] derived an expression for the velocity needed to penetrate to a radial position ℓ in a plasma characterized by density and temperature profiles varying as $n_e \sim 1 - (r/a)^2$ and $T_e \sim n_e^2$. The velocity U is given in terms of average plasma parameters, the machine minor radius a, the fuel molecular weight M, the pellet radius r_p and a function $G(\langle T_e \rangle; \ell/a)$ as

$$U = 4.57 \times 10^{-17} \frac{a \langle n_e \rangle^{1/3} \langle T_e \rangle^{1/6}}{M^{1/3} r_p^{5/3}} G(\langle T_e \rangle; \ell/a). \quad (2)$$

The function G is shown in Fig. 7 for several values of the penetration parameter ℓ/a. For the higher temperature plasmas ($\langle T_e \rangle > 1$ keV) and penetration beyond the midpoint ($1 - \ell/a > 0.5$), G has a simple power law dependence on ℓ/a and $\langle T_e \rangle$. Under these restrictions, the expression for U reduces to

$$U = 1.87 \times 10^{-13} \frac{a \langle n_e \rangle^{1/3} \langle T_e \rangle^{1.7}}{M^{1/3} r_p^{5/3}} (1 - \ell/a)^3, \text{ m/sec} \quad (3)$$

for T_e in eV, n_e in m^{-3}, r_p, ℓ, a in meters.

Application of this result to conditions typical of the proposed ignition device (TNS)[13] (a = 62 cm, r_p = 3 mm, $\langle T_e \rangle$ = 10 keV, $\langle n_e \rangle = 2 \times 10^{20}$ m^{-3}, M = 5) yields velocities of the order of 10,000 m/sec for penetration two-thirds of the way to the plasma center. Although deep penetration might eventually prove desirable, it is premature to consider such penetration as a necessary requirement. This is especially true in view of recent studies which indicate that shallow fueling (U $\gtrsim$ 1000 m/sec) may be adequate if not superior (W. A. Houlberg et al., this volume).

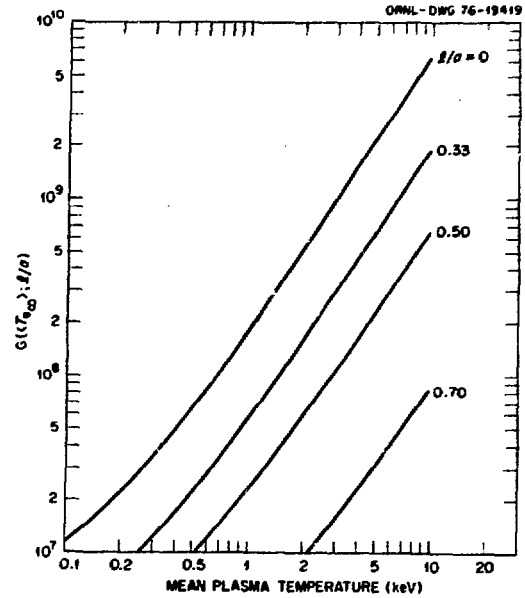

Fig. 7 Dependence of the function G of Eq. (2) on mean plasma temperature and fractional distance from the plasma center.

The principal result of Eq. (3) is that large pellets will penetrate further than small ones, and that increasing pellet size has a more pronounced effect than increasing the velocity. Future efforts at ORNL will be directed toward increasing both of these parameters in an attempt to achieve a more dramatic effect. Advanced pellet injectors are being built to inject pellets of the order of 1 mm diam at speeds approaching 1000 m/sec (C. A. Foster and S. L. Milora, this volume) into the ISX-B plasma. The anticipated results of such an experiment are shown in Fig. 8 where we have plotted theoretical fuel deposition profiles as a function of plasma radius for 0.9 mm diam pellets with speeds of 500 and 1000 m/sec. A pellet of this size would increase the plasma density by $\gtrsim$40% (compared to the $\sim$1% increase realized previously). At speeds of 1000 m/sec indications are that half the fuel would be deposited beyond the plasma midpoint, and that the pellet would penetrate to within 5 cm of the center of the plasma. As indicated by Eq. (2), decreasing the velocity by a factor of two will not substantially alter these results.

At these high velocities, the anticipated pellet lifetimes will be of the order of a few hundred microseconds. In this short time, rather large density modifications would take place. When viewed as a diagnostic tool, future pellet experiments should provide valuable information regarding plasma stability and transport as well as improved empirical pellet ablation scaling laws.

Acknowledgments

The authors would like to acknowledge the work of the many individuals who participated in this experiment. In particular, the efforts of R. J. Colchin, C. D. Hendricks, K. Kim, and R. J. Turnbull were instrumental in developing the pellet apparatus and performing the experiments. The assistance provided by the ORMAK operating crew, especially P. H. Edmonds, A. C. England, P. W. King, D. H. McNeill, M. Murakami, W. Namkung, and J. B. Wilgen is also gratefully acknowledged.

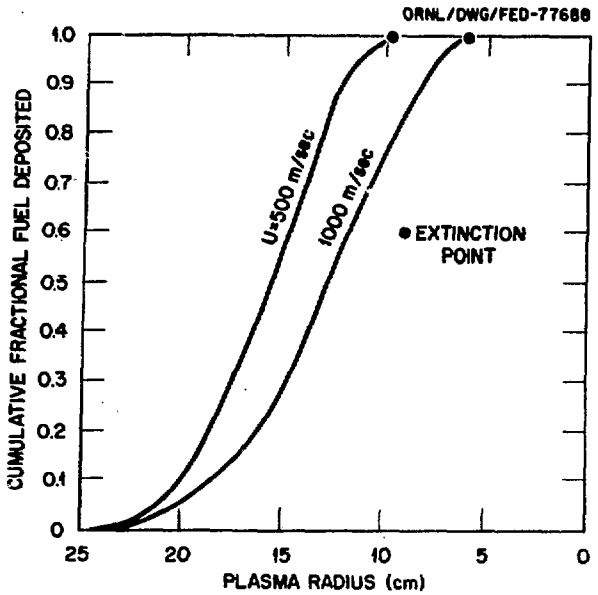

Fig. 8 Calculated values of cumulative fuel deposition as a function of plasma radius for perpendicular injection of a 0.9 mm diam pellet in a hypothetical ISX-B plasma (T_{ec} = 1 keV, n_{ec} = 7 x $10^{19} m^{-3}$).

References

1. C. A. Foster, R. J. Colchin, C. D. Hendricks, and R. J. Turnbull, Bull. Am. Phys. Soc. 20, 1300 (1975).
2. K. Kim, R. J. Colchin, C. A. Foster, S. L. Milora, and R. J. Turnbull, Bull. Am. Phys. Soc. 21, 1052 (1976).
3. C. A. Foster, R. J. Colchin, S. L. Milora, K. Kim, and R. J. Turnbull, Nucl. Fusion 17, 1067 (1977).
4. C. A. Foster, Ph.D. thesis, Department of Physics, University of Illinois, Urbana, Illinois (1977).
5. C. A. Foster, K. Kim, R. J. Turnbull, and C. D. Hendricks, Rev. Sci. Instrum. 48 625 (1977).
6. P. B. Parks, R. J. Turnbull, and C. A. Foster, Nucl. Fusion 17, 539 (1977).
7. S. L. Milora and C. A. Foster, "ORNL Neutral Gas Shielding Model for Pellet-Plasma Interactions," ORNL/TM-5776, Oak Ridge National Laboratory, Oak Ridge, Tennessee (1977).
8. L. Spitzer, D. J. Grove, W. E. Johnson, L. J. Tonks, W. F. Westendorp, USAEC Report NYO 6047 (1954).
9. D. J. Rose, Culham Laboratory Technology Division, Memorandum No. 82 (1968).
10. S. L. Gralnick, Nucl. Fusion 13, 703 (1973).
11. C. T. Chang, Nucl. Fusion 15, 595 (1975).
12. D. F. Vaslow, IEEE Trans. on Plasma Science, Vol. PS-5, 12 (1977).
13. J. F. Clarke and D. G. McAlees, "High Beta Predemonstration Fusion Devices," ORNL/TM-5692, Oak Ridge National Laboratory, Oak Ridge, Tennesee (1976).

PELLET ABLATION STUDIES AT GARCHING

W. Amenda, K. Büchl, R. Lang, L.L. Lengyel, and W. Riedmüller
Max-Planck-Institut für Plasmaphysik, D-8046 Garching

Results pertaining to ablation rate analysis, cryogenic pellet source development, and ablation rate measurements are presented.

Magnetic Diffusion Model

The analytical model used for ablation rate estimates has been described in detail elsewhere [1]. It was assumed that the pellet is initially in direct contact with the surrounding plasma and thus the ablated particles are ionized within a time $\Delta t_i = \Delta t_i (n_{eo}, T_{eo})$, where subscript "o" denotes surrounding plasma parameters. Considering collisional ionization, this time is much shorter than the ablation time in all cases of practical interest. As time goes on, the ablated particles form a blanket around the pellet, whose temperature is different from the unperturbed plasma temperature: $T_1 < T_o$. The ionization front moves some distance away from the pellet surface ($r_1 > r_p$). Some of the electrons in the blanket recombine, and, since the characteristic recombination times are also much shorter than the ablation times (owing to the high densities), the electron density in the blanket n_{e1} may be approximated to a fairly good degree of accuracy by the equilibrium density value corresponding to the temperature T_1. The particles ablated leave the pellet with a velocity v_{vap} and are ionized after a time $\Delta t_i = \Delta t_i (n_{e1}, T_1)$, where subscript "1" denotes parameter values in the blanket around the pellet. The ionization front while moving outward displaces the magnetic flux lines. If field diffusion could be neglected, only the magnetic flux lines originally imbedded in the pellet would remain imbedded in the blanket. However, the penetration depth of the magnetic field lines is comparable in some cases to the blanket radius. The magnetic field diffusion has thus been taken into account. A quasi-steady approximation has been used throughout the present analysis.

It is assumed that the electrons heating the pellet gyrate along the magnetic flux lines. Energy is thus transported only along those flux lines which either pierce the blanket or are at a distance from it not larger than the electron gyro-radius.

The energy carried by the gyrating ions is accounted for simply by doubling the corresponding electron flux term.

The phenomena associated with the finite penetration depth of the incident plasma particles in the blanket as well as electrostatic shielding are not considered in this analysis. The energy is transferred to the ablated particles at the blanket-plasma interface ($\phi_o = 1/4\, n_{eo} v_{eo}\, (2\, kT_o)$). The energy flux incident on the pellet surface ϕ_1 causes only vaporization. It is assumed that the radial velocity component of the vaporized particles v_{vap} does not change appreciably over the ionization length Δr ($\Delta r = r_1 - r_p$). The motion remains spherically symmetric up to the blanket radius r_1, and the charged particles then lose their radial momentum and leave the blanket region along the magnetic flux lines. The sonic flow constraint has not been used in the calculations reported here ($v_i \neq v_s$).

The results displayed in column "a" of Table 1 were computed in Ref. 1 by means of the ionization rate coefficients of Bates et al. [2]. The vapor velocity v_{vap} was assumed to be equal to the sonic velocity at the pellet temperature (≙ 262 m/s).

	a			b			c		
ϕ_o(W/m^2)	2×10^7	10^9	10^{11}	2×10^7	10^9	10^{11}	2.10^7	10^9	10^{11}
r_p(mm)	0.33	0.60	0.59	0.30	0.60	0.60	0.31	0.60	0.60
r_1(cm)	4.28	3.68	1.75	3.87	4.50	2.36	5.42	5.35	2.88
$n_1(10^{14}$cm$^{-3})$	0.48	9.70	17.0	0.46	11.3	47.8	0.31	9.60	90.0
T_1(eV)	2.50	1.38	1.35	2.61	1.64	1.52	3.90	2.03	1.67
τ_{abl}(μs)	433	93	56	3.86	63	18	321	54	8

Table 1 Blanket parameters and ablation times as functions of the incident energy flux ϕ_o and pellet radius r_p.

It is of interest to check the effect of the assumed vapor velocity and ionization rate values on the blanket parameters and ablation rates. For this purpose, in a group of calculations the ionization rates proposed by Kolb and McWhirter [3] have been used. The respective results are shown in point "b" ob Table 1 (v_{vap} = 262 m/s). Finally, the results displayed in column "c" correspond to a case where the energy imparted to the ablated particles at the pellet surface is of the order of the vaporization energy, i.e. v_{vap} = 1500 m/s. The ionization rates of Ref. 3 have been used in these calculations. As can be seen, at low energy flux values the blanket parameters and ablation times are not significantly affected by the particular approximation used. At higher flux values the ablation times corresponding to the different approximations may differ by almost an order of magnitude. Computations have been performed also for $\phi_o = 10^{13}$ W/m^2.

The results corresponding to the different approximations display a common characteristic: as the flux intensity ϕ_o increases, the blanket radius r_1 corresponding to a given pellet radius decreases, but, at the same time, the blanket density n_1 increases, and the blanket temperature T_1 remains practically constant (of the order of 1 eV), over 5 orders of magnitude of ϕ_o-variation. Hence the ablation process seems to be self-regulating: the constant (flux-independent) blanket temperature provides an effective shielding also at high flux intensities. The analysis performed has further shown that the magnetic Reynolds number based on the blanket parameters plays an important role in the ablation process: it determines whether the blanket remains diamagnetic or becomes magnetized, and thus affects the magnitude of the energy influx.

Cryogenic Pellet Sources

The experimental pellet development work at Garching was originally aimed at the fabrication of Deuterium pellets used as targets for filling magnetic traps with laser-produced plasmas. The following 3 major requirements had thus to be fulfilled:

- In order to exclude the possibility of impurities in laser-produced plasmas no other materials than deuterium could be contained in the pellet. For applying the pellets in the Stellarator Wendelstein IIb a pellet size of about 0.5 mm was required.
- For avoiding disturbances of the plasma confinement in the magnetic field freely falling pellets had to be used. In the given case a minimum distance of 0.3 m between the pellet source and the laser

focus was required.
- For getting the free falling pellets to the focus, the pellet trajectory had to be controlled with a high degree of accuracy.

Two different types of pellet sources are presently under development or in operation.

Following the proposal of Hendricks [4], a cryogenic apparatus had been developed for producing a fine liquid hydrogen jet. The jet is broken up into discrete droplets of well-defined size by applying a perturbation of a given frequency. Droplets so produced are shown in Fig. 1. Here the jet diameter is 0.3 mm, the velocity 10 m/sec, and the frequency 3000 cycles. The pressure surrounding the droplets is maintained slightly below the triple point of hydrogen in order to partially freeze the droplets. This pellet source is still under development. Presently a differential pumping system is being built for introducing the partially frozen droplets into a high vacuum system. A charging system may be necessary for selecting and guiding the individual pellets.

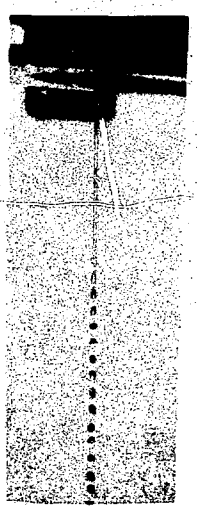

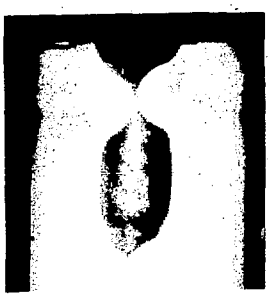

Fig. 2
Solid deuterium pellet

Fig. 1 Liquid deuterium droplets

Our extrusion type pellet source has been successfully used for laser-produced plasmas in a Stellarator [5] as well as for pellet plasma interaction studies in a Tokamak [6]. In this case the pellets are produced in high vacuum by cutting off pieces from an extruded deuterium ice stick. Deuterium is condensed in a chamber with a movable piston and pressurized with a constant pressure of about 400 atm. If the temperature is increased to a value above ∿ 8 K, the ice is forced through a nozzle (0.4 mm diameter) in the bottom of the chamber, to form a round stick of transparent deuterium ice. The extrusion velocity is controlled by the temperature and the pressure on the ice. The extrusion length is controlled by a photodiode which determines the size of the pellet. As is shown in Fig. 3, the lower end of the ice stick is cut symmetrically with respect to the axis of the stick by means of electrically heated wires. On the basis of high speed camera studies, we have minimized the uncontrolled mechanical motions of the pellet during the cutting procedure, in order to minimize the divergence of the trajectory of the falling pellet. The center of gravity of the pellet must be exactly below the point of suspension, possible oscillations of the pellet are damped if a sufficiently high ice temperature is choosen.

This pellet source is able to deliver freely falling pellets of variable size at a rate of ∿ 1 pellet per minute. The pellets so produced are characterized by a rather low spatial scattering. In Fig. 3 the measured probability is given with which a pellet passes through a horizontal circle, 200 mm below the pellet source, as a function of the diameter of this circle.

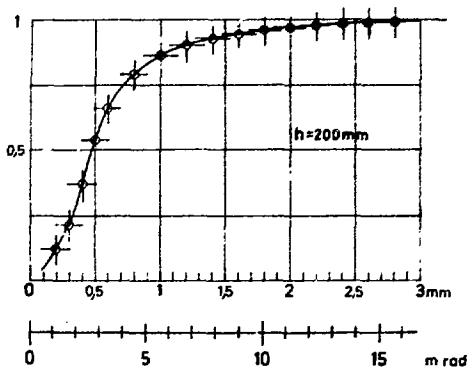

Fig. 3 Spatial dispersion of D_2 pellets

Pellet Experiment in the Tokamak Pulsator

In the pellet experiment for the Garching Pulsator we were interested in two topics: increasing the plasma density and influencing the discharge by means of the injected pellets.

To achieve an observable increase of density, relatively large pellets had to be used. We produced cylindrically shaped deuterium pellets with a diameter of 350 µm and a variable length of 600 µm to 8 mm. The shortest pellets contain 3.5×10^{18} atoms. This is about the total number of protons in Pulsator. These pellets are produced by cutting off small pieces from a stick of solid deuterium (see previous section). They were accelerated only by gravity and arrived at the axis of the discharge torus with a velocity of 6 m/s. Because of this slow speed the pellet would ablate completely in the outer zones of the plasma. The pulsator discharge was therefore ignited, when triggered by the falling pellet on reaching the torus axis. Ablation thus occured in a plasma with temporally rising temprature and density. A fast value also had to be triggered by the pellet because the cryostat runs at 10^{-7} mbars, but the basic pressure in the torus was a few times 10^{-4} mbar of hydrogen. The arrival time of the pellet at the top of the torus was measured with a light barrier. The expansion of the ablation cloud was visualized by a streak camera. Further diagnostics of the ablation was done by recording the enhanced H_α emission of the plasma. Moreover, the usual pulsator diagnostics was used.

The streak picture was taken in the light of H_β. It indicates a rapid expansion of the ablation cloud, with a velocity of 2.5×10^4 m/s. The ablation lasts for about 0.5 ms.

The H_α emission was measured with two photomultipliers directed horizontally and vertically to the axis of the torus. Without pellet injection during the first two milliseconds negligible H_α emission was observed. With pellet injection strongly enhanced H_α emission can be seen. These measurements yield an ablation time of 0.45 ms for pellets 0.35 mm in diameter and 0.8 mm in length. The ablation time varies only slowly with pellet length.

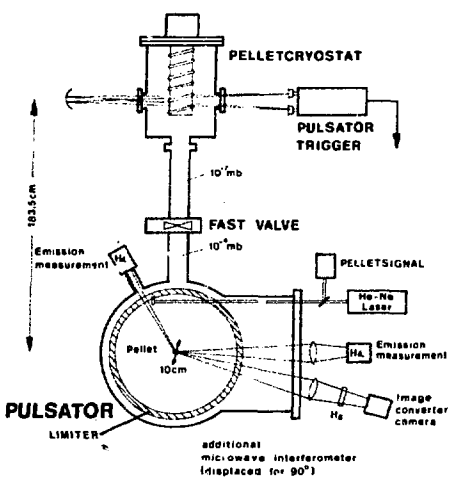

Fig. 4 Pellet experiment in Pulsator

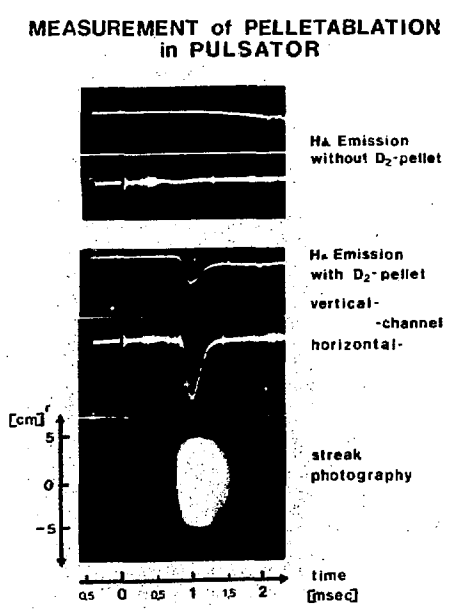

Fig. 5 H_α emission measurements and streak photography of the pellet

From these measurements a mean ablation rate of $8 \times 10^{23}/cm^2$ s is calculated. The pellet interacts with a plasma with an electron density of about 10^{13} cm^{-3} and an estimated temperature of less than 10 eV.

The electron density of the Pulsator beam was measured by microwave interferometry, not in the injection plane but in a torus plane which was rotated by 90° from the injection plane. Without pellet the density increases up to 3×10^{13} cm^{-3} within a time of 0.5 ms. With pellet injection the electron density rise starts with a small delay and becomes slower during the time when ablation is observed by means of H_α emission. After ablation the electron density overshoots the density of a standard low-density Pulsator discharge. The overshoot is not as high as expected for the size of the injected pellets. The density rises for about five milliseconds. Instead an expected factor 2 of density increase, we got values between 1.4 and 1.8.

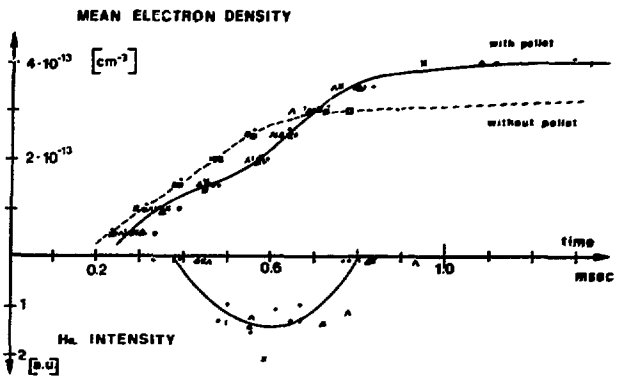

Fig. 6 Evolution of mean electron density in Pulsator (m.w. interferometry)

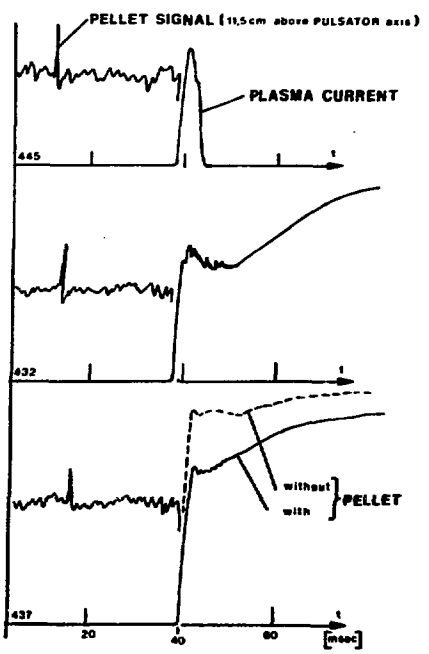

Fig. 7 Toroidal current in Pulsator

Compared with the ORMAK pellet experiment, we were using relative large pellets of the order of 100 % of the Pulsator filling. This certainly affects the discharge properties of Pulsator. This can be demonstrated by the toroidal current in the plasma. In a discharge without pellet injection the current looks nearly like a step function. With pellet injection we see different influences on the current, depending on the size of the pellet and presumably the exact location of the pellet in the torus at ignition. Disruption is already produced after 7 ms if the pellet size essentially exceeds 100 % of the plasma mass in Pulsator. Some-

times with pellets of about 100 % the current disrupts completely, but very often we observe a reduced current in the first ten to twenty milliseconds compared with a normal Pulsator discharge. Disruption seems to start, but after a while the distortion vanishes and the current grows. From this we estimate a limitation of pellet size for non-disruption in the ignition phase of the discharge of the order of 100 % tokamak plasma mass. To get an exact limit further experiments should be performed.

The results of these experiments may be summarized as follows:

1. The ablation time for D_2 pellets 350 μm in diameter and 800 μm in length is measured to be 450 μs.
2. The ablation rate is measured to be $8 \times 10^{23}/cm^2$ s for a plasma density of a few times 10^{13} cm^{-3} and an estimated temperature of less than 10 eV.
3. The observed mean electron density is increased by a factor of 1.4 to 1.8 instead of the expected factor of 2.
4. The discharge already disrupts during the built-up phase if the pellet mass exceeds the plasma mass in Pulsator

References

1 L.L. Lengyel, paper submitted for publication (see also IPP Report No. 4/160, April 1977)

2 D.R. Bates, A.E. Kingston, and R.W. McWhirter, Proc. Roy. Soc. A267, 297 (1962)

3 Kolb and R.W. McWhirter, Phys. Fluids 7, 519 (1964)

4 J.M. Schneider and C.D. Hendricks, Rev. Sci.Instr. 35, 1349 (1964)

5 H. Baumhacker, H. Brinkschulte, R.S. Lang, W. Riedmüller, and M. Salvat, Appl. Phys. Letters 30, 9, 461 (1977); see also Proc. 8th Europ. Conf. on Fusion, p. 133 (1977)

6 K. Büchl, R. Lang et al., Verh. Deutsch. Phys. Ges.,Frühjahrstagung Essen, 3, 663 (1977)

PELLET REFUELING PROGRAM AT RISØ

V. Andersen, C.T. Chang, L.W. Jørgensen, P. Nielsen, A.H. Sillesen
Association Euratom-Risø National Laboratory

The pellet refueling work at Risø has up to now been concentrated at studying the ablation rate of hydrogen pellets in hydrogen and deuterium plasmas in the Puffatron device. The main results of these studies are well known[1] and we shall only give a brief summary including some more recent results relating to the ablation process[2]. The work on the Puffatron device has been completed and we are presently preparing to start ablation studies in a small Tokamak, Dante. This tokamak has only been constructed this summer and ablation studies are expected to begin in the beginning of 1978. We shall give the expected parameters of the tokamak plasma and indicate some of the planned work. In this presentation we shall also report on the theoretical work on refueling taking place at Risø. We have particularly been interested in the effect of α-particles which could significantly alter the conclusions made from present experiments.

The Puffatron Experiment

The Puffatron is an EXB discharge apparatus. A schematic set-up of the experiment with pellet launcher is shown in Fig. 1. The plasma is created in the midplane in an axial homogeneous magnetic field of 1.5 Tesla. An electric field is applied between the inner electrode and the outer vacuum-wall. The electric field is varied, with a maximum value of 3×10^5 V/m, corresponding to an E/B velocity of up to 2×10^5 m/sec. Before the discharge is initiated a puff of gas is allowed locally into a central area of the device, the gas is extending 10-20 cm axially at the time of breakdown. For a short period of time, 4-5 μsec, the apparatus produces of plasma of density $1\text{-}4 \times 10^{14}$ cm^{-3}. The ions of this plasma are non thermalized, i.e. the ions are moving essentially in cycloid orbits, with half of the energy as drift energy and half as Larmor energy. From the velocity of the axial expansion of the plasma we judge the electrons to be thermal with a temperature of 20 eV. This means that ablation is only due to the ions. Discharges are made in either hydrogen or helium.

Hydrogen pellets are launched at 10 m/sec into this plasma. The pellets are cylindrical 0.25 mm diameter and .25 mm long. The velocity of the pellets are measured and used to trigger the time of the discharge. During the ablation time the pellet can be considered as stationary. The unablated part of the pellet continues after the discharge with a slight deviation from the original trajectory. The amount of ablated material is determined by collecting the remaining part of the pellet. The conclusion of this experiment is that an energy of .1-.2 eV is spent by the incoming ion flux per ablated hydrogen atom.

Visual observations of the pellet show light from a gas cloud around the pellet, the cloud being much larger than the pellet. By observing the H_β light at different distances from the pellet we conclude that the light is due to the excitation of pellet material that can be seen up to 2 cm away from the pellet. Fig. 2 shows a 1 μsec exposure picture of this phenomenon. The tail is in the direction of the plasma rotation.

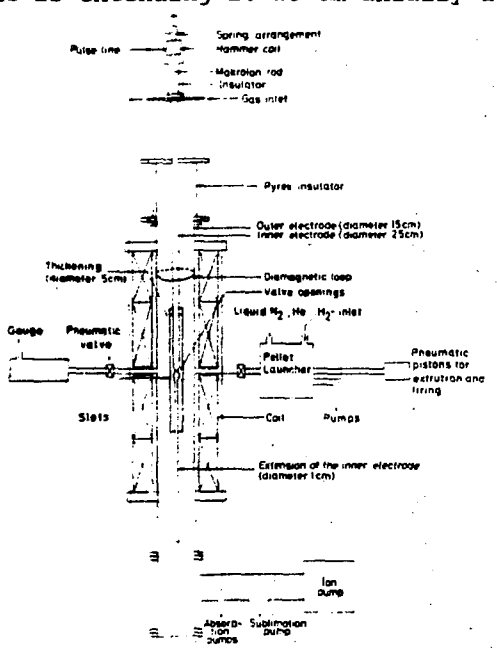

Fig. 1. Schematic diagram of the experimental set-up. The pellet launcher is in line with a collecting volume that can be closed with a valve. The pressure rise in the volume when a pellet evaporates is used as a measure of pellet size.

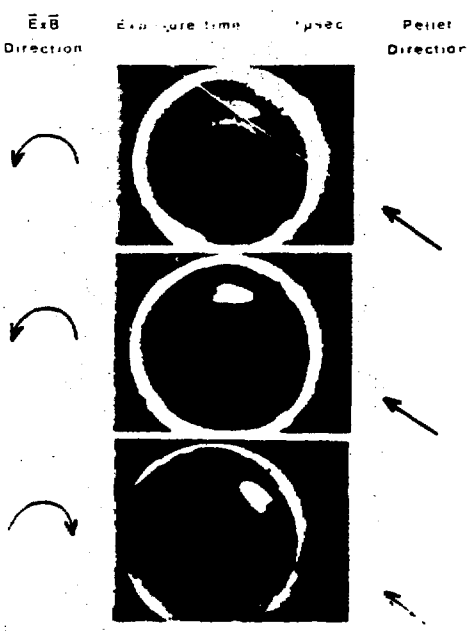

Fig. 2. A 1 μsec exposure picture of the ablated cloud around the pellet. The tail of the cloud is in the direction of plasma flow.

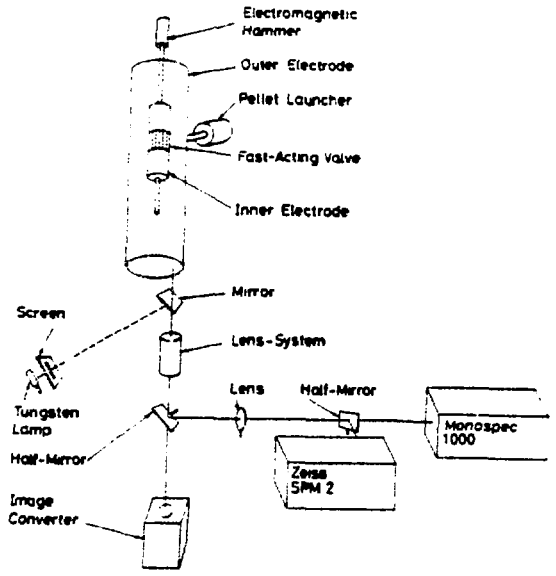

Fig. 3. Experimental set-up used to measure the velocity of expansion of the neutral cloud around the pellet.

Fig. 3 shows the experimental set-up used to make the spectral analysis of this light. The pellet position and the virtual image of the input slits at the pellet plane of the two monochromatics are recorded by an image converter camera. From this picture we know the distance from the pellet of the spatial zone analyzed. In each recording we then obtain the time history of the H_β light and some other spectral line. When injecting a hydrogen pellet in a helium plasma the other line may be anyone of the visible He-lines. In no case does the light of the He-lines show sign of the presence of a pellet. The recorded H_β light (Fig. 4) is consequently due to material evaporated from the pellet surface. By measuring the time delay of this signal as function of distance from the pellet, we find a velocity corresponding to 2 eV for hydrogen atoms.

The comet-like shape of the cloud is explained by these measurements. Pellet material is evaporated essentially isotropic. On the side facing the plasma flow the neutrals only propagate a short distance before being ionized (ionization time ≈ 1 μsec). The neutrals intercept the plasma flow of the rotating plasma, leaving a cold plasma in front of the pellet that does not rotate and a space behind the pellet without plasma. The lateral size of this region is of order the hot ion Larmor diameter. The experiment is not inconsistent with a gas shielding mechanism as proposed by other people[3,4].

Dante

The tokamak experiment Dante (Danish Tokamak Experiment) has been constructed specifically to do ablation studies. The main characteristics of the device are:

R	major radius	50 cm
a	minor radius	12 cm
ε	elongation	2
B_T	Toroidal field	.8 Tesla
I_p	plasma current	70 kA
φ	flux	.3 Vsec
T_e	expected temperature	200-500 eV

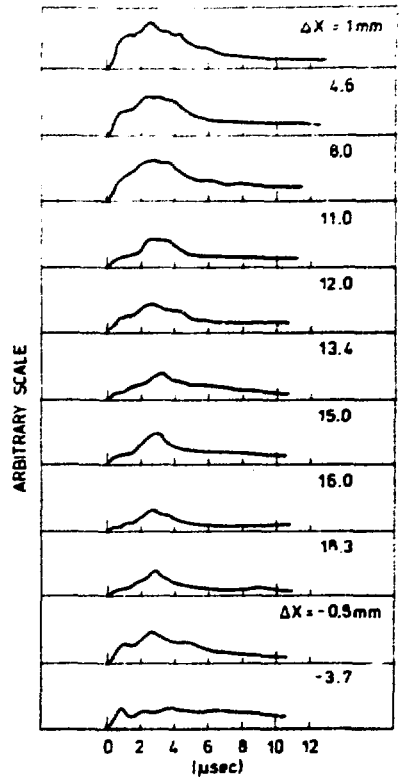

Fig. 4. The H_β-signal is displayed at different distances from the pellet center. Positive values of Δx indicates measurements in the tail of the cloud. Negative values of Δx correspond to position in front of the pellet with respect to the plasma flow. The time scale is adjusted for each trace by a time $\Delta t = \Delta x/v_c$, where $v_c = 1.82\times10^4$ m/sec, (v_c is the expansion velocity of the neutrals).

In other experiments injecting pellets into tokamak plasmas[5], the pellets only enter the outer parts of the plasma. The parameters of this plasma vary considerably over the pellet lifetime and the outer parts of tokamak plasmas are not very well diagnosed. We have therefore judged a plasma with moderate parameters to be adequate for refueling studies. We shall instead concentrate on knowing the parameters of the plasma in the interaction zone. The planned experiments include injection of pellets into plasmas of different temperature and densities in the conventional way, i.e. launching the pellet into the plasma at low velocity. An elongated plasma profile was chosen in order to obtain a higher peak temperature for a low field device. The elongation also causes a steeper temperature gradient, i.e. a shorter distance for the pellet to reach a certain temperature plasma.

In another type of experiment we shall attempt to obtain sufficient injection speed to make the pellets come to the center of the plasma. We shall directly measure the necessary speed for different size pellets at varying plasma parameters. Since we do not at present have a technique for accelerating pellets, we plan instead to move the plasma relative to a stationary pellet. The cross section of the vacuum chamber is rectangular, the height of the chamber being twice the width. In this configuration it should be

possible to locate a plasma of circular cross section which only occupies the bottom half of the vacuum chamber. We are then free to drop a pellet into the other half and the introduction of a radial field will then move the plasma relative to the pellet. We estimate by this method to be able to simulate injection speeds of 10^3-10^4 m/sec.

Theoretical Work on Refueling

On the theoretical side, some preliminary investigation on the effect of α-particles has been made. Taking the conservative point of view, assuming α-particles be able to diffuse outward from the core of the reactor, calculation based on the binary collision approximation shows that the pellet will be subjected to the bombardment of α-particles around 3 MeV regardless of its location in the reactor. A dense blanket soon will form around the pellet after the initial direct impact phase. For a reasonable combination of number density and temperature of the ablated plasma a blanket radius exceed 10 cm is required to further slow down the energy of the α-particles to the thermal range[6].

Works on α-particles will be continued by extending analysis to more realistic situations to be encountered in a reactor, and by considering the presence of possible anomalous effects.

Besides, a compilation of the currently existing ablation theories and an assessment concerning the various ways of accelerating the pellet are just initiated.

References

[1]L.W. Jørgensen, A.H. Sillesen and F. Øster, Plasma Physics 17, 453 (1975).

[2]L.W. Jørgensen, A.H. Sillesen and F. Øster, Plasma Physics, to be published.

[3]P. Parks, R.J. Turnbull and C.A. Foster, Nuclear Fusion 17, 539 (1977).

[4]D.F. Vaslow, IEEE Trans. on Plasma Science PS-5, 12 (1977).

[5]C.A. Foster, R.J. Colchin, S.L. Milora, K. Kim, and R.J. Turnbull, ORNL/TM5897 (1977).

[6]C.T. Chang, "Preliminary Considerations Regarding the Effect of α-particles on a Refueling Pellet" paper presented at the 8th European Conf. on Controlled Fusion and Plasma Physics, Prague, Czechoslovakia.

ORNL PELLET ACCELERATION PROGRAM*

C. A. Foster and S. L. Milora

Oak Ridge National Laboratory
Oak Ridge, Tennessee 37830

Summary

The Oak Ridge National Laboratory (ORNL) pellet fueling program is centered around developing equipment to accelerate large pellets of solidified hydrogen to high speeds. This equipment will be used to experimentally determine pellet-plasma interaction physics on contemporary tokamaks.

The pellet experiments performed on the Oak Ridge Tokamak (ORMAK) indicated that much larger, faster pellets would be advantageous. In order to produce and accelerate pellets of the order of 1-6 mm in diameter, two apparatuses have been designed and are being constructed. The first will make H_2 pellets by extruding a filament of hydrogen and mechanically chopping it into pellets. The pellets formed will be mechanically accelerated with a high speed arbor to a speed of 950 m/sec. This technique may be extended to speeds up to 5000 m/sec, which makes it a prime candidate for a reactor fueling device.

In the second technique, a hydrogen pellet will be formed, loaded into a miniature rifle, and accelerated by means of high pressure hydrogen gas. This technique should be capable of speeds of the order of 1000 m/sec. While this technique does not offer the high performance of the mechanical accelerator, its relative simplicity makes it attractive for near-term experiments.

Introduction

The ORNL Plasma Fueling Program is developing solid hydrogen pellet injection devices to be used in pellet-plasma interaction studies. The immediate objective is to develop equipment which can be applied to contemporary tokamak confinement devices in efforts to determine empirical pellet fueling criteria. The ultimate goal is the realization of a practical device that can be used to sustain ignited plasma conditions in a tokamak power reactor. An early survey of hydrogen pellet fabrication and acceleration techniques[1] resulted in the selection of two candidate fueling concepts for further study and development in our laboratory. One method will produce solid pellets by extruding and clipping a filament of solidified hydrogen into cylinders to be subsequently accelerated by a high speed rotating arm or disk. It is expected that development of this concept to its full potential will result in fueling devices capable of providing pellet velocities and feed rates that are sufficient to fuel the ignited plasmas of tokamak power reactors. The second concept being developed at our laboratory would utilize pressurized hydrogen gas to accelerate a frozen pellet confined in a tube. This technique is believed to be capable of providing velocities up to 1000 m/sec which would make it a useful device for performing pellet injection experiments in contemporary tokamaks (see S. L. Milora and C. A. Foster, this workshop). In this paper we discuss design aspects of both of these techniques.

Mechanical Pellet Accelerator

A pellet constrained to move in a channel on a rotating disk will be accelerated to and will exit from the disk at a speed given by $V_{pellet} = 2V_{tip}\cos(\theta/2)$, where θ is the angle of the channel exit with respect to the tangent of the disk and V_{tip} is the peripheral speed of the disk.

The accelerations are such that a pellet will reside on the disk for a fraction of a revolution of the disk, independent of both the pellet mass and rotational frequency of the disk. For example, if the pellets enter the channel at one-third the disk radius, the disk would revolve 94° in the time interval it takes the pellet to travel from the entrance point to the exit point. If all the pellets are injected onto the disk at the same angular position, they will exit at the same angle. We expect the pellet angular dispersion to be less than 6°.

The speed of the pellet is governed by the disk design and the material of construction:

$$V_{pellet} = \sqrt{\frac{\sigma\alpha}{\rho}}\cos(\theta/2),$$

where σ/ρ is the strength-to-weight ratio of the disk material, α is determined by the geometry of the disk, and θ is again the exit angle of the pellet.

The materials having the highest strength-to-weight ratios are fiber composites such as Kevlar/epoxy which have unidirectional strength characteristics. Since these materials have highly anisotropic strength characteristics, they are best suited for arbor designs which have constant stress arms, such as the two-arm design shown in Fig. 1. This shape produces a constant stress in the arbor and yields the ultimate α values which approach infinity for infinitesimally small tip sizes; the α value is 13 for the design shown. A two-armed, constant stress arbor of Kevlar could achieve a pellet velocity of 5000 m/sec, which makes a prime candidate for a reactor refueling device. However, since composite materials are rather difficult to work with, the two-arm composite design was not chosen for our initial device.

We have constructed a tapered disk made from high strength aluminum with a circular groove cut in the top face of the disk to guide pellets. This disk will give a design pellet speed of 940 m/sec. The pellet injection apparatus is shown in Fig. 2. The pellets will be formed by a hydrogen extrusion press. This device freezes a billet of solid hydrogen and then squeezes it through an orifice, continuously forming a filament of solid hydrogen the diameter of the orifice. This filament will be periodically clipped at a rate of 60 pellets per second by a rotating cutter disk with an integral knife edge. The pellet will be ejected from this low speed disk at a speed of 14 m/sec and injected onto the high speed rotating disk through a fast valve. An electronic circuit can hold the cutter disk in phase with the high speed disk to within 10° of rotation. The pellets will land at the inside edge of the high speed groove, which is undercut to trap and hold the pellet. The disks are operated at or near room temperature so that the hydrogen pellet will float on an ablated gas cushion yielding a low coefficient of fraction. However, the time the pellet spends on the warm surfaces

*Research sponsored by the Department of Energy under contract with Union Carbide Corporation.

will be short enough to prevent substantial evaporation of the total pellet mass.

The pellets spin off the disk tangentially at twice the disk peripheral speed. The peak acceleration forces occur near the periphery and are

$$A_{max} = \frac{4V_{tip}^2}{R} .$$

The inertial stresses arising from these accelerations may have to be kept below the yield strength of the frozen pellet. This implies that larger diameter devices will probably be required for the higher performance designs. Difficulties of this kind are not expected with the prototype device.

Design Aspects of High Speed Rotating Equipment

Since the tip speed of the disk is quite large, the stored angular momentum and energy in the disk are substantial. For this reason the disk is encased in a conservatively designed chamber to prevent injury in the event of failure. A 5-in.-thick steel torque ring penetration barrier surrounds the disk and the whole assembly is encased in a 1.5-in.-thick steel vacuum chamber. As more experience is gained with a given disk design or if composites are used much of this armor may be found to be unnecessary.

Pneumatic Pellet Accelerator

The pneumatic pellet guns[2] are designed to inject single pellets at moderate speeds into a tokamak. They offer the advantage of being simple to fabricate and are easily adapted to a tokamak. A single pellet will be formed and loaded into a gun barrel. A solenoid valve will apply a 200-psi drive gas at room temperature which will accelerate the pellets to speeds of ~500 m/sec. The pellet will then pass through a multiaperture baffle system, and a fast closing valve will trap the drive gas behind the pellet.

A simplified gas dynamic analysis of the performance of an ideal frictionless gun yields the following approximate result for the muzzle velocity, U, in terms of the acceleration or barrel length:

$$\frac{U}{\ell} = \frac{C_o}{\tau_c} \cdot \frac{1.66}{0.82\ U + 0.33\ C_o\ (U/C_o)^2} \qquad (1)$$

where C_o is the speed of sound of the propellant evaluated at the stagnation chamber conditions and τ_c is a characteristic time or figure of merit that accounts for the physical properties of both propellant and projectile and the gun operating conditions. It is defined in terms of the chamber pressure P_o, the propellant sound speed C_o, the mass of the projectile M, and its base area A as $\tau_c = MC_o/P_oA$.

Since short barrel lengths ℓ are desirable for high performance[3] (minimal friction effects), it is evident that low values of τ_c are needed. In view of the extremely low density of hydrogen ice (ρ = 0.07 gm/cc), this requirement can be met for the small pellets of interest to tokamak fueling ($r_p \approx 1$ mm) at very low chamber pressures ($P_o \approx 10$ atm). Such pressures would be compatible with the inherently low mechanical strength of hydrogen ice[4] and still provide high performance. For example, Eq. (1) indicates that a 1-mm cylindrical pellet could be accelerated to 800 m/sec with a chamber pressure of 10 atm using hydrogen propellant in a barrel only 3.5 cm long. The degrading effects of friction are not expected to be large since a low viscosity hydrodynamic film should form at the pellet-barrel interface.

It is expected that modest improvements in velocity could be realized with this technique by optimization of design but extrapolation to the performance limits of the light gas gun (>10,000 m/sec) is not considered to be practical at this time.[1]

Applications to Pellet Injection Experiments

Both of the devices discussed above will be tested in the laboratory before being applied in pellet injection experiments on the Impurity Study Experiment (ISX) tokamak at ORNL. With the anticipated speeds and pellet sizes (500-1000 m/sec, 0.9-mm diam pellets), a much greater fueling effect than previously observed should result. Our calculations indicate that these pellets will penetrate 15-20 cm into a 25-cm plasma and will increase the plasma density by 40% (S. L. Milora and C. A. Foster, this workshop). The information gained from these experiments will be incorporated in future pellet injector designs.

References

1. S. L. Milora, C. A. Foster, and G. D. Kerbel, Bull. Am. Phys. Soc. 21, 1052 (1976).
2. S. L. Milora and C. A. Foster, "The Gas Gun as a Device for Fueling Tokamaks," unpublished.
3. J. Lukasiewicz, AIAA Journal 5, 11 (1967).
4. Yu E. Stetsenko, D. N. Bol'shutkin, L. A. Indan, and A. A. Khudoteplaza, Sov. Phys.-Solid State 14, 1 (1972).

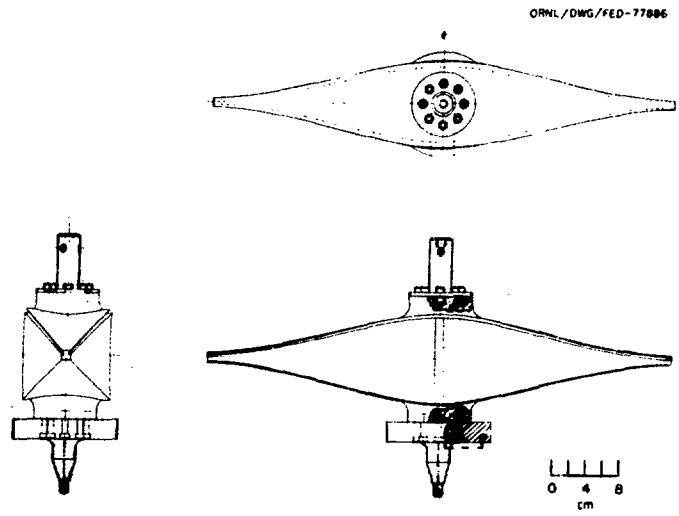

Fig. 1. Uniform Stress Arbor Design

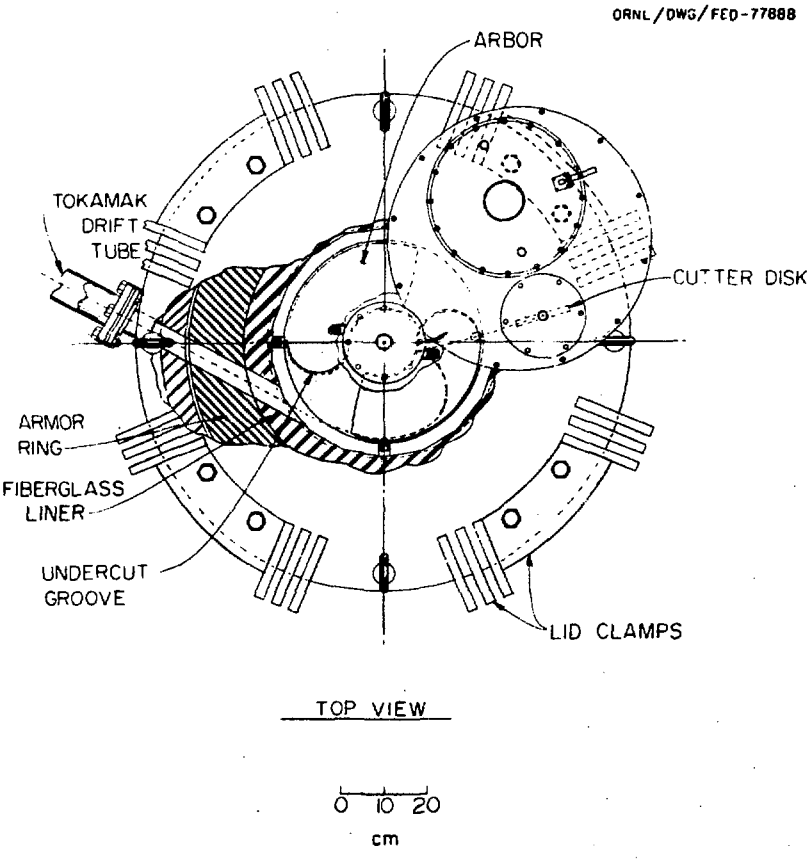

Fig. 2a. Mechanical Pellet Injection System

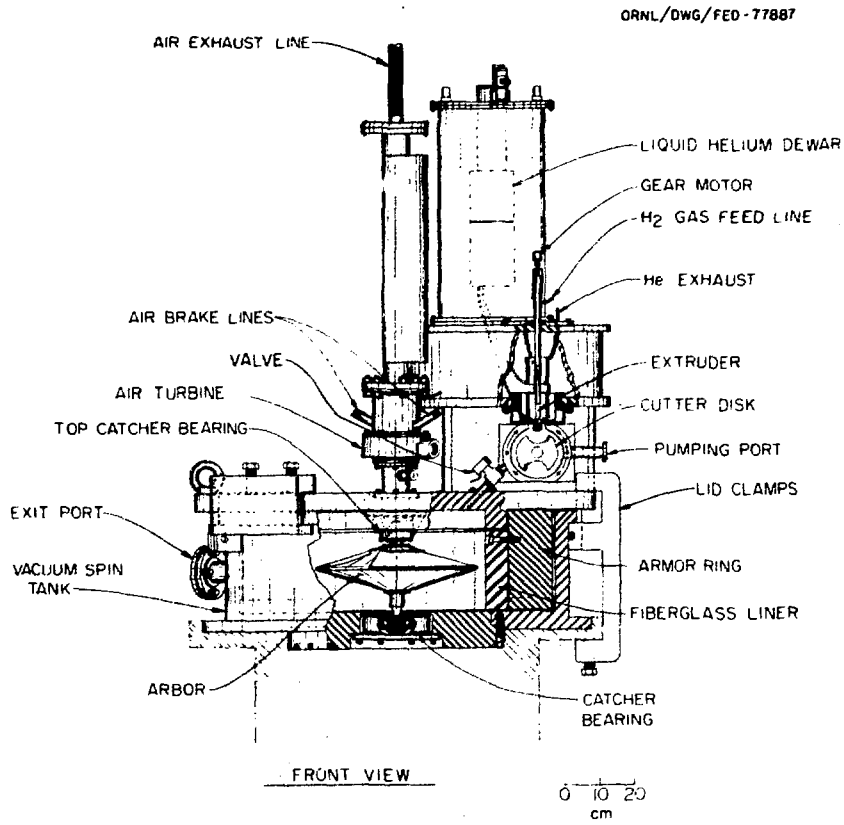

Fig. 2a. Mechanical Pellet Injection System

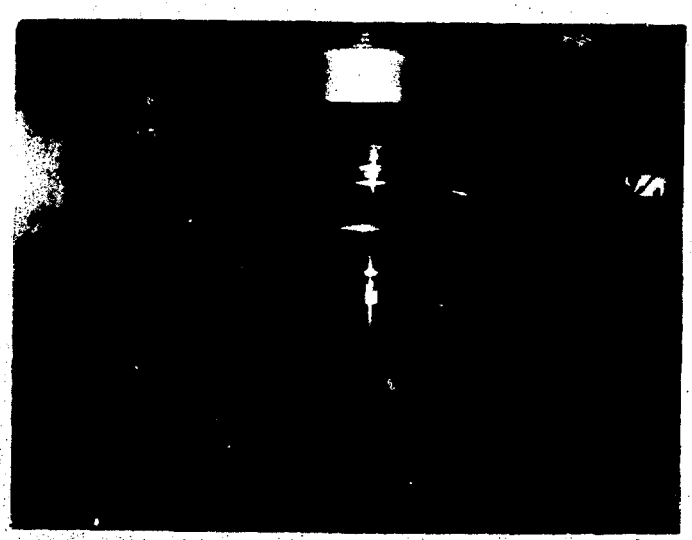

Fig. 2b. Pellet Accelerator Disk Arbor

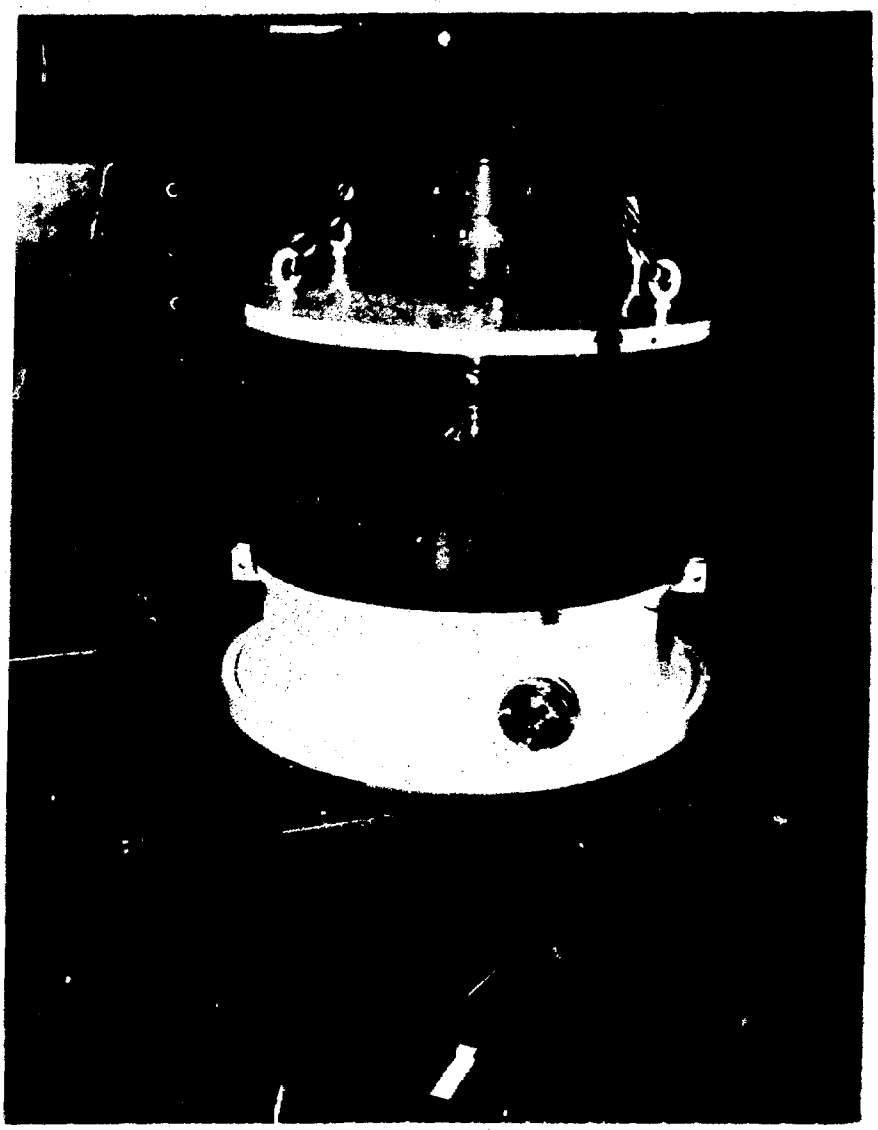

Fig. 2c. Pellet Accelerator Spin Tank

[illegible]

A review is made of current light gas gun and related hyper-velocity launcher technology with emphasis on physical and technological limits, advantages, and disadvantages as they apply to injection requirements for refueling Tokamak type nuclear fusion reactors.

It is shown that the mass and velocity requirements for refueling are well within the capabilities of the state of the art and can be produced by several of the different types of gun launching devices.

The practical problems of adapting this performance capability to the refueling task are addressed and some possible configurations are given including both single pellet and multiple pellet injection.

A short bibliography is given for those who wish additional detailed information.

Introduction and Justification

In a paper presented by Milora, Foster, and Kerbel[1] of the Oak Ridge National Laboratory at the 18th Annual Meeting of the Division of Plasma Physics of the American Physical Society, some estimates of the particle size and velocity requirements for several existing and planned fusion machines were presented. The authors, who are plasma physics specialists, noted that among the several candidates, they believed the light gas guns possessed the mass and velocity requirements necessary to be useful as a possible fuel injector and suggested that this proven technology not be overlooked in a search for a practical refueling system.

This paper, written from the viewpoint of a light gas gun specialist, expands on that point in order to permit a broader understanding of that technology and then addresses some of the practical problems of interfacing gun launcher technology with that of the fusion machine. It is shown that existing devices could be successfully applied to this task, and offers some possible configurations.

Tokamak Fueling Requirements

The operation of a Tokamak-type fusion machine requires that fuel be supplied to the interior region of the working plasma. Estimates of the particle density of the plasma range around 2×10^{14} cm^{-3}. Estimates of the minimum amount of fuel required are of the order of 4 g/MW-day and include an estimate of the amount of fuel that may be "lost" in the colder regions of the machines where it cannot react.[2]

For a reactor operating at a power level of 1000 MW (thermal), then the fueling requirement is $\dot{m} \sim 4$ kg/day or 0.05 g/sec. For a fuel density of [illegible], this implies the volume flow rate of [illegible]. These rates are minimum values for the fueling rates of current test fusion plants, hence there is little if any technology that can be carried over from existing technology and new approaches must be sought.

In addition, there is also an upper limit on the fuel flow rate. The incremental amount of fuel that may be added to maintain the reaction is of the order

$$\frac{\Delta m}{m} \sim 10^{-2} \text{ to } 10^{-1}$$

where m is the total mass of fuel within the machine. Greater amounts would quench the reaction.

If the 4 kg/day amount is injected as discrete amounts of, say, 10 to 100 separate injections per second, then the volume and mass of each injection element lies in the range of 0.005 to 0.05 cm^3 and 1×10^{-4} to 1×10^{-3} grams. For an effective total reacting volume of 100 m^3 (10^8 cm^3)* then the maximum incremental amount of mass that may be injected in each injection cycle without disrupting the reaction is

$$\Delta m \sim 3 \times 10^{-4} \text{ to } 3 \times 10^{-3} \text{ grams}$$

Hence, both mass and rate requirements are satisfied for conditions around 10 to 100 injections per second of 1.0 to 4 mg of fuel. Less number of injections per second would require greater mass injection which might quench the reaction. More injections per second, i.e., less mass per injection are permitted by the physics, but have other practical constraints, for example, survival of the pellet during the injection process.

Survival Constraints

Parks[3] and colleagues analyzed the problem of moving the particle from an injector out into the reaction zone. The particle densities are low enough that convective heating is negligible. Radiative heating, on the other hand, is very large and predominates. Parks has provided estimates of lifetimes for known pellet radii and plasma temperatures and densities where radiation is the transport mechanism. They are given in Figure 1, for an electron density of 4×10^{14}. The lifetimes taken in combination with an assumed reaction zone width gives directly a projectile velocity. Both 1 meter and 3 meter zones are included.

* Assumes a toroid of a cross section of one side of 1 meter^2 and a toroidal diameter of 10 meters.

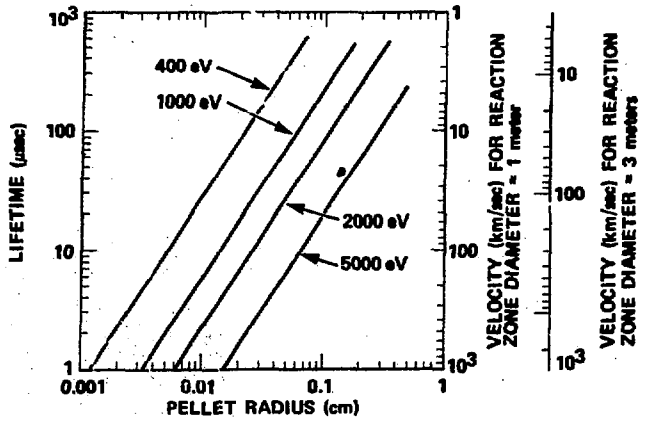

Fig. 1 Pellet lifetimes versus initial pellet radius for various plasma temperatures, Plasma electron density is $4 \times 10^{13}/cm^3$.

From the figure it is seen that the required velocities increase as pellet radii decrease and temperatures increase. For a pellet of 1 mm diameter, say, and a temperature of 1500 eV, 7000 mps are required for a 1-meter-diameter machine. A 3-meter-diameter machine would require almost 28,000 mps, a value beyond existing capability.

Milora, et. al.,[1] have also looked at the pellet injection task for several experimental devices and conclude that the required pellet dimensions are in the range of 2 to 5 mm for radius and velocities in the range of 2 to 6 km/sec. These data are summarized in Figure 2.

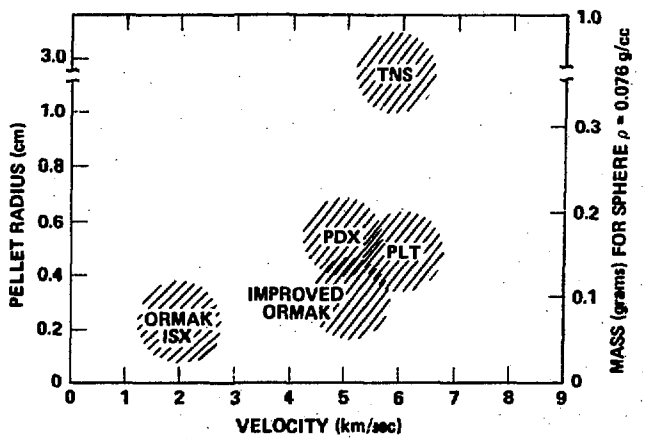

Fig. 2 Pellet radius versus injection velocity for several operating and planned nuclear machines.

Although there is some disagreement among the various sources, it would appear safe to predict that the mass-velocity requirements for injection in all likelihood will be in the range of 1 mg to 1 gram and 2 to 20 km/sec. For purposes of discussion, and to serve as a point of focus, 1 mg and 6 km/sec will be used as a "representative requirement" in the following discussion. However, as will be seen, the requirement falls essentially within the existing performance envelope of existing gas guns, and "breakthroughs" or major improvements in performance are not required. This important fact should not be overlooked in the search for a practical fuel injector.

Basic Launcher Theory

It took mankind nearly 700 years from the introduction of "guns" to reach projectile velocities of a few thousand feet per second.[4] Under the impetus of space and national defense requirements of the last 30 years, the limits have been advanced to over 40,000 feet per second with 2 gram particles.[5] The gains originated in the fruitful combination of several fields; physics, combustion, gas dynamics, materials properties, and hydrodynamic computer codes to mention a few key ones.

The devices themselves take many forms; the expendable explosively driven hypervelocity launchers pioneered by Physics International Company,[5] the large launchers at the U. S. Naval Ordnance Laboratory and the Canadian Armament Research and Development Establishment[6] that can handle launched masses up to several pounds on a routine repetitive basis, and include the novel hybrid devices such as the Institute for Aerospace Studies spherical implosion device,[7] and the Arnold Engineering Development Center electrically driven "Pot Shot" gun.[8] Some examples are shown in Figure 3.

In their basics, guns are very simple. The physical principles governing their operation have been known for a century. In their details and in present practice, they are complex pieces of sophisticated mechanical equipment that require computers for analysis.

Simple Analysis

Consider first the basic gun configuration shown in Figure 4. A constant diameter tube is separated into a driver section and a barrel, launch tube or driven section by a projectile of mass M, and cross-sectional area A. A gas, usually of high pressure, temperature, sound speed and ratio of specific heat (P_o, T_o, a_o, and γ), fills the driver region and a vacuum is assumed in the launch tube. The projectile, assumed frictionless, is accelerated toward the muzzle under the influence of the pressure on the base.

If the reservoir pressure, P_o, could be maintained at the base of the projectile, the behavior of the projectile would be described simply by Newton's Second Law:

$$P_o \cdot A = M \frac{dv}{dt}$$

and the velocity performance would be specified by:

$$V_{muzzle} = \sqrt{2 P_o \frac{AL}{M}}$$

This very simple ideal model points out some basic parameters and features of launcher technology. Clearly the muzzle velocity is an increasing function of pressure, and launch tube length and a decreasing function of mass/unit area or "areal density" as it is named. These simple concepts hold true for complex guns as well, except for only the most unusual situations. Only the details of the functional relationships change. Hence long barrels, high projectile base pressures, and low areal

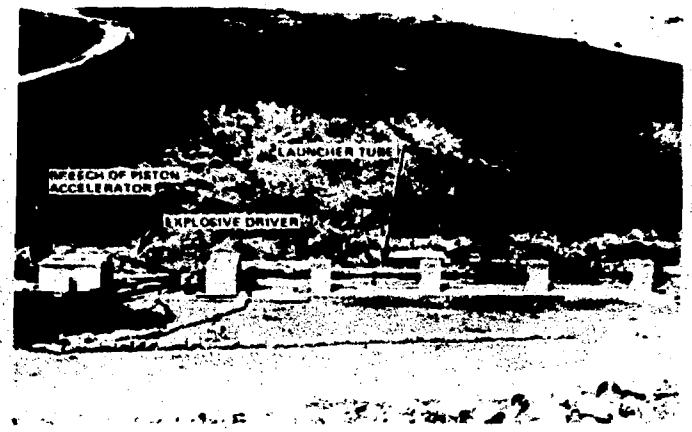

Fig. 3a Explosively driven expendable type light gas gun.

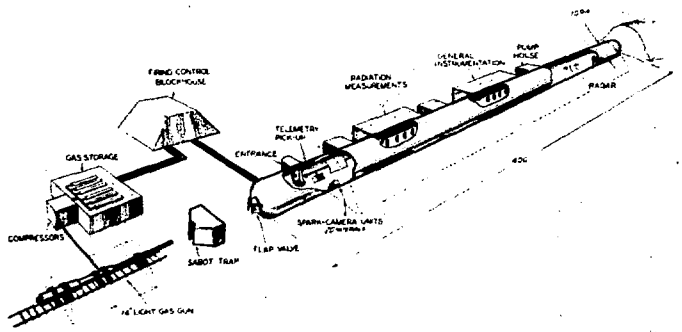

Fig. 3b Large two-stage light gas gun for laboratory environment.

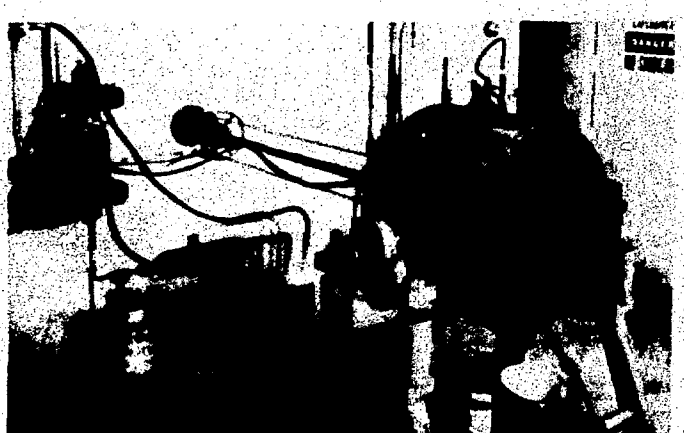

Figure 3c Novel contained explosive driven launcher for laboratory environments.

Fig. 3 Some representative examples of light gas gun/hypervelocity launcher facilties.

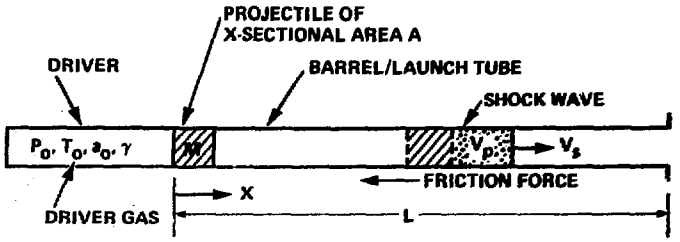

Figure 4 Simple gun/launcher configuration and nomenclature

densities are required for the production of high velocities.

Base Pressure Considerations

The key to high projectile base pressures is essentially high reservoir sound speeds or equivalently high reservoir temperatures. From elementary gas dynamics we know that a gas decreases in pressure and temperature as it expands and that there is a maximum velocity to which a given initial temperature gas can be accelerated. This velocity, the escape speed, is given for perfect gases and the geometry of Figure 4 as

$$U_{max} = \frac{2\ a_o}{\gamma - 1}$$

or in terms of temperature

$$U_{max} = \frac{2}{\gamma - 1}\sqrt{\frac{\gamma P}{\rho}} = \frac{2}{\gamma - 1}\sqrt{\gamma \frac{R}{m} T}$$

clearly low ratios of specific heat, low densities, high temperatures, or sound speeds are desirable. i.e., hence the "light gas gun." By way of example, perfect gas hydrogen ($\gamma = 1.4$) at a temperature of 20°K has an escape velocity of 6.6 km/sec (21,500 fps). Helium by comparison has a 20°C escape velocity of 3.0 km/sec (9800 fps). However, the actual muzzle velocity of most guns falls well short of this limit, as the accelerating pressure is zero as the gas velocity reaches escape velocity and friction, heat loss, counter pressure, and other deleterious effects take their toll. Further, while high pressures are desirable from performance considerations, high pressures are difficult to contain and control. Also, high pressure and low areal densities imply very high projectile accelerations. In some cases, otherwise promising launching schemes have been thwarted by the severity of the "projectile integrity" problem, as the projectiles were unable to withstand the difficult accelerations imposed by the particular launch cycle.

To overcome these limitations and to create hypervelocities in spite of them, launcher professionals have been very creative in their efforts to counter or circumvent the constraints. Some techniques are elegant--

others very creative--many promising ones never quite made it for one good reason or another.

Expansions

There are two kinds of expansions in gas dynamics--steady and unsteady. A steady expansion is the kind of flow which is produced by a gas expanding through a nozzle. A wind tunnel or rocket motor, wherein the pressure profile along the nozzle is independent of time, are two common one-dimensional planar examples. An unsteady expansion, such as the flow produced by a shock tube, the expanding driver gas in a gun, or the like, has a pressure profile or history at a point which is not uniform in time. The pressure-velocity relationships of the two are very different. For example:

$$\text{Steady } \frac{P}{P_o} = \left[1 - \frac{\gamma_4 - 1}{2}\left(\frac{U_3}{a_4}\right)^2\right]^{\gamma_4/\gamma_4}$$

$$\text{Unsteady } \frac{P}{P_o} = \left[1 - \frac{\gamma_4 - 1}{2}\frac{U_3}{a_4}\right]^{2\gamma_4/\gamma - 1}$$

These velocities are plotted for comparison on the P-U plane in Figure 5.

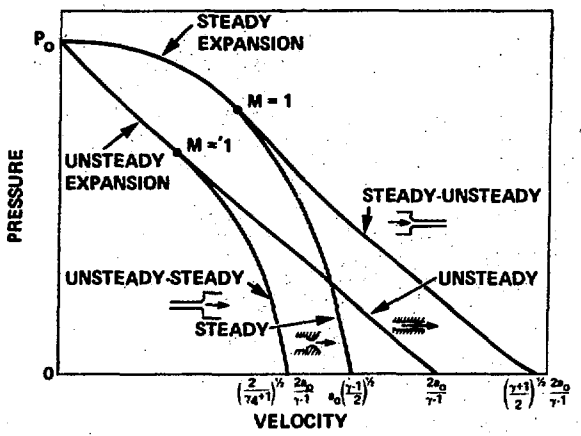

Fig. 5 The pressure-velocity behavior of a gas in steady and unsteady expansions.

It can be seen that the steady flow is more efficient in trading pressure for velocity up to a point, which corresponds to a local flow Mach number, M, of 1, after which the unsteady flow is more efficient. The range of velocities attainable by the processes is given for unsteady and steady flow by

$$\text{Steady } U_{escape} = \left(\frac{\gamma - 1}{2}\right)^{\frac{1}{2}} a_o$$

$$\text{Unsteady } U_{escape} = \frac{2}{\gamma - 1} a_o$$

Or we can combine the most efficient parts of both--i.e., steady flow up to M = 1, and unsteady for velocities greater than M = 1 to yield the highest possible escape velocity:

$$U_{escape} = \left(\frac{\gamma + 1}{2}\right)^{\frac{1}{2}} \frac{2a_4}{\gamma_4 - 1}$$

A geometry used to generate this flow is shown in Figure 5, and is called chambering or chamberage. All told, four possible combinations of expansions exist. They are also shown schematically in Figure 5.

For the most efficient process, the diameter ratio must be large in order to realize the gain. In practice area ratios of 25 give better than 90% of the gain. The improvement in escape speed over the usual unsteady (constant area tube) case is

$$\left(\frac{\gamma + 1}{2}\right)^{\frac{1}{2}} = 1.095 \Big|_{\gamma = 1.4} \quad \text{or} \quad 1.155 \Big|_{\gamma = 1.67}$$

While small, most high performance gun devices are designed with chambrage to take advantage of this effect.

Two-Stage Light Gas Guns

As it is difficult to contain high temperature gases at temperatures of several thousand degrees Kelvin under steady conditions, a "transient steady" method was developed and named the "two-stage light gas gun."

This gun shown schematically in Figure 6a, uses an additional driving stage. The first stage, usually propellant driven, accelerates a relatively massive piston into the driver gas, usually He or H_2, shock compressing it to high pressures and equally important, high temperatures. Many thousands of degrees Kelvin can be reached very readily using this method. As the temperatures are high for only short periods of time, tens to hundreds of milliseconds, the heat loss, erosion, and other mechanical problems are lessened or negated.

Further, as there is generally a maximum pressure that can be applied to the base of a projectile without destroying it, the highest velocities that are attainable for a given barrel length occur when the base pressure is held at or near this limiting value. An elegant method to create nearly this ideal situation in practice has been made using a modified two-stage light gas gun, called the "accelerated reservoir light gas gun." It is shown schematically in Figure 6b. Here a deformable piston is purposely forced into a tapered reservoir region at the end of the first stage stroke. The geometry, velocities, mass of piston, etc., are chosen to yield a generally increasing pressure history in the reservoir that yields on expansion, for a given projectile, nearly constant base pressure at the projectile. Each complex case is unique and must be optimized usually with computers for the given set of initial conditions and desired projectile velocity. However, the alleviation of projectile integrity problems and resulting net high velocities well justify the computational complexity.

Projectile Friction

The friction of the solid projectile rubbing against the barrel creates a direct deceleration force. Aside from good machining practices, choice of materials, and mechanical fits, not much can be done to alleviate it. Fortunately the velocity loss due to friction

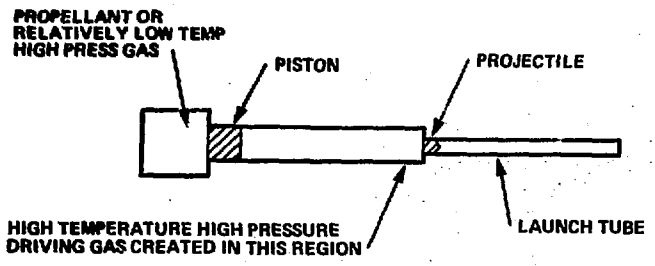

6a CONVENTIONAL 2 STAGE LIGHT GAS GUN

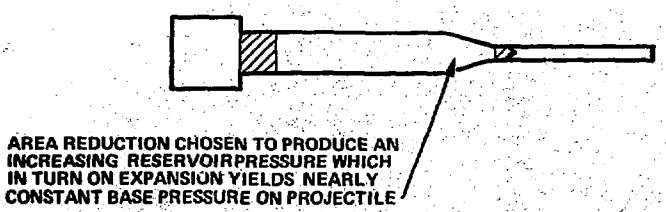

6b ACCELERATED RESERVOIR LIGHT GAS GUN

Fig. 6 Schematic of two-stage light gas guns.

is usually of the order of 15% or less.

Friction of the driver gas against the barrel wall also produces losses which show up as pressure drops at the projectile and for long launch tubes, may choke off the flow separating the projectile from its driver. As with mechanical friction, it is a second order effect provided barrel dimensions are not too small.

Counter Pressure

Counter pressure, another loss mechanism, is the pressure generated on the front face of the projectile by the compression of the atmosphere ahead of it in a rapid shock-like fashion. The projectile behaves much like a piston creating a shock induced flow ahead of it and suffers from not only the increase in pressure on the face of the model, but in turn, viscosity creates a boundary layer within that flow. The projectile-piston must re-accelerate this velocity deficient flow exchanging projectile velocity and momentum in the process. Fortunately, the barrel ahead of the projectile can be evacuated to reduce the absolute value of the counter pressure to acceptable levels.

Despite the complexity of the task, the details of which have only been touched upon in the preceding sections, the state of the art of hypervelocity launchers is such that complex shaped projectiles of many pounds are launched to several thousands of feet per second routinely and small shapes of 2 grams have exceeded 40,000 ft/sec in devices specifically optimized to reach maximum velocities.

Figure 7 is a composite of some of these mass/velocity results. It should be immediately apparent from the figure that the mass velocity requirements for a Tokamak device, outlined in the previous section, are well within the capability of these devices, and allow much room for expansion.

In the following section we outline what configuration a launcher dedicated to fuel injection might take.

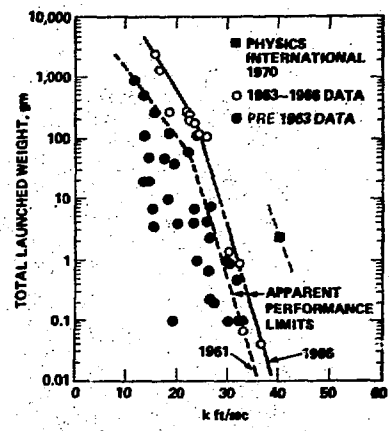

Fig. 7 Maximum launch velocities and weights.

GAS GUN INJECTOR

Requirements

The orderly development of the refueling technology of a Tokamak requires three steps. First, a single shot mode, wherein a single fuel pellet is injected into the machine and processed. Secondly, a burst mode, wherein several fuel pellets are injected, one after the other in rapid succession, to study short-time, steady state operations. Finally, the continuous mode where fueling is essentially a continuous steady-state process.

It appears to this author that the continuous mode is outside the present practical limits of gas gun technology unless the required injection velocities became so large as to outstrip the capabilities of all the other candidate injectors. One should keep in mind that many conventional guns have high repetition rates and it is within the realm of reason that ingenious mechanisms might be forthcoming to do the same with unconventional guns.

However, for the single shot and burst modes, it is clear that the light gas gun is well suited for the task.

The most difficult requirement of the gun injection, it would appear to us, is not the velocity or mass requirement, but rather the manufacture and insertion of the projectile into the barrel. Although right circular cylinders of solid hydrogen could, in principle, be made externally and fitted to the

barrel, it does not appear practical to do so, as solid hydrogen is admittedly an unusual projectile material.

An alternative approach is to create the projectile within the gun. Two possible methods suggest themselves--a steady state mode in which the projectile is manufactured prior to the launch cycle and a transient mode, in which the projectile is created during the launch cycle. Both modes require a conventional piston/projectile in addition to the fuel element.

For example, for the steady state mode, we envision injecting a known amount of liquid hydrogen immediately ahead of the projectile. Further cooling would bring it to the freezing point. The shape of the projectile could be facilitated by positioning the launcher in a vertical position under the Tokamak or loading the fuel in a vertical position and then rotating the assembly to the horizontal position for firing. The mechanical complexity of such a configuration does not appear particularly difficult, since the envisioned apparatus is relatively small.

For the transient mode, gaseous hydrogen is injected into the barrel of the launcher. The tube wall in the region immediately in front of the projectile is kept below the liquification point of the hydrogen fuel. Consequently, the fuel condenses in a thin layer on the tube wall ahead of the piston/projectile. The fuel is prepared near the projectile to minimize the mechanical loading of the projectile by the fuel being collected and reduce the subsequent shock heating of the fuel.

An injector configuration which could be operated in either mode is shown in Figure 8. It consists of a 5-mm-diameter launch tube, 200-mm long. A 25-mm-diameter pump or driver tube connects to it upstream. The launch tube tapers to 1-mm diameter at the exit plane in such a fashion that the front face of the deformable piston uniformly accelerates to a higher velocity than the rear face prior to decelerating to a stop, after the manner of the "accelerated" reservoir light gas gun. The tapered end of the tube utilizes an area reduction designed to double the front surface velocity of the fuel. Much larger ratios are, of course, possible in principle using, for example, the contraction scheme developed by Voitsekhovsky.[10] This simple geometry immediately reduces the velocity requirement by one half and the degree of abruptness also allows latitude in choosing the mass and velocity of the injected fuel.

The nominal 0.1 gram piston is large compared to the fuel which will be in the range 0.5 to 5 mg. Even if several times this amount is required to make up for boundary layer losses, losses due to vaporization, etc., the fuel mass remains a negligible amount of the launched weight, hence the piston weight is selected independently of the fuel mass requirements, which cease to be a controlling factor in the design analysis. Note in passing that the light gas gun performance at 0.1 gram is than 40,000 fps.

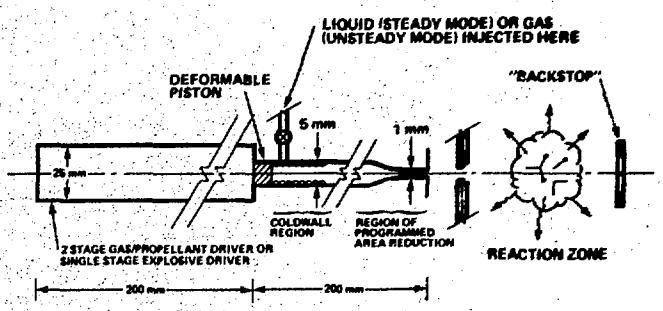

Fig. 8 A conceptual view of a light gas gun injector for inserting fuel into a fusion machine.

As the initial temperatures are chosen to create a liquid fuel projectile (or possibly a solid one which becomes liquid on shock and frictional heating in the barrel), any potential fuel projectile integrity problem becomes academic, as the projectile material is reprocessed at the contraction section, and a high velocity "spurt" of liquid hydrogen is ejected from the exit of the contraction section.

Jet breakup considerations will have to be considered but do not appear insurmountable at the pressures and velocities envisioned.

It should be noted in passing that the contraction ratio also serves as a "stop" for the piston. Other constant area designs which were considered had the failing that the projectile followed the fuel into the reactor, introducing an impurity level typically an order of magnitude greater than the fuel injected, and possibly as much as the original mass in the machine.

The contraction concept also permits sealing of the launch tube after firing, preventing driver gases from entering into the Tokamak interior and contaminating the machine, an important requirement. Further, we envision that the injected liquid hydrogen might well become solid as liquid jets near the freezing point will solidify rapidly if injected into a near vacuum. Accordingly, solid hydrogen pellets may not be an absolute requirement as the near freezing-point-hydrogen will solidify to produce the desired pellet. Hence, the manufacture of a "hard" pellet is circumvented.

It is our contention that this novel combination of what we feel are the best features of the different technologies involved can yield a practical fuel injector for single pulse fueling of Tokamak machines.

Further, multiple injections, possibly as many as 8 or 9 in a simple system could also be obtained by a permutation of this basic concept. An assembly of injectors arranged in a manner not unlike the chamber of a "six-shooter" or even separate launch tubes, driven by a single driver, as shown schematically in

Figure 9, would provide multiple projectiles for the "burst" mode.

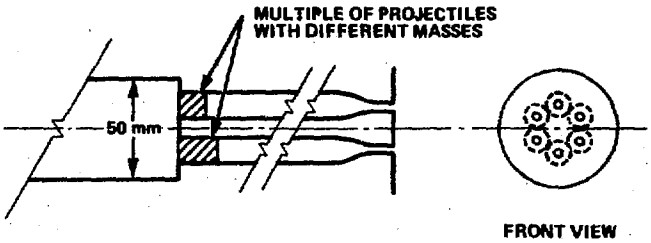

Fig. 9 A conceptual view of a light gas gun injector for inserting multiple fuel elements into a fusion machine.

The timing of the injection of the multiple pellets could be arranged by varying the projectile weight in each of the single launch tubes to give the desired exit velocity and time. A 50-mm driver would appear to be adequate for 6 or 7 driver tubes. Larger or longer drivers would be required if more barrels were added to the cluster. Even multiples of this might be used if it were necessary to increase the total fueling time even further.

Connecting such a device to a Tokamak appears to be a straightforward mechanical task. A fast action gate valve might be used as a backup seal to the deformable piston, and would facilitate the insertion of new barrels for the next shot(s). One might have to add a "splash plate" on the opposite side of the reactor to catch and defeat any high velocity fuel elements which survived the machine interior, to prevent self-destruction.

To produce 3 km/sec in a chambered single state light gas gun utilizing room temperature hydrogen requires a driver pressure of several tens of thousands of psi, hence a two-stage or explosively driven light gas gun will most likely to be required as a practical matter. An additional driver stage, 200-mm long and 50 mm in diameter, driven by propellant or room temperature hydrogen should generate 3 km/sec without difficulty. Alternatively, an explosive driven gun utilizing approximately 500 grams of safe-liquid explosive could do the same. The driver stage of the explosive gun is considerably simpler in mechanical design, however, a robust vessel to contain the resulting products of detonation would be required. Containment vessels designed to handle many pounds of explosive are common in many explosive research laboratories and offer no particular difficulty in design or operation.

Summary

In the preceding section, its has been shown that the most probably velocities and fuel mass fall well within the mass-velocity capabilities of current light gas gun technology. Indeed the fuel mass requirements are so small that the light gas gun piston/projectile mass predominates and the fuel mass can be neglected in performance calculations.

Further the velocity requirements and present capabilities allow a substantial margin for growth, should such become necessary in the evolution of the fusion machine. The guns themselves have not reached a performance barrier, and could be extended beyond present capabilities.

While a light gas gun based injector capable of continuous operation appears feasible but somewhat combersome, the light gas gun is ideally suited to the single pellet and short burst modes. The continuous mode might well become necessary to persue, if the velocity requirements outstrip all of the other candidate fueling systems.

The practical problems of adapting a gas gun to the fueling task appear straightforward and both configurations shown offer practical solutions to the many mechanical and physical requirement involved.

References

1. S. L. Milora, C. A. Foster, and G. D. Kerbel, "A Survey of Possible Pellet Injection Techniques for Refueling Tokamak Reactors," 18th Annual Meeting of the Division of Plasma Physics of the American Physical Society, San Francisco, CA., November 15-19 (1976).

2. R. G. Mills, "The Fueling of Toroidal Fusion Reactors," Proc. of the 2nd Topical Meeting on the Technology of Controlled Nuclear Fusion, 4, 1173 (1976); held in Richland WA., 21-23 September (1976).

3. T. B. Parks, R. J. Turnbull, and C. A. Foster, "A Model for the Ablation Rate of a Solid Hydrogen Pellet in a Plasma," Nuc. Fusion, 17, 3, 539 (1977).

4. A. E. Seigal, "The Theory of High Speed Guns," AGARDOgraph 91, May (1965).

5. J. D. Watson, "A Summary of the Development of Large Explosive Guns for Re-Entry Simulation," PIFR-155, Physics International Company, San Leandro, CA., (1970).

6. A. C. Charters, "The Free Flight Range: A Tool for Research in the Physics of High Speed Flight," ARS Preprint 1984-61 (1961).

7. R. F. Flagg, "The Application of Implosion Wave Dynamics to a Hypervelocity Launcher," Inst. Aerospace Studies, University of Toronto, TR-125, June (1967).

8. J. Lukasiewicz, W. B. Stephenson, P. L. Clemens, and D. E. Anderson, "Development of Hypervelocity Range Techniques at AEDC," TR-61-9, Arnold Engineering Development Center, (1961).

9. J. S. Curtis, "An Accelerated Reservoir Light Gas Gun," NASA TN-D1144,Ames Research Center, Moffett Field, CA.

10. B. V. Voitskhovsky, et al., "Some Results of the Destruction of Rocks by Means of a

Pulsed Water Jet," News of the Siberian Dept. of the Academy of Sciences, USSR, Series of Tech. Sci. 1, 2, 7-11, Novosibirsk; also U.S. Patents 3,343,794 and 3,412,554.

Bibliography

A veritable wealth of information is available on the subject of light gas guns. References 4 through 9, in addition to those below will provide an excellent introduction to the subject.

J. I. Glass, Hypervelocity Launchers, Pt. 1: Simple Launchers Review No. 22, Institute for Aerospace Studies, University of Toronto, May (1963).

J. I. Glass, Hypervelocity Launchers, Pt. 2: Compound Launchers-Driving Techniques, Rev. No. 26, Institute for Aerospace Studies, University of Toronto, December (1965).

A. E. Seigal, The Effect of the Optimum Chamberage on the Muzzle Velocity of Guns, NAVORD Report 2691, U.S. Naval Ordnance Laboratory, October (1952).

W. D. Crozier and W. Hume, High Velocity Light Gas Gun, J. Appl. Phys., 28, 892 (1957).

R. L. Bjork, The Atomic Hydrogen Gun, Report RM-1707, Rand Corporation (1961).

A.E. Seigal, R. Piacesi, and D. N. Bixler, Wall Friction, Heat Transfer and Real Gas Propellant Effects in High Speed Guns, Proc. 4th Hypervelocity Techniques Symposium, Arnold Air Force Station, November (1965).

FUELING BY LIQUID JETS

C. Bruno
Physics International Company
San Leandro, California 94577

Introduction

Maintenance of steady-state burn in tokamak fusion reactors will require a reliable method for fueling them during operation. The injection of high-velocity dense-phase DT is one solution under investigation. The eventual requirements are not known precisely but the next series of experiments in tokamak devices (e.g., Doublet III, PDX) could use millimeter size particles with velocities of the order of 2000 m/s. This paper presents results on the feasibility of a high-pressure injection system to meet these objectives.

Long Term Requirements

Neither the amount of fuel needed nor the injection conditions are known for power-plant-sized tokamaks, but some limits may be defined. A minimum rate of about 0.5 g/s or 1 cm^3/s is needed to replace fuel furned in a 1000 MWe fusion plant.

If fuel is injected as a condensed phase, the effect of collision and radiation will tend to vaporize it as it moves toward the desired region of the plasma. Thus, if sufficient mass must survive during the penetration phase, whether in jet, drop, or pellet form, it must be sufficiently fast and large.

Although uncertain at present, future requirements have been estimated for the case of solid spherical particles; they call for velocities of about 10^6 cm/s and sizes of about 1 mm in order to penetrate regions of about 1 meter. Thus, it appears that particles of 10^{-3} to 10^{-2} cm^3 are needed at repetition rates of about 10^2 pulses/s.

Current Experiments and Theory

The main injection experiments to date are those of Kim, et al (1976) in which 0.2 mm diameter pellets were injected at 100 m/s into the ORMAK plasma (80 eV, 5 x 10^{18} m^{-3}). Jorgensen, et al. (1975) observed the ablation rate of a hydrogen pellet by a plasma of $n = 2 \times 10^{20}$ m^{-3}, $T_e = 10$ eV, $T_i = 400$ eV. Ablation models have been derived by Parks, et al. (1977), Vaslow (1976), Rose (1968), Gralnick (1973), and Spitzer (1954).

Near Term Experiments

PLT is in operation at densities of 10^{20} m^{-3} and temperatures of about 1 keV. Two other devices (Doublet III and PDX) are under construction and will be available in 1979 or 1980 for experiments. Current estimates for useful experimental pellet parameters are 1 to 2 km/s and 1 to 3 mm in diameter. Experiments under these conditions would advance both the pellet and plasma parameters by an order of magnitude.

Injector Technology

During the past 10 years Physics International has developed diesel pressure injectors capable precisely and repeatedly of injecting small amounts of fuel by means of pressures in the range 700 to 1500 atmospheres. A simplified diagram of the 1450 atmosphere DELPHI injector system under development is shown in Figure 1. The repeatibility of the injection process is due to the piezoelectric PC valve technology, also developed by Physics International, and to its inherently short response time. A typical PZ injector built by PI is shown in Figure 2.

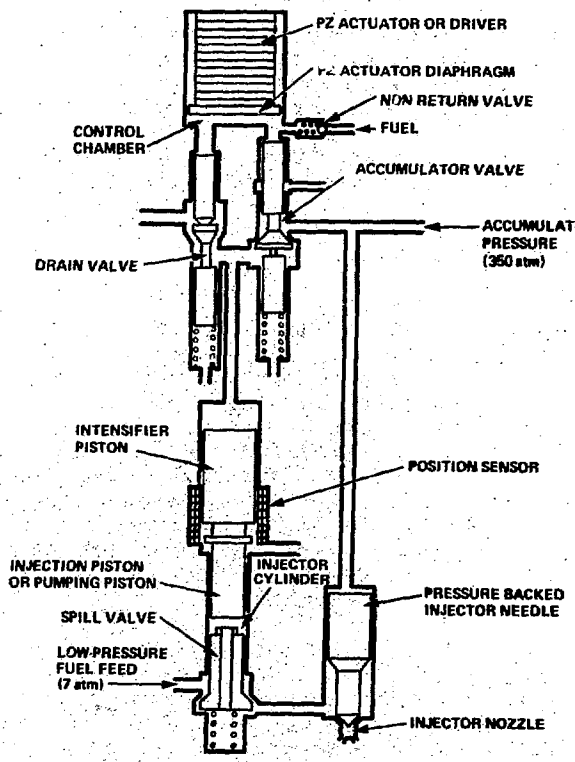

Fig. 1 Diagram of piezoelectric servo-valve fuel injector.

The injector is fed diesel fuel at the pressure of 7 atmospheres and injects it at a pressure of about 1400 atmospheres. Expansion through a short nozzle causes the pressure energy to accelerate the fuel to a velocity equal to

$$V = \left(2 \frac{\Delta p}{\rho}\right)^{1/2}$$

Neglecting friction losses, usually small, at a Δp of 1400 atmospheres, V is 580 m/s.

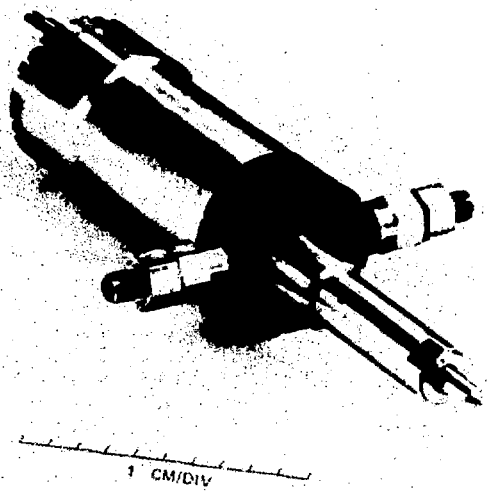

Fig. 2 Piezoelectric pump injector.

Basic LH_2 Injector Concept

Because of its lower density, liquid hydrogen would be accelerated by the same pressure (1400 atm) to over 1500 m/sec. A diesel-type fuel injector can thus deliver useful velocities and amounts of material. Application to hydrogen fueling experiments has some new requirements (formation and selection of a single particle from this jet) and different technology (cryogenic H_2) which must be applied.

To accomplish this, an injector has been designed which has a thermally isolated cryogenic high pressure portion and means for producing a short duration jet (Figure 3). In addition, the physics and implementation of jet breakup and particle selection have been investigated. Vibration-induced particle formation and rotating mechanical selectors have been chosen and conceptual designs executed. The device is designed to deliver a single high-velocity particle once each few minutes, to coincide with the repetition rates of near-term tokamaks.

A simplified sketch of the injector to show its main components is shown in Figure 4. Hydraulic fluid (glycol) pressurized by N_2 can be made to accelerate a piston when a valve is opened by a piezoelectric stack. A pushrod transmits force and motion to an intensifier piston which, because of the area difference, increases the pressure acting on externally fed LH_2. The pressure increases in the injection chamber until it becomes high enough to lift the needle valve off its seat against the force of a preset spring. At that instant the LH_2 begins to escape through the nozzle, while the piston keeps pushing it.

Physics Feasibility

Jet Formation

Compression and Expansion of Liquid Hydrogen. The liquid hydrogen present as working fluid inside the injector will be compressed nearly adiabatically by the intensifier piston up to pressures ~2 kbar. Following the opening of the needle valve, the

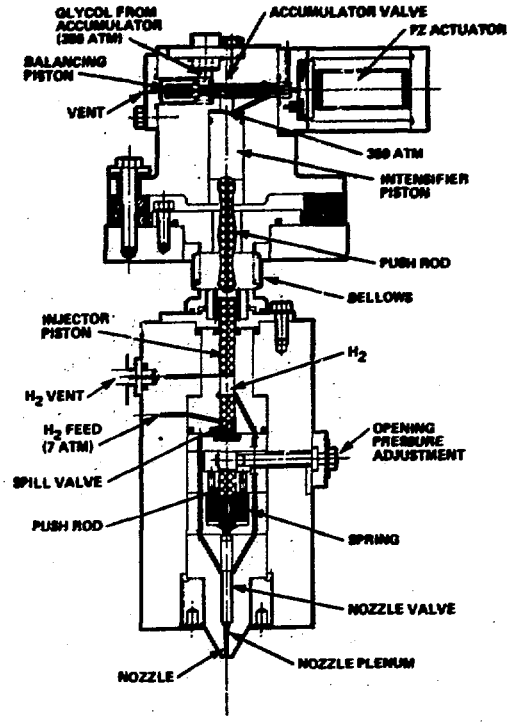

Fig. 3 Conceptual design of tokamak fueling injector.

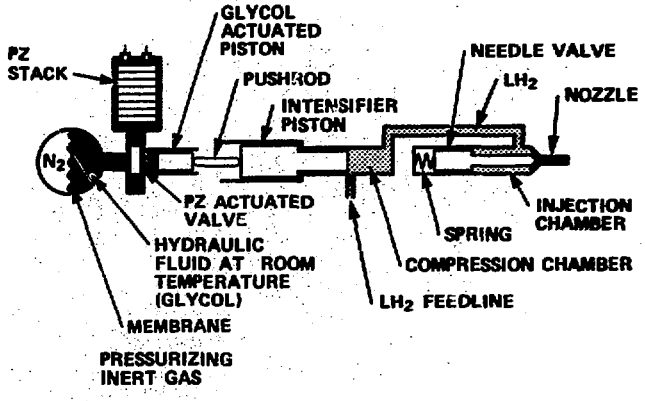

Fig. 4 Simplified sketch of LH_2 injector.

hydrogen will expand back to low pressure (~50 torr to prevent flash vaporization). Adiabatic compression data are required to predict pressures and temperatures in the hydrogen; unfortunately in the pressure range of interest they are scarce.

Hugoniot compression results can be used in lieu of adiabatic provided the pressure range is low enough, i.e., ~1 kbar (Van Thiel, 1964; Roder, 1973; and Mills, 1977). What this means is that on a P, ρ diagram, adiabatic and Hugoniot lines are very close to each other at low pressures. Therefore for a given density the pressure corresponding to an adiabatic compression can be assumed then to be a fraction (very close to 1) of the pressure obtained from the Hugoniot results (Goren, 1969). The effect of this assumption can be checked by reducing the fraction and observing the

differences that will occur.

On the basis of these considerations, a least square fit of the Van Thiel and Wasley results of the form

$$P(\mu) = A_0 + A_1 \mu + A_2 \mu^3$$

where

$$\mu \equiv \rho/\rho_0 - 1 \text{ and}$$

$$A_0 = P_0 = 1.013 \text{ bar}$$

$$A_1 = 1.170 \times 10^3 \text{ bar}$$

$$A_2 = 1.131 \times 10^4 \text{ bar}$$

was performed. The fit approximates well the density behavior when the pressure is increased by a shock compression. Its accuracy in representing an adiabatic compression will decrease with the pressure.

The greatest percentage error of the least squares fit with respect to the experimental data points was ~3.8% at 1120 atmospheres. The value of the sound speed at 1 atmosphere was 17.2% higher than the experimental value of 0.11 cm/usec. A check of the speed of sound predicted at 2 kbar indicated an error of less than 10% with respect to the data of Mills et al., (1977)(see Figure 5). The fit was used for all the LH_2 fluidynamic calculations; it combines both the equation of state and the equation for the thermodynamic change in one analytic function. While some of the assumptions made to derive the fit are crude, they are no worse than the available thermodynamic data. A test of the sensitivity of the results to the fit was performed assuming the pressure was only 80% of the fit-predicted pressure. No substantial changes were found in the results.

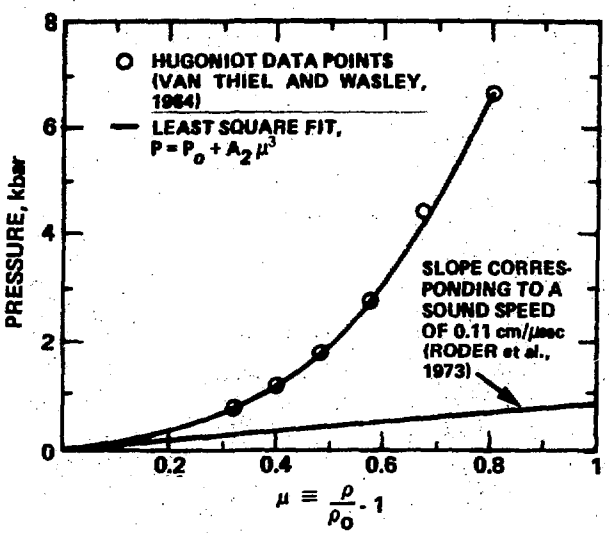

Fig. 5 Liquid hydrogen compression curve fit.

LH_2 Jet Acceleration. The velocity of the LH_2 jet depends on upstream pressure, temperature, shape of duct, and compressibility. Forced by the pressure in the reservoir the LH_2 expands in the convergent portion of the nozzle and accelerates. If the pressure head is high enough, the velocity may equal the speed of sound; the cross section where this happens is the throat. Under steady state conditions, no further velocity increase takes place past the throat, unless the cross section increases with distance; in the case of a sudden acceleration (as in the injector), a transient precedes the establishment of steady state conditions. During this transient supersonic speeds can be reached, regardless of the nozzle shape. Besides, LH_2 has an adiabatic compressibility about two orders of magnitude lower than the compressibility of a perfect gas; thus, the effect of the duct shape must be far less important in determining whether the efflux will or will not be supersonic. From the analysis of the Hugoniot data of Van Thiel and Wasley, it is also clear that the H_2 energy at ~ 2 kbar is mostly PV energy (as in a liquid) rather than internal energy (as in a gas).

To summarize these considerations, the acceleration of a liquid hydrogen is closer to the acceleration of a conventional heavy liquid than to that of a gas. The kinetic energy is imparted to the liquid mostly by pressure forces and only in small part by the change in internal energy. Supersonic velocities can be obtained if the initial reservoir pressure is large enough; the effect of a convergent-divergent nozzle shape is, in this context, the same of a simple convergent nozzle.

With the $P = P(\mu)$ fit described in a previous section, Physics International's PISCES 2DELK hydrodynamic code was used to explore the jet velocity range as a function of pressure and convergent shape. The rather irregular LH_2 reservoir of the actual injector (see Figure 3) was modeled for simplicity into a cylindrical cavity separated from the nozzle by a valve.

Three geometries of the convergent portion of the nozzle were explored: a conical surface of 45 degree angle; a quarter of circle generatrix surface, and a 45 degree cone blended with the rest of the nozzle by means of a smoothly sloping surface. Finally, two different nozzle shapes downstream of the critical (throat) area were investigated: straight duct, and divergent conical duct.

The results indicate that a speed of ~2 km/s can be reached by a pressure ~2 kbar in the reservoir and by using a 45 degree conical convergent blending with a smooth curved surface into a slightly divergent duct. As this divergence needs to be smaller than 0.001 to avoid the onset of vena contracta effects, no practical performance degradation occurs when the divergent portion of the nozzle is replaced by a constant cross section duct.

Figure 6 shows the history of the jet velocity at the nozzle exit for a reservoir pressure of 2 kbar. The initial velocity overshot is due to the fact that at early times hydrogen gas is present inside the nozzle and its acceleration is larger than that of the denser liquid. For realistic valve-opening times, this gas velocity peak would not probably occur. The velocity oscillations in the figure are chiefly due to the inviscid fluid assumption; small scale oscillations due to

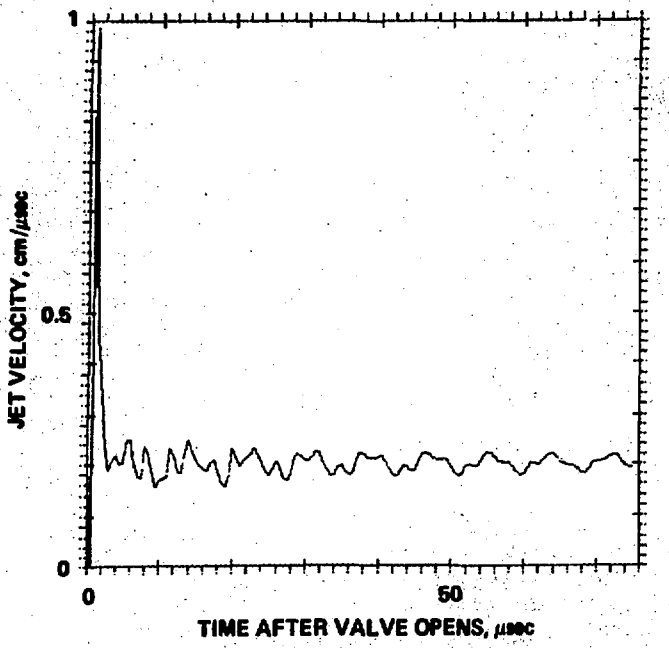

Fig. 6 Jet velocity versus time for p=2 kbar, 45-degree conical nozzle smoothly blended into a 0.1% divergent duct.

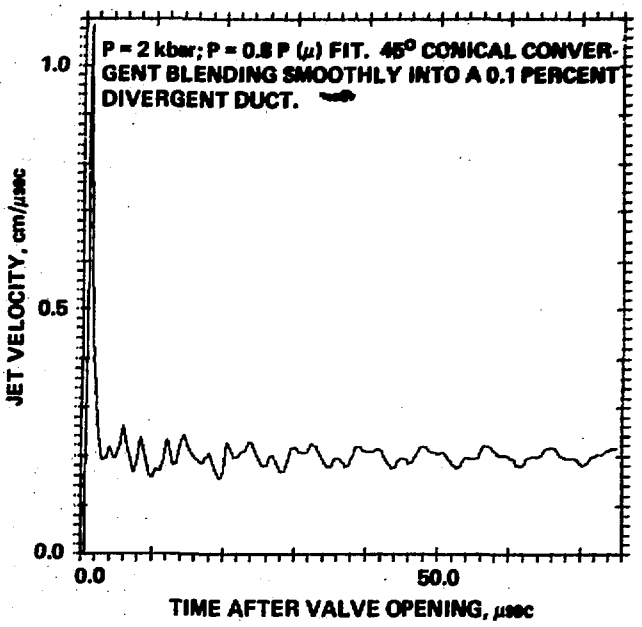

Fig. 7 Jet velocity history; p=2 kbar; p=0.8 P(μ) fit; 45-degree conical convergent blending smoothly into a 0.1% divergent duct.

mesh and time-step sizes (and to the plotting hardware) can also be detected. The estimate for frictional effects in the nozzle predicts a pressure head loss of ~3 atmospheres/nozzle diameter.

Results for the jet velocities at other pressures and geometries are summarized in Figure 7. Velocities higher than 2 km/s can be obtained at an increasing price in terms of pressure. Actually the scaling of the jet velocity [$V \sim (\Delta P)^{\frac{1}{2}}$ for inviscid and incompressible flow] appears from the results to take place with a power slightly less than one half. Therefore, it is less and less advantageous to use hydrodynamically slow, high pressures devices to accelerate LH_2. Aside from fluidynamics considerations, structural questions (stresses, tolerances) constitute by themselves a major problem in devices designed to operate in the kilobar range. Faster jets are possible instead by means of impulsive accelerations (shocks) of the liquid.

Particle Formation and Selection

Four main questions need to be analyzed in the context of particle formation: premature (i.e., unwanted) jet breakup, jet freezing, particle formation process and particle integrity during flight.

Premature Jet Breakup. Studies on jet breakup go back to Lord Rayleigh (1878, 1879) who analyzed it in the velocity regime dominated by inertia and surface tension. This produces randomly sized drops, unless a forced excitation is superimposed. The size of the drops spontaneously formed in this regime is larger than the jet diameter. After Rayleigh, extensive research on jet breakup was carried on to explain the different breakup mechanisms dominating at different regimes, i.e., when the drops formed are smaller than the jet diameter. An excellent review of the material already published is in Reitz and Bracco (1976). The majority of the theories and experimental fits agrees in predicting a critical Weber number $We_{cr} \sim 10^1$ beyond which no intact jet column exists, i.e., the jet begins to atomize as soon as it emerges from the nozzle. [The Weber number is the ratio background gas density x (jet velocity)^2 x jet diameter/jet surface tension.] Other jet breakup regimes exist, their boundaries defined by jet Reynolds number, gas/liquid density ratio, and Ohnesorge number. For a LH_2 jet of ~0.05 cm diameter at 2 km/s into a ~50 torr chamber, We ~5000, $\gg We_{cr}$. Accordingly a steady-state jet should atomize forming a spray cone immediately after emerging from the nozzle. However, there is experimental evidence that individual nozzle geometry and jet turbulence intensity can affect considerably the jet regime, both in steady and unsteady situations. A first example is supplied by fast water jet technology. Impulsively accelerated water jets are being explored as a possible means for rock cutting. Typical parameters for a pulsed water jet can be found in Young (1977)

Pulsed water jet:
- We ~40,000 $\gg We_{cr}$
- Re ~2×10^7 (U_{jet}=2500 m/s)
- ρ_{gas}/ρ_{jet} ~1×10^{-3}

Under these conditions, all more unfavorable for jet integrity than in the LH_2 jet, coherent jet distances of 500 diameters have been measured.

Secondly, Reitz (1977) injecting diesel oil and water into a high pressure chamber (to simulate diesel injection) explored the range $R_e \sim 10^4$, We ~10^3, $\rho_g/\rho_L \sim 10^{-2}$, and

found that for a sufficiently long nozzle, (i.e., L/d $\gtrsim$ 50), no breakup could be obtained inside his apparatus, indicating the intact jet length to be $\sim 10^2$ to 10^3 diameters. His tentative conclusions are that for well-developed turbulent flow the available theories and empirical fits cease to be valid, and that turbulence has a stabilizing effect on jet integrity. Possible mechanisms responsible for breakup at lower turbulence intensities are: the geometry of the nozzle and its connection with cavitating areas; the magnitude of radial velocity components, kept directed inwards in high speed water jets by a convergent nozzle shape; and the slower relaxation of the velocity profiles from turbulent (inside the nozzle duct) to plug-type profiles in the jet.

On the basis of the experimental results mentioned, it seems clear that the integrity of a fast LH_2 jet cannot be predicted by available criteria. The facts mentioned indicate the practical possibility of forming coherent, high Reynolds jets in relatively dense media. Experiments with nozzle geometries and injection parameters should be the definitive criteria for determining the feasibility of LH_2 jets.

Jet Freezing. As indicated in the previous section, turbulent liquid jets can survive even at Weber numbers greater than critical. However, it still may be necessary to have a background gas pressure so small as to be comparable with the LH_2 vapor pressure. In this case vaporization may become important, and the jet surface might freeze. The characteristic time associated with the radial penetration of the thermal wave is

$$t_{HT} \sim (\tau_{jet})^2/a$$

where a is the thermodiffusivity. For molecular conduction (purely laminar regime), $t_{HT} \sim 1$ second; at the Reynolds number typical of the LH_2 jet ($\sim 10^6$) the regime is fully turbulent, provided the nozzle L/d ratio is $\gtrsim 50$. Under this assumption $t_{HT} \sim (\tau_{jet})^2/a_T$ where the turbulent thermodiffusivity a_T may be estimated using Prandtl's analogy (Schleicher and Tribus, 1956 and Schlichtin, 1968, p. 572) The results indicate $a_T \sim 10^4$ a and thus the characteristic heat transfer time is $\sim 10^{-4}$ sec for which the freezing distance should be $\sim 10^1$ cm. The indications are therefore that a very vast jet can begin to freeze very rapidly. When this happens the vapor pressure drops and the process slows down. However, for low enough background pressure and long enough times, the jet will freeze throughout (Foster, 1977). In fact local nozzle heating has been used precisely to prevent very thin liquid jets from freezing as soon as they emerged from their capillary nozzle (Hendricks, 1977).

In conclusion, a device to break the fast LH_2 jet into particles must be able to do so prior to jet freezing, i.e., within a distance of $\sim 10^1$ cm.

Particle Formation. In laminar flow jet regime, the traditional method for orderly jet breakup into particles is to superimpose a standing wave on the jet surface by means of a mechanical or piezoelectric device (Schneider and Hendricks, 1964; Schneider, et al., 1967; Goodman and Hunt, 1976; Foster et al., 1977; Calliger, et al., 1977). Fast jet breakup can be obtained by suitably amplifying the disturbance (Foster, et al., 1977). The result in all cases is the exponential growth of the difference between neck and swell (Goedde and Yuen, 1970), due to surface tension effects, until breakup at the nodes occurs.

In a fast LH_2 jet, the flow regime is turbulent and the surface tension tends to oppose the growth of the disturbance rather than to be the driving mechanism; thus it cannot be counted upon to break the jet into drops.

A different method for particle formation was suggested by C. Hendricks (1977) and consists in "whipping" the jet as it emerges from the nozzle. Assuming the nozzle tip y_N to move up and down sinusoidally in a small arc 2β, i.e.,

$$y_N = Y_N \sin\omega t$$

and if L is the length of each jet half-wave, the jet will tend to break up at the nodes, being opposed by the surface tension γ. Equilibrium yields

$$\tfrac{1}{2}\left(L\,\frac{\pi d^2}{4}\,\rho\,Y_N\omega^2\cdot\frac{2}{\pi}\right)\sin\beta = \gamma\,\pi\,d$$

where ρ, d are density and diameter of the jet. For small angles β, and since the length L should be approximately particle size,

$$U_{jet}\,\frac{2\pi}{\omega} \sim 2d$$

from which

$$\omega \sim \frac{U_{jet}\,2\pi}{2d} \sim 1 \times 10^7 \text{ rad/sec},$$

or $f \sim 1.6$ MHz.

Replacing $\sin\beta$ by Y_N/ℓ_N yields

$$\frac{Y_N^2}{\ell_N} \sim \frac{4\pi\,\gamma}{d^2\rho\,\omega^2}$$

that can be used to dimension the nozzle and the nozzle vibrating system. This device will tend to produce a "fanning out" of the particles formed; in practice the jet may break up in sections shorter than the half wave length and only those particles close to the jet original axis will be able to continue in a straight trajectory toward the particle selection device.

Particle Integrity. Once formed, the LH_2 particle will keep vaporizing due to convective effects and vapor pressure (if it is lower than the background pressure). During this time aerodynamic forces will tend to distort the shape of the particle and slow it down. If these forces are sufficient large compared to surface tension and/or mechanical strength, they may eventually cause the particle to break into fragments.

The effect of aerodynamic drag on slowdown is very small: i.e., it would take a distance $\sim 10^3$ cm to reduce the particle energy by 10% in a $\sim$50 torr vacuum chamber.

Not negligible instead is the effect of aerodynamic forces on the particle integrity. For a liquid drop of radius R, the drop Weber number

$$We = \frac{\rho_\infty (\Delta U)^2 R}{\gamma}$$

must be less than some critical value, $We_{cr} \sim 10^1$.

In the LH_2 particle case, $We \sim 10^3$; the breakup time t_B is given by (Nicholls, 1972)

$$t_B \sim \frac{R}{\Delta U} \sqrt{\frac{\rho}{\rho_\infty}}$$

of the order of 10^{-5} seconds for 40 torr pressure. At the particle speed this points to a breakup distance $\sim$10 cm.

These estimates are based on the assumptions that surface tension is the only effect keeping the particle together and that the pressure is relatively high. If a crust of solid H_2 ice forms on the surface of the particle, the aerodynamic pressure will be opposed by the ice mechanical strength $\sigma \sim 10^5$ dyne/cm^2 (Roder, et al., 1973). The thickness t_i of the ice shell forming immediately upon vaporization is $\sim \alpha/r$, where α is the liquid thermodiffusivity and r is the surface regression rate (in cm/sec). As it is difficult to estimate the vaporization rate, we may assume for t_i a value of a few percent of the drop radius, which means a few micrometers, a number in agreement with the estimate by Foster (1977). In this case, the force opposing breakup is equal to $t_i \times 2\pi R\sigma = 10^1$ dyne; for comparison, the surface tension would give a force $2\pi R\gamma \sim 1$ dyne. Thus the effect of aerodynamic forces on a freezing particle is less important than for a liquid drop.

The particle breakup problem can be completely solved by passing the particle just formed inside a chamber at a pressure lower than the 40 or 50 torr of the LH_2 triple point. If the pressure in the vacuum chamber is kept at $\lesssim 1$ torr the Weber number becomes ~ 100 and the breakup distance becomes $\sim 10^2$ cm. A third vacuum chamber, with a pressure $\sim 10^{-2}$ torr can definitely prevent the particle from breaking up.

In conclusion, the injection of hydrogen particles of $\sim$ 0.1 cm diameter and 2 km/s will have to proceed in the following way: the LH_2 jet must be broken into particles within 10^1 cm from the nozzle exit. This can be accomplished by "whipping" the jet with $f \sim 1$ MHz. Within 10^1 cm, the particle just formed must go through a planned stepped change in gas density along the particle trajectory; this can be achieved by a properly designed, multichamber vacuum system with interchamber gates synchronized with the jet formation process.

System Design

The liquid hydrogen injection system is composed of five subsystems:

1. The jet source (injector)
2. Instrumentation and control
3. Cryogenics
4. Vacuum system
5. Particle manipulation

A sketch of the complete system is shown in Figure 8.

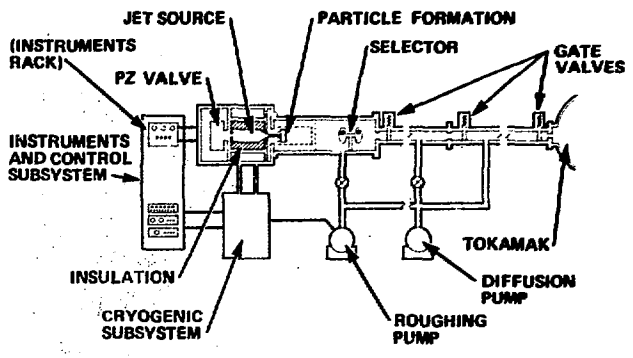

Fig. 8 Tokamak fuleing system schematic.

Jet Source

The jet source is a piezoelectric controlled, fast acting valve which initiates a high pressure liquid hydrogen jet. The jet is broken up into uniform sized droplets, each about twice the jet diameter in size, by a piezoelectric transducer at the end of the jet nozzle. The particles thus formed are frozen by passing through a region of gas at slightly below the liquid hydrogen vapor pressure ($\sim$50 torr). One particle is selected by a pair of rotating disks with appropriately spaced openings. The selected particle passes through drift tubes of lower pressure and into the tokamak plasma. Specifications call for producing a $\sim$1 mm-diameter-H_2 particle with velocity of $\sim$2 km/s repetition rate approximately once per five minutes, and for meeting tokamak interface requirements in terms of size, orientation, gas transfer, etc. Problems examined in the context of the injector design are: thermal and mechanical stresses, LH_2 leaks during injection, and sealing devices.

Thermal and mechanical stresses can be shown to fall well within the range acceptable for standard cryogenic materials (i.e., SS316). More severe are the requirements posed by limits to LH_2 leaks. At a peak pressure of $\sim$2 kbar, and considering the leak through the hydrogen compression piston, the volumetric leak flow rate V is

$$V \sim \frac{\pi r_p}{6\mu} h^3 \frac{\Delta P}{\Delta X}$$

where r_p is the piston radius and h is the gap between piston and cylinder; this gap increases from $\sim$ 2 μm to $\sim$10 μm under stress. The total volume leaked during injection may be then

approximately the volume to be injected, unless special seals or stiffer materials with higher Young's modulus are used. WC is one of such materials; as its modulus is ~ 3 times larger than for stainless steel, the total volume leaked can be reduced by a factor of ~ 27, thus solving the leak problem.

Cryogenics

The cryogenic subsystem is dictated by two requirements: the first, to cool the injector proper to LH_2-compatible temperatures and supply the LH_2 to form the jet; the second to reduce as much as possible the heat exchange between the injector region and the outside environment.

Cooling of the injector can be performed by liquifying H_2 by means of a cryostat and by passing it in a recirculating circuit. The same source provides the LH_2 that under moderate pressure (~ 5 to 6 atm) will be transferred to the injecting portion of the device to form the jet. Thermal analysis, assuming that the injector insulating vacuum chamber is maintained at the LN_2 boiling point, indicates that ~15 watts of refrigerating power at 20°K are necessary for the maintainment of a steady-state regime. This is a modest requirement that can be satisfied by commercially available cryostats.

No special problems are to be expected in the design of the vacuum chambers; at the same time some care is required by the interfacing of their operation with the injection.

Particle Formation and Selection

The function of the particle formation and selection subsystem is to extract a single solid pellet with high velocity from the liquid jet and to transfer the excess hydrogen to the vacuum system for disposal.

Jet Breakup Device. In the injector discharge nozzle, the pressure drops from 1400 bar to less than 2 bar in a few diameters. L/D ratios ~ 50 are in order for jet coherence. Consequently, the nozzle will be about 3-cm-long of which ~10 mm may be thin-walled tube. This tube will vibrate laterally to induce discontinuities in the jet with subsequent formation of particles.

Assuming a sinusoidal displacement of the jet tip and equating the mean accelerating force to the surface tension holding the jet together, we find from a previous section

$$\frac{Y_N^2}{\ell_N} \approx 9 \times 10^{-10} \text{ cm}$$

where Y_N = one half amplitude at nozzle tip and ℓ_N = length of flexible portion of nozzle. With a nozzle length of 10 mm, Y_N is 3×10^{-5} mm. This displacement must be applied at a frequency 1 MHz. The required displacement can be produced by a piezoelectric element of 0.1 inch driven to 20 volts/mil field. This element must have a natural frequency much higher than the frequency of operation. A factor of ten in the resonance frequency can be achieved with a two-element section of ferroelectrically hard ceramic such as PZT8. The PZ element can be excieted with a sinewave high voltage generator given ± 1 kV. A sketch of the proposed configuration is given in Figure 9.

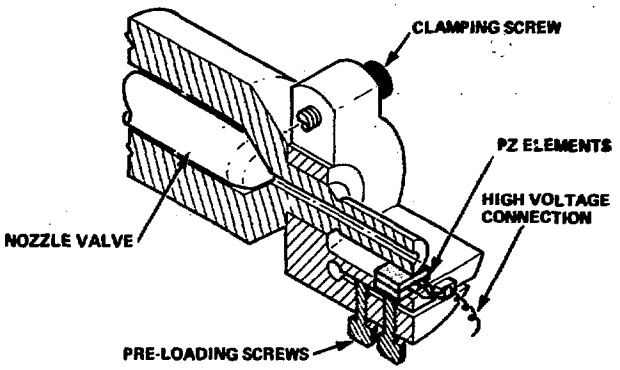

Fig. 9 Sketch of nozzle vibrator.

Pellet Selection. In the pellet selection method studied, two rigidily coupled, 10-cm spaced disks rotate at 750 rpm. Each disk carries a 4-mm-diameter hole at a radius of 7.6 cm. By rotating this assembly, a 1-mm section of jet may be passed through at 2 km/s. Since the repetition times is ~8 ms, the injector firing point may be triggered from the disk rotation to allow the highest velocity portion of the jet to pass through the selection device.

The rejected pellets must be removed from the system as H_2 gas is pumped out of the drift vacuum chambers.

Summary and Conclusions

The production of high velocity particles of hydrogen by piezoelectrically controlled pressure injection has been found to be feasible on the basis of analyses, existing experimental data and an assessment of the necessary technology. By applying known technologies in a new combination, a device can be developed for use in fueling experiments in near term tokamaks such as PDX and Doublet III.

Using the best available equation of state for hydrogen, jet velocities of 2000 m/s can be achieved with pressures of 2000 atmospheres. To prevent freezing of this jet as a solid rod will require a background bas at the nozzle exit with a pressure approximately that of the hydrogen vapor pressure, viz ~ 50 torr. Under these conditions available theories would predict atomization of the jet but recent experiments with turbulent jets under similar conditions tend to indicate that turbulence in the liquid flow stabilizes the jet. Such a jet must be broken over about 10^1 cm into particles. Of several possibilities considered, one is a piezoelectric element at the nozzle exit to couple inertial oscillations into the fluid. The stream of particles formed will be passed through regions of lower gas pressure to cause

them to freeze. A single particle can be selected from the stream by one of several methods, the first choice being a rotating orificed disk.

A conceptual design of a complete fueling device has been made with detailed design of the jet source, which is the major new component in terms of technology. The piezoelectrically controlled valve is state of the art and operates at room temperature. The high pressure cryogenic portion will require careful design, fabrication and testing to achieve the required high precision fits, dimensional stability, and thermal control, but several design and material options are available to accomplish these objectives.

The particle formation systems considered are state of the art. The rotating selector is mechanically straightforward. The remaining subsystems (instrumentation and control, cryogenics, and vacuum) are standard applications of existing technologies. A development plan leading to a fueling device has been examined. It has two main objectives, first to confirm our understanding of the jet behavior, including practical aspects such as the effects of nozzle shape and surface finish upon the pressure drop in the fluid. The second is the development of the device hardware for the complete system. The physics of the jet breakup is a key element which is to be examined further both theoretically and by experiments as soon as possible. This can be started rapidly using simple injection devices and (initially) stand-in fluids from H_2O to liquid N_2. Then small quantities of LH_2 can be used to conduct definitive experiments on jet breakup, while the remaining fluid flow and solidification analyses can be refined and the design of the system can be completed.

Subsequently, a developmental fueling system can be constructed and tested. During this testing period the precise specifications for fueling devices to be delivered to ERDA users would be defined and devices would be designed to meet these requirements.

References

Calliger, R.T., Turnbull, R.T., and Hendricks, C.D., (1977), "Hollow Drop Production by Injection of Gas Bubbles into a Liquid Jet," Rev. Sci. Instr., 48, 7, 846.

Foster, C.A., Kim, K., Turnbull, R.T., and Hendricks, C.D., (1977), "Apparatus for Producing Uniform Solid Spheres of Hydrogen," Rev. Sci. Instr., 48, 6, 625.

Goedde, E.F., and Yuen, M.C., (1970), "Experiments on Liquid Jet Instability," J. Fluid Mech., 40, 3, 445.

Goodman, R.K. and Hunt, A.L., (1976), "Ammonia-Pellet Generation System for the Baseball II-T Target Plasma Experiment," LLL preprint UCRL-78611.

Goren, S.L. and Wrongski, S., (1969), "The Shape of Low Speed Capillary Jets of Newtonian Liquids," J. Fluid Mech., 25, 689.

Gralnick, S.L. (1973), Nucl. Fusion 13, 703.

Hendricks, C.D. (1977), consulting communication, August 12.

Jorgensen, et al., (1975), Plasma Phys. 17, 453.

Kim, K., et al., (1976), Bull. Am. Phys. Soc., 21, 1052.

Mills, R.L., Liebenberg, D.H., Bronson, T.C., and Schmidt, L.C., (1977), "Equation of State of Fluid N-H_2 from P-V-T and Sound Velocity Measurements to 20 Kbar," J. Chem. Phys. 66, 7, 3076.

Parks, P.B. (1977), Nucl. Fusion 17, 539.

Rayleigh, Lord (1878), Proc. Lond Math. Soc., 10, 4.

Rayleigh, Lord (1879), Proc. Royal Soc. Lond., 29, 71.

Reitz, R. and Bracco, F.V., (1976), "Breakup Regimes of a Single Liquid Jet," paper presented at Fall Meeting of Combustion Institute, Eastern Section, November 18-19, 1976, Drexel University, Philadelphia, PA.

Reitz, R., (1977), private communication, September 14.

Roder, H.M., Childs, G.E., McCarty, R.D., and Angerhofer, P.E., (1973), "Survey of the Properties of the Hydrogen Isotopes Below Their Critical Temperatures," NBS Technical Note 641.

Rose, D.J. (1968), "On the Fusion Injector Problem," Culham Technology Division, Memo. No. 82.

Schleicher, C.A. and Tribus, M., (1956), "Heat Transfer in a Pipe with Turbulent Flow and Arbitrary Wall-Temperature Distribution," Preprint of paper presented at the 1956 Meeting of Heat Transfer and Fluid Mechanics Institute, Stanford, CA., June 21-23.

Schlichting, H., (1968), Boundary Layer Theory, McGraw-Hill Book Company, New York, N.Y.

Schneider, T.M. and Hendricks, C.D., (1964), "Source of Uniform-Sized Liquid Droplets," Rev. Sci. Instr. 35, 10, 1349.

Spitzer, L., et al., (1954), "Problems of the Stellerator as a Useful Power Source," NYO-6047 USAEC.

Vaslow, D.F., (1976), General Atomic Report, GA-A13659.

Young, C., (1977), "Rock Breakage with Pulsed Water Jets," paper presented at the Energy Technology Conference and Exhibit, Houston, Teas, September 18-22, ASME paper 77-PET-78.

LINEAR RESONANCE ACCELERATION OF PELLETS

Robert G. Mills
Princeton University
Princeton, New Jersey 08540

ABSTRACT

A possible requirement for the acceleration of macroscopic pellets to velocities exceeding 10^4 meters per second implies the development of new apparatus. A satisfactory approach might be the linear resonance accelerator. Such apparatus would require the charging of pellets to very high values not yet demonstrated. The incompatibility of phase stability with radial stability in these machines may require abandoning phase stability and adopting feedback control of the accelerating voltage to accommodate statistical fluctuations in the charge to mass ratio of successive pellets.

Introduction

Figure one, drawn from the report on Princeton's reference design for a fusion reactor[1] predicts that a pellet velocity of 5×10^4 m/sec would be necessary to penetrate that large plasma. The model was conservative, and it is quite conceivable that lower velocities will suffice. It is only prudent, however, to consider what the implications might be should it develop that it is really necessary to accelerate large pellets (1 mm radius) to velocities exceeding 10^4 meters/second.

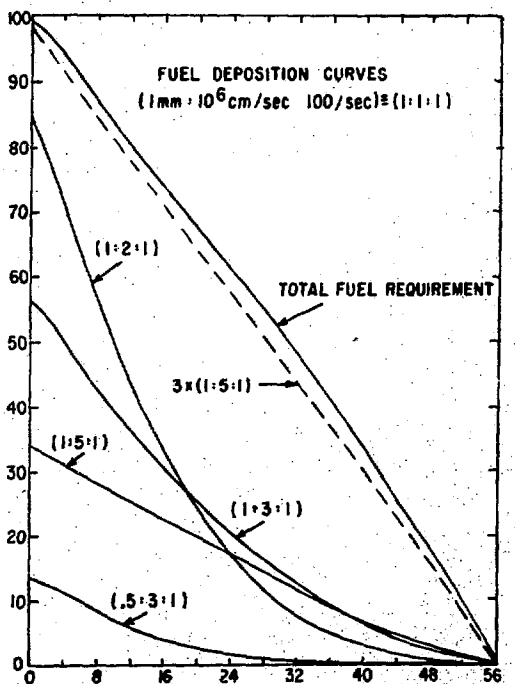

Fig. 1. Requirement curve for PRDM and several fuel-deposition curves generated by hypervelocity ballistic injection.

To accelerate charged pellets of this size to those velocities electrically in apparatus of reasonable size is a rather formidable undertaking. The charge must be as large as possible to minimize the equivalent voltage difference which is quite large in any case. If we have a pellet of specific gravity ρ, radius r (in mm), charged to within a safety factor k_E of an ultimate limit (discussed below), and accelerated through a potential drop of V megavolts, its final velocity in units of 10^4 m/sec is given by

$$v = 0.0728 \left(\frac{V}{k_E \rho r} \right)^{1/2} . \qquad (1)$$

This relation is plotted in Figure two for a pellet of density equal to that of liquid DT.

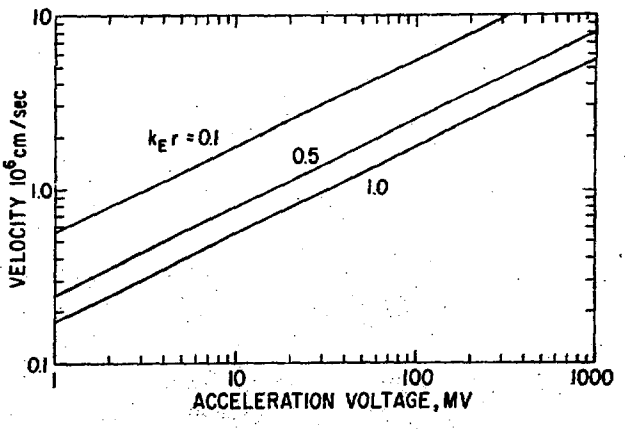

Fig. 2. Velocity as a function of accelerating voltage for several pellets.

The (e/m) ratios of these pellets are so small, and the velocities such that magnetic forces will be less than one percent of electric forces, suggesting purely electrostatic acceleration. Although the large voltages required introduce technical difficulties, the large mass and low velocities compared to those encountered in particle accelerators provide opportunities not available to designers of accelerators of nuclei. For example, the rf power amplifiers will operate at frequencies in the neighborhood of 50 kilohertz, and the transit time of the pellet through the apparatus can be 10^{-2} seconds or longer permitting detection of the position of the particle in the machine as a function of time with appropriate feedback control of the accelerating potentials.

For orientation it is convenient to consider one specific example of such a machine. It is diagrammed in Figure 3. This design is to accelerate pel-

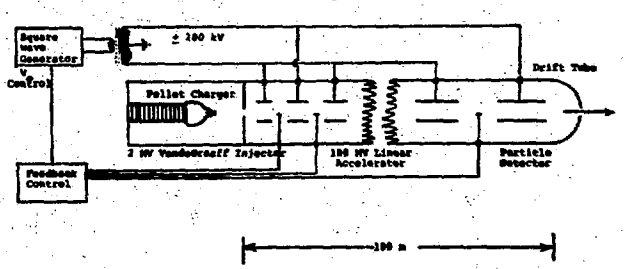

Fig. 3. Machine schematic.

lets, 0.39 mm in radius, weighing 5×10^{-8} kg of frozen DT thinly coated with a metallic shell to a final velocity of 1.86×10^{4} m/sec. The e/m ratio of this pellet is 1.73 coulomb/kilogram (cf. 4.82×10^{7} C/kg for deuterons and alpha particles). Techniques for charging droplets [2] commonly produce e/m ratios of 10^{-3} - 10^{-4} C/kg. The machine is about 100 m long, is driven at 50 kilohertz with a 100 kV switching circuit and produces pellets charged to 2 MV by a small Van de Graaf injector. The average accelerating field is 10 kV/cm. Table I lists various pertinent parameters. The pellet detectors are located midway between the drift tubes in the virtual ground plane to minimize pickup from the drift tubes and detect the passage of the pellet by electrostatic induction. The outputs from the pellet detectors are used to monitor the velocity gain of the pellet and control the accelerating potential.

Table I

Pellet and Pellet Accelerator Typical Characteristics

Pellet Data:	
Composition	Metallic coated frozen DT
Equivalent Specific Gravity	0.2
Mass	5×10^{-8} kg
Radius	0.39 mm
Charge Data:	
Charge on Pellet	260 statcoulombs
	8.67×10^{-8} coulomb
Surface Field Strength	5.13×10^{7} volts/cm
Safety Factor, k_E (see Eq. 1)	1.95
Pellet Potential	2×10^{6} volts
e/m	1.73 coulombs/kilogram
$k_E r$ (see Eq. 1)	0.76
Linear Resonance Accelerator:	
Length	100 m
Average Accelerating Field	10 kV/cm
Nominal Equivalent Potential	100 MV
Injection Velocity	2.6×10^{3} m/sec
Final Velocity	1.9×10^{4} m/sec
Driving Frequency	50 kHz
Accelerating Time	0.01 second
Number of Drift Tubes or Apertures	~ 1000

Charging of Pellets

It should be noted that the apparatus proposed here would be limited to the acceleration of pellets, not of droplets. Charged droplets of liquids are in a state of unstable equilibrium as first pointed out by Lord Rayleigh, [3] and they will explode when charged to only a few thousand volts. To achieve the very high charges visualized here, they must be frozen so that their shear strength will resist deformation. It is also proposed here to coat them with a conductor to facilitate their charging.

The maximum electric fields that can be placed on metals has been investigated by Müller. [4] He has charged tungsten to about 5×10^{8} volts/cm, but for most materials 10^{8} is a practical limit. We adopt a safety factor k_E such that the surface field strength is $10^{8}/k_E$ volts/cm. The low mechanical strength of solid hydrogen is another reason for coating the pellet with metal in order to withstand the stresses of large surface electric fields. The pellets must be formed first and then charged. A suitable procedure is illustrated in Figure 4. Prepared conducting microspheres are pushed out from the high voltage electrodes on a needle. Charge flows onto the sphere along the needle, and the unbalanced electric force accelerates the sphere away from the needle, but as separation takes place, the needle is more rapidly accelerated (mechanically) back into the shield while the sphere is still close enough to shield the needle from the high potential gradient that would otherwise trigger a discharge from the needle tip.

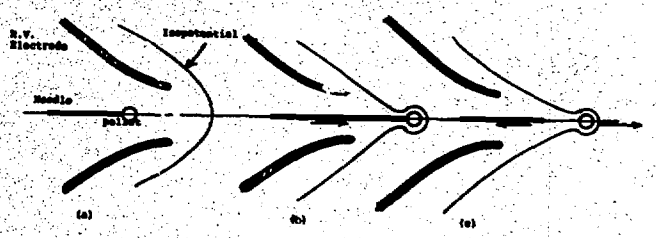

Fig. 4. Charging of pellets to high voltage.

Trajectory Stability of Linear Resonance Accelerators

The type of machine proposed here was first conceived by Wideröe[5] and developed by Sloan and Lawrence.[6] The problems of radial stability (focusing) vs phase stability (uniform acceleration of all entering particles) in electrostatic accelerators were appreciated promptly; see, for example, Zworykin et al.[7] E. M. McMillan found a general proof of this incompatibility in 1945, but did not publish it until 1950.[8] A simplified version of his argument for paraxial trajectories in cylindrically symmetric electrostatic accelerators follows.

The equilibrium trajectory is the z axis of a cylindrical accelerator equipped with drift tubes. We consider a slightly idealized version of a single cell between two tubes both of length equal to twice the interelectrode gap excited by a nominally square voltage wave. This is shown in Figure 5. The particle moves at synchronous speed so that the voltage waves and E-field waves shown are those seen by the particle at each point in space.

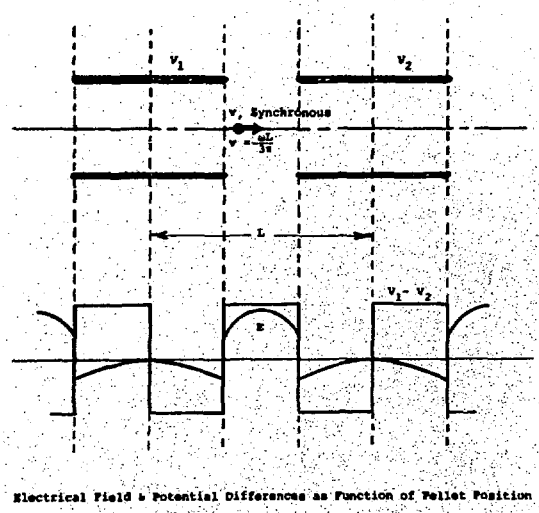

Fig. 5. Single cell of accelerator is of length L.

To reduce the overall length of the apparatus, it will probably prove desirable to replace the drift tubes with simple apertures as illustrated in Figure 6. Sloan and Lawrence[6] decided against this approach, saying it would reduce the voltage gain per gap to about 63%, but if the alternate is a drift tube a full cycle in equivalent length (see Figure 5), the apertures are probably preferable. The length of the accelerating cell, L, in a Wideröe machine is given by

$$L = \frac{\pi v (2k+1)}{\omega} \quad , \quad k = 0, 1, 2$$

Figure 5 shows a system of k = 1. Figure 6 shows a system of k = 0. Sloan and Lawrence also used k = 0, but had the gaps narrow, most of the length devoted to the drift tube. This makes high voltage differences difficult.

Due to various imperfections no particle will remain precisely on the axis; therefore we are concerned with restoring forces in the radial direction as a particle departs from the axis, where, by symmetry, $F_r = e E_r = 0$. To first order, $F_r = -\alpha r$,

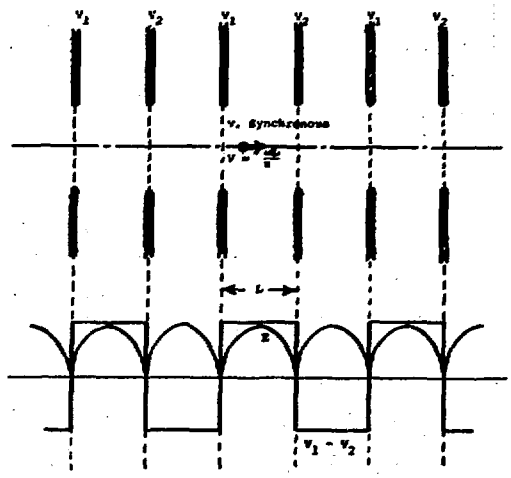

Fig. 6. Use of apertures instead of drift tubes.

and the average of F_r over a cycle must be towards the axis ($\bar{\alpha} > 0$) if the trajectory is to be bounded. It follows from $\nabla \cdot \bar{E} = 0$ that, near the axis of a system of cylindrical symmetry

$$E_r = -\frac{r}{2}\frac{\partial E_z}{\partial z} \quad ,$$

and

$$\frac{\partial E_r}{\partial r} = -\frac{1}{2}\frac{\partial E_z}{\partial z} \quad .$$

Let us calculate the average value of α over the unit cell:

$$\bar{F}_r = \frac{1}{L}\int_0^L e E_r \, dz$$

$$\bar{\alpha} = -\frac{\partial \bar{F}_r}{\partial r}$$

$$\bar{\alpha} = \frac{e}{L}\int_0^L -\frac{\partial E_r}{\partial r}\, dz = \frac{e}{L}\int_0^L \frac{1}{2}\frac{\partial E_z}{\partial z} \quad . \qquad (2)$$

We are considering the radial force acting on the particle moving down the tube at a velocity v = dz/dt. Therefore

$$\frac{\partial}{\partial z} \equiv \frac{d}{dz} - \frac{1}{v}\frac{\partial}{\partial t}$$

allowing us to write (2) as

$$\bar{\alpha} = \frac{e}{2L}\int_0^L \frac{\partial E_z}{\partial z}\, dz - \frac{e}{2Lv}\int_0^L \frac{\partial E_z}{\partial t}\, dz$$

$$\bar{\alpha} = \frac{e}{2L}\left(E_z(L) - E_z(0)\right) - \frac{e}{2Lv}\int_0^L \frac{\partial E_z}{\partial t}\, dz \quad . \qquad (3)$$

By symmetry (see Figure 5) the first term is zero. For radial focussing $\bar{\alpha}$ must be positive, requiring the second term to be negative. We can interpret the second term in terms of the energy, W, gained in crossing the gap.

$$W = e \int_0^L E_z \, dz$$

If E_z is not constant in time, this will depend on the time of entry, t_e, of the particle into the acceleration cell, and the resulting change in energy gain will be given by

$$\frac{\partial W}{\partial t_e} = e \int_0^L \frac{\partial E_z}{\partial t} \, dz \quad .$$

Thus

$$\bar{\alpha} = - \frac{1}{2Lv} \left(\frac{\partial W}{\partial t_e} \right) \quad . \qquad (4)$$

The property of phase stability provides for automatic correction of v_z en route by giving less acceleration to fast particles and more acceleration to slow particles, i.e., $\partial W/\partial t_e$ must be positive (greater W for late arrivals). But (4) shows that this property implies a negative $\bar{\alpha}$, or radial instability. This dilemma is met in the design of linear particle accelerators by placing a foil over the entrance to the drift tube to allow a positive contribution to $\bar{\alpha}$ from the first term on the right of (3). Energetic charged particles lose little energy in traversing the foil. In some cases grids have been used, but the transparency must be very high if there are very many drift tubes. Neither is possible for our application. Since we must have radial stability to keep our trajectories bounded, we shall excite the drift tubes with drooping square waves as illustrated in Figure 7. Thus $\partial W/\partial t_e$ is negative, and radial focussing is provided. At the low frequencies contemplated such wave shaping can be produced as demonstrated by Mills.[9] The simple modification of his circuit in Figure 7 provides the required wave shape.

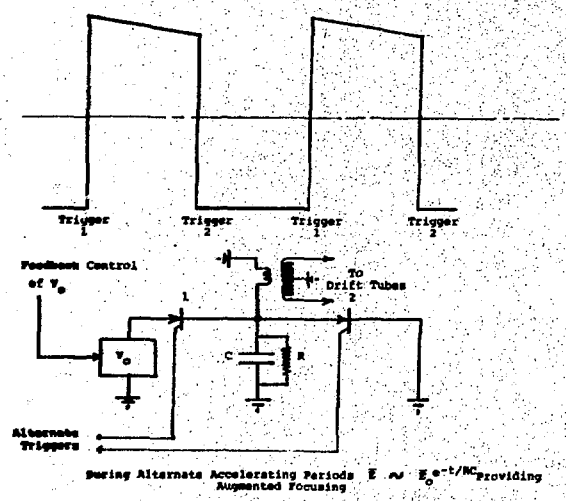

Fig. 7. Voltage wave generation and control.

Having abandoned phase stability one would wonder how any particle could be fortunate enough to find its way through a substantial portion of the machine before getting out of step. The nuclear particle accelerator designer is at least presented with particles of precisely defined (e/m). We shall be faced with presumably small but nevertheless finite variations in (e/m). Complete passage would indeed be impossible if we were not dealing with such massive and slow (by linear accelerator standards) particles that feedback control can be accomplished. Figures 6, 7, and 3 illustrate the system. The passage of the particle is detected by electrostatic probes located adjacent to the trajectory. They are located in the virtual ground plane between two drift tubes and are not sensitive to the driving voltage. The accelerating voltage supply, V_o, is initially set high enough to accelerate the lowest (e/m) particles expected through the system. Most particles will be accelerated somewhat more rapidly, and the times of the detected passages are interpreted by the feedback electronics to reduce the applied voltage to the proper value to carry the particle through the system synchronously.

Work Done To Date

In addition to the work reported here, Davis[10] has been investigating particle trajectories to determine the radial excursions to be expected in practical devices. Preliminary indications are that such a machine need not be extremely large, but the acceptance cone may turn out to be inconveniently small. Note added after conference: In the discussion following the presentation of this paper, the author's attention was called to work of very similar nature in the acceleration of iron particles by Friichtenicht and associates.[11, 12]

These workers used a 92 drift tube machine to accelerate micron diameter microparticles to 3×10^4 m/sec in a reliable manner. The principal difference is their control of frequency whereas we propose feedback control of accelerating voltage. Their experience suggests this approach to have merit.

Acknowledgment

This work was supported in part by the Department of Energy Contract EY-76-C-02-3073.

References

[1] A Fusion Power Plant, R. G. Mills, ed., Princeton Plasma Physics Laboratory Report MATT-1050 (1974).

[2] R. K. Goodman and A. L. Hunt, Rev. Sci. Instr. 48, 176 (1977).

[3] Lord Rayleigh, Phil. Mag. XIV, 184 (1882).

[4] E. W. Müller, Phys. Rev. 102, 618 (1956).

[5] R. Widerõe, Arch. F. Elektrot. 21, 387 (1928).

[6] D. H. Sloan and E. O. Lawrence, Phys. Rev. 38, 2021 (1931).

[7]V. K. Zworykin et al., Electron Optics and the Electron Microscope (John Wiley and Sons, Inc., New York, 1945) pp. 660-664.

[8]E. M. McMillan, Phys. Rev. 80, 493 (1950).

[9]R. G. Mills, Princeton Plasma Physics Laboratory Report TM-181 (1963).

[10]C. A. Davis, private communication.

[11]D. G. Becker, J. F. Friichtenicht, B. Hamermesh, and R. V. Langmuir, Rev. Sci. Instr. 36, 1480 (1965).

[12]J. C. Slattery, D. G. Becker, B. Hamermesh, and N. L. Roy, Rev. Sci. Instr. 44, 755 (1973).

SUMMARY OF FUELING BY PELLET INJECTION

L. D. Stewart, Exxon Nuclear Company
on assignment at Princeton Plasma Physics Laboratory
Princeton, N. J. 08540

Pellet-Plasma Interaction

Model-based studies were presented which indicated in all cases that shielding will occur, but there was not total agreement in these studies on the mechanism of the shielding. The data from the pellet ablation experiment on ORMAK was explained by considering the plasma electron flux, incident on the pellet surface, to create an ablated neutral cloud which self-consistently attenuates the incident electron flux. The lack of total agreement in the studies comes about when extending this to tokamak reactor plasmas. Various groups contended either that this mechanism would continue to dominate in reactor plasmas, or that it would be modified by a comparable heat flux from alphas, or that it would be modified somewhat by electrostatic shielding because of electron flux induced charge buildup on the pellet, or that it would be modified by ionization of the neutral cloud yielding a plasma cloud shield, or that this same plasma cloud would exclude magnetic field causing deflection of the incident electron flux and therefore additional shielding.

For tokamak reactors, depending on the reactor design chosen and on the model chosen, the predicted required pellet velocities range from ~ 5×10^5 cm/ sec to ~ 5×10^6 cm/sec for pellet diameters ranging from ~ 1 mm to ~ 10 mm. ORNL simulation studies of a tokamak plasma being fueled by pellets indicated that deep penetration may not be required and therefore the lower end of the velocity range might be sufficient. The predicted range of velocities is important because it goes from difficult at 5×10^5 cm/sec to possibly not feasible at 5×10^6 cm/sec.

Experiments

Formation and acceleration of pellets or liquid jets requires a knowledge of the physical properties of solid and liquid deuterium and tritium. Although a program is in progress at LLL to determine the properties of solid and liquid H_2, D_2, T_2, and DT, most available data is for H_2, and even this is not nearly complete. It is expected that fairly accurate extrapolations can yield D_2 from H_2 data, but extrapolations to T_2 and DT data, because of β-decay, are not straightforward. Beta particle ionization is predicted to increase electrical conductivity by as much as 10^6, and β-induced radiation damage is predicted to degrade thermal conductivity by as much as 10^5, to cause hardening and brittleness, and possibly to cause an increased vapor pressure at 4K. It was noted that DT is actually a mixture of D_2, DT and T_2 which will fractionate during freezing.

Three sets of experiments were reported involving pellet-plasma interactions. At ORNL, hydrogen pellets were injected into the ORMAK tokamak with velocities of 10^4 cm/sec. Pellets with 70 μm dia. had lifetimes of 420 μsec while pellets with 210 μm dia. had lifetimes of 850 μsec. The penetration of the larger pellets was to a position where the plasma had T_e ~ 80 eV and $n_e = 2$ to 5×10^{12} cm^{-3}. The observed pellet lifetimes, and the ablation rates and distribution of mass in ablated hydrogen cloud as a function of pellet position, were found to be in good agreement with shielding of the energetic plasma electrons by ablated neutral hydrogen molecules. A 75% shielding effect was inferred. A deflection of the pellet from its injection path was noted and attributed to a rocket effect due to an anisotropic electron flux. The largest pellets, which contained about 1% of the total particles contained in the plasma, did not affect the tokamak discharge.

At Garching, deuterium rods 600 μm long and with a 350 μm dia. were dropped into the Pulsator tokamak, then the tokamak discharge was initiated. A 450 μsec lifetime was observed along with a cloud expansion velocity of 2.5×10^6 cm/sec. The plasma electrons had T_e ~ 10 eV and n_e ~ 10^{13} cm^{-3}. The pellets contained ~ 100% of the total particles contained in the plasma, and n_e was in fact observed to double after pellet injection. Larger pellets caused the plasma to disrupt, implying that this 100% refueling per pellet may be an upper limit on pellet size. The observed pellet ablation did not agree well with the neutral shielding model, but it was felt that the significant energy flux of runaway electrons during discharge initiation caused the disagreement.

At Risφ, hydrogen cylinders 250 μm long and with a 250 μm dia. were put into the Puffatron EXB discharge apparatus. A discharge was then initiated which for 5 μsec had n_e ~ 4×10^{14} cm^{-3}, T_e ~ 20 eV, an EXB velocity of 2×10^7 cm/sec, and for the ions a maximum energy of 400 eV. The energy flux to the pellet was due mainly to the ions, and, as on ORMAK, a pellet deflection was observed which was attributed to the anisotropy of the flux. The pellets were not totally ablated in this experiment. An energy input per ablated atom of ~ 0.2 eV and an ablation cloud expansion velocity of ~ 2×10^6 cm/sec were observed. The observations were not inconsistent with the neutral cloud ablation models.

Acceleration Techniques

Studies were described on four different techniques for acceleration of pellets to

velocities suitable for future research tokamaks and tokamak reactors.

ORNL reported that after a survey of all known ideas for pellet acceleration, the rotating arbor technique and the gas gun technique were selected as having the best combinations of feasibility and ultimate achievable velocities. From the survey, it was concluded that size was easier to come by than velocity, so pellets containing 10 to 50% of the fuel load should be used.

A rotating arbor uses centrifugal acceleration to throw out a pellet after 90 - 100°, with the exact angle being independent of pellet mass and arbor rotational frequency and dependent on the loading position. The ultimate pellet velocity is limited by the arbor strength/weight ratio and is ~ 5×10^5 cm/sec. The device is inherently capable of tens to hundreds of pellet accelerations per second. The stored energy of the rotating arbor is high, and a thick, steel-walled containment vessel is required. An arbor has been built and accelerated to a tip speed of 5×10^4 cm/sec, which is projected to yield a pellet velocity of 1×10^5 cm/sec. A gas gun is being built which will use high-pressure hydrogen to accelerate a pellet to 8×10^4 cm/sec. The gas gun is difficult to extrapolate beyond 10^5 cm/sec and beyond single-shot capability, but its relative simplicity makes it attractive for near term experiments. It is expected that both of the acceleration devices will be applied to the ISX tokamak and may be applied to the PLT and PDX tokamaks.

Physics International reported studies of tokamak pellet fuel accelerators based on gas guns and on liquid jets. It was pointed out that the military has spent years investigating techniques for acceleration of particles to hypervelocities, techniques including electromagnetic, plasma, and electrostatic acceleration, and that the 2-stage gas gun has survived the investigations. A 2-stage gas gun has accelerated a 2 gm metallic particle to 1.2×10^6 cm/sec. Although no H, D, or T acceleration has been done, it was projected that the acceleration of one milligram particles of such materials to 6×10^5 cm/sec could be done in a straightforward manner. A device capable of more than single-shot would be a problem, and a continuously operating device might not be possible. It was suggested that because a single-shot device is only ~ 40 cm long, there would be room for multiple single-shot systems and that this might satisfy the requirements for near-term research tokamaks.

Liquid jets was reported as a technology which had achieved 5×10^4 cm/sec, with 0.1 to 0.5 mm dia. jets of diesel fuel. Using simple density scaling or using more detailed calculations or simulations indicates 2×10^5 cm/sec jets of liquid hydrogen should be attainable. Experimental verification is needed, as is experimental verification of jet stability, of the ability to break up the jet into correctly sized liquid particles, of the integrity of these particles, of the ability to freeze these particles, and of a pellet selection mechanism such as rotating discs.

PPPL reported a study of an electrostatic accelerator, which, although bulky and expensive, may be the only way of getting to $\geq 10^6$ cm/sec should that be required. It was proposed that a metal coating on the pellets be used to hold the charge. An initial design uses a 100 m, 100 MeV accelerator to yield a velocity of 2×10^6 cm/sec, with higher velocities requiring more length. The incompatibility of phase stability and radial stability in such a device would be circumvented by providing feedback control in lieu of phase stability.

TECHNOLOGY ASSESSMENT

Chairman: H. S. Cullingford
(Department of Energy, U.S.A.)

AN ASSESSMENT OF FUSION FUELING TECHNOLOGY

G. W. Stuart

Laboratory for Applied Plasma Studies
Science Applications, Inc., La Jolla, CA 92037

Introduction and Summary

We have performed an assessment on the status of fueling technology as of the Spring of 1977. Hence more recent developments, such as may be reported at this meeting, are not included in the survey. The yardstick used to measure the adequacy of refueling technology is whether or not it appears possible at present (and with what risk factor) to develop equipment (on a timely basis) to achieve the quantitative refueling requirements of: firstly, future large scale experiments, and finally, of power reactors. The assessment covered the range of different magnetically confined fusion machine types.

The conclusions of the assessment are summarized as follows:

- Refueling may be by neutral beams, plasma guns, gas blankets, or by pellet injection. The two dichotomies that control the difficulty of refueling are between pulsed and steady state (much longer than the particle confinement time) operation, and between open and closed magnetic geometries. Substantial difficulties in refueling are envisaged only for steady state, closed geometry machines; that is, for tokamak, EBT, stellerators, and machines of similar ilk.

- Mirror machines require special comment. Because in mirrors the neutral beam particle injection energy essentially equals the plasma ion temperature, the neutral beam heating source simultaneously satisfies the refueling requirements.

- There is no assurance at present that tokamak (and EBT) can be refueled. Refueling a tokamak EPR with neutral beams, which must have particle energies of 100's-of keV to penetrate the plasma results in a beam heating power several times that for the fusion alpha power. This implies a huge circulating power and a machine that is possibly endothermic, or else has a severely limited energy multiplication. Refueling with gun injected plasma may be possible, but a scientific data base is lacking that such plasma will penetrate tokamak (or EBT) closed magnetic geometry, and then be trapped within the machine plasma. We suggest that modest experiments be performed to determine such behavior. Insofar as gas blanket refueling is concerned, some present tokamak experiments show anomalous refueling by gas blankets. Since the mechanisms underlying gas blanket refueling are not known, (however, explanations based on the Ware pinch have had some success), it cannot be predicted whether they will remain effective in the much larger, higher temperature, EPR regime. It seems likely that, if at all, gas blanket refueling would continue to be effective in an Alcator-type EPR because of its small plasma dimensions, and because operating conditions in such a reactor would be less of an extrapolation from present experiments than for a main line EPR. This leaves as a refueling possibility only pellet injection.

- If the most optimistic predictions on the ablation rate of D-T ice pellets in hot plasma pertain, then the pellet velocities required for it to reach the plasma center region before disappearing can probably be attained; however, there is no assurance that the pellets will remain intact and solid (the melting point of hydrogen is about 15°K) during the acceleration and injection processes. If the median or more pessimistic estimates of ablation rates pertain, then it is extremely unlikely, based on experience obtained during a plethora of Department of Defense programs to produce hypervelocity pellets, that adequate pellet velocities can be attained within the foreseeable future.

Discussion

The essential dichotomies on refueling are between pulsed and steady state or quasi-steady state machines, and between open and closed magnetic geometry machines. A "quasi"-steady state machine is one in which the burn time substantially exceeds the particle confinement time. Tokamak operation is anticipated to be quasi-steady state.

For short pulsed machines, such as linear confinement schemes and toroidal theta pinches operated in such mode, the refueling problem is minimal. After each burn pulse the cold residual plasma is pumped out and fresh D-T gas valved in. The technology problems have to do with pumps and valves. There are also scientific problems on just how the burning plasma is to be non-destructively quenched, but these are outside the present scope.

Refueling of linear confinement devices that operate steady state also appears to be doable. Plasma guns of the deflagration type, or other, can be used to inject plasma along the open field lines at the end. More likely, neutral gas can be introduced through valves penetrating the first wall that are spaced along the machines' length. The small plasma radius, a few centimeters for proposed machines, allows the injected particles, after ionization, to penetrate to the center even with classical transport processes.

Mirror reactors of say the MX-type are open geometry, steady state machines that require special consideration. In order to break even ($Q > 1$) such

machines must have ion temperatures greater than about 200 keV. The electron temperature is an order of magnitude lower. The ion and energy confinement times are essentially equal; hence the refueling and heating are simultaneously taken care of with neutral beams, which because they must have particle energies greater than 200 keV have to be of the negative ion type in order to have reasonable power efficiency. In order to start the machine a plasma is gun injected through the mirror; this acts as the initial target for the neutral beam. (In mirror experiments, such as 2-X, the plasma is sometimes created sans neutral beams by gun injection alone; the gun injected plasma is trapped and compressively heated by increasing the field magnitude; this procedure is not adequate nor practical for reactors.)

Finally, we come to the machines where serious refueling problems may exist; steady (or quasi-steady) state machines with closed magnetic geometry. These include tokamak, stellerators, and EBT. Recalling that charged particle beams cannot be used to refuel closed magnetic geometry, the possible refueling techniques for such machines are:

(1) neutral beams,
(2) gas blanket refueling,
(3) plasma guns,
(4) hypervelocity pellets.

Each of these are discussed in the following subsections.

Neutral Beams

Fueling tokamak or EBT reactors with neutral beams does not appear to be practical. In order to penetrate into a typical EPR plasma the deuteron energy must be in the range of 200 to 400 keV, and triton energies must be half again as large. (A recent suggestion by Jassby [PPPL] to trap ionized beam particles between induced field ripples and let them perform a toroidal drift into the plasma interior may, if it proves feasible, cut the particle energy requirements for penetration by a factor of two or more.) Now, counting nuclear events in the blanket the energy release per fusion is about 20 MeV. But in typical reactors only 2-5% of the ions fuse, the others leak out. If we say that it requires 500 keV to inject a D-T pair by neutral beam, take a 5% fuel burnup, assume that the blanket heat is converted to electricity with a 1/3 thermodynamic efficiency, and assume that electric power is converted to neutral beam power with an efficiency of 0.5, then the electrical multiplication of a neutral beam fueled tokamak or EBT is limited to be less than

$$Q_e = \frac{\text{output power}}{\text{input power for fueling}} = \frac{1}{3}\,\frac{(20\ \text{MeV})(.05\ \text{burnup})}{2\ (0.5\ \text{MeV})} = \frac{1}{3}$$

Instead of an energy source tokamaks are now energy sinks. With minor modifications, replacing heat engine recovery of leaking plasma energy with direct conversion recovery, this result carries over and shows why at best mirror reactors have $Q_e \approx 1$.

Although the argument in the preceding paragraph is lethal, except perhaps for a fusion-fission hybrid, there is still another extremely serious difficulty with refueling tokamaks using neutral beams. This is, the beam energy is set by penetration considerations (but see Jassby's suggestion, above). This energy is not needed for heating the plasma, indeed, it exceeds the fusion alpha power by a typical factor of 2 to 5, and overheats the plasma.

Gas Blanket Refueling

This is the best refueling approach of all if nature permits it. A dilute neutral gas blanket lies between the plasma and the first wall. This blanket may in part originate from the leaking plasma ions which neutralize on the wall. Gas atoms penetrating the plasma are ionized by impact processes and charge exchange, the resulting ions diffuse through the plasma. For gas blanket refueling to succeed the inward flux of particles through each surface within the plasma must approximately equal the outward flux. (The small imbalance of these rates determining the global increase or decrease in plasma density.) Older calculations using known plasma processes predict that gas blanket refueling will not work; the ions created near the plasma boundary cannot effectively diffuse to the central regions. However, experiments performed on, inter alia, Ormak, Alcator, and T-10 indicate that these tokamaks are refueled by the gas blanket since the discharges persist much longer than the particle confinement times.

The question is then, what processes are responsible for gas blanket refueling. Recent calculations at ORNL and PPPL which invoke both a higher injection velocities for neutrals (recycle off the wall) and the Ware pinch, a neoclassical effect, do succeed in predicting refueling; some aspects of these calculations are controversial. In any event, the present experiments are performed with low temperature collisional plasmas (electron temperatures from 1 to 2 keV) confined within small (minor plasma radius from 10 to 60 cm) machines. The question is whether the (probably) unknown mechanisms responsible for the anomalous gas blanket refueling observed in present experiments will continue to be effective for refueling large machines containing thermonuclear plasma. This is a scientific question, and its answer is unknown. If nature is kind, and gas blanket refueling of reactors is possible, then present concern on refueling tokamak reactors is a chimera and no special technologies will have to be developed. If gas blanket refueling is to work for tokamak reactors, it is most likely to work for an Alcator-type because of: (1) the small plasma radius, and (2) the nearness of the reactor regime to the present experimental regime.

Gas blanket refueling may be substantially affected by pumping the plasma chamber to remove ash (alphas) and impurities. Of course, the pumping may be simultaneous with a feed of pure D-T gas. In this sense divertors are pumps since they remove ions leaking from the plasma from the plasma chamber (such ions cannot neutralize at the walls and recycle back into the plasma).

Plasma Guns

Plasma guns of the Marshall or deflagration types may provide a means to refuel closed geometry machines. Such guns provide remarkably pure plasma with energies up to about 10 keV. However, it is uncertain if the gun injected plasma can penetrate the closed magnetic geometry and then be trapped in its interior. Until such scientific questions are answered the technology development of large guns for refueling is not warranted. If the scientific answers, when found, are positive, then it seems certain that the necessary hardware can be developed.

Pellets

In this procedure high velocity pellets of D-T ice are periodically injected into the plasma. Once in the plasma the pellets rapidly ablate due to the impinging flux of energetic plasma particles. The physics is the same as for a missile reentry vehicle heat shield; the material already ablated off the pellet forms a protective layer that reduces the ablation rate at the pellet's surface. The cryogenic pellet refueling scheme is based on getting the pellet to survive to the vicinity of the plasma center. Obviously, the larger the pellet and the higher its velocity the greater its penetration distance before it disappears. There is a limit on pellet size; if it is too large it will produce substantial cooling of the plasma, even extinguishing an ignited plasma. If, to get a feel for the problem, we stipulate that the pellet can contain no more than one-half the fuel particles in the tokamak that it is being injected into, then for a plasma density of $10^{14}/cm^3$ the pellet radius is limited to

$$r_p = 5.2 \times 10^{-3} a A^{\frac{1}{3}} = 7.8 \times 10^{-3} a \text{ (cm)}$$

where a is the plasma minor radius and A the aspect ratio; in the form on the right A = 3.5 .

Ablation rates for D-T pellets in thermonuclear plasma have been calculated by Tonks, Rose, Gralnick, Vaslow, and others. Their results are shown in Figure (1), which relates injection velocity, pellet radius, and penetration distance. Figure (1) can be combined with the equation above limiting r_p, and by assuming the penetration distance should be equal to the minor radius the required injection velocity is found. These are shown in Table 1 for the most optimistic and pessimistic curves in Figure (1); Gralnick's and Vaslow's pessimistic bound, respectively. It should be noted that Vaslow's calculations are the most recent and complete.

It has been proposed that the effective ablation rate may be lessened if a stream of smaller pellets are used instead of injecting the entire refuel mass as a single pellet. The hope here is that the material wake left by earlier particles will remain to reduce the ablation on subsequent particles. This conjecture is presently unsupported by calculations or experiment.

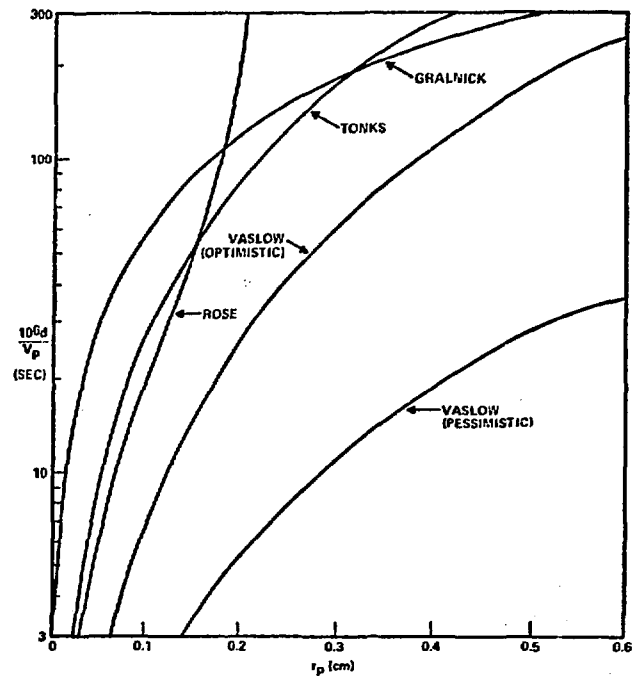

Figure 1. D-T pellet penetration depth into thermonuclear plasmas as a function of pellet radius (r_p) and speed (v_p) . Ablation models of Gralnick, Rose, Tonks, and Vaslow.

TABLE 1

Pellet velocities required to refuel tokamaks (A = 3.5), $n = 10^{14}/cm^3$.

r_p (cm)	a (cm)	$v_p \times 10^{-6}$ (cm/sec) Optimistic	$v_p \times 10^{-6}$ (cm/sec) Pessimistic
0.1	12.7	0.24	5.1
0.3	38.2	0.25	3.8
0.5	63.7	0.21	2.1
0.7	89.2	0.20	1.8

Now, the key to pellet injection is obtaining the necessary pellet velocities. To obtain the velocities in the "optimistic" column of Table 1 is difficult but possible with present technology, at least for strong projectiles. Whether D-T ice can be accelerated to these velocities while remaining an intact solid is uncertain. To obtain the velocities in the "pessimistic" column for any projective material is not possible with technology that can be anticipated over the next decade or so.

Pellets may be accelerated with light gas guns, centrifuges, and by placing a charge on the pellet and using electrostatic acceleration, or by placing the pellet in a metal carrier and using electromagnetic acceleration. Light gas guns have been used to accelerate projectiles of up to about 12. x 10^5 cm/sec. Such experiments were conducted with high strength projectiles; D-T ice has a yield stress estimated to be only 34 bars and fracture during acceleration is a concern. Also, a pellet temperature rise greater than about 10°K during acceleration cannot be

tolerated; the melting point of hydrogen is about 15°K. Temperature rises during acceleration can come from compression of the pellet, heat transfer from the propellent gas, or friction with the gun barrel. To insulate the pellet from the hot propellent gas, an insulating disk insert may be used. If the disk fits too tightly in the barrel, frictional heating, ultimately transmitted to the pellet, is of concern. If too loose, hot gas can leak around the disk to the pellet. Finally, only the D-T pellet is to be injected into the plasma. Means must be developed so that the insulating disk and the (probably) light hydrogen propellent gas can be diverted from entering the plasma. Differential pumping as in neutral beam lines could remove the gas.

Using a centrifuge or other mechanical rotating device is another approach to pellet acceleration. An accelerator of this type has been proposed by Oak Ridge. Most of the same comments apply here as do for light gas guns in the previous paragraph. It is probable that the centrifuge approach can give the velocities in the optimistic column of Table 1, but no assurance that an accelerated pellet will remain intact and cold enough to remain solid. In the centrifuge approach the pellet is injected near the centrifuge axis and is allowed to free fall through an open tube that extends to the centrifuge rim; the trajectory will lead to the plasma. An advantage relative to light gas guns is the absence of a disk and propellent gas which must be prevented from entering the plasma.

An accelerator that produces liquid droplets with velocities of about 10^4 cm/sec has been used to perform refueling experiments on Ormak. In this, liquid hydrogen held in a high pressure chamber is forced through a small orifice. This technique cannot be extrapolated to the velocities in Table 1.

Electrostatic acceleration of charged particles does not appear to be a practical approach to refueling, primarily because the charge to mass ratio that can be obtained is so low. Estimates are that an electrostatic accelerator would have to be about 100 km long.

A somewhat more promising approach is electromagnetic acceleration, being pursued at General Atomic. Here the cryogenic pellet is placed in a metal carrier that is pushed by a magnetic wave traveling down a metal guide structure. (A similar system has been proposed for inter-urban transport.) At peak velocity the pellet is ejected into the plasma, and the carrier must be somehow diverted. Theoretical studies show that velocities of about 10×10^5 cm/sec can be obtained with a guide structure ca. 50 meters long. As with the other pellet acceleration procedures, there are considerations on retaining the pellet intact and cryogenic through the injection procedure.

Acknowledgement

This work was supported by DOE/ERDA under contract #EG-77-C-03-1401.